Final Report

Nitrogen Oxides in the Nocturnal Boundary Layer: Chemistry of Nitrous Acid and the nitrate Radical

U.S. Department of Energy
Project Number: DE-FG02-01ER63094

Jochen Stutz
Department of Atmospheric and Oceanic Sciences
University California Los Angeles
7127 Math Sciences,
Los Angeles, CA 90095-1565

May 24, 2005

Summary

Chemical processes occurring at night in the lowest part of the urban atmosphere, the so called nocturnal boundary layer (NBL), can influence the composition of the atmosphere during the night as well as the following day. They may impact the budgets of some of the most important pollutants, such as ozone and nitrogen oxides, as well as influence size and composition of particular matter. Few studies have thus far concentrated on the nocturnal chemistry of the urban NBL, most likely due to the strong influence of vertical transport and mixing, which requires the measurement of trace gas profiles instead of simple point observations.

Motivated by our lack of observations and understanding of nocturnal chemistry, the focus of this project was the study of the vertical distribution of trace gases and the altitude dependence of nocturnal chemistry under polluted conditions through field observations and modeling studies. The analysis of three field experiments (TEXAQS, Houston, 2000; Phoenix Sunrise Ozone Experiment, 2001; NAPOX, Boston, 2002), two of which were performed in this project, showed that ozone concentrations typically increase with height in the lowest 150m, while NO_2 typically decreases. NO_3, the dominant nocturnal radical species, showed much higher concentrations in the upper part of the NBL, and was often not present at the ground. With the help of a one-dimensional chemical transport model, developed in this project, we found that the interaction of ground emissions of NO_x and hydrocarbons, together with their vertical transport, is responsible for the vertical profiles. The dominant chemical reactions influencing ozone, NO_2 and NO_3 are the reaction of ozone and NO_3 with freshly emitted NO. Sensitivity studies with our model showed that the magnitude of the trace gas gradients depend both on the emission rates and the vertical stability of the NBL. Observations and model analysis clearly show that nocturnal chemistry in urban areas is altitude dependent. Measurements at one altitude, for example at the ground, where most air quality monitoring stations are located, are not representative for the rest of the NBL.

Our model also revealed that radical chemistry is, in general, altitude dependent at night. We distinguish three regions: an unreactive, NO rich, ground layer; an upper, O_3 and NO_3 dominated layer, and a reactive mixing layer, where RO_2 radicals are mixed from aloft with NO from the ground. In this reactive layer an active radical chemistry and elevated OH radical levels can be found. The downward transport of N_2O_5 and HO_2NO_2, followed by their thermal decay, was also identified as a radical source in this layer.

Our observations also gave insight into the formation of HONO in the NBL. Based on our field experiments we were able to show that the NO_2 to HONO conversion was relative humidity dependent. While this fact was well known, we found that it is most likely the uptake of HONO onto surfaces which is R.H. dependent, rather than the NO_2 to HONO conversion. This finding led to the proposal of a new NO_2 to HONO conversion mechanism, which is based on solid physical chemical principles. Noteworthy is also the observation of enhanced NO_2 to HONO conversion during a dust storm event in Phoenix.

The final activity in our project investigated the influence of the urban canopy, i.e. building walls and surfaces, on nocturnal chemistry. For the first time the surface area of a city was determined based on a Geographical Information System database of the city of Santa Monica. The surface to volume areas found in this study showed that, in the

lower part of the NBL, buildings provide a much larger surface area than the aerosol. In addition, buildings take up a considerable amount of the volume near the ground. The expansion of our model and sensitivity studies based on the Santa Monica data revealed that the surface area of buildings considerably influences HONO levels in urban areas. The volume reduction leads to a decrease of O_3 and an increase of NO_2 near the ground due to the stronger impact of NO emissions. Our project shows that the urban canopy should be included in future air quality models to better represent nocturnal chemistry.

This project has considerably advanced our understanding of the chemistry of the urban nocturnal boundary layer. The results of this project have implications for air quality studies in the urban nocturnal boundary layer. The study has also identified new questions on nocturnal processes, which we will continue to address through other projects.

Table of Contents

1 Introduction

Nocturnal chemistry and physics play a crucial role in the conversion and removal of air pollutants such as ozone, nitrogen oxides, and VOCs, which would otherwise be available for daytime ozone formation [*Finlayson-Pitts and Pitts*, 2000]. Photolytic reactions, which are the driving force of atmospheric chemistry during the day, are absent at night. As a consequence, the NO_3 radical, which is rapidly photolysed during the day [*Geyer et al.*, 2001; *Harris et al.*, 1983; *Magnotta and Johnson*, 1980; *Platt et al.*, 1980; *Wayne et al.*, 1991] is the dominant radical species. Besides NO_3, ozone plays an important role as an oxidant of NO and unsaturated VOCs [*Paulson and Orlando*, 1996]. In addition, various heterogeneous reactions become important in the comparably slower chemistry at night. One of the most prominent examples is the formation of HONO [*Finlayson- Pitts et al.*, 2003; *Stutz et al.*, 2002; *Winer and Biermann*, 1994], which acts as an OH radical precursor during the following morning [*Alicke et al.*, 2003; *Alicke et al.*, 2002].

The goal of this project was the investigation of various aspects of nocturnal chemistry in the polluted nocturnal boundary layer (NBL). We were particularly interested in the chemistry of NO_3 and N_2O_5 and the conversion of NO_2 to HONO. A complication of the study of nocturnal chemistry is given by the influence of the weak vertical transport at, night which can lead to vertical profiles of trace gases. The project therefore adopted a one-dimensional view of chemistry in the NBL, i.e. measurements and models covered the entire altitude of the NBL. The following final report summarizes our main findings. We will concentrate on the immediate results of our activities. The publications that resulted from our efforts are appended at the end of the report.

We begin this report with a short introduction in the state of knowledge before the start of this project in order to provide a perspective for the discussion of our results in the following sections. Section 2 will summarize our field observations, while Section 3 describes the 1D chemical transport model that was developed during the project. The main scientific findings are described in Section 4.

1.1 Vertical Mixing in the NBL and its Impact on Trace Gases Profiles

Meteorological conditions have a strong influence on the distribution of trace gases. This is particularly true at night, when radiative cooling of the earth's surface can lead to a stable vertical stratification of the NBL. Nocturnal vertical turbulent transport, which is predominately produced by wind shear, is consequently reduced by the negative buoyancy in the NBL [*Arya*, 1988; *Businger et al.*, 1971; *Rao and Snodgrass*, 1979]. In polluted environments, such as urban areas, trace species are emitted near the surface. Due to the suppressed mixing, these gases can accumulate close to the ground which influences their vertical distribution, as well as those of other species which are chemically connected to them. This is a well known effect that has been described with respect to the accumulation of CO and NO during the morning rush hour.

The influence of vertical mixing often makes it challenging to use point measurements or zero-dimensional modeling approaches [*Allan et al.*, 2000; *Bey et al.*, 1997; *Faloona et*

al., 2001; *Geyer et al.*, 2003; *Platt et al.*, 1990]. While during the day, when turbulent mixing is strong, the omission of vertical transport will only lead to small uncertainties, ignoring the vertical structure of the NBL may give an incomplete picture of the chemical composition and the chemical processes occurring at night. As mentioned above, the challenge of considering both chemistry and meteorology for the polluted NBL was one of the main motivations for this project .

Investigations on the vertical trace profiles in the NBL are sparse. Most reports have concentrated on ozone, which often has lower concentrations near the ground than aloft in both rural and urban areas [*Cros et al.*, 1992; *Glaser et al.*, 2003; *Gusten et al.*, 1998; *Pisano et al.*, 1997; *Zhang and Rao*, 1999]. The positive O_3 gradients are explained by dry deposition of O_3, and the reaction of O_3 with freshly emitted NO. Two studies also report negative NO_2 gradient [*Glaser et al.*, 2003; *Guesten et al.*, 1998], most likely caused by the emission of NO and its reaction with ozone. The obvious lack of observations was the major obstacle for the systematic study of the altitude dependence of nocturnal chemistry and the reason for our field efforts.

A number of studies have investigated the vertical structures of the NO-O_3-NO_2 system in the boundary layer. However, most of them concentrated on the day the boundary layer [*Fitzjarrald and Lenschow*, 1983; *Gao and Wesely*, 1994; *Gao et al.*, 1991; *Hov*, 1983; *Kramm et al.*, 1991; *Lenschow and Delany*, 1987; *Thompson and Lenschow*, 1984]. All studies show the important role of the NO-O_3-NO_2 chemistry in the lower boundary layer. They are also particularly useful since they often focus on the impact of chemistry on turbulent mixing, which is an important aspect of nocturnal chemistry models. The few studies that have studied the NBL show that the effects of vertical mixing are enhanced, and strong trace gas gradients are observed [*Galmarini et al.*, 1997; *Hov*, 1983; *Riemer et al.*, 2003]. Few of these studies, however, considered a full set of chemistry, and validation with field data is also missing. In addition, the studies rarely analyzed the detailed chemical mechanisms in the NBL, and how these interact with vertical transport.

1.2 Chemistry of NO_3

The following equations describe the main chemical pathways of the nocturnal chemistry of NO_3 [*Finlayson-Pitts and Pitts*, 2000].

$$NO_2 + O_3 \rightarrow NO_3 + O_2 \quad (1)$$

$$NO_3 + NO \rightarrow NO_2 + NO_2 \quad (2)$$

$$NO_3 + NO_2 + M \leftrightarrow N_2O_5 + M \quad (3)$$

$$N_2O_5 + H_2O \xrightarrow{H_2O,aerosols} 2\ HNO_3 \quad (4)$$

$$NO_3 + VOCs \rightarrow \ldots\ldots \rightarrow \text{organic nitrate} + \text{other products} \quad (5)$$

The formation of NO_3 proceeds through the reaction of NO_2 with O_3 (eq. 1). Due to the presence of high levels of NO_2 and O_3 in the polluted NBL this reaction leads to an

efficient production of NO_3. NO_3 can be converted back to NO_2 through its reaction with NO (eq. 2). This reaction is quite fast and is primarily responsible for the low daytime NO_3 levels in urban environments [*Geyer et al.*, 2003]. NO_3 and NO_2 can also establish a temperature dependent equilibrium with N_2O_5 (eq. 3). This equilibrium is of particular interest since the loss of N_2O_5 through uptake on particles or its reaction with water vapor (eq. 4) is a loss pathway for NOx in the NBL. NO_3 can also react with a number of hydrocarbons forming organic nitrates and other products, such as RO_2 radicals (eq. 5).

A large number of publications have presented studies on the chemistry of NO_3. Most of these studies were, however, performed in the marine boundary layer or in remote areas [*Allan et al.*, 2000; *Allan et al.*, 1999; *Carslaw et al.*, 1997; *Geyer et al.*, 2001; *Heintz et al.*, 1996]. Publications on urban NO_3 are surprisingly sparse. In fact, we only found one study [*Platt et al.*, 1980] that focused on urban environments and one that addressed the polluted suburban case [*Smith et al.*, 1995]. The general results of these studies have been extensively discussed in atmospheric chemistry text books [*Finlayson-Pitts and Pitts*, 2000].

In the following overview we will therefore only concentrate on those measurement and modeling studies that addressed NO_3 gradients in the NBL [*Aliwell and Jones*, 1998; *Allan et al.*, 2002; *Fish et al.*, 1999; *Friedeburg et al.*, 2002; *Galmarini et al.*, 1997; *Povey et al.*, 1998; *Riemer et al.*, 2003; *Weaver et al.*, 1996]. NO_3 concentrations were generally found to be higher at the top of the NBL than near the surface. [*Aliwell and Jones*, 1998] explain this behavior by NO emission near the surface, which destroys NO_3 through reaction 2, and the weak vertical mixing at night. Model studies of the concentration profile of NO_3 in the lowest 2 km by [*Fish et al.*, 1999] confirm this observation. [*Riemer et al.*, 2003], for an urban plume case, modeled a strong positive gradient of NO_3 in the lowest ~150 m of the NBL with low levels at the surface and up to several hundred ppt at 150 m. Besides these few reports, little systematic information on the altitude dependence of NO_3 chemistry was available in the literature before the start of this project.

1.3 HONO Chemistry

The formation of nitrous acid, HONO, has been one of the most elusive processes in air pollution research over the past three decades. In the early morning and under cloudy conditions HONO photolysis is often the dominant OH source in urban areas, with diurnally averaged contributions to the OH budget of up to 34% [*Alicke et al.*, 2003; *Alicke et al.*, 2002; *Aumont et al.*, 2003]. Consequently HONO formation and photolysis impacts ozone formation [*Aumont et al.*, 2003; *Harris et al.*, 1982; *Jenkin et al.*, 1988] and the oxidation of various pollutants, as well as the formation of aerosol through the oxidation of SO_2 , NO_2, and various hydrocarbons [*Aumont et al.*, 2003].

Despite its importance for air quality, the details of HONO formation remain a mystery. Laboratory studies show that HONO is formed through the conversion of NO_2 on surfaces in a process that is first order in NO_2 and depends on surface adsorbed water [*Finlayson- Pitts et al.*, 2003; *Jenkin et al.*, 1988; *Kleffmann et al.*, 1998; *Pitts et al.*, 1984; *Sakamaki et al.*, 1983; *Svensson et al.*, 1987]. Because HONO is often observed with a yield of nearly 50%, and the remaining nitrogen as surface adsorbed HNO_3

[*Goodman et al.*, 1999; *Kleffmann et al.*, 1998; *Svensson et al.*, 1987] the following stochiometry is regarded today as the best description of HONO formation:

$$NO_2 + NO_2 + H_2O \rightarrow HONO + HNO_3 \quad (6)$$

Other suggested chemical HONO formation mechanisms, for example involving NO [*Calvert et al.*, 1994; *Saliba et al.*, 2000; *Sjödin and Ferm*, 1985], or soot particles [*Ammann et al.*, 1998], have been shown to play only a minor role in the atmosphere [*Gerecke et al.*, 1998; *Kalberer et al.*, 1999]. The formation of HONO in various combustion processes is also insufficient to explain mixing ratios of several ppbv observed in urban areas [*Kirchstetter et al.*, 1996; *Kurtenbach et al.*, 2001; *Pitts et al.*, 1984] and indoor environments.

Besides the phenomenological descriptions of the NO_2 to HONO conversion via R1, we know very little about the detailed molecular processes. *Jenkin et al.*, [1988] proposed a reaction mechanism in which a $H_2O \bullet NO_2$ water complex on the surface reacts with a gas-phase NO_2 molecule. In a recent publication by *Finlayson- Pitts et al.*, [2003] proposed a mechanism that proceeds through N_2O_4 adsorbed on surface films where it isomerizes to the asymmetric form, $ONONO_2$. The $ONONO_2$ autoionizes to $NO^+NO_3^-$, which reacts with surface adsorbed water to generate HONO and HNO_3. HONO can then escape into the gas-phase or undergo secondary reactions.

The non-photolytic loss of HONO also plays an important role in the nocturnal atmosphere [*Harrison et al.*, 1996; *Pitts et al.*, 1984; *Sakamaki et al.*, 1983; *Stutz et al.*, 2000; *Svensson et al.*, 1987; *TenBrink and Spoelstra*, 1998]. All studies report that the loss of HONO in the atmosphere proceeds via heterogeneous reactions or surface uptake. However, the reaction order, as well as the chemical mechanism, are uncertain. One proposed reaction mechanism has the stochiometry:

$$HONO + HONO \rightarrow NO_2 + NO + H_2O \quad (7)$$

Recently *Syomin et al.*, [2003] suggested, based on laboratory observations, a different mechanism in the presence of surface adsorbed HNO_3:

$$HONO_{(surface)} + HNO_{3(surface)} \rightarrow 2\ NO_{2(gas)} + H_2O_{(surface)} \quad (8)$$

A large number of atmospheric observations of HONO have been reported over the years (see [*Lammel and Cape*, 1996] for a review). Nevertheless, little direct information on the chemical mechanism dominating the behavior of HONO followed from these observations. As will become clear below, the main reason for insufficient understanding of atmospheric HONO is founded in the strong influence of micrometeorology. Few measurements of vertical HONO gradients or fluxes have been reported [*Harrison and Kitto*, 1994; *Kitto and Harrison*, 1992; *Stutz et al.*, 2002]. Our earlier studies [*Stutz et al.*, 2002] showed that not only the formation of HONO on the ground, but also its loss, are important processes. As a consequence of this observation we could determine a steady state of HONO in the atmosphere. The observations of gradients also illustrated the

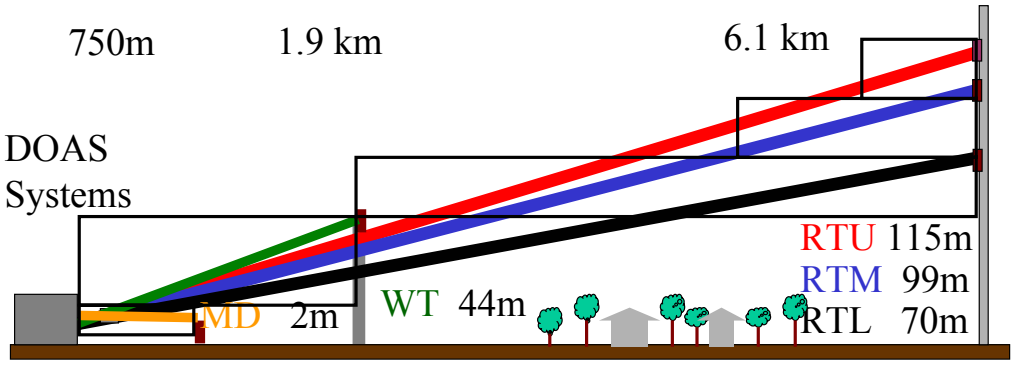

Figure 1: Setup of the DOAS light path in Houston (figure from [*Stutz et al.*, 2004])

influence of vertical mixing. However, the gradients were only measured in the lowest 4m of the atmosphere. There was therefore also a clear need for more HONO and HONO gradient observations.

For many years chemical processes occurring in the nocturnal urban boundary layer have received little attention, most likely because the strong influence of vertical transport and mixing on the distribution of pollutants emitted at the ground posed an obstacle for the study of various chemical processes. As a consequence, observational data was sparse and the description of the nocturnal chemistry in atmospheric models was incomplete prior to the beginning of this project. The goal of this project was to overcome the challenges posed by the influence of meteorology and chemistry, and to provide insights into the chemistry in the NBL and the consequences this chemistry has for air quality. The following two sections describe our experimental and modeling efforts.

2 Experimental Activities

The acquisition of field observations of the chemical composition and its altitude dependence in the NBL was one of the main activities of this project. Consequently we performed field experiments in Phoenix, in summer 2001, and Boston, in summer 2002. The analysis of data from an earlier experiment in Houston, in 2000, was also part of this effort. The data sets of these experiments are the basis of our scientific results, which will be discussed in Section 4.

All our measurements were made using Differential Optical Absorption Spectroscopy, DOAS, [*Platt*, 1994]. The details on our instrument and the analysis methods have been described elsewhere [*Alicke et al.*, 2002; *Geyer et al.*, 1999; *Stutz et al.*, 2001; *Stutz and Platt*, 1996; *Stutz and Platt*, 1997]. We will therefore concentrate on the description of the different field setups and observational data acquired in the three field studies.

2.1 TEXAQS 2000

While the measurements during the Texas Air Quality Study 2000 predate this project, the interpretation of this data set was one of our first activities. The TEXAQS

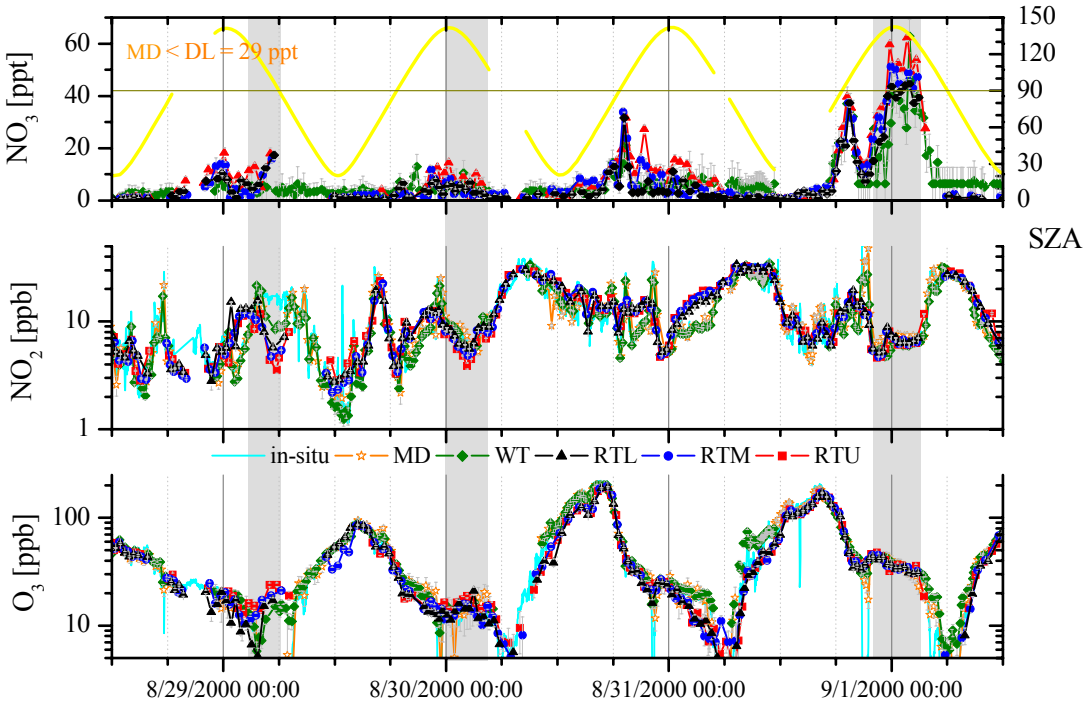

Figure 2: Overview of path averaged DOAS data from noon of August 28 to noon September 2, 2000. The data is color coded according to the colors in Figure 1. Please note the logarithmic scale for NO_2 and O_3. (figure from [*Stutz et al.*, 2004 b])

2000 study took place at La Porte, near Houston, TX, during July and August, 2000. We set up two long-path DOAS instruments measuring on five different light paths (Figure 1). The lightpaths spanned different height intervals, thus allowing the retrieval of vertical concentration profiles of O_3, NO_2, NO_3, and HONO. Figure 2 shows three days from the original, path-averaged, data set. While LaPorte, was a more suburban environment, petrochemical refineries to the east of La Porte contributed considerably to the high pollutant levels observed during periods of easterly winds. As Figure 2 shows, ozone mixing ratios reached up to 200 ppb during these days. NO_2 levels were elevated during the day but were lower during the night. This behavior stems from the origin of the nocturnal air, which came from west and southwest during the nights and was not under the influence of large direct emissions. During the day, the air often originated directly from the industrial complexes east of La Porte, explaining the high levels of all pollutants.

Based on our path-averaged measurements (five light paths pointing from H = 2 m to altitudes h_i of 2, 44, 70, 99, and 115 m) we developed a method to derive vertical mixing ratio profiles for O_3, NO_2, HONO, and NO_3. All data was temporally interpolated to the time of the RTU observation, i.e. along the i^{th} light path a concentration S_i was observed at this time. The concentrations in a specific height interval, C_i, were derived as follows: C_1 and C_2 directly represent the concentrations of the lower height intervals. C_3, C_4, and C_5 in the height intervals (44 m – 70 m), (70 m – 99 m), and (99 m – 115 m) were calculated with the following equation:

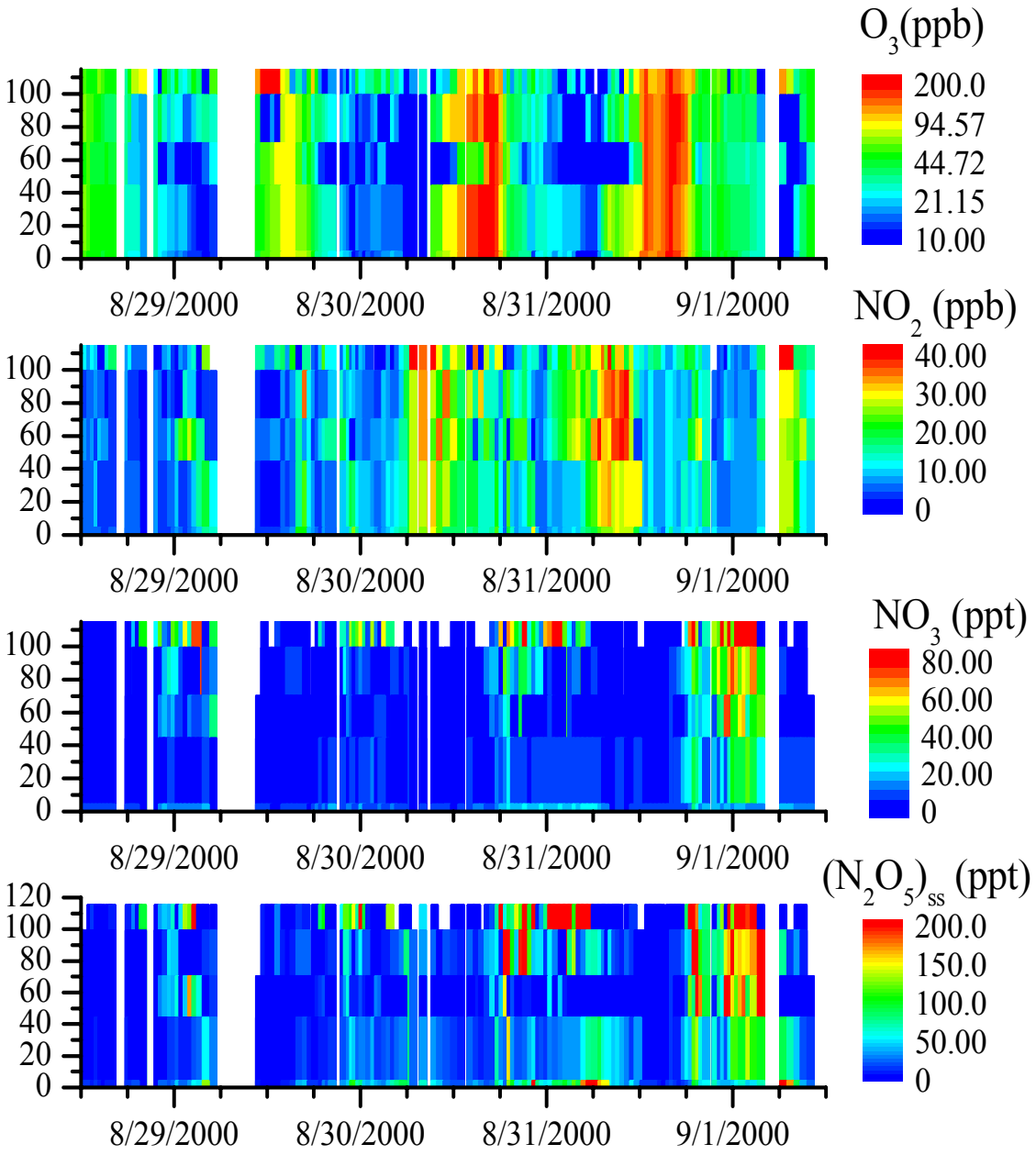

Figure 3: Vertical profiles of O_3, NO_2, NO_3, and steady state N_2O_5 at La Porte. (figure from [*Stutz et al.*, 2004])

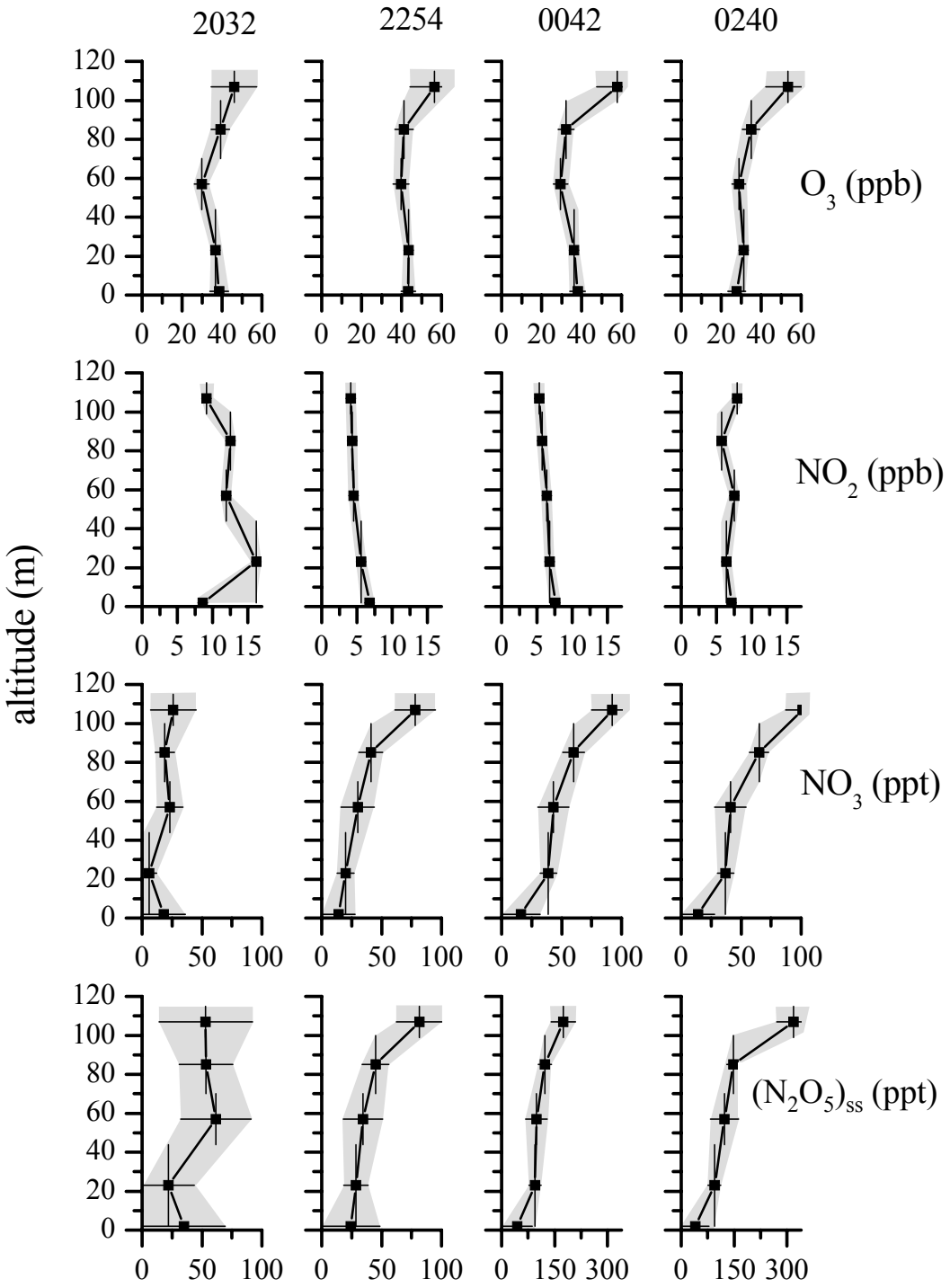

Figure 4: Vertical distribution of O_3, NO_2, NO_3, and steady state N_2O_5 at La Porte. (figure from [*Stutz et al.*, 2004])

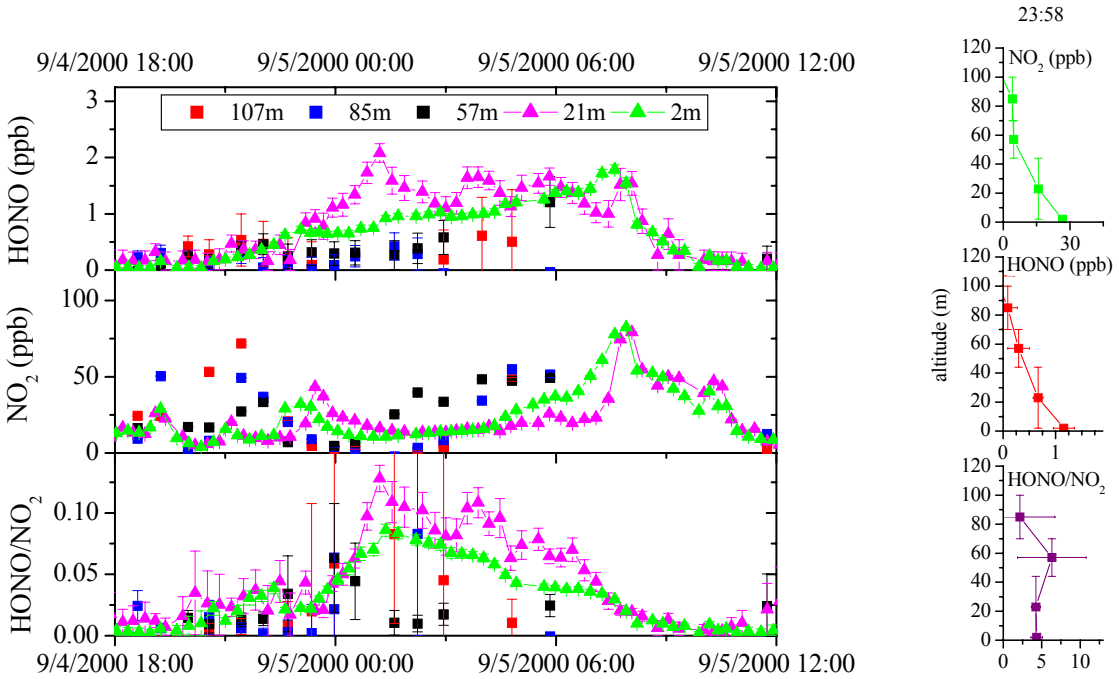

Figure 5: Time series of NO_2, HONO, and the HONO/NO_2 ratio at various altitudes at La Porte on Sept 5, 2000. The profiles on the right were taken from the measurements at 23:58. Vertical bars show the extent of the height intervals.

$$C_i = \frac{h_i - H}{h_i - h_{i-1}} S_i - \frac{h_{i-1} - H}{h_i - h_{i-1}} S_{i-1} \tag{9}$$

Because horizontal gradients can lead to erroneous vertical profiles, we filtered our data using various tests, for these periods. The data shown here is only of those time periods when the atmosphere was horizontally well mixed.

Figures 3, 4, and 5 show the result of this procedure. Ozone and NO_3 show positive gradients (higher concentrations aloft), and NO_2 and HONO have negative profile (lower concentrations aloft). NO_3 concentrations above 100m altitude reached above 100 ppt, showing an active radical chemistry. In contrast, close to the ground, NO_3 concentrations were negligible.

We also observed negative HONO profiles at La Porte, which point towards a conversion of NO_2 to HONO on the ground (Figure 5). The path-averaged HONO data (not shown here) has been used for the investigation of the relative humidity dependence of NO_2 to HONO conversion.

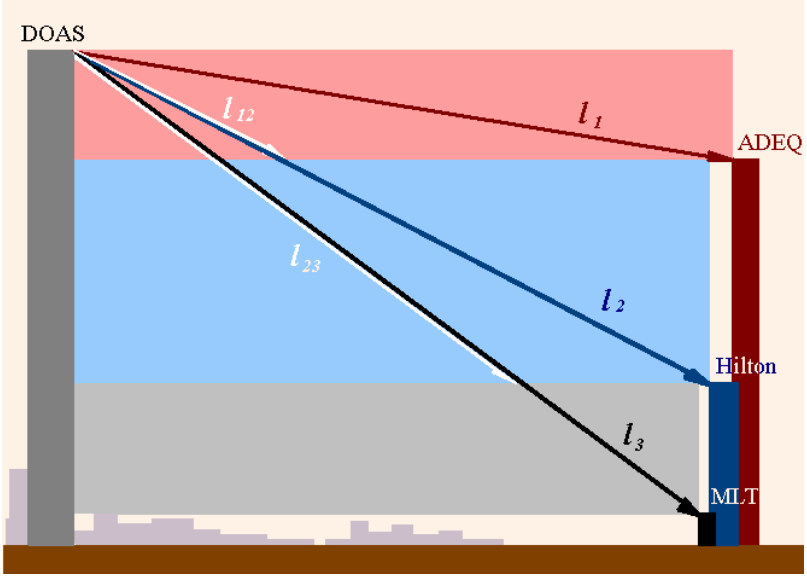

Figure 6: DOAS setup during the Phoenix 2001 experimens. The three lights paths are distinguished by color.

2.2 Phoenix 2001

In June 2001, a field experiment organized by DOE'a Pacific Northwest National laboratory, PNNL, was conducted in the downtown area of Phoenix, AZ. As part of this project UCLA's long-path Differential Optical Absorption Spectroscopy (DOAS) system was operated to provide 24-hour continuous measurements of vertical distributions of a number of trace species in the open atmosphere. Meteorological parameters, such as relative humidity, wind direction and speed, and potential temperature profiles, were monitored at various fixed altitudes and with balloon sondes operated by PNNL. In addition, in-situ measurements of NO were made at different altitudes by Batelle Ohio.

During the two-week field studies (6/16/2001 – 7/1/2001), our long path DOAS instrument was set up on the 39th floor of BankOne, 140 m above ground (Figure 6). Three retroreflector arrays were mounted on the roofs of buildings (ADEQ, Hilton, and MLT) with different heights, at a distance of about 3.3 km north from BankOne (see Figure 6). The average trace gas concentrations along each light path were monitored by sequentially aiming the telescope to the three retroreflector arrays. The duration of a typical measurement cycle covering all three light paths was 15~20 min, depending on atmospheric visibility. The light paths were aligned in the horizontal but separated in the vertical direction. The paths ran along one direction of the street grid which connnects the downtown and northern uptown region of Phoenix. As during TEXAQS, we made an effort to ensure that horizontal inhomogeneities would not lead to erroneous vertical trace gas profiles. Because traffic was, to a large extent, spatially homogeneous in downtown Phoenix, inhomogeneities of the trace gas distributions in the horizontal direction were small. Freeway I10, which crossed the light paths close to the BankOne building, had light traffic during the night. An impact from the freeway emissions was thus not expected. The area between downtown and uptown Phoenix therefore offered an ideal location for our measurements, since the impact of street canyons was expected to be small.

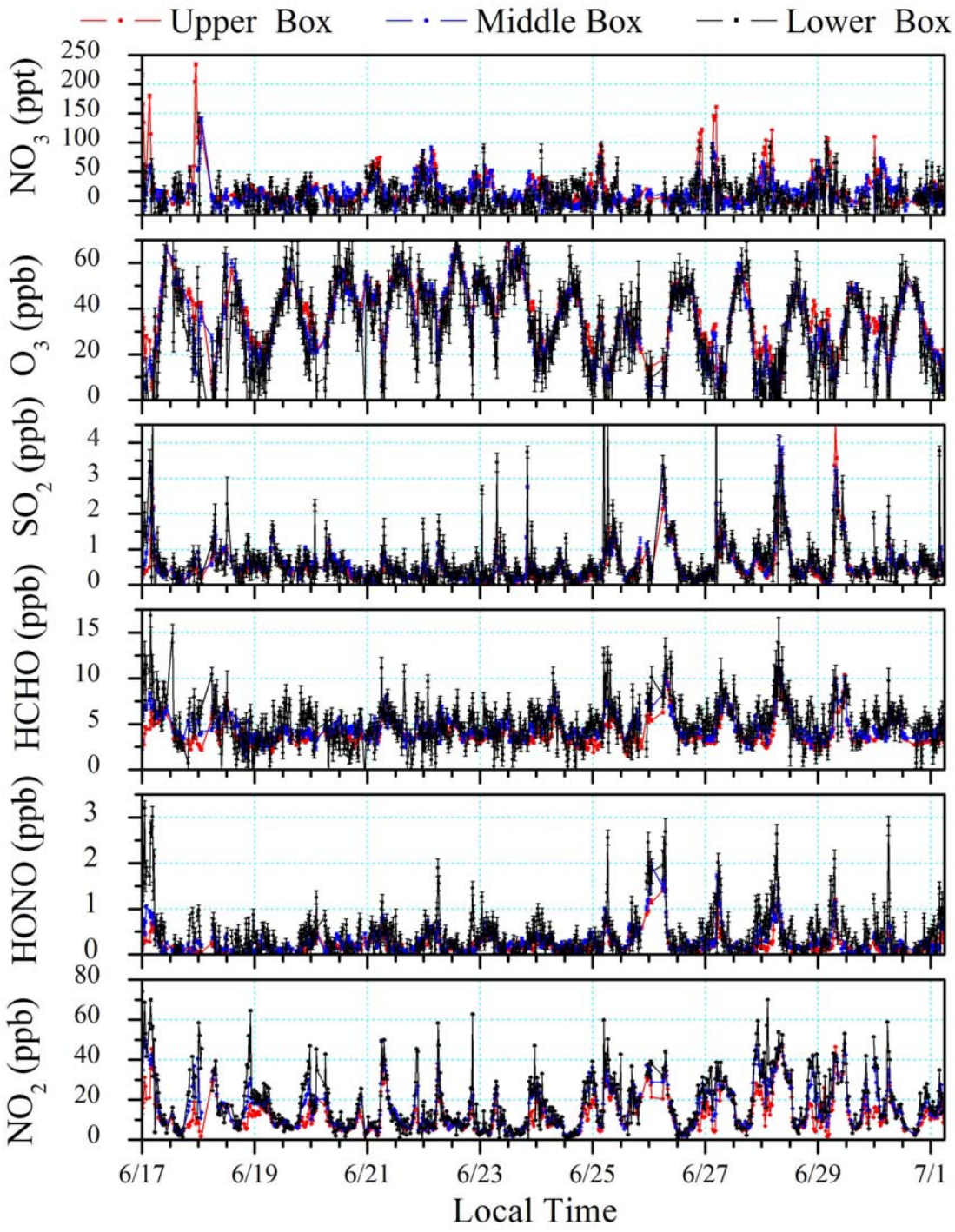

Figure 7: Overview over the entire DOAS data set acquired in Phoenix.

NO_2, HONO, HCHO and O_3 were measured in the near UV spectral region according to their distinctive absorption structure in the wavelength range of 300-380 nm. NO_3 was detected separately at higher wavelengths (610-680 nm) [*Alicke et al.*, 2002; *Geyer et al.*, 1999]. We used a similar approach to that described above for the TEXAQS 2000 experiment to derive trace gas concentrations averaged over a certain height interval, C_{low}, C_{mid}, and C_{up}. Due to the error propagation in the calculation, the concentration in the lower height interval, C_{low} has larger errors and higher detection limits than those in the upper and middle height intervals C_{up} and C_{mid}. Figure 7 shows an overview over the entire data set acquired by our group in Phoenix. The diurnal variations of O_3 and NO_2 are typical for a strongly polluted urban site. Ozone shows high daytime and low nighttime mixing ratios. The behavior of NO_2 is exactly opposite to that of O_3. NO_3 levels were very high, up to 200 ppt, in the upper height interval. In this overview one can already recognize that the NO_3 mixing ratio is higher in the upper height interval than close to the ground (see also below). Formaldehyde mixing ratios were in the range of 5 ppb during the day. Surprisingly, HCHO increased to twice this value during some nights. Since HCHO formation processes are slow at night, we attribute the elevated HCHO to direct emissions from the ground. This is confirmed by the negative HCHO concentration profiles during most nights. SO_2 mixing ratios vary independently from the other trace gases, which is most likely due to a few SO_2 point sources in the Phoenix area. HONO levels were surprisingly low for a heavily polluted urban area such as Phoenix. The reason for the low HONO is the low relative humidity in Phoenix (see Section 4.4).

Based on these results, the vertical gradients of trace gas concentrations between 27.5 m and 125m altitude were also calculated, using:

$$\frac{dC}{dz} = \frac{C_{up} - C_{low}}{z_{up} - z_{low}} \tag{10}$$

where z_{up} and z_{low} refer to the central height of the upper and lower box respectively. This gradient is a linear approximation for the more complex vertical profiles of the various trace gases. It is, however, a good quantity to study nocturnal chemistry and the various transport processes.

The fact that the Phoenix measurements were performed in a fairly polluted downtown area helped this study, since the gradients were much stronger than those in Houston. Figures 8 and 9 show two nights, June 16 – 17 and June 26 – 27. The first night is characterized by strong stability and high emissions. A morning rush hour is missing since 6/16 was a Saturday. Gradients of O_3 and NO_2 were in the range of 0.1 - 0.3 ppb/m throughout this night. Interestingly, the gradient of the sum of O_3 and NO_2, O_x, was much smaller, showing the importance of the NO + O_3 reaction. NO_3 also shows very strong gradients, with the highest NO_3 levels measured aloft during the campaign. The N_2O_5 mixing ratio was calculated based on the NO_3 + NO_2 equilibrium (reaction 3). The NO_3 production rate according to reaction 1 is shown together with the lifetime of NO_3 calculated based on production rate and NO_3 concentration. The second night shown here illustrated the influence of the stability of the NBL.

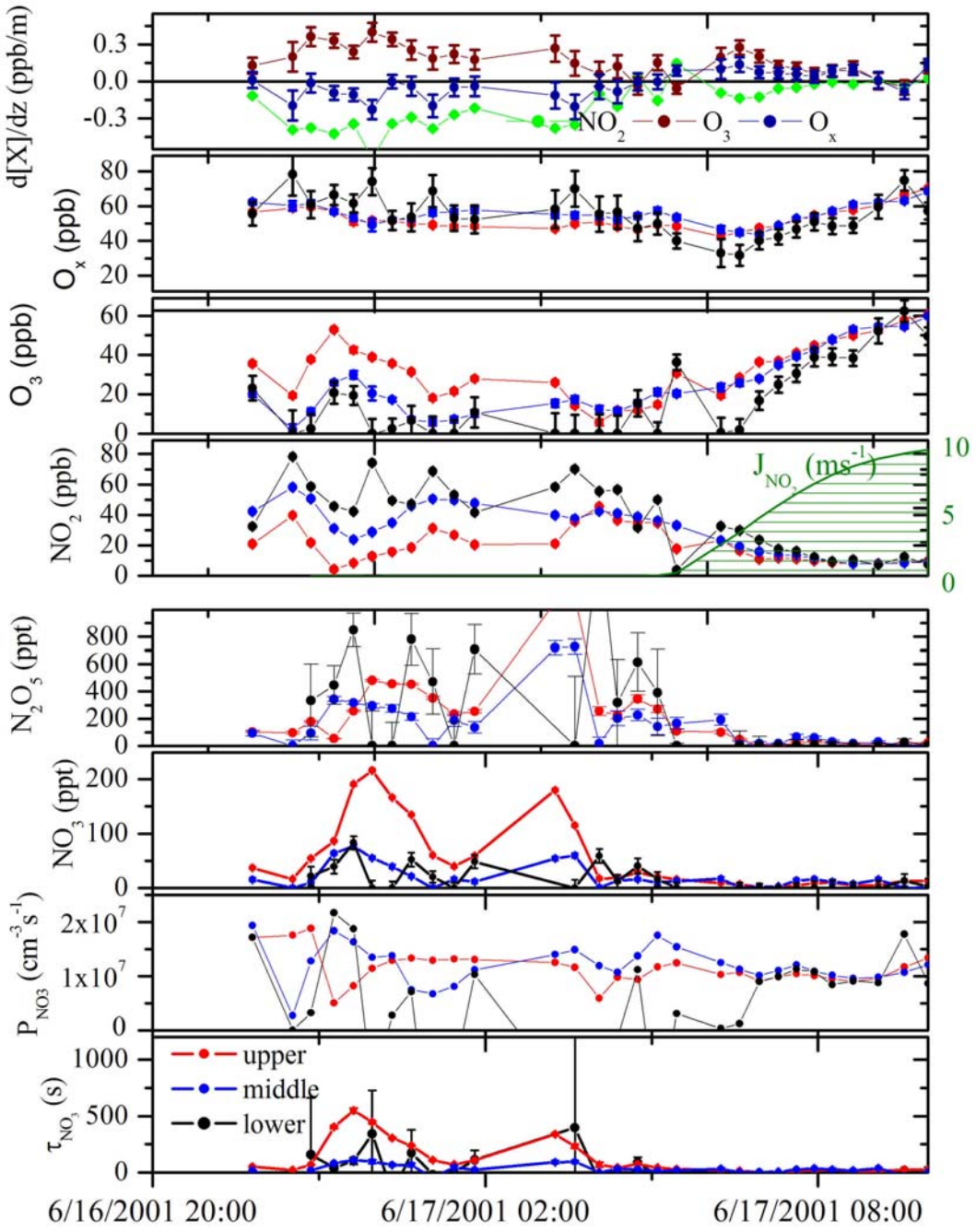

Figure 8: Data from the night of June 16 -17 in Phoenix

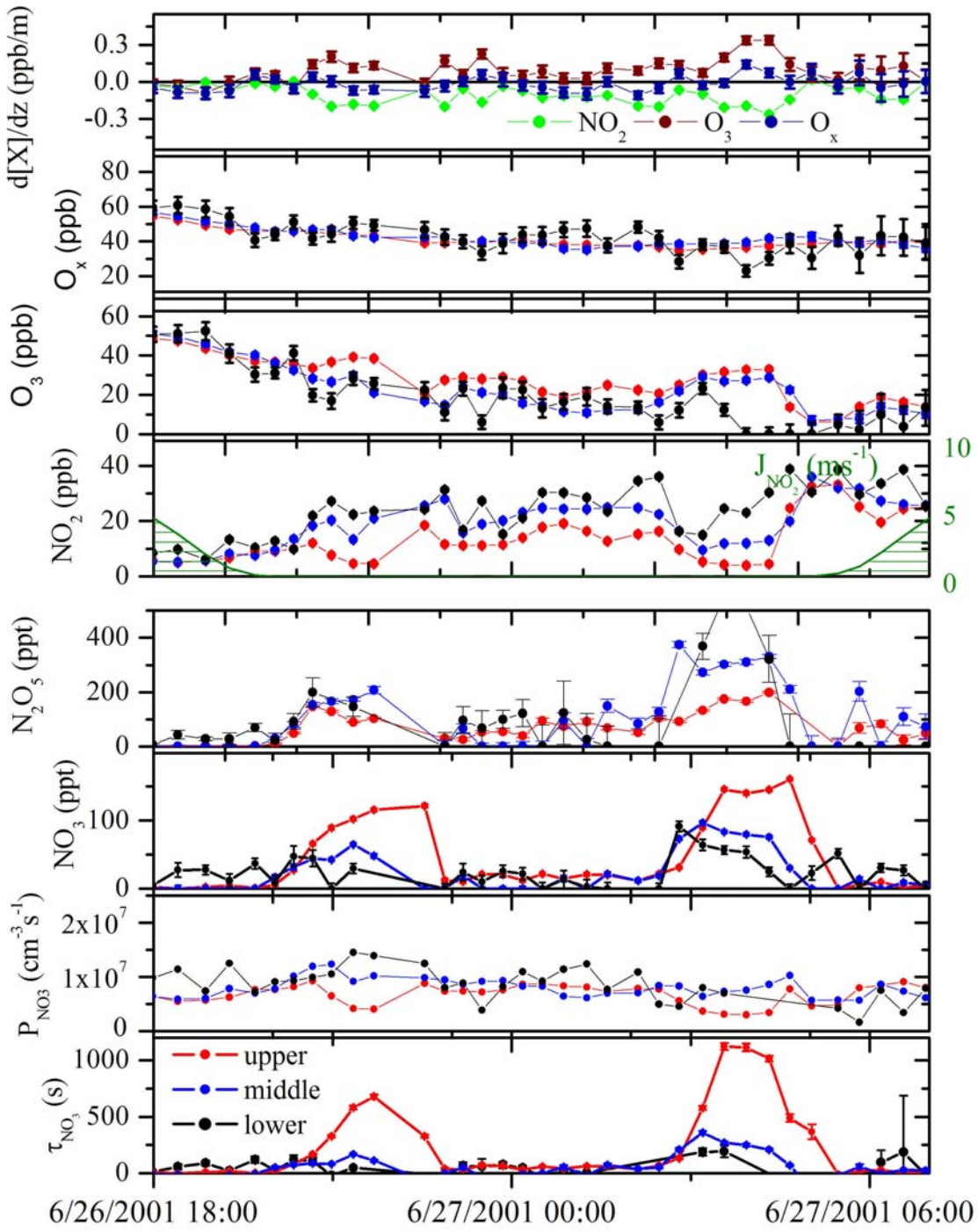

Figure 9: Data from the night of July 26 – 27 in Phoneix

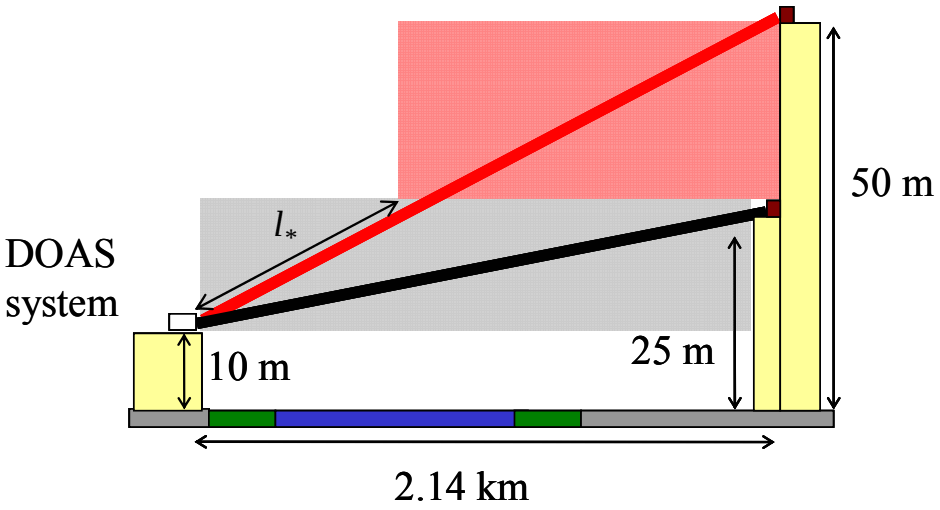

Figure 10: Setup during the NAOPEX field experiment in Boston

Two periods of strong vertical gradients in all trace gases, which can be identified at 2200 and 0400 in Figure 9, are correlated with large temperature gradients (not shown here), and thus strong vertical stability. Again NO_3 levels were quite high in the upper height interval. This is clearly related to an increased atmospheric lifetime of NO_3, most likely due to missing sinks aloft (lower panel Figure 9). The gradients of O_3 and NO_2 were somewhat smaller than during the first night, but the O_x gradients were again smaller than those of O_3 and NO_2. A number of other nights have been studied (see appended manuscript by Wang et al.).

In summary, the Phoenix 2001 experiment has been extremely successful. It has provided a wealth of unique observations that are still being further interpreted. The data has been presented during many meetings and is used in a number of publications.

2.3 Boston 2002

The NAOPEX Experiment in Boston 2002, was the last performed within this project. As in Phoenix, the experiment was a collaborative effort between UCLA and various DOE laboratories, such as PNNL and Argonne National Laboratory. Figure 10 shows the DOAS setup that was used during the experiment. The area around Boston College, where our instrument was located, was characterized by a larger amount of vegetation and less traffic that downtown Phoenix. Nevertheless, the location was fairly polluted since it was often downwind of downtown Boston. We also flew temperature balloon sondes and deployed thermometers at three different altitudes during the campaign. While we did not achieve the altitude range of our Phoenix experiment, the high time resolution makes this another interesting data-set.

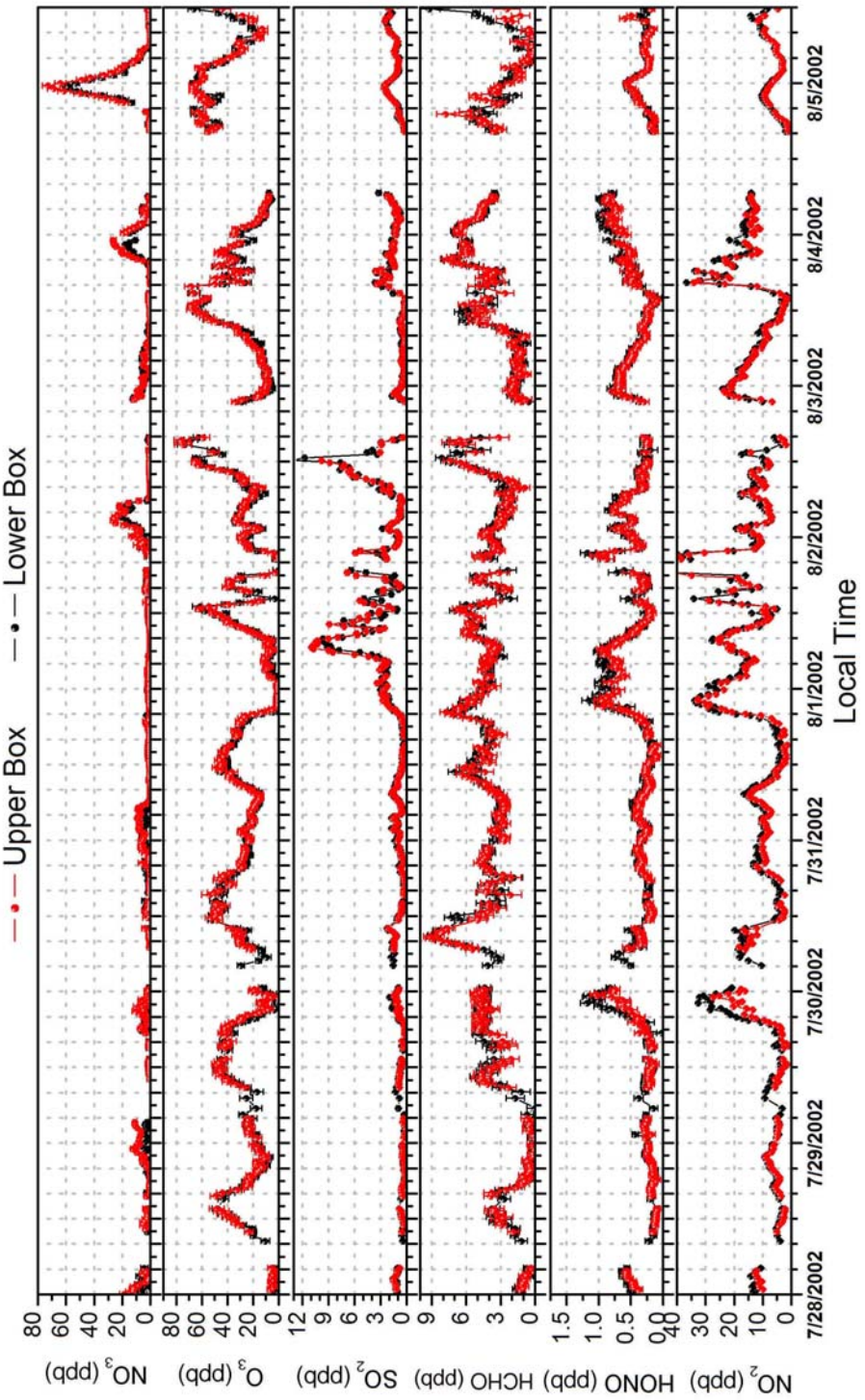

Figure 11: One week of the Boston data set

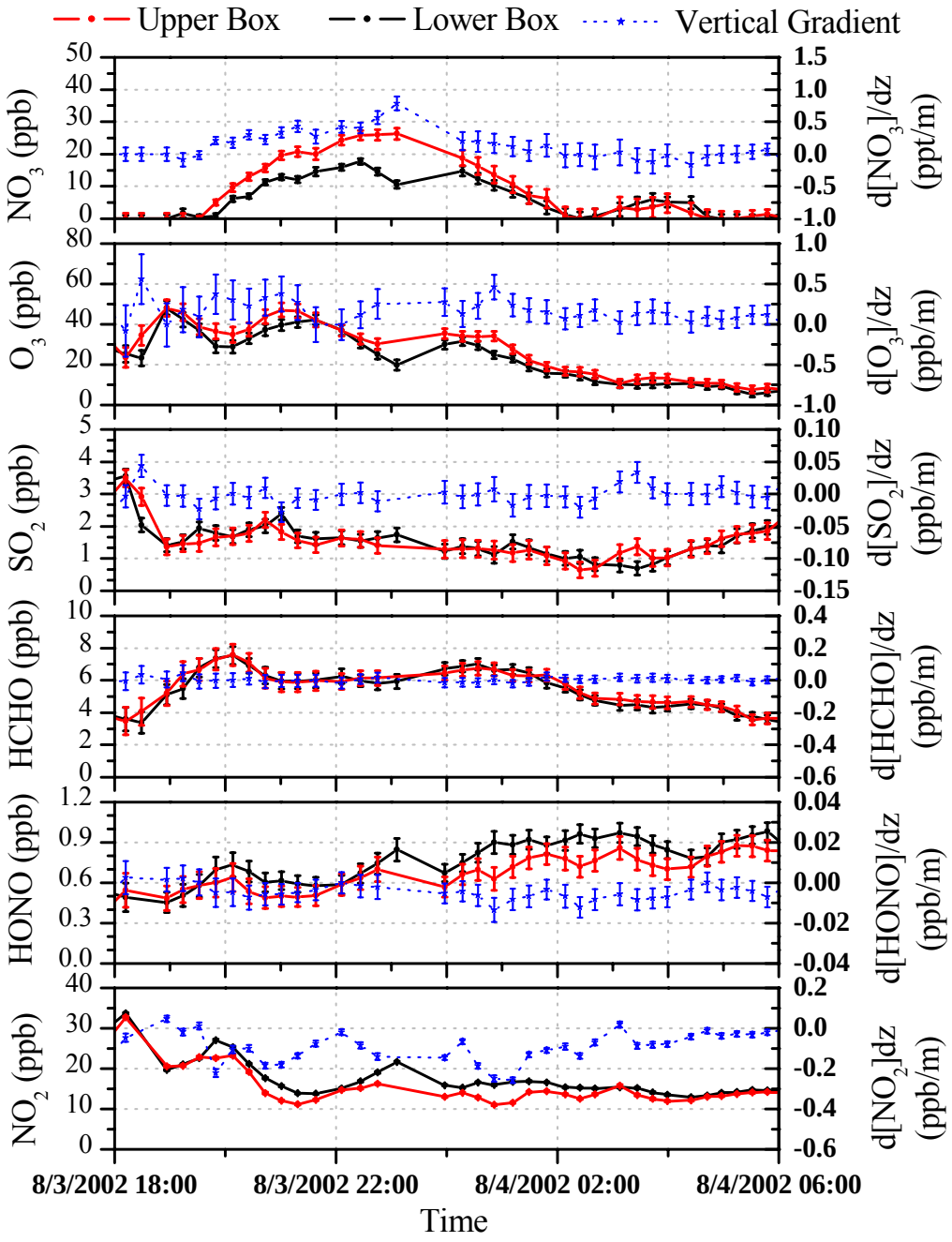

Figure 12: Vertically resolved mixing ratios and gradients for the night of August 3 – 4 in Boston.

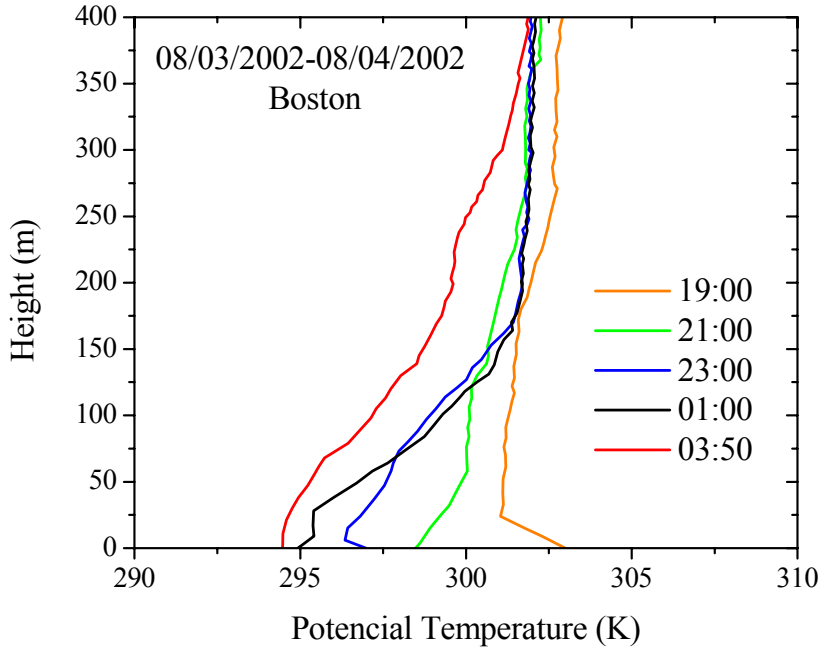

Figure 13: Balloon soundings during the night of August 3 -4 in Boston.

Figure 11 gives an overview of the entire Boston data set. As in Phoenix, the O_3 and NO_2 mixing ratios show the diurnal variation expected for a polluted site. The mixing ratios of both gases were of similar magnitude to those in Phoenix. SO_2 mixing ratios were typically low, except for certain periods during which we were influenced by the Boston College power plant. Formaldehyde was also in the same range as in Phoenix. However, daytime values were higher than those at night. This is in contrast to our observations of Phoenix, and we can conclude that direct HCHO sources do not seem to be as important in Boston. HONO levels were quite high, most likely due to the higher R.H. in Boston compared to Phoenix. NO_3 mixing ratios were generally smaller than in Phoenix. A number of possible explanations can be found for the lower NO_3 levels. Higher R.H. and higher VOC emissions could have increased the loss of NO_3 and N_2O_5, thus reducing NO_3. Our Boston observations were also made at much lower heights than in Phoenix, and the NO_3 + NO reaction could have been more important.

Vertical gradients of various trace gases were also observed in Boston. Figure 12 shows the night of August 3-4, during which all gases, with the exception of HCHO and SO_2, show gradients. The sign of these gradients is similar to those in Phoenix, confirming that the general behavior observed in Houston and Phoenix apply also to other environments. It is particularly interesting that NO_3 shows a fairly strong gradient over a small height interval of 20m. As in Phoenix, O_x did not show vertical gradients (not shown here). Figure 13 shows the balloon soundings during this night, showing that the NBL on August 3 –was quite stable, contributing to the formation of the observed vertical gradients

The various field experiments have provided a unique data set, which has allowed us to constrain our modeling activities and has given us observational evidence that the processes that we believed would control the chemistry and composition of the nocturnal boundary layer are indeed occurring. Furthermore, the different environments of Houston, Phoenix, and Boston showed that our findings are not restricted to one location, but seem to be universally applicable. The comparison of various locations was used in our analysis of HONO formation, which combined the Houston and Phoenix data with an earlier data set from Nashville. The scientific findings derived from our observations will be discussed in Section 4.

3 Modeling Activities

As part of the original proposal we proposed to develop a one-dimensional chemical transport model to study nocturnal chemistry. Throughout the project we realized that this model was indeed an essential tool for understanding the complex mechanisms occurring at night in an urban NBL. We therefore dedicated a considerable portion of the project to the development of this model. The initial purpose of the model was to provide a tool to understand the general behavior of the chemistry ion the NBL. The model was therefore based on a detailed chemistry and a prescribed vertical mixing, the latter often being constrained by the observations of the vertical distribution of O_3 and NO_2, or, when available, micrometeorological data. We found that the model also described our observations surprisingly well. Consequently it has also been used to extract quantitative information from our measurements. The model has a number of unique features. In particular, the explicit treatment of the vertical transport of reactive trace gases will be described below (Section 3.2.2). It should be noted here that some of the most exciting scientific results produced in this project stem from the model (see Section 4). The following sections describing the model are adapted from the manuscripts of [*Geyer and Stutz*, 2004 a, b].

3.1 Model Description

The one-dimensional **N**octurnal **C**hemical **A**nd **T**ransport model, NCAT, is based on a system of 1D transport kinetics equations, which express the change of the concentration $c_i(z, t)$ of a trace gas i at an altitude z at the time t as follows:

$$\frac{dc_i(z,t)}{dt} = \Psi_i(z,t) + P_i(z,t) - L_i(z,t) + E_i(z,t). \qquad (11)$$

Here, $\Psi_i(z,t) = -\frac{\partial j_i(z,t)}{\partial z}$ is the rate of the concentration change caused by the net vertical flux $j_i(z,t)$, $P_i(z,t)$ the total chemical production rate, $L_i(z,t)$ the total chemical loss rate, and $E_i(z,t)$ the emission rate of compound i. The equation system is solved with a Gear-type solver (Facsimile [*Curtis and Sweetenham*, 1987]). Concentration changes by advection are neglected.

The height range and the number of grid-points, also called boxes, covering the altitude range of the model can be easily varied, allowing high vertical resolutions. For most of our model runs we subdivided the lowest 250 m of the nocturnal atmosphere into 20 boxes (sensitivity tests show that the results are identical to that of model runs using more than 100 grid points). An additional box between 250 m and 1000 m is used to

provide an upper boundary for the model. Considering the reduced vertical transport efficiency near the ground we adopted a logarithmically decreasing box height towards the ground in the lowest meters.

The model includes an explicit computation of vertical exchange and the temperature profile, gas-phase and heterogeneous nocturnal NO_x-NO_3-HO_x-O_3 chemistry, a simplified VOC oxidation scheme, emission of NO from soil and cars, CO emission from cars, emission of monoterpenes from the biosphere, and dry deposition on the ground.

3.2 Vertical transport calculation

3.2.1 Vertical flux of an inert gas

The vertical flux, $j_i(z,t)$, of an inert or slow reacting trace gas, for example CO and CH_4, is calculated in the model using a linear flux-gradient relationship (*K* model, we implicitly assume that atmospheric density does not change over the height of the NBL):

$$j_i(z,t) = -K_{inert}(z,t) \cdot \frac{\partial c_i(z,t)}{\partial z} \tag{12}$$

In this first-order model, the vertical flux $j_i(z,t)$ only depends on the vertical concentration gradient of a gas *i*, $\frac{\partial c_i(z,t)}{\partial z}$, and on the altitude dependent eddy diffusivity $K_{inert}(z,t)$ (laminar diffusion is considered only close to the ground surface). The eddy diffusivity is identical for all inert gases, and is calculated by Monin-Obukhov similarity theory using the empirical equations for the dimensionless stability correction factor, $\Phi_S(\frac{z}{L^*},t)$, for turbulent molecular transport given by *Businger et al.* [1971] for the lowest 50 m.

$$K_{inert}(z,t) = \frac{\kappa \cdot u^*(t) \cdot z}{\Phi_S(\frac{z}{L^*},t)} \tag{13}$$

In equation 13, $\kappa \approx 0.4$ is the von-Karman constant, and $u^*(t)$ the Prandtl layer friction velocity. Above 50 m the inert eddy diffusivity is set to its value at 50 m altitude. The correction factor $\Phi_S(\frac{z}{L^*},t)$ is a function of altitude and atmospheric stability, which is described by the Monin-Obukhov length $L^*(t)$. In later versions of the model we also included the possibility of a rough surface by using the surface roughness and displacement height to calculate K_{inert} with an expanded equation 13.

3.2.2 Vertical flux of a reactive gas

As pointed out by several studies [*Brost et al.*, 1988; *Fitzjarrald and Lenschow*, 1983; *Galmarini et al.*, 1997; *Gao et al.*, 1991; *Hamba*, 1993; *Lenschow*, 1982; *McDonald-Buller et al.*, 1999; *Schumann*, 1989; *Thompson and Lenschow*, 1984; *Vila-Guerau de Arellano*, 2003; *Vila-Guerau de Arellano et al.*, 1995], the unmodified K model is restricted to inert or slow reacting gases because the effect of chemistry on the vertical flux of a trace gas is not considered. Since second order closure models, as applied for example by *Galmarini et al.* [1997] and *Vila-Guerau de Arellano et al.* [1995] for

reactive gases, are difficult to use with complex chemical frameworks, we included a modified K model in NCAT which considers the effects of both vertical mixing and chemistry on the vertical flux of a trace gas.

The vertical net flux of a reactive species i can therefore be approximated by

$$j_i(z,t) = \overline{w'(z,t)\cdot z'}\cdot\frac{\partial c_i(z,t)}{\partial z} + \overline{w'(z,t)\cdot z'}\cdot\frac{\partial(P_{ij}(z,t) - L_{ij}(z,t))}{\partial z}\cdot\tau_{i\,eff}(z,t), \qquad (14)$$

where $w'(z,t)$ is the fluctuation of the vertical component of the wind speed, z' the turbulent mixing length, and $\tau_{i\,eff}(z,t)$ an effective time scale for the transport. Using the definition $K_{inert}(z,t) = \overline{w'\cdot z'}$, the flux of a reactive species can be expressed by

$$j_i(z,t) = -K_{inert}(z,t)\cdot\left(\frac{\partial c_i(z,t)}{\partial z} + \frac{\partial(P_i(z,t) - L_i(z,t))}{\partial z}\cdot\tau_{i\,eff}(z,t)\right) \qquad (15)$$

Equation 5 is similar to the modified *K* model discussed in *Hamba* [1993] (also [*Hamba*, 1994; *Verver*, 1994]). The effective time $\tau_{i\,eff}$ was approximated by *Hamba* [1987] using the Two Scale Direct Interaction Approximation (TSDIA) theory [*Yoshizawa*, 1982].

$$\tau_{i\,eff}(z,t) = \frac{1}{\tau^{-1}_{i\,turbulent}(z,t) + \sum_l |j_{il}| + \sum_{l,m} |k_{ilm}(c_l + c_m)|} \qquad (16)$$

In equation 16, j_{il} represents the reaction rate constant of a unimolecular reaction, k_{ilm} the rate constant of a bimolecular reaction involving the gas *i*. The turbulence time scale $\tau_{i\,turbulent}(z,t) = \frac{z}{\kappa\cdot u^*(t)}$ is on the order of 100 s in the NBL [*Fitzjarrald and Lenschow*, 1983; *Lenschow*, 1982].

By introducing the modified *K* model (equation 14), vertical transport of a gas is no longer only a function of its concentration profile, but also of the concentration profiles of other gases that react or are educts of this gas (cross-diffusion). Equation 14 is particularly useful if turbulent transport and chemistry occur on comparative timescales. If the chemical timescale of a gas is very short, its vertical flux is influenced little by chemistry, either because it is in a steady state or because $\tau_{i\,eff}$ is small. At the other extreme, vertical transport of a gas is hardly influenced by chemistry if its chemical timescale is very long, and equation 2 can be used to calculate $j_i(z,t)$.

The explicit treatment of the vertical mixing of reactive trace gases is a unique feature of our model. To ensure that this treatment is indeed necessary, we used the model to compare the effective eddy diffusivity of a reactive trace gas with that of an unreactive tracer. The effective eddy diffusivity of a gas, $K_i(z,t)$, is defined as the negative ratio of its vertical flux and concentration gradient:

$$K_i(z,t) = -\frac{j_i(z,t)}{\frac{\partial c_i(z,t)}{\partial z}}. \qquad (17)$$

Because chemical reactions alter the vertical flux of a reactive trace gas, the effective eddy diffusivity of a reactive gas can be different from that of an inert gas. Applying

equation 17, $K_i(z,t)$ can be expressed as product of the eddy diffusivity of an inert gas and a chemistry correction factor.

$$K_i(z,t) = K_{inert}(z) \cdot \left[1 + \frac{\frac{\partial (P_i(z,t) - L_i(z,t))}{\partial z} \cdot \tau_{i\,eff}(z,t)}{\frac{\partial c_i(z,t)}{\partial z}} \right] \tag{18}$$

The chemistry correction factor is closer to unity if a gas a) has a strong concentration gradient, b) is in chemical steady state (because $\frac{\partial (P_i(z,t) - L_i(z,t))}{\partial z}$ is negligible), and c) has a short chemical lifetime. $K_i(z,t)$ is larger than $K_{inert}(z)$ if $\frac{\partial (P_i(z,t) - L_i(z,t))}{\partial z}$ has the same trend as its concentration gradient. Likewise, $K_i(z,t)$ is smaller than $K_{inert}(z)$ if both gradients have opposite directions.

In Figure 14 the vertical profiles of the concentration gradients, vertical fluxes, and effective eddy diffusivities of NO, O_3, NO_2, NO_3, and N_2O_5 are shown using data of a typical urban scenario one hour after model start. Note that we did not calculate effective diffusivities for NO, NO_3, and N_2O_5 above 50 m, since equation 16 is no longer applicable at very weak concentration gradients. The vertical profile of $K_{NO}(z,t)$ in Figure 14 reveals three layers with different chemistry correction factors. Below 10 m the chemistry correction term in equation 16 is, in principle, negligible because the effective time, $\tau_{NO\,eff}(z,t)$, is very short (e.g., ~1 s in 3 – 4 m). The causes of the short effective time close to the ground are the short turbulent time scale, which increases linearly with altitude, and the fast reaction frequency of NO. In a layer between 10 and 30 m, the effective eddy diffusivity of NO is, however, strongly reduced. In the example in Figure

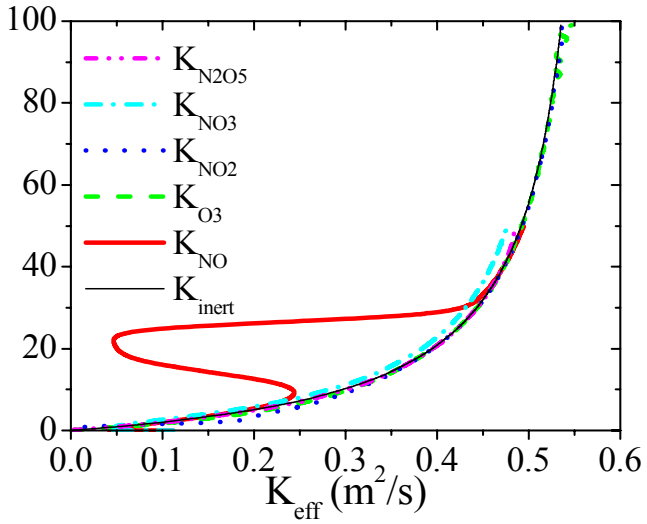

Figure 14: Vertical profiles of concentration gradients, vertical fluxes, and effective eddy diffusivities for the reactive trace gases NO, O_3, NO_2, NO_3, and N_2O_5 (scenario 1, one hour after start). Additionally, the eddy diffusivity of an inert gas is shown. (figure from [Geyer and Stutz, 2004 a])

14, $K_{NO}(z,t)$ is as low as 0.05 m^2/s at an altitude of 20 m. This value is almost an order of magnitude lower than the eddy diffusivity of an inert gas of 0.40 m^2/s. The strong reduction of $K_{NO}(z,t)$ in this height interval is mainly caused by the long effective time scale $\tau_{NO\,eff}(z,t)$ of ~30 s. In addition, the ratio of $\frac{\partial L_{NO-O3}(z,t)}{\partial z}$ and $\frac{\partial [NO](z,t)}{\partial z}$ in equation 18 is a factor of 2 – 3 higher in this layer than it is near the ground. Since both gradients have the same trend, $K_{NO}(z,t)$ is smaller than $K_{inert}(z,t)$. The chemistry correction factor for $K_{NO}(z,t)$ again becomes negligible above 30 m because NO establishes a chemical pseudo steady state at higher altitudes.

While we found that a chemistry correction of the eddy diffusivity is necessary for NO, no important changes of the vertical fluxes by chemical reactions were calculated for O_3, NO_2, NO_3, and N_2O_5. In the case of O_3 and NO_2, the eddy diffusivities are only weakly changed by chemistry because for both gases the gradient of the total reaction rate is small compared to its concentration gradient. In the case of NO_3 and N_2O_5, the fast inter-conversion of both gases leads to very short effective times $\tau_{NO_3\,eff}(z,t)$ and $\tau_{N_2O_5\,eff}(z,t)$ on the order of a few seconds at all altitudes. In addition, the gradients of the total reaction rate are weak compared to the concentration gradients for both gases.

Our results show that it is important to consider a chemistry correction for the eddy diffusivity of NO to correctly calculate vertically resolved chemistry in the NBL. The reduced effective eddy diffusivity of NO around 20 m results in a suppression of the mixing of NO from the ground into higher altitudes, thus forming a sharper borderline between the chemistry in the NO filled ground layer and in higher altitudes. Since NO is important for a number of chemical transformations, its suppressed mixing can have various secondary effects, for example for the vertical profiles of $[NO_3]$, $[RO_2]$, $[HO_2]$, and [OH].

3.2.3 Calculation of the temperature profile

The profile of the potential temperature $\Theta(z,t)$ in the lowest 50 m is calculated from the heat flux $H(t)$ according to $\frac{d\Theta(z,t)}{dz} = -\frac{H(z,t)}{c_p \cdot \rho} \cdot \frac{1}{\kappa \cdot u^*(t) \cdot z} \Phi_H(\frac{z}{L*},t)$ [*Arya*, 1988; *Haugen*, 1973]. Here, c_p represents the mass heat capacity of air, ρ its density, and $\Phi_H(\frac{z}{L*},t)$ the dimensionless correction factor for heat transport suggested by *Businger et al.* [1971]. Above 50 m the potential temperature is set to its value at 50 m altitude. The temperature profile is explicitly used to calculate temperature dependent rate constants and the profile of $[H_2O]$.

3.3 Chemical mechanisms

Two reaction frameworks were adopted in our study. The initial framework was based on a reduced set of reactions from the Master Chemical Mechanism 3 [*Saunders et al.*, 2003]. The reaction rates for the NO_3 self-reaction and gas-phase hydrolysis of N_2O_5 were taken from *Sander et al.* [2003] and *Atkinson et al.* [2002], respectively. The gas-phase chemistry module is limited to the nocturnal key species NO, NO_2, NO_3, N_2O_5,

HONO, O_3, CO, the HO_x radical group OH and HO_2 (with the reservoir species HO_2NO_2), α-pinene, isoprene, propene, propane, CH_4, various RO_2 radicals, and PAN. The chemistry of reaction products, such as HNO_3, aldehydes, and H_2O_2, which show slow chemistry at night, is not further considered in NCAT. The complex VOC reaction system in the atmosphere is simplified in the NCAT model by including the explicit oxidation mechanisms of four VOCs representing different classes of VOCs. This obvious simplification of the VOC chemistry should not affect the analysis of the chemical transport mechanisms at night. Biogenic VOCs are represented by α-pinene and isoprene. These species often account for a major part of the nocturnal VOC reactivity towards NO_3 and O_3, even in urban environments [*Berndt and Boge*, 1997; *Fuentes et al.*, 2000; *Geyer et al.*, 2001; *Guenther et al.*, 2000; *Kesselmeier and Staudt*, 1999; *Paulson et al.*, 1998]. Alkanes and alkenes are represented by propane and propene, respectively. The VOC oxidation chains initiated by reactions with NO_3 and OH generally follow the sequence VOC – RO_2 – (RO) – HO_2 – OH, which is discussed in detail by *Geyer et al.* [2003]. The direct formation of HO_2 and OH radicals by ozonolysis is also included in the NCAT model [*Paulson and Orlando*, 1996]. Another source of peroxy radicals is the thermal decay of photochemically produced peroxyacetyl nitrate (PAN), which can persist into the night.

The latest version of NCAT contains the gas-phase chemical mechanism RACM contains 77 model species, and considers a total of 237 reactions [*Stockwell et al.*, 1997]. This mechanism gives a more realistic picture of nocturnal radical species, which was the topic of one of our studies. In short, RACM aggregates hundreds of VOCs into 23 model classes (4 alkanes, 4 alkenes, 3 biogenic, 3 aromatics, and 9 carbonyls). RACM distinguishes 24 different types of organic peroxy radicals, which are formed by the oxidation of VOCs initiated by NO_3, O_3, and OH. The RO_2 radicals can react with NO, NO_3, and other RO_2 radicals, forming a wide variety of secondary VOCs (mostly carbonyls), as well as HO_2. The hydro peroxy radical is further converted into OH, for example, by reactions with NO. It is important to note that, in the case of the OH + VOC reactions, one peroxy radical is formed in RACM, i.e. these reactions are neutral in [OH] [*Stockwell et al.*, 1997].

3.4 Deposition, aerosol uptake, and emission

Dry deposition and uptake onto aerosols is calculated for a number of species including O_3, NO_2, NO_3, N_2O_5, HONO, and HO_2. The range of uptake coefficients for the various aerosol and ground surfaces is large (see the IUPAC recommendation under http://www.iupac-kinetic.ch.cam.ac.uk). NCAT therefore uses uptake coefficients that are in the middle of the range of measured data.

Dry deposition is calculated from the number of molecules of a gas in the lowest box colliding with the surface and the respective uptake coefficient. Initially we assumed a flat ground surface for the calculation of the deposition rate, which may lead to an underestimation of the dry deposition. In the latest version of NCAT we have also included building walls and roofs as possible surface (see Section 4). The uptake rate of a gas onto aerosols is calculated from the aerosol surface area (assuming a particle diameter of 150 nm) and the uptake coefficient according to the mass-transfer equation given by *Fuchs and Sutugin*, [1971].

Biogenic emissions of NO from the soil and α-pinene from vegetation (uniformly in altitudes between 1 – 10 m) are included in the model. Additionally, traffic emissions of NO and CO between 0.1 – 1 m altitude are considered in the urban case scenarios, with a [CO]/[NO] emission ratio of 6 [*Klemp et al.*, 2002].

3.5 Initialization of the model

Typically NCAT is initialized with meteorological parameters, emission rates, and concentrations of O_3, NO_2, PAN, and VOCs typical for the early part of the night (e.g., [*Atkinson*, 2000; *Finlayson-Pitts and Pitts*, 2000]). All other compounds start at near-zero concentration. Because of the convective conditions during the day, all trace gases start with uniform concentrations in the NBL. The variations of trace gas concentrations are calculated for up to 2 hours following model start.

3.6 Typical Results of NCAT

A large number of model runs were performed with NCAT, both to investigate the mechanisms in the NBL as well as for the interpretation of our field measurements. Details of these model runs can be found in the appended publications [*Stutz et al.*, 2004b, *Geyer and Stutz*, 2004 a,b]. Here we only want to show one example of a model run to illustrate the results of NCAT. The nocturnal stability in this case (standard case in [*Geyer and Stutz*, 2004a]) was weakly stable (K_{inert}(10 m) = 0.3 m^2/s). The ambient temperature at 50 m altitude was chosen as 290 K, while the atmospheric pressure was fixed at 1013 mbar at the ground. The relative humidity was set to 50% at all heights. A uniform aerosol surface area of 200 $\mu m^2/cm^3$, a level which is typical for urban areas [*McMurry*, 2000; *Seinfeld and Pandis*, 1997], was used. The flux of NO from soil was set to 10^{10} molecules/cm^2s. Additionally, emission of NO and CO from cars between 0.1 – 1 m, of 2 x 10^9 and 12 x 10^9 molecules/cm^3s, respectively, were used. Emission rates of α-pinene from vegetation in 1 – 10 m were set to 3 x 10^6 molecules/cm^3s.

Figure 15 shows the first six hours of the model run with these parameters and initial 60 ppb of ozone and 5 ppb of NO_2. Similar to our field observations, the model calculates persistent positive vertical profiles of O_3, and negative profiles of NO and NO_2. In addition, one finds a decrease of O_3 throughout the night and an increase of NO_2. In this case the decrease of ozone was mainly caused by dry deposition. NO_3 and N_2O_5 also show positive gradients throughout the night, as in the observations. Due to the decrease of O_3 the mixing ratios of NO_3 and N_2O_5 also decrease throughout the night. The model is also able to predict the behavior of gases that were not observed in the field. For example, NCAT predicts negative α-pinene vertical profiles, due to the emissions near the ground and the increasing NO_3 mixing ratios of NO_3, which destroy this compound.

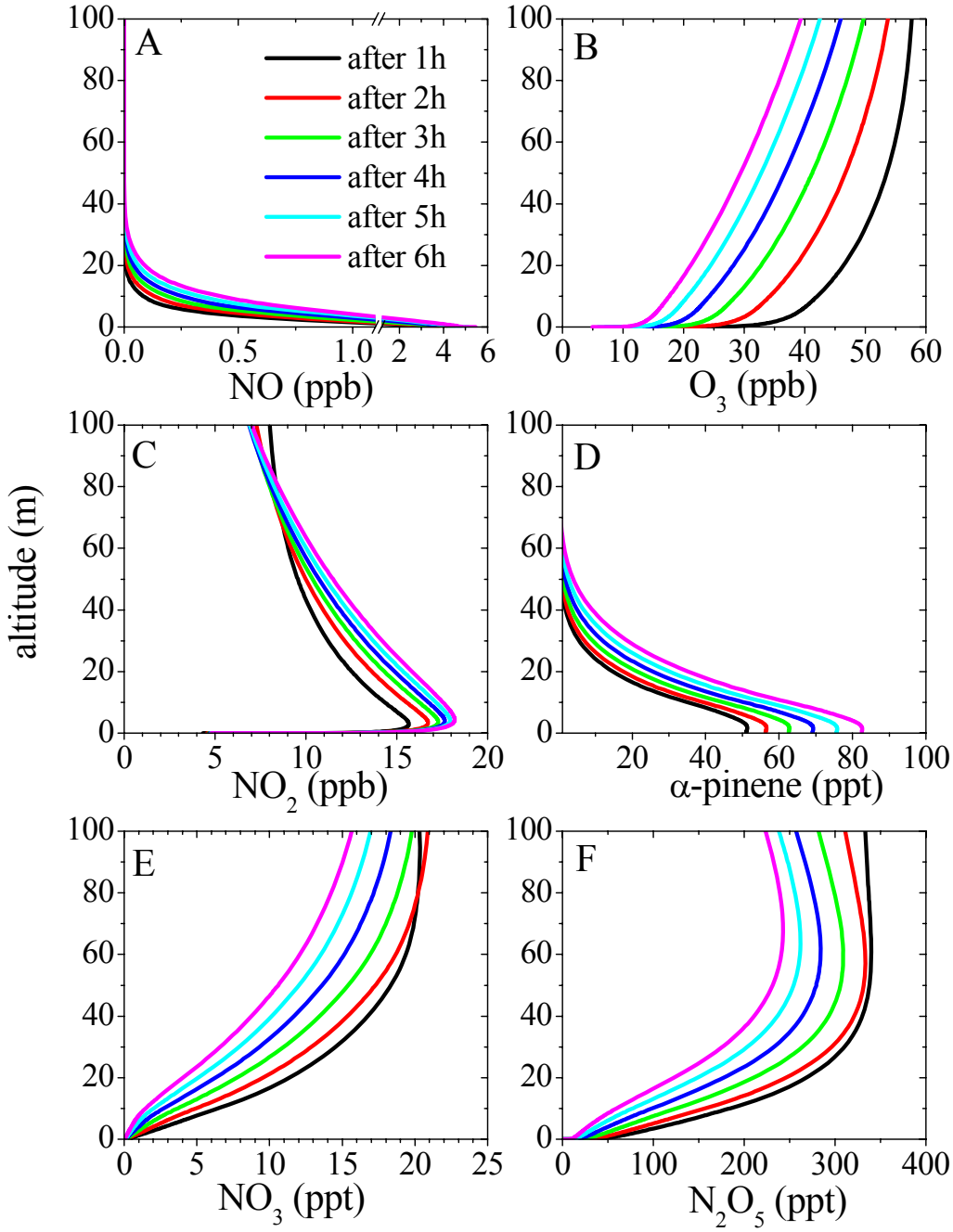

Figure 15: Hourly snapshots of the modeled vertical profiles of [NO], [O_3], [NO_2], [α-pinene], [NO_3], and [N_2O_5] in the first 6 hours after model start for an urban scenario with weak nocturnal inversion. (Figure taken from [Geyer and Stutz, 2004 a)

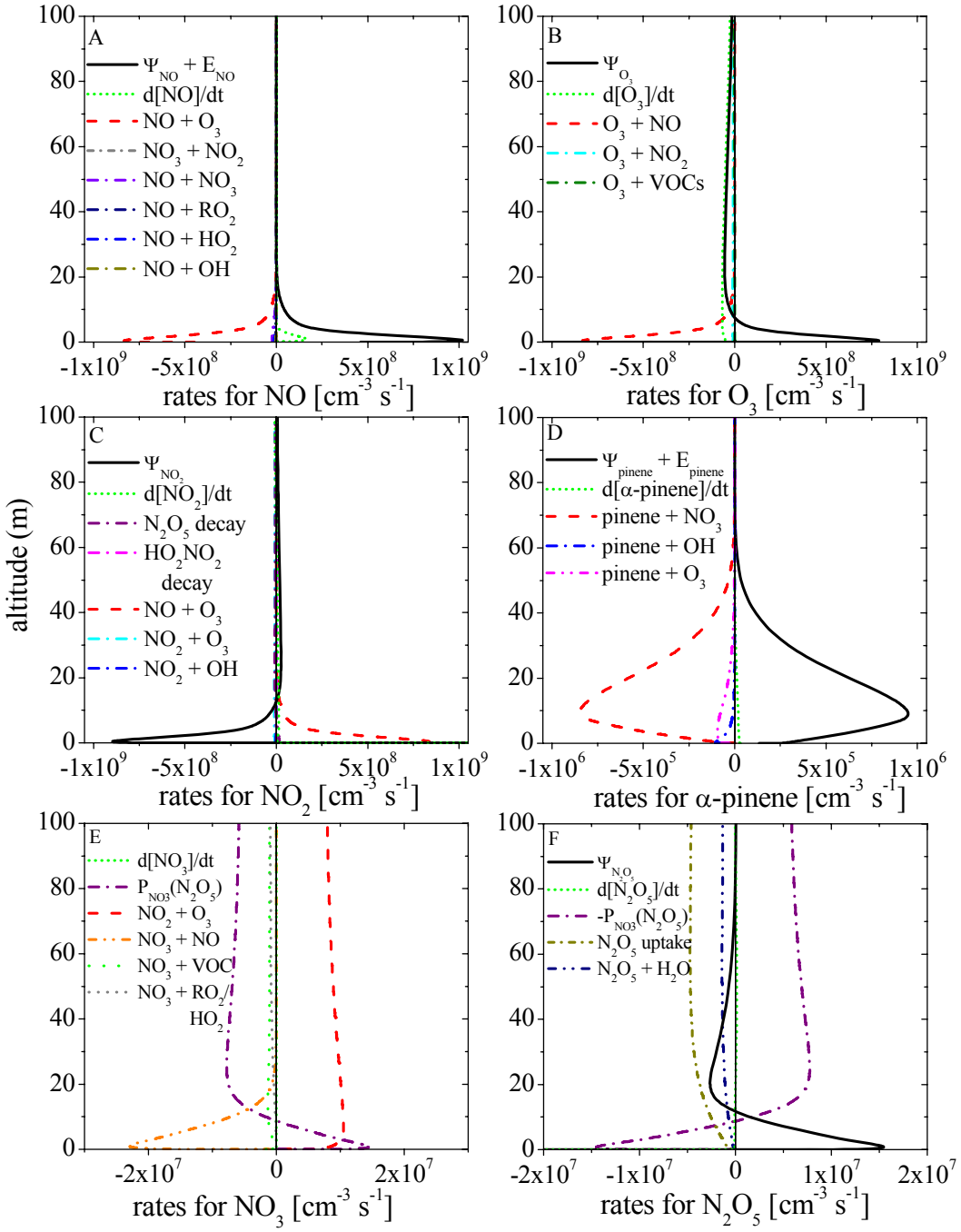

Figure 16: Vertical distribution of chemical rates and the rate of change by vertical transport and emission of NO, O_3, NO_2, α-pinene, NO_3, and N_2O_5, one hour after model start. [Figure taken from [Geyer and Stutz, 2004a]

One of the main advantages of NCAT, and its relative simplicity compared to higher dimensional chemical transport models, is the ability to easily extract reaction and transport rates from the model. Figure 16 shows these rates one hour after model start. The dominant role of the NO + O_3 reaction can clearly be identified (figure 16 A, B and C). The vertical transport rates of O_3, Ψ_{O3}, shows that the ozone that is lost through this reaction and dry deposition is replenished trough downward transport (figure 16 B). The α-pinene rates show that its reaction with NO_3 is the main loss path. This loss is balanced by the upwards transport of freshly emitted α-pinene. The analysis of the NO_3 reaction rates shows surprising results. The production of NO_3 (reaction 1) depends only weakly on the altitude. The reaction of NO_3 with NO (reaction 2) is the dominant loss process of NO_3 close to the ground. The equilibrium with N_2O_5 serves both as a source and sink of NO_3. In the upper part of the NBL the losses of N_2O_5, for example through N_2O_5 aerosol uptake and its reaction with water vapor, lead to a destruction of NO_3. In the lower part of the NBL, however, the N_2O_5 equilibrium acts as a net NO_3 source. This surprising result can be explained by the downward transport of N_2O_5 into the lower NBL, which can be clearly identified in the graph of the N_2O_5 rates (figure 16F). This result has not been predicted by any previous studies, and illustrated the value of a detailed nocturnal chemical transport model. We will show in Section 0 that other transport processes can influence the radical levels in the atmosphere.

The results of NCAT have provided unique insights into the chemistry in the NBL, which resulted in two publications [*Geyer and Stutz*, 2004 a,b]. Some of the results, such as the vertical transport of N_2O_5 and the fact that N_2O_5 is a source of NO_3 in the lower NBL, were not predicted previously and illustrate how little was known about nocturnal chemistry before this project. NCAT has also become an essential tool for our research efforts in the interpretation of the field experiments. Figure 17 shows the comparison of a vertical profile observed in La Porte in 2000 (grey area, see also Figure 3) with the respective NCAT model run. Based on this comparison, we were able to validate our model and to extract information from out field observations, such as the budgets of O_3, NO_2 and NO_3 (see [Stutz et al, 2004 b]).

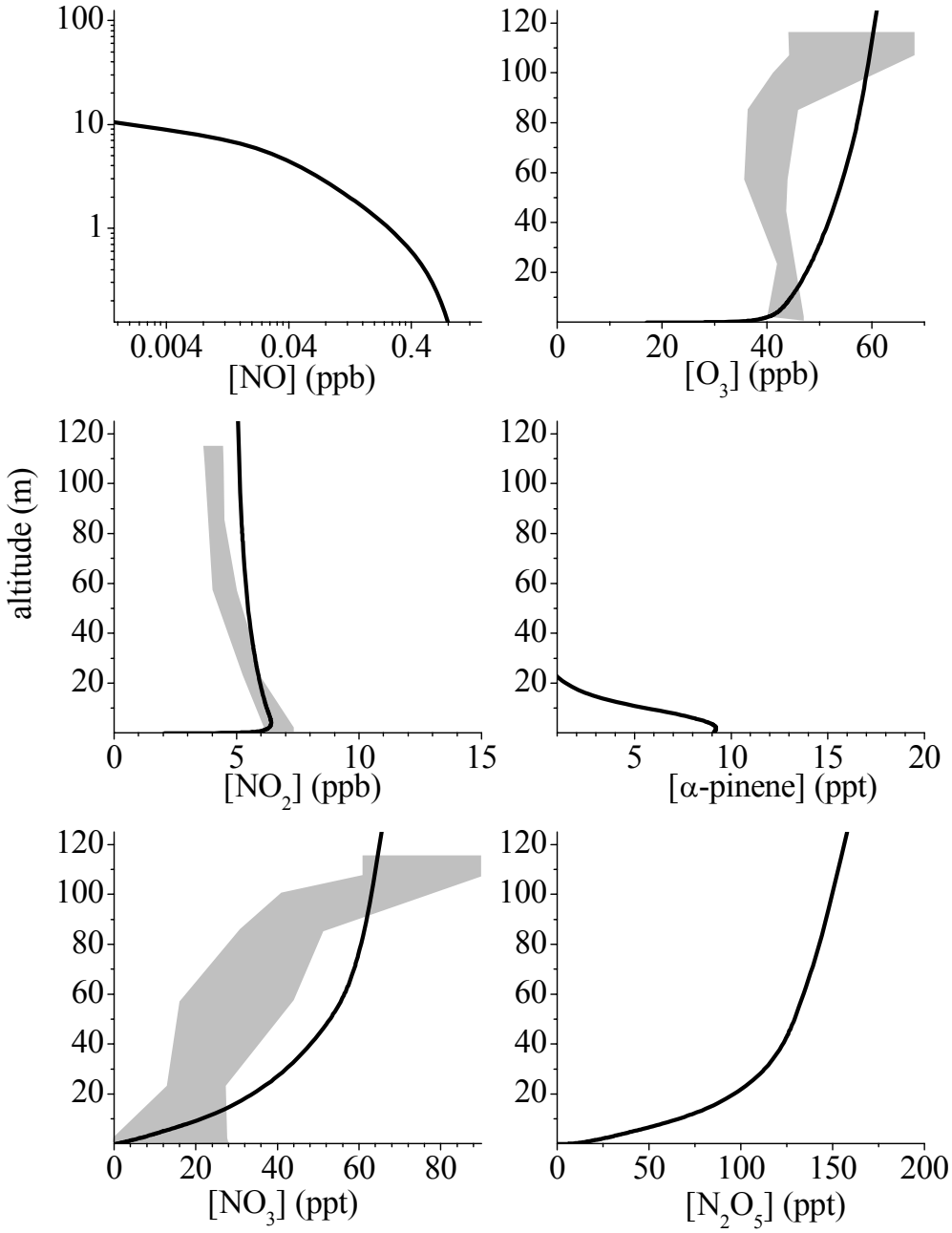

Figure 17: Vertical profiles of [NO], [O_3], [NO_2], [α-pinene], [NO_3], and [N_2O_5] modeled by NCAT for the La Porte conditions three hours after sunset (8/31 2254). The grey area shows the observations with their uncertainties. (figure from [Stutz et al, 2004 b]

4 Results and main scientific findings

The experimental and modeling activities described above lead to a number of interesting scientific results. The following sections concentrate on the final results, without describing details of the methods used. All results were derived based on the observations and modeling studies described in Sections 2 and 3. Most of the results have been published (see attached publications).

It should be noted here that the last few sections on HONO chemistry, as well as the urban canopy and its role in heterogeneous chemistry, describe topics that only emerged towards the end of the project, and research on these topics is still ongoing through another project. However, we anticipate that several publications will be submitted in the near future. The contribution of this project to these publications will be acknowledged.

4.1 Vertical distribution of O_3, NO_2 and NO_3 and the

The main result of our field activities was the observation of vertical concentration profiles of the dominant trace gases in the polluted NBL, O_3, NO_2, and NO_3. The field activities provided us with an extensive data set in three environments with different relative humidity, emissions ratios, etc. This allowed us to find the general features of the altitude distribution of the various trace gases and study the chemistry in the NBL. Figures 3, 8, 9, and 12 show examples of our observations in Houston, Phoenix and Boston.

The following list describes the common features found in the lowest 100m of the NBL at the three locations:

- Ozone shows negative altitude gradients in all environments we have studied, while NO_2 shows positive profiles. Through measurements made by other groups, we also know that NO shows positive profiles. Our DOAS data, which is averaged over an extended volume of the NBL, shows that on scales of one kilometer the O_3 and NO_2 profiles persist throughout the night, except for cases when the nocturnal stability suddenly changes.
- The sum of NO_2 and O_3, O_x, shows negligible or only small gradients, even in situation when O_3 and NO_2 show large gradients (see, for example, Figure 18). This behavior illustrates clearly the role of the NO + O_3 reaction in urban environments. Small positive or negative O_x gradients, as observed in Phoenix, can be caused by dry deposition of O_3 or direct emission of NO_2, respectively.
- NO_3 always shows negative gradients in the NBL. NO_3 mixing ratios can reach above 100 ppt in the upper part of the NBL (see, for example, Figure 8). The often elevated NO levels at the ground lead to very low NO_3 in the lower NBL. These observations illustrate that NO_3 chemistry is important for urban nocturnal chemistry, with implications for the NO_x and ozone budgets, as well as the processing of aerosol particles.

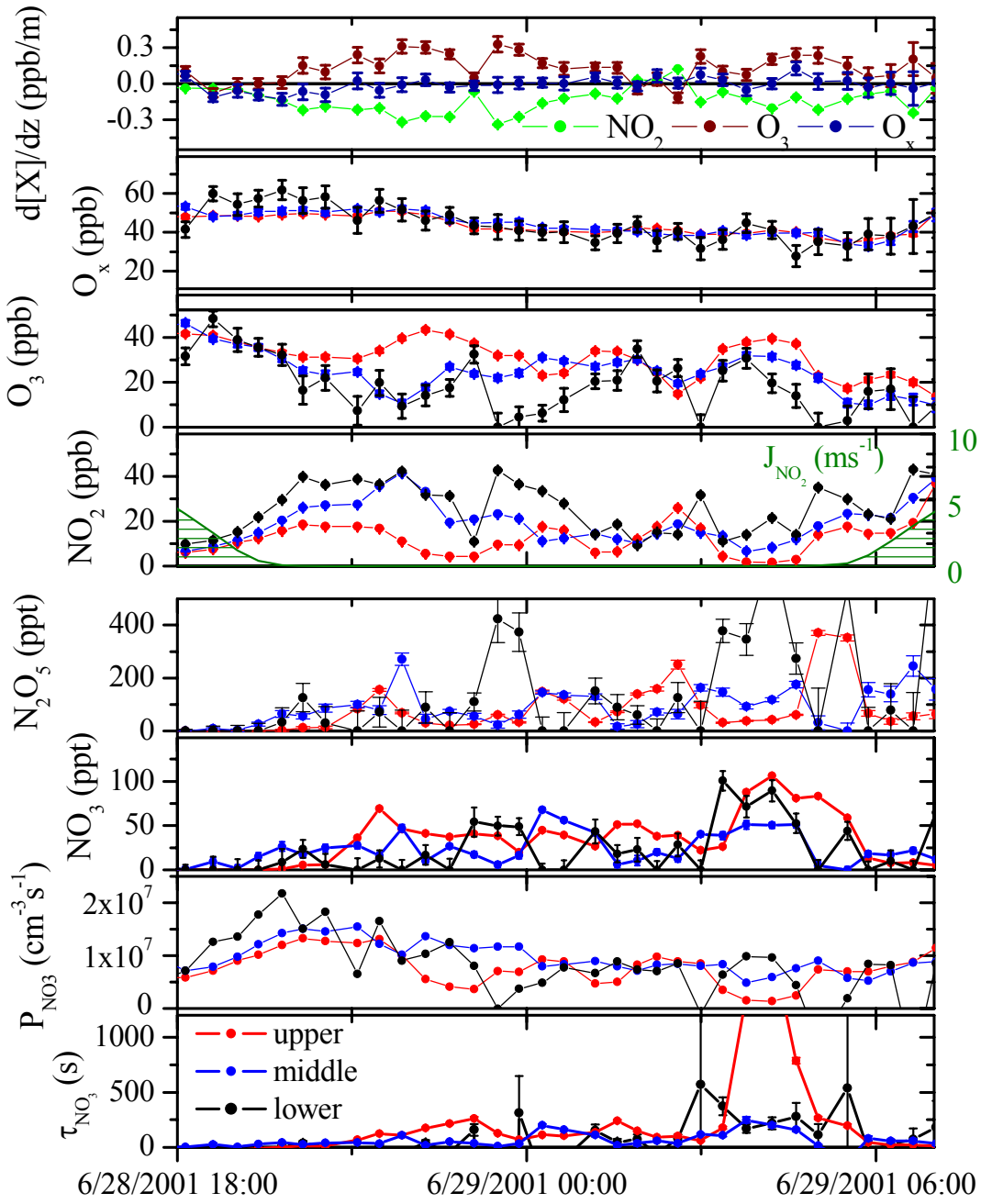

Figure 18: Example of O_3, NO_2, and O_x gradients in the night of 6/28 - 6/29 in Phoenix

•

- N_2O_5, calculated from the steady state between NO_3 and NO_2, shows mostly negative gradients. The gradients follow those of NO_3. Mixing ratios of N_2O_5 reach several hundred ppt. A few observations in Phoenix also showed different N_2O_5 gradients. In general, the uptake of N_2O_5 on the aerosol will occur in the upper NBL, where one expects the largest changes of aerosol properties at night.
- Positive HONO gradients were also observed in all locations. This points towards a surface source of HONO, i.e. NO_2 to HONO conversion on the ground, or direct emissions. Again, this behavior was common to all three locations and seems to be an universal property of nocturnal NO_2 and HONO chemistry.
- HCHO gradients were only observed in Phoenix. Other locations do not seem to show nocturnal HCHO gradients. We believe that direct emission of HCHO in Phoenix are the cause for the observed behavior.
- All trace gas gradients are stronger in the more heavily polluted environment of Phoenix than in the suburban locations of Houston and Boston. Nights with lower emissions also show smaller gradients in these locations. One can therefore conclude that higher emissions, predominately of NO, increase the gradients of the various trace gases.
- The gradients depend on the vertical stability, i.e. stronger temperature gradients are accompanied by stronger trace gas gradients (see Figure 9). Other examples from Houston and Boston show the same behavior. It is therefore clear that vertical stability plays an important role for nocturnal chemistry.
- The trace gas gradients disappear in the early morning when the boundary layer starts to break up (Figures 8 and 9). At this time, the various chemical regimes that occur at different altitudes in the NBL are mixed together and determine the starting conditions for the chemical processes during the following day.

Our observations show that it is important to measure the vertical distribution of trace gases in the urban NBL. Sufficient information on the chemical composition of the NBL can only be obtained when the entire extent of the NBL is probed.

Based on these general observations, we used our 1D chemical transport model (see Section 3) to investigate the chemical and meteorological mechanisms that lead to the altitude dependence of nocturnal chemistry. We first validated our model for one night of the Houston study (Figure 17). During this night, positive gradients of O_3, NO_3, and steady state N_2O_5, as well as negative gradients of NO_2, were observed. NO and VOC concentrations at 10m latitude were measured by the NOAA Aeronomy laboratory. Using the measured micrometeorological data and vertically evenly distributed levels of all trace gases, we modeled the concentration profiles in Figure 17, showing that the model indeed does reproduce our observations. Differences between observations and model in Figure 17 are most likely caused by the unknown aerosol and VOC concentrations aloft. In addition, our description of vertical transport in the NBL is highly simplified and most likely does not accurately describe the true vertical exchange.

The NCAT model was then used to study the dependence of nocturnal chemistry on parameters such as vertical stability, emission ratios, temperature, etc. through sensitivity studies (see [*Geyer and Stutz*, 2004a]). The following summarizes the general results from the modeling efforts, with respect to nocturnal O_3, NO_2, and NO_3 chemistry:

- The model shows, in agreement with the observations, that in urban areas the NO-O_3-NO_2 system is characterized by negative NO and NO_2 gradients, and a positive O_3 gradient. The cause for this behavior is the reaction of O_3 with freshly emitted NO. In addition, dry deposition of ozone and NO_2 can influence the vertical profiles, in particular in rural areas. Under heavily polluted conditions the direct emission of NO_2 also plays a role.
- Biogenic VOCs, such as α-pinene, show negative gradients because they are emitted near the ground, and their loss frequency is highest at the top of the NBL. The loss proceeds predominately through the high NO_3 and O_3 levels in the upper NBL.
- Both NO_3 and N_2O_5 have positive gradients in the NBL. This is again in agreement with our observations. The cause for the profiles is the reaction of NO_3 with NO and, in rural environment, α-pinene close to the ground. The model also shows that a temperature gradient in the NBL can also lead to positive NO_3 gradient.
- The vertical structure of chemistry in the NBL can have a significant effect on the effective eddy diffusivities of reactive trace gases (see Figure 14). In a layer near the ground, the eddy diffusivity of NO is significantly reduced by the reaction of NO with O_3. A chemistry correction factor for NO should be considered in *K* models.
- The model shows that the two main factors controlling the vertical structure of nocturnal chemistry are the emission strength of NO (Figure 20) and, to a certain extent, α-pinene, and the vertical stability of the NBL (Figure 19). At high emissions larger gradients are modeled, in agreement with our observations. Weaker stabilities lead to an enhanced vertical mixing, decreasing the trace gas gradients, as also observed in the atmosphere.
- The downward transport of N_2O_5, followed by its thermal decay, is a major source of NO_3 near the ground (Figure 17). Vertical transport of N_2O_5 has to be considered in steady state calculations of [NO_3] and [N_2O_5], which are often used for the interpretation of field data.
- The loss processes of NOx, and VOC's are altitude dependent at night, i.e. mostly higher in the middle or upper NBL. Only by considering the entire height of the NBL can the loss rates be determined accurately.

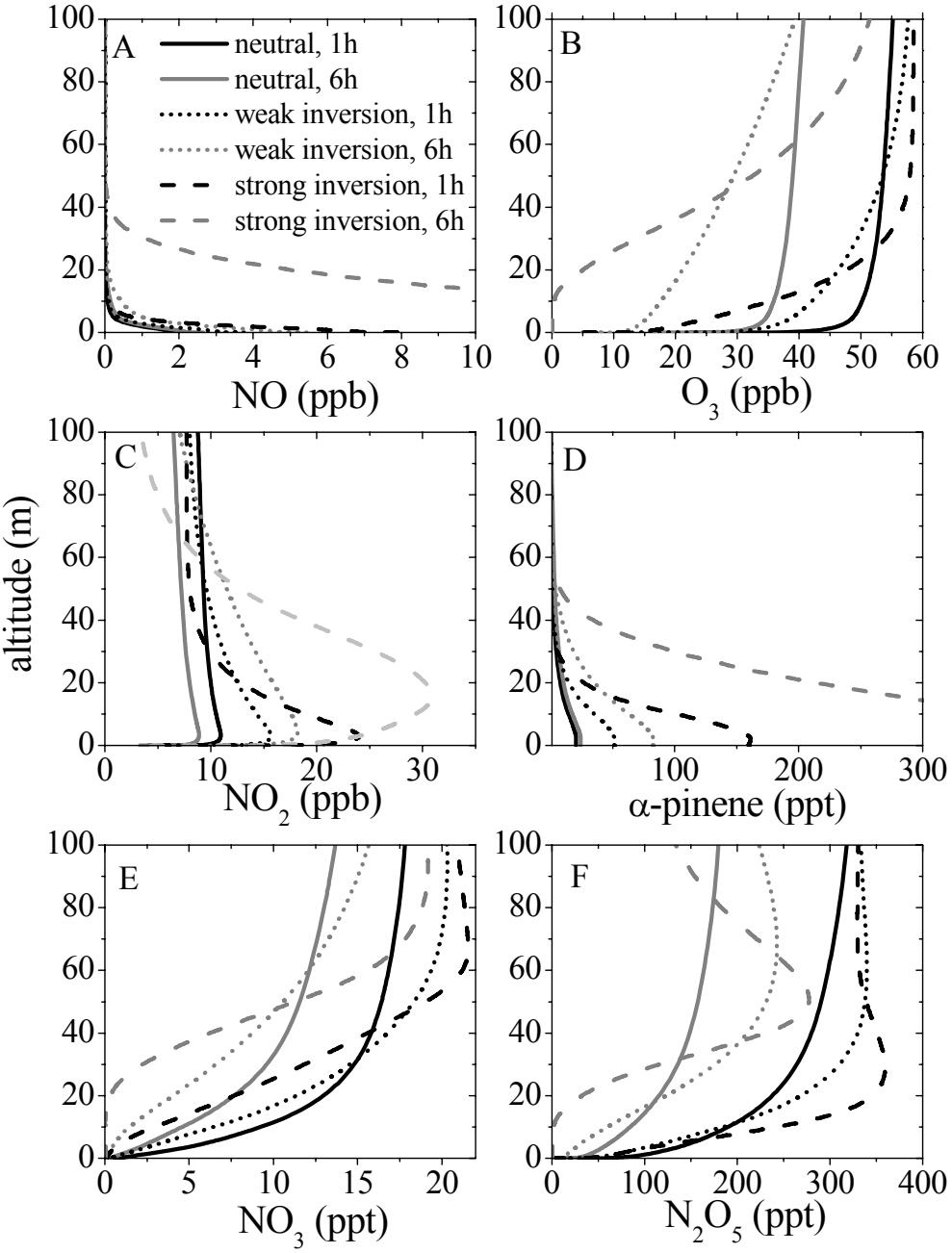

Figure 19: Variation of the vertical profiles of [NO], [O_3], [NO_2], [α-pinene], [NO_3], and [N_2O_5] 1 and 6 hours after model start under urban conditions with atmospheric stability. All model parameters, except stability, were kept at the same levels. (figure from [Geyer and Stutz, 2004 a])

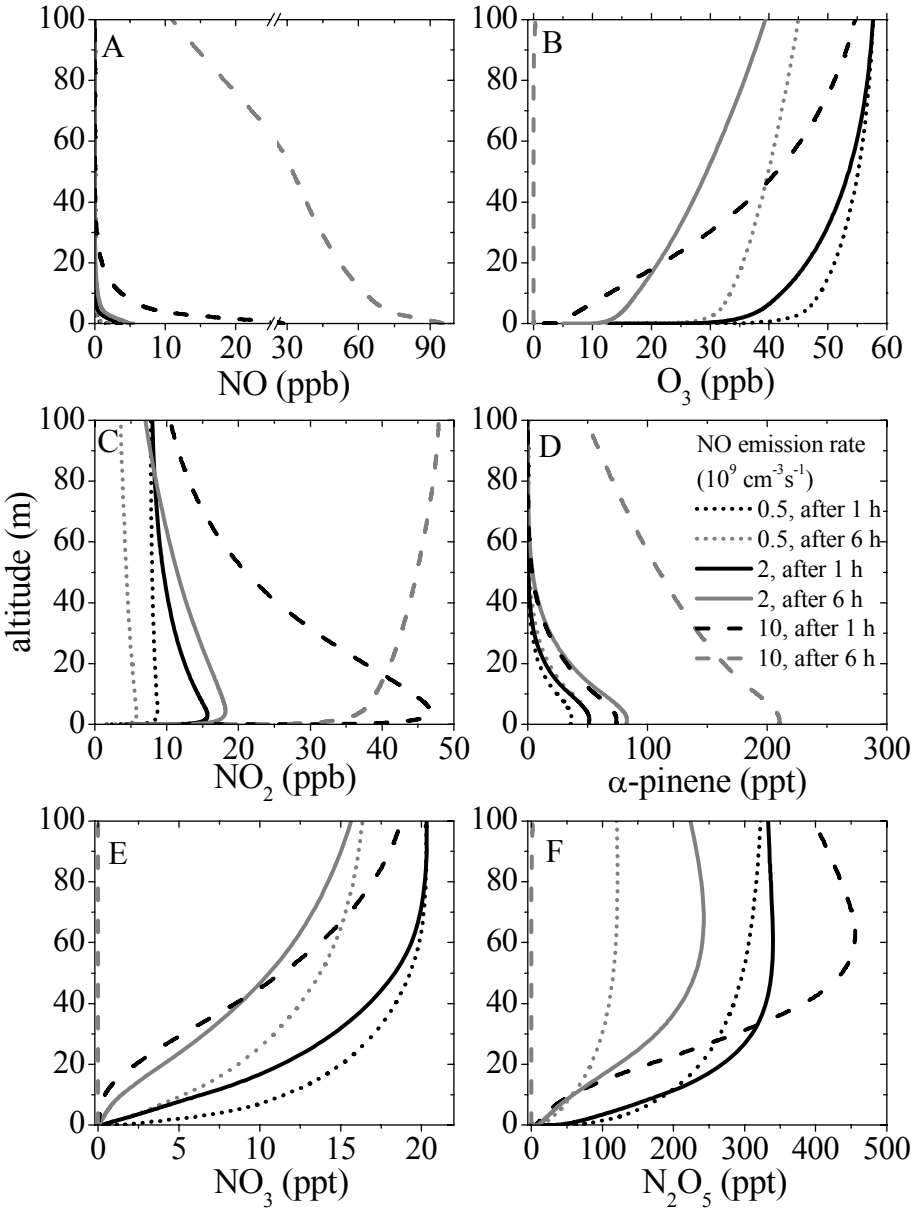

Figure 20: Variation of the vertical profiles of [NO], [O_3], [NO_2], [α-pinene], [NO_3], and [N_2O_5] 1 and 6 hours after model start under urban conditions with the NO emission rate. All model parameters, except the NO emission rate, were kept at the same levels. (figure from [Geyer and Stutz, 2004 a])

These results from our observations and modeling studies lead to the first major result of our study:

The chemistry in the polluted nocturnal boundary layer is very altitude dependent. Measurements at one height are not representative for the entire extent of the NBL or, for that matter, the residual layer.

A correct description of nocturnal chemistry is only possible if the vertical distributions of trace gas concentrations and vertical transport rates are considered. A change in the approach to observe and model nocturnal chemistry, i.e. using vertical profiles, is therefore required.

4.2 Budget of O_3, NO_2, and O_x

Based on our observations and modeling studies we also studied the budgets of O_3, NO_2 and O_x. The often very low ozone levels at the ground, where most air quality monitoring stations are located, as well as the fact that O_x shows very weak gradients, motivated this aspect of our project. The overreaching questions were: How much ozone is really lost in the urban NBL? Which processes are responsible for the loss?

We based our analysis on our La Porte and Phoenix data, as well as on the sensitivity studies with NCAT. Table 1 shows the results from our Houston study for the night shown in Figure 3. In Houston, dry deposition was the largest loss of O_3. NO_3 chemistry was the second most important loss process for O_3, and the most important process for the NO_2 budget. The fact that dry deposition played such an important role is due to the low NO emission rates in La Porte. This case is thus not representative for a true urban environment.

Table 1: Comparison of O_3 and NO_2 loss rates averaged over the lowest 100 m of the NBL during the night 8/31 – 9/1 at La Porte. [*Stutz et al.*, 2004 b]

Sink	Loss rates averaged over lowest 100 m (ppb/h)
Ozone	
$NO + O_3$	0.6
$NO_2 + O_3$	1.0
Dry deposition	2.4
$VOC + O_3$	0.1
Total	4.1
NO_2	
$NO_2 + O_3$	1.0
$NO_2 + NO_3$	0.5
Dry deposition	0.7
Total	2.3

To study the O_3 and NO_2 budget in urban environments we used our Phoenix data. The altitude integrated loss rate of O_3 and O_x, as well as the change in NO_2 in the NBL, were determined based on our path-averaged measurements from 140-10m altitude. We chose two nights, with different characteristics to

study the budgets. The night of 6/16 – 6/17 (Figure 8) had a strong vertical stability and strong ground emissions of NO_x and VOCs. During the night of 6/30-7/1 (Figure 18) both stability and emissions were weak. It should be added that both nights were between Saturday and Sunday, and did not show strong rush hour effects. Ozone loss during these nights was found to be -3.2±1.5 ppb/h and -2.6±0.2 ppb/h, respectively, while NO_2 increased by 1.5±1.6 ppb/h and 0.3±0.2 ppb/h, respectively. The high errors during the first night are due to temporal changes in the trace gas mixing ratios throughout the night. The determination of the loss rate of O_x does not suffer this difficulty, since the variations of O_3 and NO_2 balance each other. The O_x loss during the night of 6/16 – 6/17 was -1.8±0.4 ppb/h, that of 6/30-7/1 was -2.6±0.2 ppb/h.

The analysis of these two different nights reveals a number of interesting features in the budgets of these species. The ozone loss and NO_2 increase is somewhat larger during the first night showing the influence of the emissions on the budgets. About 40% of the ozone loss during 6/16-6/17 is due to the conversion of O_3 to NO_2. This can be deduced from the comparison of the O_x and O_3 loss rate. The situation is different during the second night when the NO + O_3 reaction plays only a secondary role. The O_x loss is larger during the second night. From our model studies we believe that this is caused by the weaker stability during this night. The O_x loss does not seem to be altitude dependent, or alternatively the O_x residence time is much larger than that of either O_3 or NO_2, and O_x is thus better mixed in the NBL. The opposite gradients of NO_2 and O_3, together with the negligible gradients of O_x, show that the downward transport of O_3 is counterbalanced by an upward flux of NO_2. This has some interesting implications for the chemistry in the residual layer, i.e. transport into the NBL exchanges O_3 for NO_2 in the residual layer

A theoretical analysis of the different loss processes shows that the following mechanisms are important of the O_3, NO_2 and O_x budgets in urban environments:

4.2.1 Conversion of O_3 to NO:

The reaction of NO + O_3 is responsible for the conversion of ozone to NO_2.

$$NO + O_3 \rightarrow NO_2 + O_2 \qquad (19)$$

However, this transformation of O_3 to NO_2 only temporarily removes O_3 from the boundary layer, since the photolysis of NO_2 during the next morning will lead to a re-release of O_3. A simple calculation, based on the photostationary state between NO, NO_2 and O_3 with the assumption that other NO_2 and O_3 losses are absent, illustrates the ultimate impact of nocturnal NO emissions on the O_3 budget. The distribution between NO, NO_2 and O_3 during daytime can be described by the Leighton ratio $[O_3] = \frac{J_{NO2}}{k_1} \cdot \frac{[NO_2]}{[NO]}$ [*Finlayson-Pitts and Pitts*, 2000]. O_x will remain constant in this description if no other O_3 or NO_2 loss processes other than (R19) and NO_2 photolysis are considered. One can then derive an expression for the steady state O_3 concentration before sunset and after sunrise:

$$[O_3] = \frac{1}{2}\left([O_x] - [NO_x] - \frac{J_{NO2}}{k_1} + \sqrt{\left([NO_x] - [O_x] + \frac{J_{NO2}}{k_1} \right)^2 + 4\frac{J_{NO2}}{k_1}[O_x]} \right) \qquad (20)$$

To determine the influence of nocturnal NO emissions, we assume an initial NO_x concentrations at sunset, $[NO_x]_{ss}$. Sunrise NO_x is defined by $[NO_x]_{sr} = [NO_x]_{ss} + E_{NO}$, where E_{NO} represents the total emissions of NO throughout the night. The difference between O_3 levels at sunset and the next sunrise shows the effective O_3 destruction, assuming that J_{NO2} is equal in both cases. We then define the efficiency of ozone destruction by NO emissions as $D_{O3} = ([O_3]_{sr} - [O_3]_{ss})/E_{NO}$.

We can discuss an example with $[O_x]$=60ppb and J_{NO2}=0.005s^{-1}. At low $[NO_x]_{ss}$ levels (< 10 ppb) and low to moderate E_{NO}, D_{O3} is found in the range of -0.7 ~ -0.9. At high levels of $[NO_x]_{ss}$ (40ppb), D_{O3} decreases to -0.4 ~ -0.5. Similarly, the magnitude of D_{O3} is also found to decrease with increasing E_{NO}. Therefore, the impact of nocturnal NO emissions on the O_3 budget depends on various parameters and needs to be determined for every case separately. However, it is clear that (R19) does ultimately destroy O_3, considering the difference in O_3 levels before sunset and after sunrise.

This calculation shows that nocturnal NO emissions can destroy ozone during the next day by changing the NOx levels. This effect is typically not considered in the analysis of the ozone budget. However, our simple calculation shows that the change of NOx levels at night indeed has an impact on daytime chemistry.

4.2.2 NO_3 and N_2O_5 chemistry:

The formation of NO_3 consumes one ozone and one NO_2 molecule, i.e. 2 O_x molecules. The formation of N_2O_5 consumes another NO_2 molecule. Any loss of NO_3 and N_2O_5 therefore constitutes a loss of O_x, O_3 and NO_2. A number of chemical mechanisms can remove NO_3 and N_2O_5 from the atmosphere. The reaction with VOC's can lead to a removal of NO_3. The uptake of N_2O_5 on the aerosol is another major sink of O_x in the NBL. However, in Phoenix, where relative humidities at night were mostly below 40% at night, the reactive uptake coefficients are rather small, making N_2O_5 uptake inefficient. In La Porte, where R.H. was high at night, N_2O_5 uptake was a major factor. We therefore concluded that NO_3 and N_2O_5 chemistry plays an important role in certain environments.

4.2.3 Dry deposition of O_3 and NO_2:

The dry deposition of O_3 and NO_2 leads to a removal of both species. During many nights in Phoenix, for example 6/16 – 6/17, ozone concentrations near the ground were small, making the uptake of ozone on the ground inefficient. However, our observations show that the low ozone is accompanied by high NO_2 near the ground. Deposition of NO_2 will thus become quite important in these case. If we assume that the uptake coefficients of O_3 and NO_2 on the ground are similar, we can thus describe the O_x ,O_3, and NO_2 loss in the NBL though an O_X loss at the ground. We believe that this dry deposition is the dominant loss process for O_x in Phoenix. This is supported by the positive gradient of O_x during the night of 6/31-7/1, which indicates a downward flux of O_x. Our observations in Houston confirm the role of dry deposition of ozone (Table 1)

In summary, we found that the NO + O_3 reaction, together with emissions of NO, has a major impact on the NO_2 and O_3 budgets. However, since this ozone loss is partially reversible in the morning at the onset of photolysis, one has to be careful in its

interpretation. The loss of O_x will lead to a loss of ozone and NO_2. We believe that this loss predominately happens through dry deposition of ozone and NO_2. In urban areas with high relative humidities, the chemistry of NO_3 and N_2O_5 can also play an important role in the removal of O_x, as we have shown in our Houston study. A sensitivity study of the different loss processes with NCAT was presented in [Geyer and Stutz, 2004 a]. Since the dependence is quite complex we refer to the attached publication.

4.3 Altitude dependence of ROx chemistry

One of the most exciting results of our project was the investigation of the altitude dependence of the radical chemistry at night. We used our model to analyze the vertical distribution of the various radical species at night, NO_3, RO_2, HO_2, and OH. This addressed the much discussed question about the origin of nocturnal OH radicals, which have been observed at various locations. The following section was adapted from [*Geyer and Stutz*, 2004 b], and summarize the results presented in this paper.

Our model results show that the vertical profiles of organic peroxy radicals, RO_2, show a maximum in the lower part of the NBL (see Figure 21). The strong positive gradient below the maximum is caused by the high loss rate of RO_2 through its reaction with NO close to the ground and downward transport. Above the maximum [RO_2] slowly decreases with altitude because of the decreasing RO_2 production by reactions of NO_3 and O_3 with unsaturated VOCs (figure 22). The reaction of NO_3 with monoterpenes is the most important net RO_2 source at night. Hydroperoxy radicals, HO_2, develop a similar profile to RO_2. The maximum is, however, located closer to the ground. The positive gradient of HO_2 below this maximum is caused by the fast removal of HO_2 by reaction with NO. Above the maximum HO_2 mixing ratios decrease because the HO_2 production by RO_2 + NO reactions decreases. The concentration of the hydroxyl radical, OH, is ~10^5 molecules/cm^3 in the upper part of the NBL. However, in a layer close to the ground, a high concentration maximum of a few 10^6 molecules/cm^3 can develop. These high nighttime levels of OH are caused by the maximum of the reaction rate of HO_2 and NO in this layer. Nighttime OH can significantly contribute to the removal of VOCs.

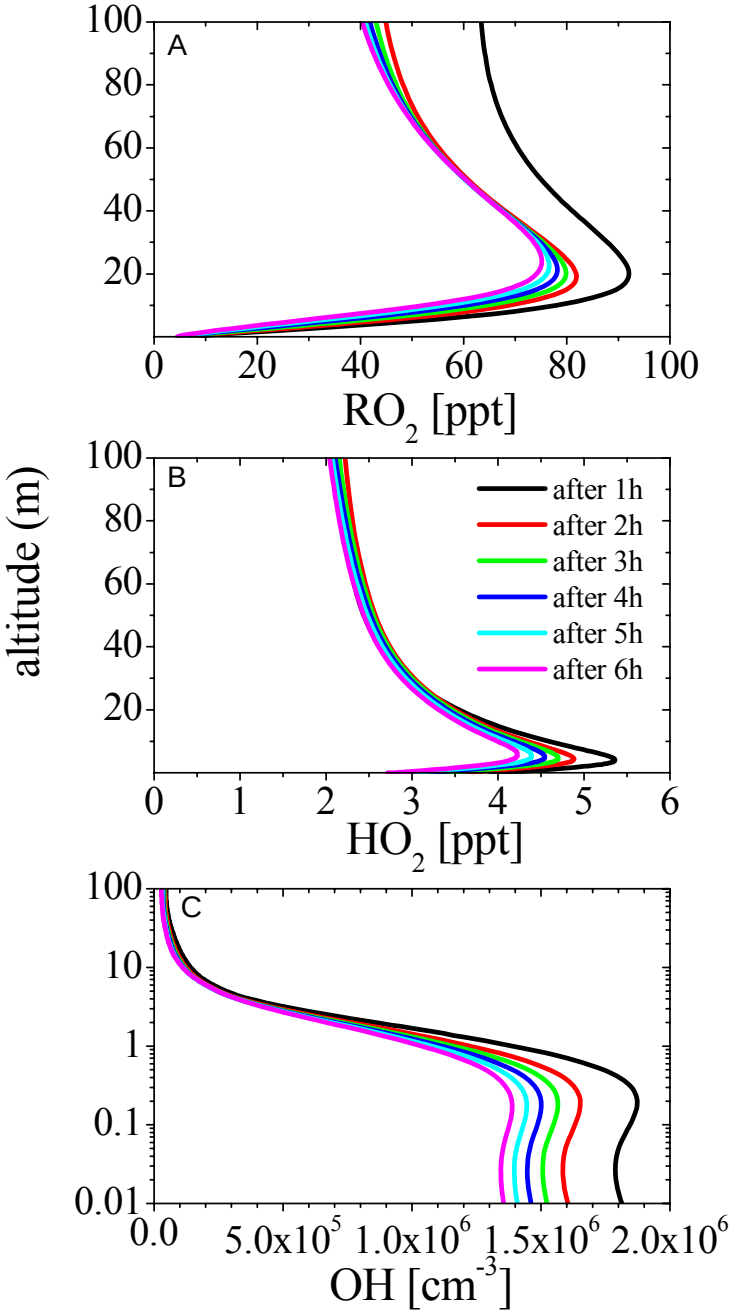

Figure 21: Hourly snapshots of the modeled vertical profiles of [RO_2], [HO_2], and [OH] in the first six hours after model start for an urban scenario with moderate NO emission and weak nocturnal stability. Note the logarithmic scale for the vertical profile of [OH]. (figure from [*Geyer and Stutz*, 2004 b])

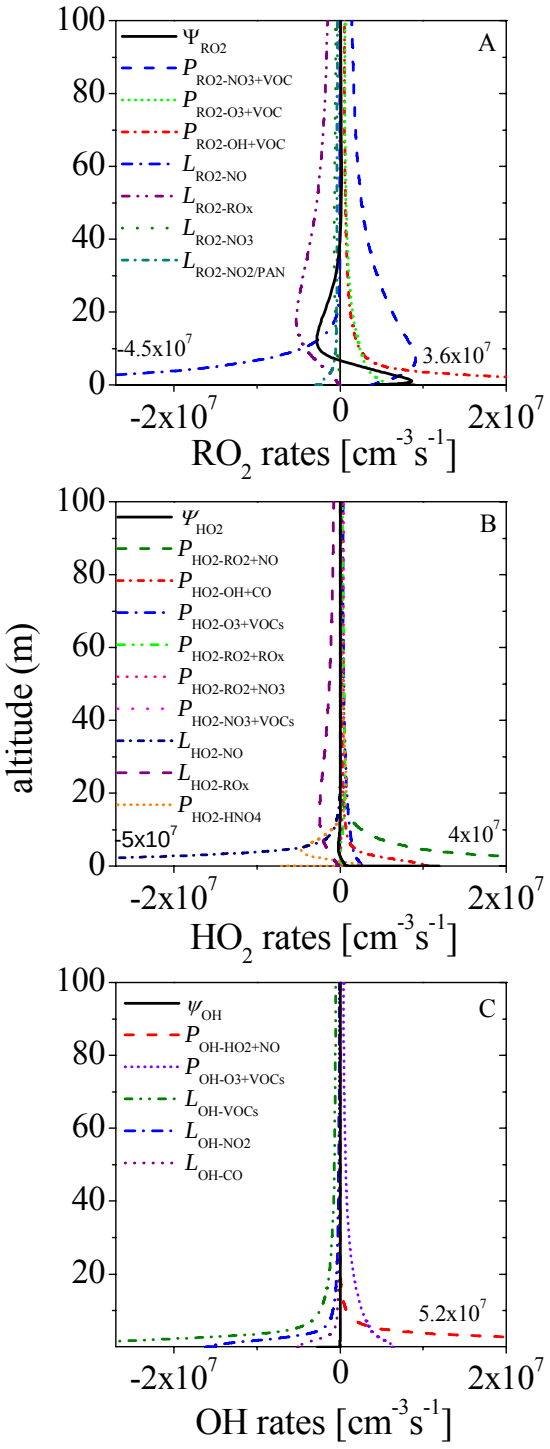

Figure 22: Vertical profiles of chemical rates and the rate of change by vertical transport of RO_2, HO_2, and OH three hours after model start. (figure from [*Geyer and Stutz*, 2004 b])

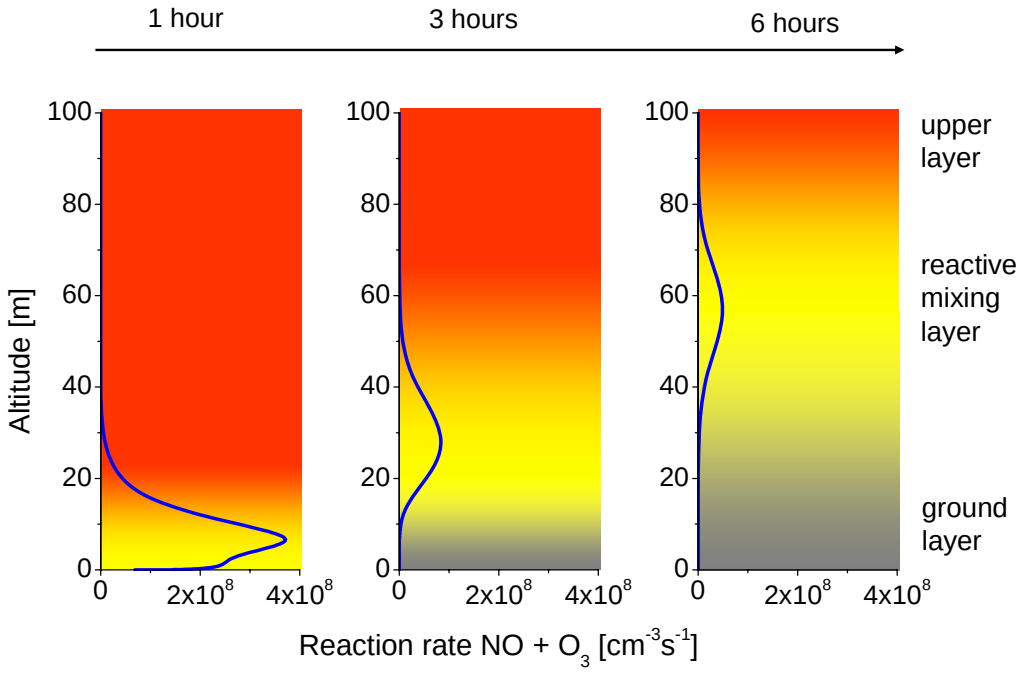

Figure 23: Illustration of the three layer concept of the NBL: The evolution of the unreactive ground layer, the reactive mixing layer, and the upper layer during the night is exemplified by the NO + O_3 reaction rate for an urban case with high traffic emissions and stability. (figure from [*Geyer and Stutz*, 2004 b])

To simplify the description of the altitude dependent RO_x chemistry in the NBL, we propose to distinguish three chemical regimes based on their RO_x chemistry and OH production rates (see Figure 23). The regimes can be easily distinguished by using the NO + O_3 formation rate as an indicator:

a) The ground layer near the surface is defined by high levels of NO, which suppress the presence of NO_3 and O_3, reducing the NO + O_3 formation to near zero. All radical levels in this layer are low, and radical chemistry is basically inactive. The ground layer only forms when the destruction of O_3 by NO emissions at the ground surpasses the replenishing of ozone through downward transport.

b) The upper layer at the top of the NBL is characterized by high levels of NO_3, O_3, and organic peroxy radicals, but negligible NO concentrations. Here, VOCs are oxidized by NO_3 and O_3 but the peroxy radicals are only slowly converted into OH radicals. OH is mostly produced by the ozonolysis of alkenes. Again the NO + O_3 rate is very low due to the low NO levels. The nocturnal RO_2 maximum typically develops in the lower part of the upper layer.

c) The reactive mixing layer is located between the ground layer and the upper layer. In this height interval NO from the ground layer, and NO_3, O_3, and RO_2 from the upper layer, are mixed together. It is important to realize that in this layer the otherwise chemically unlikely simultaneous presence of RO_2, NO_3 and NO is maintained by vertical mixing. In addition to their downward transport, organic

peroxy radicals are produced by NO_3 + VOC and O_3 + VOC reactions. RO_2 is rapidly converted into HO_2 and OH by reactions with NO. This fast radical propagation chain leads to high HO_2 and OH production. The concentration maxima of HO_2 and OH are located in the reactive layer. The reactive mixing layer is thus the height interval with the most active radical chemistry in the NBL.

Our results illustrate a number of unique chemical transport mechanisms in the NBL that have thus far not been discussed in the literature:

- Vertical transport of RO_2 radicals plays a crucial role in nocturnal chemistry. This transport is driven by the RO_2 concentration gradient, which is formed by high RO_2 production rates through the NO_3/O_3 + VOC reactions in the lower part of the upper layer, and destruction of RO_2 through its reaction with NO in the reactive mixing layer. Downward mixing of RO_2 acts as sink for RO_2 above the NO rich layer and as an important source close to the ground. This mechanism is important in all scenarios we investigated, but in particular in scenarios with high monoterpene concentrations and weak stability.
- Vertical transport of HNO_4, followed by its thermal decay, also often acts as important source of HO_2, and thus indirectly of OH, near the ground. A positive vertical gradient of HNO_4 is formed through the destruction of HO_2 by NO near the ground that reduces [HNO_4] compared to its much higher pseudo steady state value aloft. This gradient leads to a downward transport of HNO_4, which then acts as a HO_2 source near the ground. This mechanism increases in importance with the degree of pollution and the vertical stability in the atmosphere. It is particularly important in urban environments.
- In addition, the vertical transport of N_2O_5 (see Section 4.1) is an important source of NO_3 radicals in the lower NBL.

These first two chemical-transport mechanisms, in combination with purely chemical OH formation mechanisms, such as the ozonolysis of VOCs, can lead to significant amounts of OH in the reactive mixing layer. We can draw the following main conclusion from our study:

Nocturnal NO_3 and RO_x radical chemistry is altitude dependent. A three layer approach explains the different regimes of radical chemistry in the NBL. Vertical transport causes a unique radical chemistry through the mixing of RO_2 and NO, which can lead to chemistry similar to that occurring during the day.

4.4 HONO formation in the NBL, influence of dust and R.H.

We also investigated the formation of HONO in the nocturnal boundary layer during the Phoenix campaign. Two different publications arose from these activities [*Wang et al.*, 2002; *Stutz et al.*, 2004 a]. Both of them rely on the idea that HONO reaches a chemical pseudo steady state in the NBL. Considering the formation and loss reactions described in Section 1.3 of this report, we set up an equation describing the temporal evolution of HONO concentrations in the NBL. The chemical formation of HONO is

described as a first order process in NO_2 occurring on surfaces with a surface area, S, to air volume, V, ratio of (S/V) [*Finlayson- Pitts et al.*, 2003; *Jenkin et al.*, 1988; *Kleffmann et al.*, 1998; *Pitts et al.*, 1984b; *Sakamaki et al.*, 1983; *Svensson et al.*, 1987]. The influence of water observed in various laboratory studies [*Finlayson- Pitts et al.*, 2003; *Jenkin et al.*, 1988; *Kleffmann et al.*, 1998] is incorporated by using a R.H. dependent reactive conversion probability $\gamma_{NO2\rightarrow HONO}$(R.H.). The heterogeneous loss of HONO is assumed to be first order in HONO. In analogy to the observed water dependence of NO_2 and HNO_3 uptake [*Finlayson- Pitts et al.*, 2003; *Saliba et al.*, 2001], we also assumed a R.H. dependent HONO uptake probability, γ_{HONO}(R.H.). This R.H. dependence was recently observed by *Syomin and Finlayson-Pitts*, [2003], between 0% and 50% R.H. Equation 21 describes this simple model mathematically:

$$\frac{d[HONO]}{dt} = \gamma_{NO2\rightarrow HONO}(R.H.)\times\frac{S}{V}\times\frac{v_{NO2}}{4}\times[NO_2] - \gamma_{HONO}(R.H.)\times\frac{S}{V}\times\frac{v_{HONO}}{4}\times[HONO] \tag{21}$$

Here v_{NO2} and v_{HONO} are the mean molecular velocities of the respective species, which are similar for both species. From equation 21 it is clear that the NO_2 - HONO system will ultimately reach a pseudo steady state (PSS), which is determined by the ratio of the two reaction probabilities $\gamma_{NO2\rightarrow HONO}$ and γ_{HONO}.

$$\left([HONO]/[NO_2]\right)_{PSS} = \frac{\gamma_{NO2\rightarrow HONO}(R.H.)}{\gamma_{HONO}(R.H.)} \tag{22}$$

It is essential to understand that the HONO-NO_2 system will always try to reach this PSS. The [HONO]/[NO_2] ratio can exceed the PSS value only if direct emissions add HONO to the system without adding a corresponding amount of NO_2. The system will then, however, move back into the PSS by an increased loss of HONO onto the surface.

One can now plot the HONO/NO_2 ratio against R.H. to determine the R.H. dependence of the ratio of the two uptake coefficients in equation 22. To cover a wide range of relative humidities we combined data from three field experiments we performed over recent years, SOS 1999 in Nashville, TEXAQS 2000, and Phoenix 2000 (see Figure 24). The data of Phoenix in Figure 24 are essential since they cover the low R.H. range. Care has to be taken in the interpretation of Figure 24, since only the maximum values of [HONO]/[NO_2] at each R.H. correspond to the PSS. However, it is clear that this maximum depends nearly linearly on R.H. up to R.H. = 90%, after which is seems to decrease again.

While we cannot determine which of the two uptake parameters in equation 22 are responsible for the observed R.H. dependence, we can conclude that the R.H. dependence of $\gamma_{NO2\rightarrow HONO}$(R.H.) must be stronger than that of γ_{HONO}(R.H.) to explain the observations:

$$\frac{d\left(\gamma_{NO2\rightarrow HONO}(R.H.)\right)}{d(R.H.)} > \frac{d\left(\gamma_{HONO}(R.H.)\right)}{d(R.H.)} \tag{23}$$

It is important to note that there is currently little information on the R.H. dependence of γ_{HONO}(R.H.). It is possible that this mechanism is only weakly dependent or even

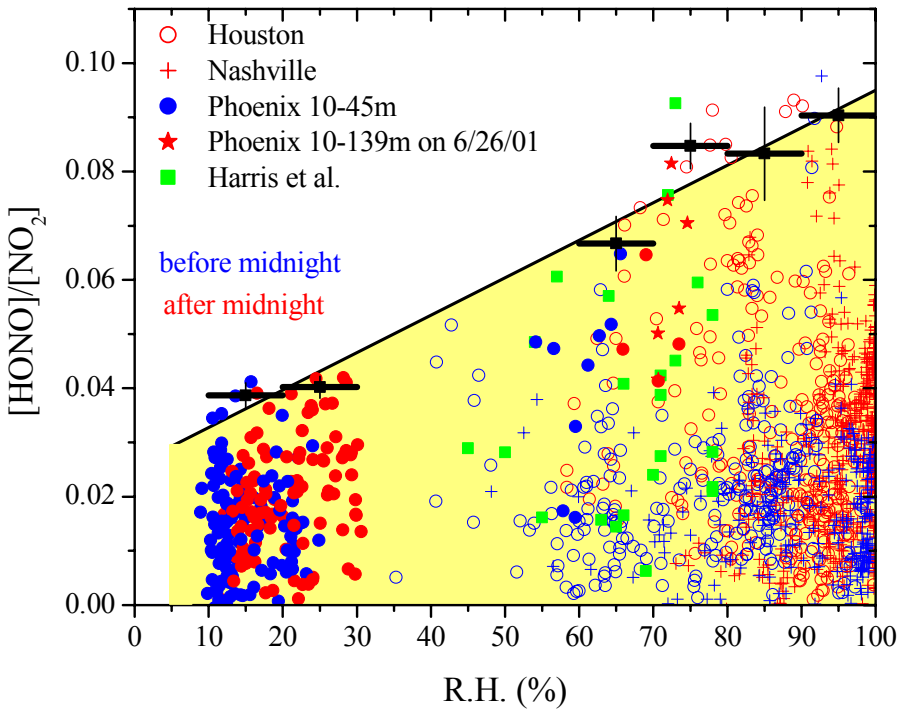

Figure 24: [HONO]/[NO_2] ratios versus R.H. for four different locations in the United States. Errors for [HONO]/[NO_2] are in the range 0.002 – 0.01, and were omitted in this plot for clarity. (figure from [*Stutz et al.*, 2004 a])

independent of R.H., at least over a certain range of R.H. In this case the observed change is purely due to the R.H. dependence of the NO_2 to HONO conversion. Since the [HONO]/[NO_2] maxima in Figure 24 are linearly dependent on R.H., we can conclude in this case that the NO_2 to HONO conversion would be proportional to the R.H., $\gamma_{NO2\rightarrow HONO}(R.H.) \propto R.H.$ This is in agreement with various laboratory results that find a linear dependence on R.H. *Syomin and Finlayson-Pitts*, [2003], recently reported that the HONO loss decreases with increasing R.H. between 0% and 50% R.H., which would lead to a negative $d(\gamma_{HONO}(R.H.))/d(R.H.)$. If this is the case for the entire R.H. range, the R.H. dependence of $\gamma_{NO2\rightarrow HONO}(R.H.)$ could be less than linear, or $\gamma_{NO2\rightarrow HONO}(R.H.)$ could even be independent of R.H. The results of our field observations led to the proposal to a new HONO formation mechanism that will be explained below.

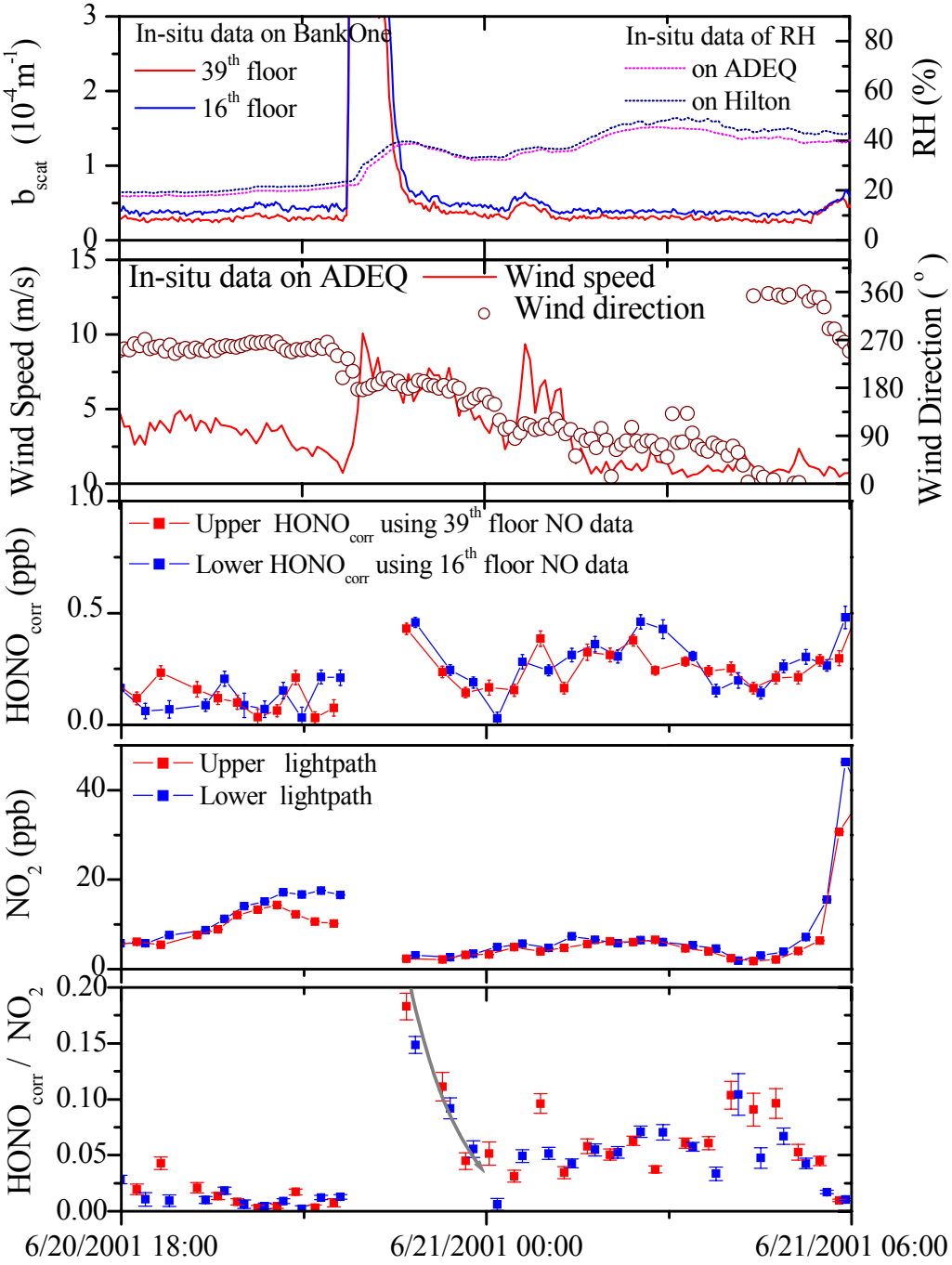

Figure 25: b_{scat}, R.H., wind speed and direction, NO_2 mixing ratio, calculated $[HONO]_{corr}$, and $[HONO]_{corr}/[NO_2]$ during the night of June 20-21, 2001 in Phoenix. Upper light path, 39th floor data, and ADEQ building data are printed in gray. The lower sampling sites and light path are marked black. The error bars show the 1σ standard deviation. (figure from [*Wang et al.*, 2002]

A unique opportunity to study HONO chemistry emerged during three dust storms that passed through downtown Phoenix. While the conversion of NO_2 to HONO in Phoenix never exceeded a HONO/NO_2 ratio of 0.07, during the dust storms this ratio increased considerably to 0.19 (see Figure 25). Considering the fact that the [HONO]/[NO_2] ratio never exceeded 10-12% in our other observations, or any other urban/sub-urban measurement, this is quite a surprising observation. One should note here that the PSS is independent of the surface-volume-ratio. Thus the pure fact that more aerosol surface is available in the dust storms does not explain the higher ratio. We believe that the chemical property of the dust particles, which was also measured during the experiment, is responsible for changing the PSS ratio. Since we do not entirely understand the NO_2 to HONO conversion on mineral dust no further chemical analysis of this data was possible. However, the increased [HONO]/[NO_2] ratios have important implications for the chemistry inside polluted dust storms, such as those often observed in southern Asia. The higher ratio indicates a higher efficiency in the formation of HONO, which leads to a enhanced formation of OH radicals through the photolysis of HONO. Further studies of HONO formation in dust storms therefore seem to be warranted.

4.5 A new mechanism of HONO formation

Based on our field observation of the R.H. dependency of HONO chemistry and through a collaboration with the University of Heidelberg, where, in laboratory experiments a dependence of [HONO] on the R.H. was observed, we also propose a new HONO formation mechanism that describes the atmospheric and the laboratory observations at the same time. Based on the results from the Heidelberg experiment, where HONO seems to be directly proportional to R.H. in the absence of NO_2 (not shown here), we adopt a Langmuir type approach to describe gas-phase and surface adsorbed HONO. On the surface a finite number of sites with a density N are available to HONO molecules. The out-gassing frequency of HONO is proportional to the amount of adsorbed HONO, $[HONO]_w$: $f_{out} = k_1 \cdot [HONO]_{wall} = k_1 \cdot S/V \, \Theta_{HONO} \cdot N$, where Θ_{HONO} is the percentage of surface coverage, S/V is the surface – to – volume ratio, and k_1 is the probability for an absorbed HONO molecule to leave the surface. The uptake of HONO is proportional to the free surface sites. A competition between H_2O and HONO for surface sites occurs on all surfaces we have investigated in the laboratory. The uptake frequency can thus be expressed as $f_{upt} = k_{-1} \cdot \frac{\bar{v}}{4} \frac{'S}{V} \cdot N \cdot (1 - \Theta_{HONO} - \Theta_{H_2O}) \cdot [HONO]_{(g)}$ where Θ_{H2O} is the percentage of water surface coverage on the sites that have similar energetics to those taking up HONO, k_{-1} is the uptake probability and $\bar{v}$ is the mean velocity of HONO. Based on these simple model assumptions, one expects an equilibrium between gas-phase and surface adsorbed HONO described as:

$$K = \frac{[HONO]_{(g)}}{[HONO]_{wall}} = \frac{k_1}{k_{-1} \cdot \bar{v}/4 \, (1 - \Theta_{HONO} - \Theta_{H_2O})} \qquad (1)$$

In the atmosphere and in the Heidelberg experiment, where HONO concentrations are many orders of magnitude lower than water vapor levels, one can assume that $\Theta_{HONO} <<$

$\Theta_{H2O.}$ With $\Theta_{H_2O} = \frac{K^{H_2O} \cdot [H_2O]_{(g)}}{1 + K^{H_2O} \cdot [H_2O]_{(g)}}$, where K^{H2O} is the equilibrium constant between gas-phase and surface adsorbed water, one can simplify equation 6 to:

$$K = \frac{[HONO]_{(g)}}{[HONO]_{wall}} = \frac{k_1}{k_{-1} \bar{v}/4} \left(1 + K^{H2O} [H_2O]_{(g)}\right) \qquad (24)$$

K^{H2O} $[H_2O]_{(g)}$ expresses the amount of surface adsorbed water which can, in good approximation, be assumed to be linearly dependent on R.H. over an R.H. range from ~10% - 80% [*Lammel*, 1999]. The equilibrium of gas-phase and adsorbed HONO is thus linearily dependent on the R.H.

Equation 24 explains the PSS observed in our field studies rather well. Incorporating this simple mechanism into our nocturnal chemistry model, we are able to describe the general dependencies on R.H. observed in the laboratory. Because this result was derived rather late in the project, we are currently still working in refining this model before publishing the results. However, this theory has been presented at a number of meetings.

4.6 Heterogeneous chemistry on the urban canopy

Heterogeneous chemistry plays an important role in the NBL, both for the uptake of N_2O_5 and the conversion of NO_2 into HONO. Current air-quality models assume that this chemistry mostly occurs on particles. The ground is, in most cases, only considered as a sink for gases, i.e. through a dry deposition parameterization. Urban areas contain, however, other surfaces, such as building walls and roofs. These surfaces are currently not considered in atmospheric chemistry models.

The fact that building surfaces are not considered is partially founded in the fact that

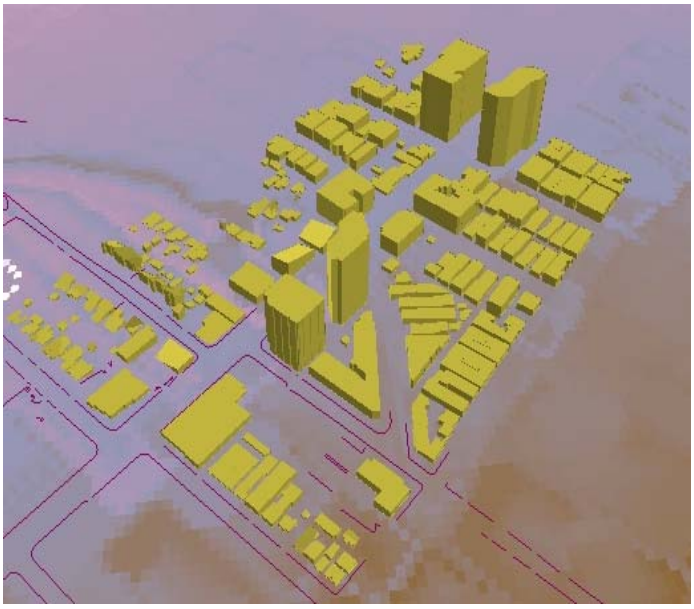

Figure 26: Area chosen for the calculation of the S/V of the urban canopy. (GIS data courtesy of the city of Santa Monica).

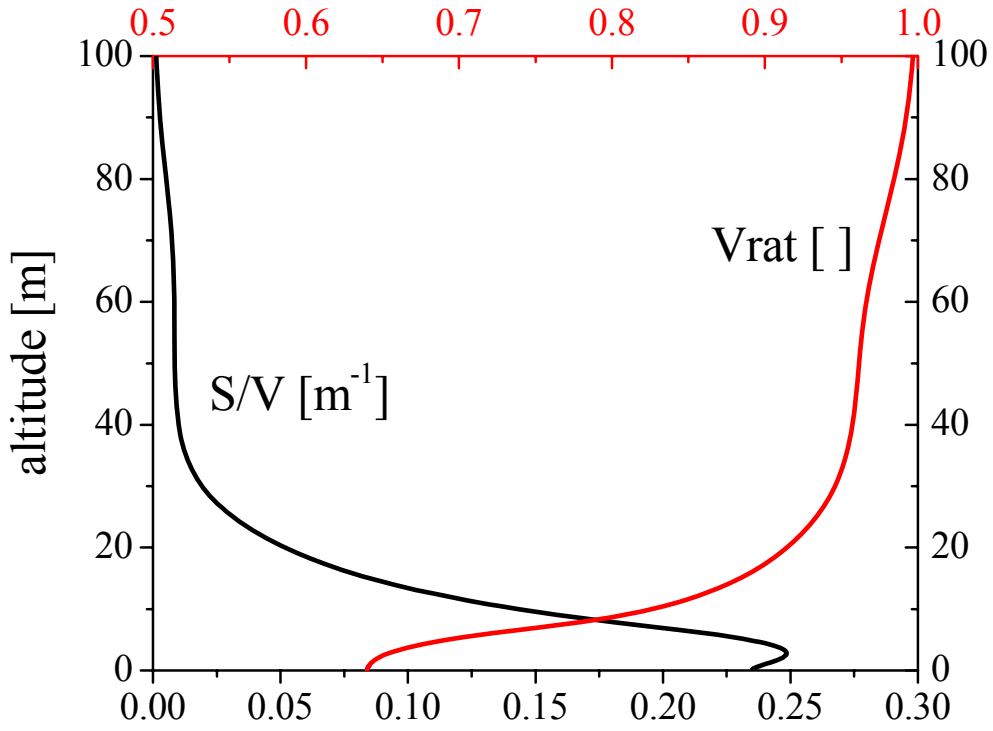

Figure 27: Surface to volume ratio and volume reduction in the target area in Santa Monica. (GIS data courtesy of the city of Santa Monica)

no information on the size of this surface area was available before this project. We therefore searched for a method to characterize the surface area of a city. The solution of this problem presented itself in the form of Geographical Information System data bases, which are available for many urban areas. We used the GIS database provided by the city of Santa Monica for our initial investigation. A part of Santa Monica (see Figure 26) was chosen for our initial surface determination. In short, the GIS data base describes all buildings in this area by using polygons for walls and roofs in three dimensions. An algorithm was developed to average this information to derive an altitude dependent surface to volume ratio in the selected city (Figure 27). In addition, the volume occupied by the buildings was also derived (Figure 27). These results led to the following conclusions about the role of the urban canopy, i.e. buildings and other man-made structures:

- The surface to volume area in the lowest 10-20 m can reach up to 0.25m-1. This number is many times larger than the typical surface area of an urban aerosol. One would thus expect a strong influence of the urban canopy on the heterogeneous processing of pollutants.
- Buildings take up a considerable amount of the volume of the atmosphere, i.e. 30-40% in the lowest 20m. This volume reduction influences trace gas concentration, in particular for any directly emitted gas and its reaction product, i.e. NO and O_3.

- Both S/V and the volume reduction decrease with altitude, but contribute even above 50m due to the presence of high-rise buildings.

It should be noted here that these results will depend considerably on area of the city, i.e. downtown areas have a higher concentration of high-rise building and thus more S/V, and the city itself. However, our results are the first direct quantification of the S/V and the volume reduction for a real city.

Based on these findings we expanded our chemical transport model to include the urban canopy. We developed a new module that is based on a resistance approach, distinguishing between the laminar layer above the surface and the rest of the atmosphere. Chemistry is treated independently in the laminar layer, and heterogeneous reactions are parameterized through the molecular collisions with the surface. Exchange between the laminar layer and the rest of the atmosphere depends on the wind speed and thus the height above the ground. This approach proved to be essential since a simple increase of the surface to volume area in the model increases the effect of heterogeneous chemistry too much. It also shows that the transport to and from the urban surfaces is an essential step when modeling the influence of the urban canopy on the atmospheric composition. To quantify the impact of the urban canopy we performed three model runs, one with a flat ground, one with a grass surface, and one with the urban canopy of our study area in Santa Monica. The meteorological conditions, initial trace gas concentrations, and emission rates, were identical in all three cases. Figure 28 compares the vertical profiles of our simulations. It is clear that the urban canopy has a considerable influence on the concentrations of various pollutants. For example, ozone is reduced at the ground due to the larger NO levels which are caused by the volume reduction. On the other hand, the higher S/V at the ground leads to considerably higher HONO at the ground.

Our results show that building surfaces cannot be ignored in the study of urban nocturnal chemistry. Based on these initial efforts we will further refine our model and the GIS algorithms to improve our model predictions in the future. A publication on our results is currently in preparation.

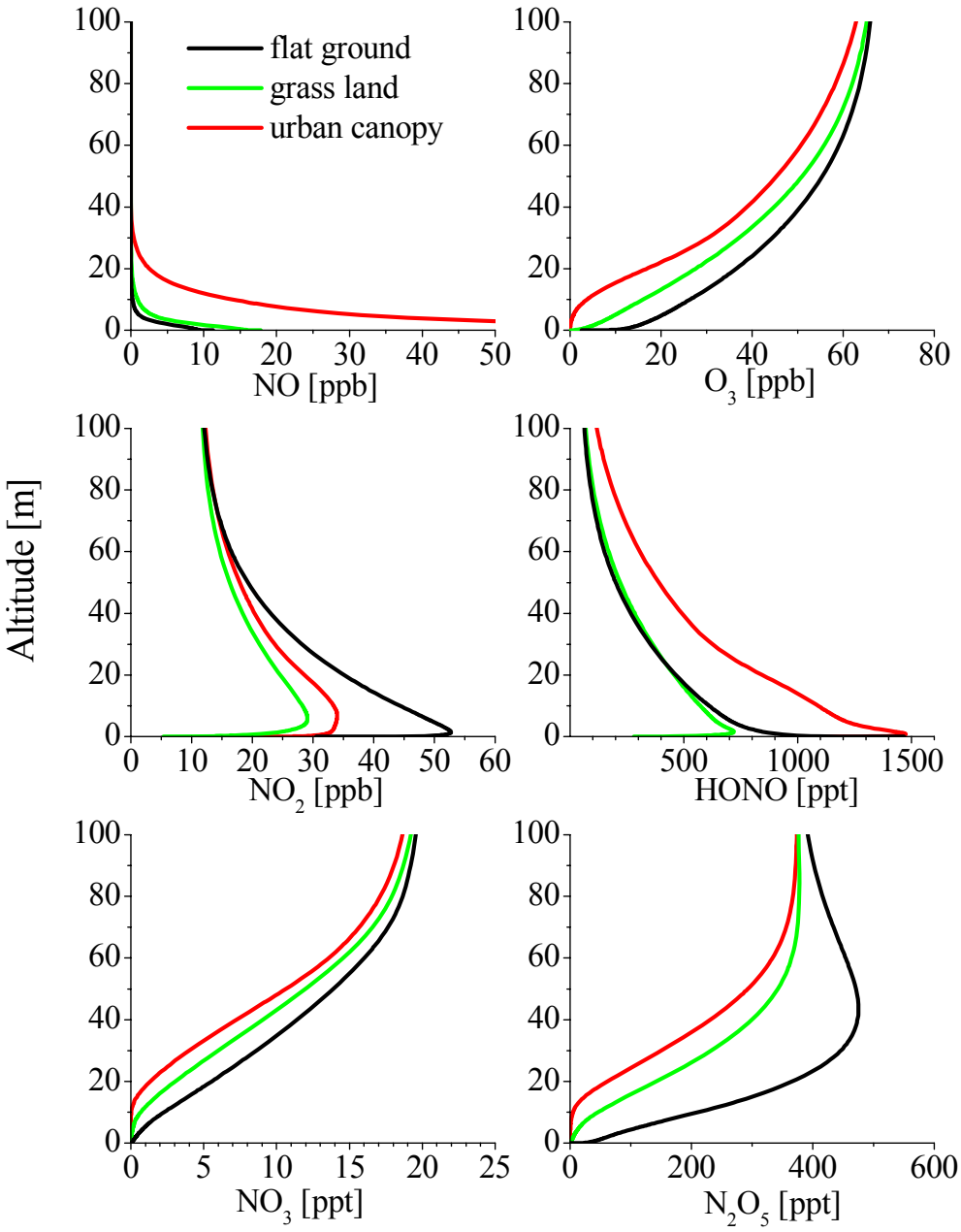

Figure 28: Comparison of NCAT model runs with different surfaces. The influence of the urban canopy can be clearly distinguished.

4.7 Educational Activities

This project also led to a number of educational activities. Most importantly it financed Shuhui Wang, a graduate student, throughout her PhD thesis. Shuhui participated in the Phoenix and the Boston field activities, and was responsible for the data evaluation. In addition, she played an important role in the development of our model. Shuhui published one of the manuscripts that resulted from this project and is currently writing two more manuscript on the results of the Phoenix study (one of this is attached to this report). These papers will be the basis of her thesis, which she will submit by the end of this year.

The project also financed Dr. Andreas Geyer, who did his postdoctoral research at UCLA. Dr. Geyer developed the NCAT model and is the first author on two of the publications that resulted from the modeling activities within this project

Many of the results from this project were incorporated into the classes of the PI. In particular, non-science students enjoyed real world examples in the General Education classes of our department.

5 Conclusions

This project has focused on the investigation of various aspects of the chemistry in the polluted nocturnal boundary layer. We have provided experimental evidence and numerical process studies to advance our understanding of chemistry at night. Our main conclusions can be summarized as follows.

- Nocturnal chemistry in a polluted boundary layer is altitude dependent due to the interaction of emissions of NO and VOC's at the ground, and the slow vertical mixing in the stable NBL. The magnitude of the observed and modeled vertical trace gas distributions depends on the emissions rates and the atmospheric stability.

- Ground observations at one altitude do not give a representative picture of the chemical composition and the chemical processes in the NBL.

- NO_3 and N_2O_5 display strong vertical gradients, with often negligible concentrations at the ground and very high levels in 100m altitude. The loss of NO_x through N_2O_5 aerosol uptake proceeds predominately in the upper part of the NBL, and is not captured by ground observations.

- An active radical chemistry occurs at night, in particular at certain altitudes. We can distinguish three regions: An unreactive region at the ground which is dominated by high NO concentrations which suppress radical chemistry a region dominated by the reaction of O_3 and NO_3 with VOC, which is located in the upper part of the NBL, and a region where radicals from the upper and the unreactive region mix, leading to a daytime like radical propagation. It is this region that our model predicts the most active radical chemistry and high OH levels.

- The mixing of gases that could otherwise not co-exist in one airmass, i.e. NO_3 / RO_2 and NO, leads to unique chemical processes at night. We have identified a number of these transport driven chemical processes, such as the nocturnal formation of OH through the mixing of RO_2 and NO. The nature of these processes and their possible presence during the day should be further analyzed.

- Our field observations reveal that NO_2 to HONO conversion depends on relative humidity. We propose a new HONO chemistry, based on established physical-chemical principles. The application of this new mechanism can explain laboratory and field observations

- NO_2 to HONO conversion appears to be enhanced on mineral dust. This has implications for the chemistry in polluted dust storms.

- We showed that the urban canopy, i.e. building walls and roof, provides a large surface area for heterogeneous chemistry which cannot be ignored when modeling nocturnal chemistry in urban areas. In addition, the volume reduction due to the presence of buildings also needs to be considered.

Finally, it should be mentioned that this project has considerably increased the interest in nocturnal chemistry in the atmospheric chemistry community. Through our publications and the presentations given throughout this project (see Section 7) other researchers have become interested in this topic. Nocturnal chemistry is now an important aspect of most field experiments, in contrast to five years ago. Our project has considerably increased the understanding of the chemistry in the polluted NBL. However, a number of new questions have emerged which will be addressed in studies following this one.

6 References

Alicke, B., A. Geyer, A. Hofzumahaus, F. Holland, S. Konrad, H.-W. Pätz, J. Schäfer, J. Stutz, A. Volz-Thomas, and U. Platt, OH formation by HONO photolysis during the BERLIOZ experiment, *J. Geophys. Res.*, *108* (D4), doi:10.1029/2001JD000579, 2003.

Alicke, B., U. Platt, and J. Stutz, Impact of nitrous acid photolysis on the total hydroxyl radical budget during the Limitation of Oxidant Production/Pianura Padana Produzione di Ozono study in Milan, *J. Geophys. Res.*, *107* (D22), doi: 10.1029/2000JD000075, 2002.

Aliwell, S.R., and R.L. Jones, Measurements of tropospheric NO_3 at midlatitude, *J. Geophys. Res.*, *103* (D5), 5719 - 5727, 1998.

Allan, B., G. McFiggans, J. Plane, H. Coe, and G. McFadyen, The nitrate radical in the remote marine boundary layer, *J. Geophys. Res.*, *105* (D19), 24,191 - 24,204, 2000.

Allan, B.J., N. Carslaw, H. Coe, R.A. Burgess, and J.M. Plane, Observation of the nitrate radical in the marine boundary layer, *J. Atmos. Chem.*, *33*, 129 - 154, 1999.

Allan, B.J., J.M.C. Plane, H. Coe, and J. Shillito, Observations of NO_3 concentration profiles in the troposphere, *J. Geophys. Res.*, *107* (D21), doi:10.1029/2002JD002112, 2002.

Ammann, M., M. Kalberer, D.T. Jost, L. Tobler, E. Rossler, D. Piguet, H.W. Gaggeler, and U. Baltensperger, Heterogeneous production of nitrous acid on soot in polluted air masses, *Nature*, *395* (6698), 157-160, 1998.

Arya, S.P., *Introduction to Micrometeorology*, Academic Press, Inc., San Diego, 1988.

Atkinson, R., Atmospheric chemistry of VOCs and NO_x, *Atmos. Environ.*, *34* (12 - 14), 2063 - 2101, 2000.

Atkinson, R., D.L. Baulch, R.A. Cox, R.F. Hampson, J.A. Kerr, M.J. Rossi, and J. Troe, Evaluated kinetic and photochemical data for atmospheric chemistry: IUPAC Subcommittee on Gas Kinetic Data Evaluation for Atmospheric Chemistry, 2002.

Aumont, B., F. Chervier, and S. Laval, $NO_x/HO_x/O_3$ chemistry in the polluted boundary layer, *Atmos. Environ.*, *37* (4), 487-498, 2003.

Berndt, T. and O. Boge, Gas-phase reaction of NO_3 radicals with isoprene: A kinetic and mechanistic study, *Int. J. Chem. Kin.*, *29* (10), 755 - 765, 1997.

Bey, I., B. Aumont, and G. Toupance, The nighttime production of OH radicals in the continental troposphere, *Geophys. Res. Lett.*, *24* (9), 1067-70, 1997.

Brost, R.A., A.C. Delany, and B.J. Huebert, Numerical modeling of concentrations and fluxes of HNO_3, NH_3 and NH_4NO_3 near the surface, *J. Geophys. Res.*, *93* (D6), 7137-7152, 1988.

Businger, J.A., J.C. Wyngaard, Y. Izumi, and E.F. Bradley, Flux profile relationships in the atmospheric surface layer, *J. Atmos. Sci.*, *28*, 181-189, 1971.

Calvert, J.G., G. Yarwood, and A.M. Dunker, An evaluation of the mechanism of nitrous acid formation in the urban atmosphere, *Res Chem Interm.*, *20* (3-5), 463-502, 1994.

Carslaw, N., L. Carpenter, J.M.C. Plane, B.J. Allan, R.A. Burgess, and K.C. Clemitshaw, Simultaneous observations of nitrate and peroxy radicals in the marine boundary layer, *J. Geophys. Res.*, *102*, 18917 - 18933, 1997.

Cros, B., J. Fontan, A. Minga, G. Helas, D. Nganga, R. Delmas, A. Chapuis, B. Benech, A. Druilhet, and M.O. Andreae, Vertical profiles of ozone between 0 meters and 400 meters in and above the African equatorial forest, *J. Geophys. Res.*, *97*, 12877-12887, 1992.

Curtis, A.R., and W.P. Sweetenham, FACSIMILE release H user's manual, London, 1987.

Faloona, I., D. Tan, W. Brune, J. Hurst, D. Barket, T.L. Couch, P. Shepson, E. Apel, D. Riemer, T. Thornberry, M.A. Carroll, S. Sillman, G.J. Keeler, J. Sagady, D. Hooper, and K. Paterson, Nighttime observations of anomalously high levels of hydroxyl radicals above a deciduous forest canopy, *J. Geophys. Res.*, *106* (D20), 24315-24333, 2001.

Finlayson- Pitts, B.J., L.M. Wingen, A.L. Sumner, D. Syomin, and K.A. Ramazan, The heterogeneous hydrolysis of NO_2 in laboratory systems and in outdoor and indoor atmospheres: An integrated mechanism, *Phys Chem Chem Phys*, *5*, 223-242, 2003.

Finlayson-Pitts, B.J., and J.N. Pitts, *Chemistry of the upper and lower atmosphere: theory, experiments and applications*, Academic Press, San Diego, CA; London, 2000.

Fish, D.J., D.E. Shallcross, and R.L. Jones, The vertical distribution of NO_3 in the atmospheric boundary layer, *Atmos. Environ.*, *33* (5), 687 - 691, 1999.

Fitzjarrald, D.R., and D. Lenschow, Mean concentration and flux profiles for chemically reactive species in the atmospheric surface layer, *Atmos. Environ.*, *17* (12), 2505-2512, 1983.

Friedeburg, C., T. Wagner, A. Geyer, N. Kaiser, B. Vogel, H. Vogel, and U. Platt, Derivation of tropospheric NO_3 profiles using off-axis-DOAS measurements during sunrise and comparison with simulations, *J. Geophys. Res.*, *107* (13), doi: 10.1029/2001JD000481, 2002.

Fuchs, N.A., and A.G. Sutugin, *Highly dispersed aerosols*, Ann Arbor Science, Ann Arbor, MI, 1971.

Fuentes, J.D., M. Lerdau, R. Atkinson, D. Baldocchi, J.W. Bottenheim, P. Ciccioli, B. Lamb, C. Geron, L. Gu, A. Guenther, T.D. Sharkey, and W.R. Stockwell, Biogenic Hydrocarbons in the atmospheric boundary layer: A review, *Bull. Am. Met. Soc.*, *81* (7), 1537 - 1575, 2000.

Galmarini, S., P.G. Duynkerke, and J. Vilà-Guerau de Arellano, Evolution of nitrogen oxide chemistry in the nocturnal boundary layer, *J. Appl. Meteo.*, *36* (7), 943 - 957, 1997.

Gao, W., and M.L. Wesely, Numerical modeling of the turbulent fluxes of chemically reactive trace gases in the atmospheric boundary layer, *J. Appl. Meteo.*, *33* (7), 835-847, 1994.

Gao, W., M.L. Wesely, and I.Y. Lee, A numerical study of the effects of air chemistry on fluxes of NO, NO_2, and O_3 near the surface, *J. Geophys. Res.*, *96*, 18,761-18,770, 1991.

Gerecke, A., A. Thielmann, L. Gutzwiller, and M.J. Rossi, The chemical kinetics of HONO formation resulting from heterogeneous interaction of NO_2 with flame soot, *Geophys. Res. Lett.*, *25*, 2453-2456, 1998.

Geyer, A., R. Ackermann, R. Dubois, B. Lohrmann, T. Muller, and U. Platt, Long-term observation of nitrate radicals in the continental boundary layer near Berlin, *Atmos. Environ.*, *35* (21), 3619-3631, 2001.

Geyer, A., B. Alicke, R. Ackermann, M. Martinez, H. Harder, B. Brune, E. Williams, T. Jobson, S.R. Hall, R. Shetter, and J. Stutz, Direct observations of daytime NO_3: Implications for urban boundary layer chemistry, *J. Geophys. Res.*, doi:10.1029/2002JD002967, 2003.

Geyer, A., B. Alicke, A. Hofzumahaus, F. Holland, S. Konrad, T. Klüpfel, H.-W. Pätz, D. Perner, A. Volz-Thomas, and U. Platt, Nighttime production of peroxy and hydroxyl radicals during the BERLIOZ campaign. Observations and modelling studies., *J. Geophys. Res.*, doi 10.1029.2001JD000656, 2003.

Geyer, A., B. Alicke, D. Mihelcic, J. Stutz, and U. Platt, Comparison of tropospheric NO_3 radical measurements by differential optical absorption spectroscopy and matrix isolation spin resonance, *J. Geophys. Res.*, *104* (D21), 26,097 - 26,105, 1999.

Geyer, A., and J. Stutz, Vertical profiles of NO_3, N_2O_5, O_3, and NO_x in the nocturnal boundary layer: 2. Model studies on the altitude dependence of composition and chemistry, *J. Geophys. Res.*, *109*, doi:10.1029/2003JD004211, 2004 a.

Geyer, A., and J. Stutz, The vertical structure of OH-HO_2-RO_2 chemistry in the nocturnal boundary layer: A one-dimensional model study, *J. Geophys. Res.*, *109*, doi:10.1029/2003JD004425, 2004 b.

Glaser, K., U. Vogt, G. Baumbach, A. Volz-Thomas, and H. Geiss, Vertical profiles of O_3, NO_2, NO_x, VOC, and meteorological parameters during the Berlin Ozone Experiment (BERLIOZ) campaign, *J. Geophys. Res.*, *108* (D4), doi:10.1029/2001JD002475, 2003.

Goodman, A.L., G.M. Underwood, and V.H. Grassian, Heterogeneous reaction of NO_2: Characterization of gas-phase and adsorbed products from the reaction, $2NO_2$ (g)+H_2O(a)->

HONO(g)+HNO_3(a) on hydrated silica particles, *J. Phys. Chem. A*, *103* (36), 7217-7223, 1999.
Guenther, A., C. Geron, T. Pierce, B. Lamb, P. Harley, and R. Fall, Natural emissions of non-methane volatile organic compounds, carbon monoxide, and oxides of nitrogen from North America, *Atmos. Environ.*, *34* (12-14), 2205-2230, 2000.
Guesten, H., G. Heinrich, and D. Sprung, Nocturnal depletion of ozone in the Upper Rhine Valley, *Atmos. Environ.*, *32* (7), 1195-1202, 1998.
Hamba, F., Statistical analysis of chemically reacting passive scalars in turbulent flows, *J. Phys. Soc. Jpn.*, *56*, 79-96, 1987.
Hamba, F., A modified K model for chemically reactive species in the planetary boundary layer, *J. Geophys. Res.*, *98* (D3), 5173-5182, 1993.
Hamba, F., Reply to comment on: A modified K model for chemically reactive species in the planetary boundary layer, *J. Geophys. Res.*, *98* (D3), 5173-5182, 1994.
Haugen, D.A., *Workshop on Micrometeorology*, A. Haugen, Eprata, 1973.
Harris, G.W., W.P.L. Carter, A.M. Winer, J.N. Pitts, U. Platt, D. Perner, Observations of nitrous acid in the Los Angeles atmosphere and implications for the predictions of ozone-precursor relationships, *Environ. Sci. Technol.*, *16*, 414-419, 1982.
Harris, G.W., A.M. Winer, J.N. Pitts, U. Platt, D.P.D.K. Killinger, A. Mooradian, , Measurement of HONO, NO_3 and NO_2 by long-path differential optical absorption spectroscopy in the Los Angeles basin: Optical and Laser Remote Sensing, *Springer Ser. Opt. Sci.*, *39*, 106-113, 1983.
Harrison, R.M., and A.M.N. Kitto, Evidence for a surface source of atmospheric nitrous acid, *Atmos. Environ.*, *28* (6), 1089-1094, 1994.
Harrison, R.M., J.D. Peak, and G.M. Collins, Tropospheric cycle of nitrous acid, *J. Geophys. Res.*, *101*, 14429-14439, 1996.
Heintz, F., H. Flentje, R. Dubois, and U. Platt, Long-term observation of nitrate radicals at the TOR-Station Kap Arkona (Rügen), *J. Geophys. Res.*, *101* (22), 891-910, 1996.
Hov, O., One-dimensional vertical model for ozone and other gases in the atmosphere boundary layer, *Atmos. Environ.*, *17*, 535-550, 1983.
Jenkin, M.I., R.A. Cox, and D.J. Williams, Laboratory studies of the kinetics of formation of nitrous acid from the thermal reaction of nitrogen dioxide and water vapour, *Atmos. Environ.*, *22*, 487-498, 1988.
Kaiser, E.W., and C.H. Wu, A kinetic study of the gas phase formation and decomposition reactions of nitrous acid, *J. Phys. Chem.*, *81*, 1701-1706, 1977.
Kalberer, M., M. Ammann, F. Arens, H.W. Gaggeler, and U. Baltensperger, Heterogeneous formation of nitrous acid (HONO) on soot aerosol particles, *J Geophys Res-Atmos*, *104* (D11), 13825-13832, 1999.
Kesselmeier, J., and M. Staudt, Biogenic volatile organic compounds (VOC): An overview on emission, physiology, and ecology, *J. Atmos. Chem.*, *33*, 23-88, 1999.
Kirchstetter, T.W., R.A. Harley, and D. Littlejohn, Measurement of nitrous acid in motor vehicle exhaust, *Environ Sci Technol*, *30* (9), 2843-2849, 1996.
Kitto, A.M.N., and R.M. Harrison, Nitrous and nitric acid measurements at sites in South-East England, *Atmo., Environ.*, *26* (2), 235-241, 1992.
Kleffmann, J., K.H. Becker, and P. Wiesen, Heterogeneous NO_2 conversion processes on acid surfaces: possible atmospheric implications, *Atmos. Environ.*, *32*, 2721 - 2729, 1998.
Klemp, D., K. Mannschreck, H.W. Paetz, M. Habram, P. Matuska, and F. Slemr, Determination of anthropogenic emission ratios in the Augsburg area from concentration ratios: results from long-term measurements, *Atmos. Environ.*, *36* (Suppl. No. 1), 61-80, 2002.
Kramm, G., H. Mueller, D. Fowler, K.D. Hoefken, F.X. Meixner, and E. Schaller, A modified profile method for determining the vertical fluxes of NO, NO_2, ozone, and HNO_3 in the atmospheric surface layer, *J. Atmos. Chem.*, *13*, 265-288, 1991.

Kurtenbach, R., K.H. Becker, J.A.G. Gomes, J. Kleffmann, J.C. Lorzer, M. Spittler, P. Wiesen, R. Ackermann, A. Geyer, and U. Platt, Investigations of emissions and heterogeneous formation of HONO in a road traffic tunnel, *Atmos. Environ.*, *35* (20), 3385-3394, 2001.

Lammel, G., Formation of nitrous acid: Parameterisation and comparison with observations, Max-Planck-Institut fuer Meteorologie, Hamburg, 1999.

Lammel, G., and J.N. Cape, Nitrous acid and nitrite in the atmosphere, *Chem Soc Rev*, *25* (5), 361, 1996.

Lenschow, D.H., and A.C. Delany, An analytic formulation for NO and NO_2 flux profiles in the atmospheric surface layer, *J. Atmos. Chem.*, *5*, 301-309, 1987.

Lenschow, D.H., Reactive trace species in the boundary layer from a micrometeorological perspective, *J. Meteorol. Soc. Japan*, *1*, 60, 1982.

McDonald-Buller, E.C., H.M. Liljestrand, and K. Sepehrnoori, Numerical modeling of dry deposition coupled to 22 photochemical reactions, *Atmos. Environ.*, *33* (10), 1491-1502, 1999.

McMurry, P.H., A review of atmospheric aerosol measurements, *Atmos. Environ.*, *34* (12-14), 1959-1999, 2000.

Magnotta, F., and H. Johnson, Photodissociation quantum yields for the NO_3 free radical, *Geophys Res Lett*, *7*, 769 - 772, 1980.

Paulson, S.E., and J.J. Orlando, The reactions of ozone with alkenes: an important source of HO_x in the boundary layer, *Geophys. Res. Lett.*, *23* (25), 3727-30, 1996.

Paulson, S.E., C. Myeong, A.D. Sen, and G. Orzechowska, Measurement of OH radical formation from the reaction of ozone with several biogenic alkenes, *J. Geophys. Res.*, *103* (D19), 25533-9, 1998.

Pisano, J.T., I. McKendry, D.G. Steyn, and D.R. Hastie, Vertical nitrogen dioxide and ozone concentrations measured from a tethered balloon in the Lower Fraser Valley, *Atmos. Environ.*, *31* (14), 2071-2078, 1997.

Pitts, J.N., H.W. Biermann, A.M. Winer, and E.C. Tuazon, Spectroscopic identification and measurement of gaseous nitrous acid in dilute auto exhaust, *Atmos. Environ.*, *18*, 847-854, 1984.

Pitts, J.N., E. Sanhueza, R. Atkinson, W.P.L. Carter, A.M. Winer, G.W. Harris, and C.N. Plum, An investigation of the dark formation of nitrous acid in environmental chambers, *Int. J. Chem. Kinet.*, *XVI*, 919-939, 1984.

Platt, U., Differential Optical Absorption Spectroscopy (DOAS), in *Monitoring by Spectroscopic Techniques*, M. W. Sigrist, J. Wiley, New York, 1994.

Platt, U., G. Lebras, G. Poulet, J.P. Burrows, and G. Moortgat, Peroxy radicals from night-time reaction of NO_3 with organic compounds, *Nature*, *348* (6297), 147-149, 1990.

Platt, U., D. Perner, G.W. Harris, A.M. Winer, and J.N. Pitts, Detection of NO_3 in the polluted troposphere by differential optical absorption, *Geophys. Res. Lett.*, *7*, 89 - 92, 1980.

Povey, I., A. South, A. Kint de Roodenbeke, C. Hill, R. Freshwater, and R. Jones, A broadband lidar for the measurement of tropospheric constituent profiles from the ground, *J Geophys. Res.*, *103* (D3), 3369 - 3380, 1998.

Rao, K.S., and H.F. Snodgrass, Some parameterizations of the nocturnal boundary layer, *Bound.-Layer Meteor.*, *17*, 15-28, 1979.

Riemer, N., H. Vogel, B. Vogel, B. Schell, I. Ackermann, C. Kessler, and H. Hass, Impact of the heterogeneous hydrolysis of N_2O_5 on chemistry and nitrate aerosol formation in the lower troposphere under photosmog conditions, *J. Geophys. Res.*, *108* (D4), doi:10.1029/2002JD002436, 2003.

Sakamaki, F., S. Hatakeyama, and H. Akimoto, Formation of nitrous acid and nitric oxide in the heterogeneous dark reaction of nitrogen dioxide and water vapor in a smog chamber, *Int. J. Chem. Kinet.*, *XV*, 1013-1029, 1983.

Saliba, N.A., M. Mochida, and B.J. Finlayson-Pitts, Laboratory studies of sources of HONO in polluted urban atmospheres, *Geophys. Res. Lett.*, *27* (19), 3229-3232, 2000.

Sander, S.P., R.R. Friedl, D.M. Golden, M.J. Kurylo, R.E. Huie, V.L. Orkin, G.K. Moortgat, A.R. Ravishankara, C.E. Kolb, M.J. Molina, and B.J. Finlayson-Pitts, Chemical Kinetics and Photochemical Data for Use in Atmospheric Studies - Eval. No. 14, NASA-JPL, Pasadena, CA, 2003.

Saunders, S.M., M.E. Jenkin, R.G. Derwent, and M.J. Pilling, Protocol for the development of the Master Chemical Mechanism, MCM v3 (Part A): tropospheric degradation of non-aromatic volatile organic compounds, *Atmos. Chem. Phys.*, *3*, 161-180, 2003.

Schumann, U., Large-eddy simulation of turbulent diffusion with chemical reactions in the convective boundary layer, *Atmos. Environ.*, *23* (8), 1713-1727, 1989.

Seinfeld, J.H., and S.N. Pandis, *Atmospheric chemistry and physics: From air pollution to climate change*, John Wiley & Sons, New York, 1997.

Sjödin, A., and M. Ferm, Measurement of nitrous acid in an urban area, *Atmos. Environ.*, *19*, 985-992, 1985.

Smith, N., J.M.C. Plane, C. Nien, and O.A. Solomon, Nighttime radical chemistry in the San Joaquin Valley, *Atmos. Environ.*, *29*, 2887-2897, 1995.

Stockwell, W.R., F. Kirchner, M. Kuhn, and S. Seefeld, A new mechanism for regional atmospheric chemistry modeling, *J. Geophys. Res.*, *102* (D22), 25,847-25,879, 1997.

Stutz, J., B. Alicke, R. Ackermann, A. Geyer, S.H. Wang, A.B. White, E.J. Williams, C.W. Spicer, and J.D. Fast, Relative humidity dependence of HONO chemistry in urban areas, *J. Geophys. Res.*, *109*, doi:10.1029/2003JD004135, 2004 a.

Stutz, J., B. Alicke, R. Ackermann, A. Geyer, A. White, and E. Williams, Vertical profiles of NO_3, N_2O_5, O_3, and NO_x in the nocturnal boundary layer: 1. Observations during the Texas Air Quality Study 2000, *J. Geophys. Res.*, *109*, 10.1029/2003JD004209, 2004 b.

Stutz, J., B. Alicke, and A. Neftel, Nitrous acid formation in the urban atmosphere: Gradient measurements of NO_2 and HONO over grass in Milan, Italy, *J. Geophys. Res.*, *107* (D22), doi: 10.1029/2001JD000390, 2002.

Stutz, J., and U. Platt, Numerical analysis and estimation of the statistical error of differential optical absorption spectroscopy measurements with least-squares methods., *Appl. Opt.*, *30*, 6041-6053, 1996.

Stutz, J., and U. Platt, Improving long-path differential optical absorption spectroscopy with a quartz-fiber mode mixer, *Appl. Opt.*, *36* (6), 1105-15, 1997.

Svensson, R., E. Ljungström, and O. Lindqvist, Kinetics of the reaction between nitrogen dioxide and water vapour, *Atmos. Environ.*, *21*, 1529-1539, 1987.

Syomin, D. A., and B. J. Finlayson-Pitts, HONO decomposition on borosilicate glass surfaces: Implications for environmental chamber studies and field experiments, *Phys. Chem. Chem. Phys.*, 5(23), 5236–5242, 2003

TenBrink, H.M., and H. Spoelstra, The dark decay of HONO in environmental (SMOG) chambers, *Atmos. Environ.*, *32* (2), 247-251, 1998.

Thompson, A.M., and D. Lenschow, Mean profiles of trace reactive species in the unpolluted marine surface layer, *J. Geophys. Res.*, *89* (D3), 4788-4796, 1984.

Verver, G., A modified K model for chemically reactive species in the planetary boundary layer - comment, *J. Geophys. Res.*, *99* (D9), 19021-19023, 1994.

Vila-Guerau de Arellano, J., Bridging the gap between atmospheric physics and chemistry in studies of small-scale turbulence, *Bull. Am. Met. Soc.*, *84* (1), 51-56, 2003.

Vila-Guerau de Arellano, J., P.G. Duynkerke, and K.F. Zeller, Atmospheric surface layer similarity theory applied to chemically reactive species, *J. Geophys. Res.*, *100* (D1), 1397-1408, 1995.

Wang, S.H., R. Ackermann, C.W. Spicer, J.D. Fast, M. Schmeling, and J. Stutz, Atmospheric observations of enhanced NO_2-HONO conversion on mineral dust particles, *Geophys. Res. Lett.*, *30*, doi:10.1029/2003GL017014, 2003.

Wayne, R.P., I. Barnes, P. Biggs, J.P. Burrows, C.E. Canosa-Mas, J. Hjorth, G. Le Bras, G. Moortgat, D. Perner, G. Poulet, G. Restelli, and H. Sidebottom, The nitrate radical: Physics, chemistry, and the atmosphere, *Atmos. Environ.*, *25A*, 1-203, 1991.

Weaver, A., S. Solomon, R.W. Sanders, K. Arpag, and H.L. Miller, Atmospheric NO3.5. Off-axis measurements at sunrise: Estimates of tropospheric NO_3 at 40 degrees N, *J Geophys Res-Atmos*, *101* (D13), 18605-18612, 1996.

Winer, A.M., and H.W. Biermann, Long Pathlength Differential Optical Absorption Spectroscopy (DOAS) Measurements of Gaseous HONO, NO_2 and HCHO in the California South Coast Air Basin, *Res Chem Interm.*, *20* (3-5), 423-445, 1994.

Yoshizawa, A., A statistical investigation of shear turbulence: the Reynolds-stress transport equation, *J. Phys. Soc. Jpn.*, *51*, 658-666, 1982.

Zhang, J., and S.T. Rao, The role of vertical mixing in the temporal evolution of ground-level ozone concentrations, *J. Appl. Meteo.*, *38*, 1674-1691, 1999.

7 List of presentations and publications resulting from the project

7.1 Publications

1. Geyer, A., and J. Stutz, The vertical structure of OH-HO_2-RO_2 chemistry in the nocturnal boundary layer: a one-dimensional model study, *J. Geophys. Res.*, *109*, doi:10.1029/2003JD004425, 2004.
2. Stutz, J., B. Alicke, R. Ackermann, A. Geyer, A. White, and E. Williams, Vertical profiles of NO_3, N_2O_5, O_3, and NO_x in the nocturnal boundary layer: 1. Observations during the Texas Air Quality Study 2000, *J. Geophys. Res., 109*, doi:10.1029/2003JD004209, 2004.
3. Geyer, A., and J. Stutz, Vertical profiles of NO_3, N_2O_5, O_3, and NO_x in the nocturnal boundary layer: 2. Model studies on the altitude dependence of composition and chemistry, *J. Geophys. Res.*, *109*, doi:10.1029/2003JD004211, 2004.
4. Stutz, J., B. Alicke, R. Ackermann, A. Geyer, S.H. Wang, A.B. White, E.J. Williams, C.W. Spicer, and J.D. Fast, Relative humidity dependence of HONO chemistry in urban areas, *J. Geophys. Res., 109*, doi:10.1029/2003JD004135, 2004.
5. Wang, S.H., R. Ackermann, C.W. Spicer, J.D. Fast, M. Schmeling, and J. Stutz, Atmospheric observations of enhanced NO_2-HONO conversion on mineral dust particles, *Geophys. Res. Lett., 30*, doi:10.1029/2003GL017014, 2003.

7.2 Conference Proceedings

1. Stutz, J, Geyer, A., and Wang, S., Chemistry in the urban nocturnal boundary layer: Influence of vertical mixing on the processing of urban pollutants, extended abstract for *13'th International Scientific Symposium on Transport and Air Pollution*, Boulder, CO, 2004
2. Stutz, J., Geyer, A., Wang, S., "Influence of vertical mixing on nocturnal chemistry in the urban boundary layer", extended abstract for AMS meeting, Long Beach, 2003.
3. Wang, S. Ackermann, R., Geyer, A., Doran, C., Shaw, W.J., Fast, J.D., Spicer, C.W., Stutz, J., "Vertical variation of nocturnal NO_x chemistry in the urban environment of Phoenix", extended abstract for AMS meeting, Long Beach, 2003.
4. Geyer, A., Wang, S., Stutz, J., "Vertical profiles of free radicals in the polluted nocturnal boundary layer: A one-dimensional model study", extended abstract for AMS meeting, Long Beach, 2003.
5. Berkowitz, C.M., Fast, J., Doran, C., Spicer, C.W., Stutz, J., Wang, S., "Vertical mixing and chemistry over an arid urban site: First results from Skyscraper observations made during the Phoenix Sunrise Campaign", extended abstract for AMS meeting, Florida, 2002.

7.3 Publications in preparation

Wang, S, R. Ackermann., C.W. Spicer, J.D. Fast, C.C. Doran, and J. Stutz, Vertical Profiles of NOx Chemistry in the Polluted Nocturnal Boundary Layer in Phoenix, AZ: I. Field Observations by a Long-path DOAS system, to be submitted to ACP May 2005.

7.4 Invited Talks

1. Stutz, J., "Radical chemistry in the nocturnal boundary layer: Observations and modeling studies", Telluride Workshop on Atmospheric Radicals, 2004
2. Stutz, J., "Influence of vertical mixing on the chemistry in the nocturnal urban boundary layer", Pacific Northwest National Laboratory lecture series, 2003
3. Stutz, J, Geyer, A., Wang, S., "Nocturnal chemistry in the urban boundary layer", poster at the Atmospheric Chemistry Gordon Conference, 2003
4. Stutz, J, Geyer, A., Wang, S., "Nocturnal chemistry in urban areas", Southern California Symposium on Photochemistry and Kinetic Processes in the Atmosphere, Riverside, 2003
5. Stutz, J, Geyer, A., Wang, S., "Chemistry in the nocturnal boundary layer: A one-dimensional view", invited talk, JPL Atmospheric Chemistry Seminar Series, Pasadena, 2003
6. Stutz, J., Alicke, B., Ackermann, R., Hönninger, G. "Nighttime Chemistry of Nitrogen Oxides in the Urban Environment", invited talk to SOS Review meeting, Research Triangle Park, NC, 2001.
7. Stutz, J., Alicke, B., Ackermann, R., Hönninger, G. "Nighttime Chemistry of Nitrogen Oxides in the Urban Environment", invited talk, NOAA Aeronomy Laboratory, Boulder, 2001.
8. Stutz, J., Ackermann, R., Wang, S., , "Nocturnal Chemistry of HONO and the Nitrate Radical", invited talk, JPL Atmospheric Chemistry Seminar Series, Pasadena, 2001.
9. Stutz, J., Alicke, B., Ackermann, R., Wang, S., Hönninger, G., "Nighttime Chemistry of Nitrogen Oxides: Results from Field Experiments in the Urban and Suburban Environment ", invited talk, CU Boulder, 2001.
10. Stutz, J., Alicke, B., Hönninger, G., Neftel, A., "Investigation of the Nighttime Chemistry of Nitrogen Oxides by Differential Optical Absorption Spectroscopy", invited talk, Atmospheric Chemistry Workshop, Telluride, 2000.

7.5 Conference Presentations

1. Stutz, J., Geyer, A., Wang, S., and Hurlock, S., Chemistry in the Urban Nocturnal Boundary Layer : Influence of Vertical Mixing on the Processing of Pollutants, Transport and Air Pollution Meeting, NCAR, Boulder, 2004
2. Stutz, J., Wang, S., and Hurlock, S., Formation of nitrous acid in the urban nocturnal

boundary layer, Annual meeting of the American Chemical Society, Philadelphia, 2004

3. Hurlock, S, and Stutz, J., GIS in air pollution research, the role of building surfaces, Paper 2042, 2004 ESRI International User Conference, San Diego, Ca, 2004
4. Wang, S., Geyer, A., and Stutz, J., Vertical profiles of atmospheric trace gases and their chemistry in the urban boundary layer — field observations and model studies, Southern California Symposium on Photochemistry and Kinetic Processes in the Atmosphere, Fullerton, CA, 2004
5. Stutz, J., Geyer, A., and Wang, S., Nocturnal chemistry in urban areas: A one-dimensional view, DOE Atmospheric Science Meeting, Orlando, Fl, 2003
6. Stutz, J., Geyer, A., and Wang, S., Formation of nitrous acid, HONO, in the polluted urban atmosphere, Fall meeting of the American Geophysical Union, San Francisco, CA, 2003
7. Wang, S., Geyer, A., and Stutz, J., Vertical variations of boundary layer chemistry in the urban environment of Boston, Fall meeting of the American Geophysical Union, San Francisco, CA, 2003
8. Stutz, J., Geyer, A., and Wang, S., Formation of nitrous acid, HONO, in the polluted urban atmosphere, Fall Meeting of the American Geophysical Union, San Francisco, CA, 2002
9. Wang, S., Spicer, C W., Ackermann, R ., Fast, J. D., and Stutz, J., Influence of dust storms on the nocturnal chemistry of NO_2 and HONO in Phoenix, Fall Meeting of the American Geophysical Union, San Francisco, CA, 2002
10. Stutz, J., Ackermann, R., Wang, S., Nighttime Chemistry of Nitrogen Oxides: Measurements of Vertical Trace Gas Gradients during the Phoenix 2001 Study, DOE Atmospheric Science Meeting, Albuquerque, NM, 2002

8 Appended publications

1. Stutz, J, Geyer, A., and Wang, S., Chemistry in the urban nocturnal boundary layer: Influence of vertical mixing on the processing of urban pollutants, extended abstract for *13'th International Scientific Symposium on Transport and Air Pollution*, Boulder, CO, 2004
2. Stutz, J., Geyer, A., Wang, S., "Influence of vertical mixing on nocturnal chemistry in the urban boundary layer", extended abstract for AMS meeting, Long Beach, 2003.
3. Wang, S. Ackermann, R., Geyer, A., Doran, C., Shaw, W.J., Fast, J.D., Spicer, C.W., Stutz, J., "Vertical variation of nocturnal NO_x chemistry in the urban environment of Phoenix", extended abstract for AMS meeting, Long Beach, 2003.
4. Geyer, A., Wang, S., Stutz, J., "Vertical profiles of free radicals in the polluted nocturnal boundary layer: A one-dimensional model study", extended abstract for AMS meeting, Long Beach, 2003.
5. Berkowitz, C.M., Fast, J., Doran, C., Spicer, C.W., Stutz, J., Wang, S., "Vertical mixing and chemistry over an arid urban site: First results from Skyscraper observations made during the Phoenix Sunrise Campaign", extended abstract for AMS meeting, Florida, 2002.

6. Geyer, A., and J. Stutz, The vertical structure of OH-HO_2-RO_2 chemistry in the nocturnal boundary layer: a one-dimensional model study, *J. Geophys. Res.*, *109*, doi:10.1029/2003JD004425, 2004.
7. Stutz, J., B. Alicke, R. Ackermann, A. Geyer, A. White, and E. Williams, Vertical profiles of NO_3, N_2O_5, O_3, and NO_x in the nocturnal boundary layer: 1. Observations during the Texas Air Quality Study 2000, *J. Geophys. Res., 109*, doi:10.1029/2003JD004209, 2004.
8. Geyer, A., and J. Stutz, Vertical profiles of NO_3, N_2O_5, O_3, and NO_x in the nocturnal boundary layer: 2. Model studies on the altitude dependence of composition and chemistry, *J. Geophys. Res.*, *109*, doi:10.1029/2003JD004211, 2004.
9. Stutz, J., B. Alicke, R. Ackermann, A. Geyer, S.H. Wang, A.B. White, E.J. Williams, C.W. Spicer, and J.D. Fast, Relative humidity dependence of HONO chemistry in urban areas, *J. Geophys. Res., 109*, doi:10.1029/2003JD004135, 2004.
10. Wang, S.H., R. Ackermann, C.W. Spicer, J.D. Fast, M. Schmeling, and J. Stutz, Atmospheric observations of enhanced NO_2-HONO conversion on mineral dust particles, *Geophys. Res. Lett., 30*, doi:10.1029/2003GL017014, 2003.

Extended Abstract for 13'th International Scientific Symposium on Transport and Air Pollution

CHEMISTRY IN THE URBAN NOCTURNAL BOUNDARY LAYER: INFLUENCE OF VERTICAL MIXING ON THE PROCESSING OF URBAN POLLUTANTS

Jochen Stutz, Andreas Geyer, and Shuhui Wang
Department of Atmospheric Sciences, University of California Los Angeles
7127 Math Science, Los Angeles, CA 90095-1565
(email: jochen@atmos.ucla.edu)

Abstract

Nocturnal chemistry in urban areas can considerably influence the composition of the boundary layer by removing pollutants, and changing size and composition of particles. Nocturnal processes also determine the state of the atmosphere in the morning, and thus influence photochemistry during the next day. The investigation of nocturnal boundary layer (NBL) chemistry is challenging because the interplay of chemical processes and weak turbulent mixing leads to a strong altitude dependence. In addition, various heterogeneous chemical transformations can occur on the ground and buildings.

Here we present results from field experiments and 1D-modeling studies of the vertical variation of chemistry and the influence of various surface in the urban NBL. Our results show that the degree of altitude dependence of nocturnal chemistry is determined by the emission strength of NO_x and the magnitude of vertical mixing. The removal of urban pollutants was found to be altitude dependent, and can, for certain species, be comparable to daytime loss. Urban surfaces were found to play an important role, in particular with respect to the chemistry of nitrogen compounds, such as NO_2, NO_3, N_2O_5 and HONO. A number of novel chemical-transport mechanisms, which are driven by the mixing of radicals, radical precursors, and NO, were identified in the model.

1. INTRODUCTION

Chemical processes in the nocturnal urban and suburban boundary layer can considerably impact the composition of the atmosphere and therefore influence the starting conditions for photochemical smog formation during the next morning (see for example [*Aumont et al.*, 2003; *Bey et al.*, 1997; *Geyer et al.*, 2001]). Various chemical processes, such as the conversion of NO_x to N_2O_5 and the oxidation of VOCs, lead to the loss of pollutants at night. N_2O_5, on the other hand, can also directly influence size and composition of aerosol particles at night [*Li et al.*, 1993; *Makar et al.*, 1998; *Riemer et al.*, 2003]. In addition, the OH radical precursor HONO can be formed at night, leading to enhanced formation of OH during the next morning [*Alicke et al.*, 2003; *Alicke et al.*, 2002].

Many investigations of nocturnal urban chemistry have relied on 0-dimensional or very coarsely resolved higher dimensional models. While this approach has been used successfully in the well mixed daytime boundary layer, it can be highly inaccurate at night for the following reasons:

- Vertical mixing is slower than during the day. Gradients of trace gases are therefore more pronounced in particular in the lowest 100 m of the urban atmosphere.

- The vertical mixing of direct emissions, for example of NO and certain VOCs, is slower than their chemical conversion in the NBL. Their concentrations therefore remain elevated close to the ground.
- The nitrate radical and ozone take over the role as dominant radical species at night. Due to their longer lifetimes they can be transported more efficiently than OH radicals during the day. This has important consequences for the removal rates of hydrocarbons and NO_x at various altitudes in the NBL.
- Heterogeneous reactions appear to play a more important role at night. Examples are the formation of HONO and the uptake of N_2O_5.
- In comparison to the day, the ground and buildings play a more important role for heterogeneous chemistry in the boundary layer at night.

To study how the interaction of chemistry and vertical mixing and the heterogeneous transformations at urban surfaces influence the chemistry in the NBL, in particular with respect to the fate of pollutants emitted by urban traffic, we adopted a one-dimensional view of the NBL. We performed vertical trace gas profile measurements in various cities and interpreted these observations with a highly resolved one-dimensional chemical transport model.

Here we will present the general findings from our studies and discuss the mechanisms that lead to the formation of the observed

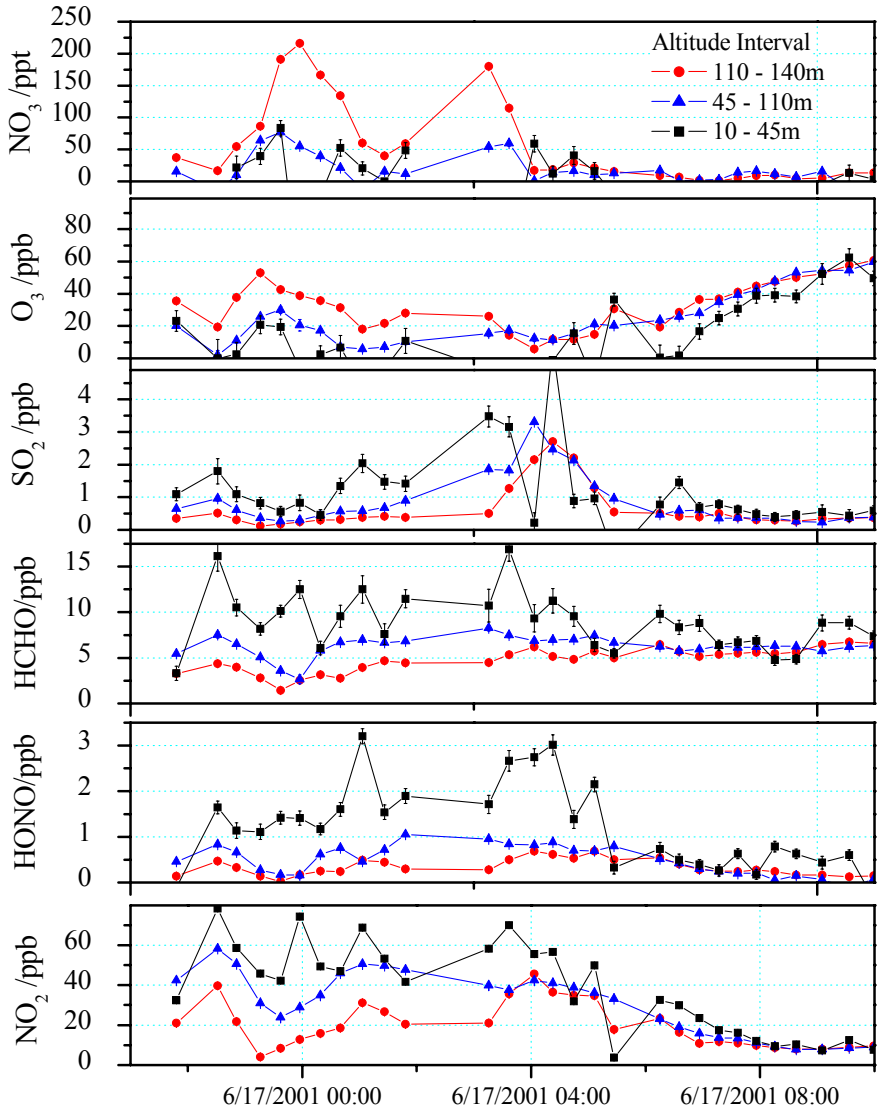

Figure 1: Observations of various trace gas gradients in Phoenix, AZ. The curves show the mixing ratios of the various compounds averaged over three height intervals. The night was characterized by vertically stable conditions. The vertical gradients disappeared after sunrise, around 6 am.

and modeled vertical profiles. We will also focus on the investigation of nocturnal radical levels and their influence on the transformation of pollutants, as well as the role of urban surfaces in nocturnal chemistry.

2. Field Observations

2.1 Experimental

In a number of field experiments we measured vertical concentration profiles of important nocturnal species such as O_3, NO_2, NO_3, and HONO by long-path Differential Optical Absorption Spectroscopy (DOAS) [*Platt*, 1994]. Our DOAS instrument consists of a xenon arc lamp, a coaxial sending/receiving telescope, and a spectrograph-detector system. The light beam is folded once by arrays of quartz corner-cube-reflectors that are typically mounted at 1 – 6 km distance at various altitudes. The multiple light paths between the instrument and the different retroreflector altitudes allow the derivation of vertical concentration profiles. Our field measurements took place in a variety of urban and suburban environments in the United States: Nashville, TN, (SOS 99), Houston, TX, (TEXAQS 2000), Phoenix, AZ, (POE 2001), and Boston, MA (NAOPEX 2002). The conditions in these environments varied in relative humidities, primary emissions, and urban surface composition, thus covering a wide range of conditions.

2.2 Results

A typical example of our observations is shown in Figure 1. Strong vertical gradients were found for all trace gases. For example, NO_3 levels were often negligible at the ground but reached above 100 ppt aloft. From the numerous nocturnal observations a consistent picture of the chemistry in the NBL emerged:

- Ozone shows a positive gradient (higher concentrations aloft than at the ground), while NO_2 typically shows a negative gradient (higher concentrations at the ground).
- O_x ($NO_2 + O_3$) shows a much smaller gradient than O_3 and NO_2.
- NO_3 levels are always elevated in the upper part of the NBL and very low near the ground.
- Calculated equilibrium N_2O_5 levels are higher aloft, and in general follow the NO_3 profile.
- HONO shows negative gradients, however the $HONO/NO_2$ ratio is in many cases constant with altitude.
- HCHO shows negative gradients.

3. Modeling studies

We used a 1-dimensional model that subdivides the NBL into 20 boxes, with a log-linear spacing for the data interpretation and various sensitivity studies. The chemical mechanism is based on RACM [*Stockwell et al.*, 1997] and includes direct emissions of VOCs, CO, and NO from various sources. Vertical transport between the boxes is calculated based on a height dependent turbulent exchange coefficient, for which the influence of chemical transformations is explicitly considered, leading to fluxes of reactive trace gases that also depend on the gradients of other reactants [*Hamba*, 1993; *Lenschow*, 1982]. The ground is treated as a reactive surface in the lowest box of the model, using published uptake coefficients [*Jacob*, 2000]. The influence of

the building roofs and walls is considered by an altitude dependent surface to volume ratio and a resistance approach to describe transport to and from the walls.

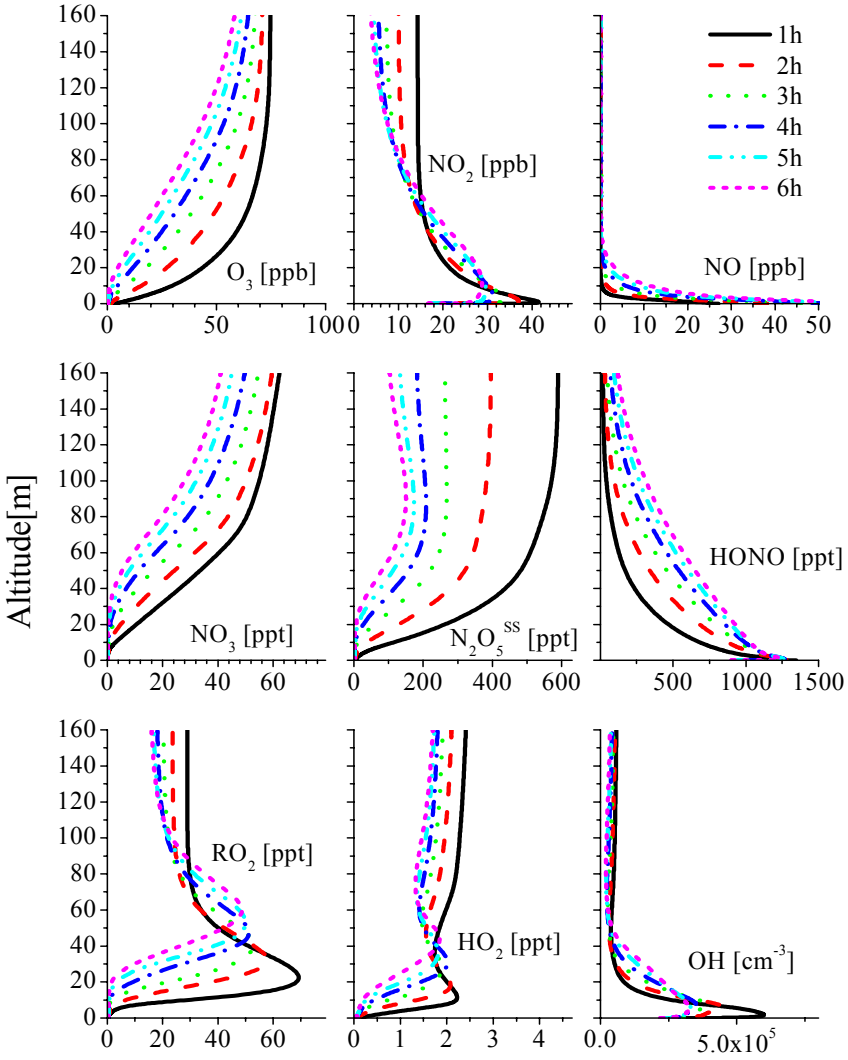

Figure 2: Variation of the mixing ratio profiles for various trace gases in a typical polluted urban NBL.

3.1 Results

To investigate the general behavior of the NBL we performed a number of model studies of the vertical distribution of the most important trace gases, as well as the chemical-transport mechanisms determining these profiles. Figure 2 shows the first six hours of a typical polluted urban area with a weakly stable NBL. The strong vertical variation of all trace gases follows the findings of our field observations, showing the high NO and low O_3 and NO_3 levels at the ground. The upper part of the NBL is characterized by negligible NO and high O_3 and NO_3 mixing ratios. As a consequence, strong variations of RO_x radical levels are predicted by the model, The maximum in the RO_2 profile is caused by an active mixing of NO, O_3, and NO_3 at this altitude, which leads to an accelerated radical chemistry. The maximum of OH at the ground is

caused by the HO_2 + NO reaction. HONO is formed by the heterogeneous conversion on urban surfaces and through direct emissions. The behavior of HONO is similar to that observed in Phoenix (figure 1).

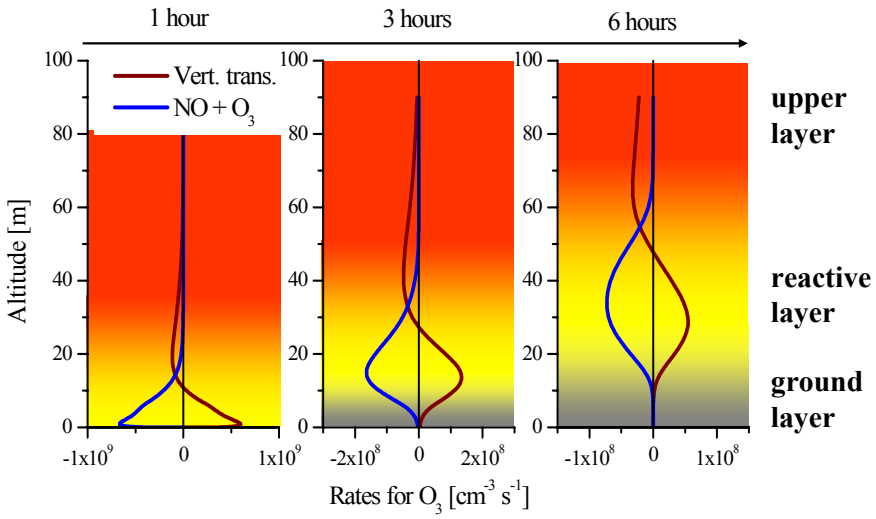

Figure 3: Three layer concept of the urban nocturnal boundary layer. The reactive mixing layer is characterized by the simultaneous presence of NO, O_3, and NO_3, here visualized by the reaction rate of the NO + O_3 reaction. The chemistry in this layer is driven by the vertical mixing of these three species and other radicals.

4. Discussion

Our observations and model studies showed that the emission rate of NO and the vertical stability are the dominant factors determining the vertical trace gas profiles in the NBL. Vertical mixing of various species, such as O_3, NO, NO_2, and N_2O_5 plays an important role in the chemistry in the NBL. To conceptualize our results we have developed a simplified view of the chemistry in the NBL (figure 3). We distinguish three layers in the NBL. The ground layer is dominated by high NO concentrations, leading to low radical levels and very slow chemistry. The upper layer has very low NO, and is thus dominated by NO_3 and O_3 chemistry. In between these two layers a zone forms where RO_2 radicals, O_3, and NO_3 from the upper layer are mixed with NO from the ground layer. In this reactive layer radical chemistry takes place that is very similar to that found during the day, i.e. HO_2 + NO and RO_2 + NO reactions are the dominant radical propagation steps.

An important aspect of nocturnal chemistry is the loss of NO_x and VOC's from traffic emissions. Figure 4 illustrates the vertical variation of the loss rates for the case shown in Figure 2. Loss of VOC proceeds through oxidation by OH, O_3, and NO_3. Because of the vertical distribution of these species and the VOCs, oxidation rates for each oxidant is altitude dependent (figure 4). The total VOC removal rate is higher near the ground, but considerable removal also occurs aloft. The loss of NO_x proceeds predominately through the uptake of NO_2 on urban surfaces and the uptake of N_2O_5 onto the aerosol (figure 4). The latter is more important in the upper part of the NBL, while the NO_2 uptake occurs near the ground.

5. Conclusions

Our field observations and modeling studies show that the chemistry in the NBL is strongly altitude dependent. The combination of chemistry and vertical mixing leads to processes that would be impossible if vertical transport is not considered. In particular, the fast radical chemistry in the reactive layer is driven by the mixing of radicals and NO. This complex structure of the NBL leads to an altitude dependent loss of various pollutants. Urban surfaces, such as walls and roofs contribute to the processing of pollutants and the formation of HONO.

Our results show that a description of nocturnal chemistry omitting vertical mixing is inadequate. Only models that have sufficient vertical resolution in the lowest 100 m of the urban atmosphere will reproduce the chemistry in the urban NBL accurately.

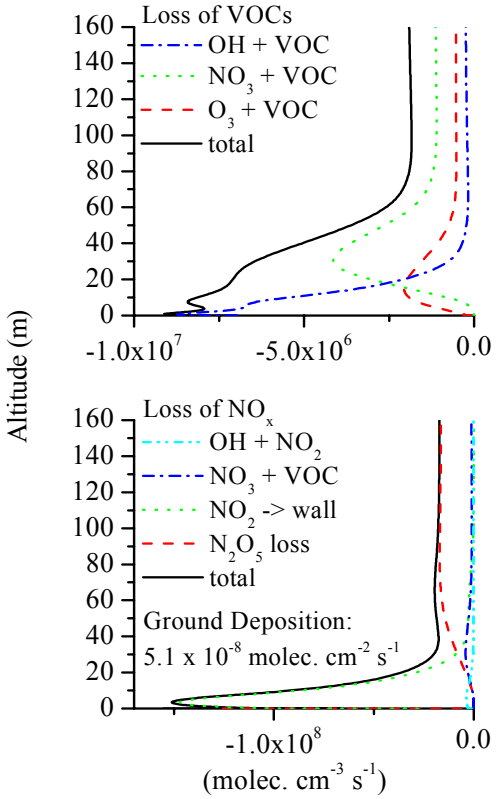

Figure 4: Vertical profiles of different loss processes for NO_x and VOCs. The averaged NO_x removal rate from the NBL is 3.75 ppb/h. The NO_2 uptake on urban surfaces contributes ~50% to the total NO_x loss.

6. References

Alicke, B., et al., OH formation by HONO photolysis during the BERLIOZ experiment, *J. Geophys. Res.*, *108* (D4), doi: 10.1029/2001JD000579, 2003.

Alicke, B., U. Platt, and J. Stutz, Impact of nitrous acid photolysis on the total hydroxyl radical budget during the Limitation of Oxidant Production/Pianura Padana Produzione di Ozono study in Milan, *J. Geophys. Res.*, *107* (D22), doi: 10.1029/2000JD000075, 2002.

Aumont, B., F. Chervier, and S. Laval, Contribution of HONO sources to the $NO_x/HO_x/O_3$ chemistry in the polluted boundary layer, *Atmos. Environ.*, *37* (4), 487-498, 2003.

Bey, I., B. Aumont, and G. Toupance, The nighttime production of OH radicals in the continental troposphere, *Geophys. Res. Lett.*, *24* (9), 1067-1070, 1997.

Geyer, A., B. Alicke, S. Konrad, T. Schmitz, J. Stutz, and U. Platt, Chemistry and oxidation capacity of the nitrate radical in the continental boundary layer near Berlin, *J. Geophys. Res.*, *106* (D8), 8013-8025, 2001.

Hamba, F., A modified K model for chemically reactive species in the planetary boundary layer, *J. Geophys. Res.*, *98* (D3), 5173-5182, 1993.

Jacob, D.J., Heterogeneous chemistry and tropospheric ozone, *Atmos.Environ.*, *34* (12-14), 2131-2159, 2000.

Lenschow, D.H., Reactive trace species in the boundary layer from a micrometeorological perspective, *J. Meteorol. Soc. Japan*, *1*, 60, 1982.

Li, S.-M., K.G. Anlauf, and H.A. Wiebe, Heterogeneous nighttime production and deposition of particle nitrate at a rural site in North America during summer 1988, *J. Geophys. Res.*, *98* (D3), 5139-5158, 1993.

Makar, P.A., H.A. Wiebe, R.M. Staebler, S.M. Li, and K. Anlauf, Measurement and modeling of particle nitrate formation, *J. Geophys. Res.*, *103* (D11), 13095-13110, 1998.

Platt, U., Differential optical absorption spectroscopy (DOAS), *Chem. Anal. Series*, *127*, 27 - 83, 1994.

Riemer, N., H. Vogel, B. Vogel, B. Schell, I. Ackermann, C. Kessler, and H. Hass, Impact of the heterogeneous hydrolysis of N_2O_5 on chemistry and nitrate aerosol formation in the lower troposphere under photosmog conditions, *J. Geophys. Res.*, *108* (D4), 2003.

Stockwell, W.R., F. Kirchner, M. Kuhn, and S. Seefeld, A new mechanism for regional atmospheric chemistry modeling, *J. Geophys. Res.*, *102* (D22), 25847-25879, 1997.

4.1 INFLUENCE OF VERTICAL MIXING ON NOCTURNAL CHEMISTRY IN THE URBAN BOUNDARY LAYER

Jochen Stutz*, Andreas Geyer, and Shuhui Wang
Department of Atmospheric Sciences, University of California Los Angeles

Abstract

Nocturnal chemistry in urban areas can considerably influence the composition of the boundary layer (BL) and therefore determine the conditions at sunrise. Since the trace gas levels in the morning BL influence the photochemistry of the day it is crucial to understand the nocturnal processes. Studying the chemical composition of the nocturnal BL is difficult because of the interplay of homogeneous and heterogeneous chemical processes and weak turbulent mixing. This interaction together with direct emissions of NO and hydrocarbons at the ground can lead to strong vertical gradients of all compounds. This is particularly significant for the chemistry of the main oxidants ozone, and NO_3, which are responsible for the removal of NO_x and various VOC's. It also plays an important role in the formation of daytime OH precursors such as nitrous acid.

Here we present data from a number of recent field studies (SOS 1999, Nashville, TN; TEXAQS 2000, Houston, TX; Phoenix 2001, AZ; etc.) showing the vertical distribution of various trace gases measured by differential optical absorption spectroscopy (DOAS). The measurements show vertical gradients of ozone, NO_2, NO_3, and HONO during many nights. A comparison of the results of the individual campaigns and the results from a one-dimensional chemical box model allows us to compose a picture of the chemistry in the nocturnal boundary layer. Common features are elevated HONO levels at the ground, and high NO_3 levels aloft. Our measurements also allow us to determine the significance of processes such as NO_x and VOC removal, as well as the investigation of several heterogeneous reactions. The implications of our findings for air quality monitoring and the photochemistry of the following day will also be discussed.

1. INTRODUCTION

It has been recognized in recent years that chemical processes in the nocturnal urban and sub-urban boundary layer can considerably impact the composition of the atmosphere and therefore influence the starting conditions for photochemical smog formation during the next morning (see for example [*Bey et al.*, 1997; *Geyer et al.*, 2001; *Platt and Heintz*, 1994; *Wayne et al.*, 1991]). Examples of such nocturnal processes are the removal of NO_x and VOCs by NO_3 and the build-up of HONO which serves as a OH precursor after sunrise.

Many investigations of nocturnal chemistry have relied on a 0-dimensional box model approach. While this approach has been used successfully in the well mixed daytime boundary layer, it can be inaccurate at night for the following reasons:

- Vertical mixing is slower than during the day. Therefore gradients of trace gases are more pronounced at night.
- The vertical mixing of direct emissions, for example of NO and VOCs, is slower than their chemical conversion in the NBL. Their concentrations therefore remain elevated close to the ground.
- Radical chemistry is slower and less efficient since OH concentrations are small. The nitrate radical, which takes over the role as dominant radical species at night, only reacts with unsaturated hydrocarbons, in particular with terpenes.
- Heterogeneous reactions appear to play a more important role, for example the formation of HONO and the uptake of N_2O_5.
- In comparison to the day, the ground offers a much larger surface to volume ratio at night.

Based on these considerations we have adopted a 1-dimensional vertical view of the nocturnal chemistry for both our experiments (Wang et al., Poster P1.1) and our modeling efforts (Geyer et al., Poster P1.16).

In the following manuscript we will present our general findings from a number of field experiments, to give a picture of the typical vertical distribution of trace gases. A 1-dimensional vertical chemical transport model is used to interpret our observations, in particular with respect to nocturnal radical levels and the removal of NO_x.

2. Field Observations

2.1 Experimental

To study the variation of nocturnal chemistry with height we have performed a number of field experiments in recent years. All of the experiments had in common that the vertical trace gas gradients were measured by Differential Optical Absorption Spectroscopy (DOAS) [*Platt*, 1994]. Our DOAS instruments consist of a xenon arc lamp, a coaxial sending/receiving telescope, and a spectrograph-detector system. The light beam is folded once by an array of quartz corner-cube-reflectors that are typically mounted in 1 – 6 km distance.

**Corresponding author address*: Jochen Stutz, University of California Los Angeles, Dept. of Atmospheric Sciences, 7127 Math Sciences Bldg., Los Angeles, CA 90095-1565;
Email: jochen@atmos.ucla.edu

The principle of DOAS is the identification and quantification of trace gases by their narrow band absorption structures. The absorption takes place along the light path. Therefore DOAS measures the concentration averaged over this light path. To measure vertical trace gas gradients we typically mount 2 – 3 reflector arrays at different altitudes and consecutively aim our telescope at the arrays. It is obvious that the DOAS light beam also averages in the vertical and a deconvolution of the height-integrated absorptions has to be performed (see for example Wang et al. P1.1). Typical time resolution for a gradient measurement is ~15 min.

Our field measurements took place in a variety of urban and sub-urban environments in the United States. In Nashville, TN, (SOS 99) and Houston, TX, (TEXAQS 2000) we encountered humid and hot conditions. While the SOS 99 measurements took place in a suburban environment of a city without much industry, the TEXAQS 2000 data was taken in a heavily industrialized area with large direct emissions. In contrast, the conditions during the Phoenix ozone experiment in 2001 (POE 2001) were very dry and the DOAS system was set up in the center of the city (see Wang et al, P1.1 for the POE 2001 results).

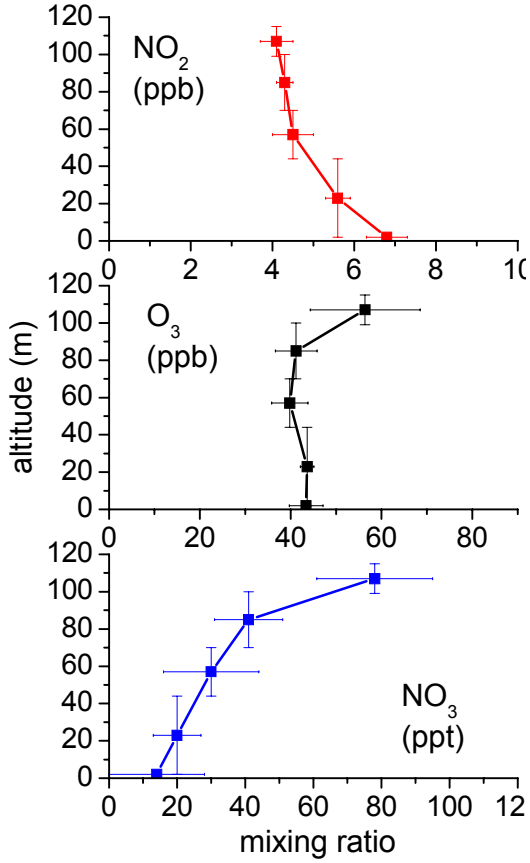

Figure 1: Vertical distribution of NO_2, O_3, and NO_3 on 8/31/00 at 22:58 CST at LaPorte near Houston

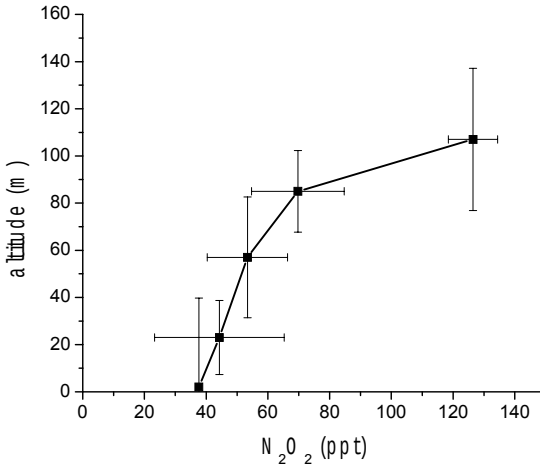

Figure 2: Vertical distribution of the calculated steady state N_2O_5 mixing ratio on 8/31/00 at 22:58 CST at LaPorte.

2.2 *Results*

Figure 1 shows an example of the vertical distribution of O_3, NO_2, and NO_3 on Aug 31, 2254 CST in Houston. The data was taken by two DOAS instruments measuring on a total of 5 light paths. The profiles show a negative gradient of NO_2 (more NO_2 at the ground than aloft) and positive gradients of O_3 and NO_3. We have observed similar vertical distributions in all our field studies (see Wang et al, P1.1). The following summarizes the common features of our observations in urban environments:

- Ozone shows a positive gradient, while NO_2 typically shows a negative gradient.
- O_x (NO_2 + O_3) shows no gradient, or at least a smaller gradient than O_3 and NO_2
- NO_3 shows positive gradients.
- HONO shows negative gradients.
- HCHO shows positive gradients

In addition to our direct observations we are able to calculate the vertical distribution of the steady state N_2O_5 mixing ratio by assuming the N_2O_5 levels are dominated by the NO_2 + NO_3 $\leftrightarrow$ N_2O_5 equilibrium [*Wangberg et al.*, 1997b]. Figure 2 shows the steady state N_2O_5 profile corresponding to the profiles in figure 1. It should be noted that this calculation is only an approximation of the real N_2O_5 mixing ratios since other loss processes of N_2O_5 and temperature effects were not considered here.

3. Modeling studies

The interpretation of our observation is difficult since it requires an accurate quantification of chemistry, micrometeorology, and direct emissions.

We have therefore developed a 1-dimensional model of the nocturnal boundary layer (NBL) that is described in detail by Geyer et al. (P1.16). In short, the model subdivides the NBL into 14 boxes, with a log-

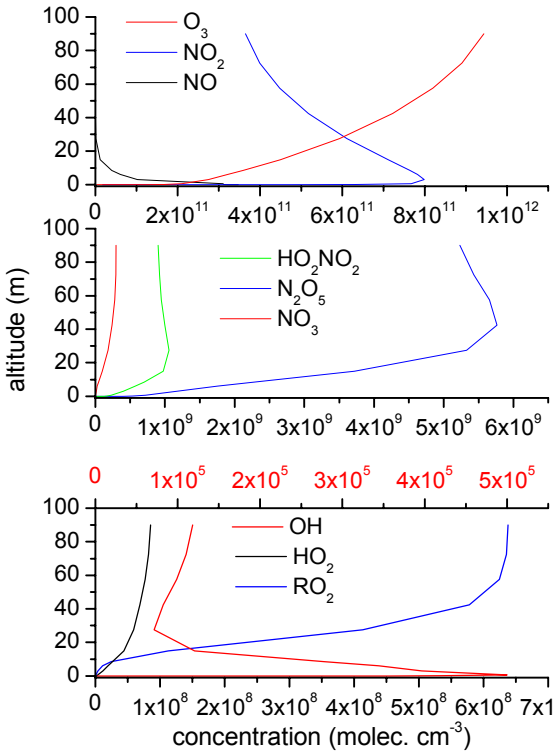

Figure 3: Modeling results after 1 hour for an urban case with an emission of NO of 5×10^{11} molec. s^{-1} at 0.5m height (details of the model are given in Geyer et al., P1.16)

linear spacing. The model contains a chemical mechanism that includes reactions of the NO_x-O_3-NO_3 system, a simplified HO_x/RO_2 reaction scheme, and a small number of VOCs and their degradation pathways representing the more complex VOC mixture found in a city. Vertical transport between the boxes is calculated based on a height dependent turbulent exchange coefficient. Direct emissions of VOCs, CO, and NO at the ground and the lower boxes are also included.

The purpose of the model is to study common features in our observations rather than to simulate the field results in detail. We are specifically interested in studying the height dependence of the removal of NO_x and VOCs, the influence of vertical transport on radical chemistry, and the interaction of NO_x with the ground and other surfaces that lead to the formation of HONO.

3.1 Results

Figure 3 shows the results of a model run after one hour. The model was initialized with a vertically uniform distribution of all trace gases, as is typically observed at the beginning of the night. We chose slightly stable conditions in the NBL, leading to a negligible temperature gradient. The values for NO and CO emissions were chosen to represent a case of an urban or sub-urban environment.

Figure 3 illustrates that the model reproduces the features we have observed in our field studies. In particular, we find a positive gradient of ozone, NO_3, and N_2O_5, while NO_2 and NO show negative gradients.

Figure 3 also shows vertical gradients of the HO_x/RO_2 radical family. While there is currently no experimental data available to verify the vertical distribution of these radicals, the OH concentrations in the lower NBL are in agreement with observations in the field. The large OH, HO_2, and RO_2 gradients are mainly caused by the elevated NO levels close to the ground, which lead to a decrease of the RO_2 lifetime and an accelerated conversion of HO_2 into OH. The latter also seems to explain the very high OH concentrations close to the ground.

3.2 Formation of HO_x radicals

The modeling results (figure 3) show the OH levels increase towards the ground, reaching levels of up to 5×10^5 molec cm^{-3}. This is at first surprising since both ozone and NO_3 levels decrease towards the ground and therefore one would expect that the HO_x formation by NO_3 + terpene reactions and the ozonolysis of VOCs become more inefficient. On the other hand, the levels of VOCs and NO increase towards the ground, which lead to an increased RO_2/HO_2 to OH conversion.

We used our model to investigate if the transport of certain species could be responsible for the radical gradients we found in our model. The most obvious species is ozone, which is continuously destroyed in the lowest region of the NBL by NO. The downward flux of ozone keeps the NO_3 concentration close to the ground elevated and forms HO_x through its reaction with VOCs.

Another trace gas effectively transported is N_2O_5. Our model indicates that due to the positive N_2O_5 gradient a net downward flux exists that leads to a net input of NO_3 following the N_2O_5 thermal decomposition. The magnitude of this effect in the urban NBL is discussed by Geyer et al. (P1.16).

Our model shows that there is a net downward flux of RO_2 radicals in the lowest 20 m of the NBL. This flux leads to the formation of HO_2 following the reaction of RO_2 with NO close to the ground.

We also found that HO_2NO_2 serves as an effective reservoir species for HO_2. The concentration peak of OH at the ground is caused by the downward transport of HO_2NO_2 followed by its thermal decomposition and the HO_2 + NO reaction.

Our model suggests that vertical transport of radicals and radical reservoir species form effective mechanisms to introduce radicals to the lower part of the NBL.

3.3 NO_x loss in the NBL

One of the most important aspects of nocturnal chemistry is the loss of NO_x through different processes. The quantification of these processes is difficult since they are altitude dependent (see figure 4). We used our model to determine the role of different NO_x loss processes:

Deposition of NO_2 is relatively unimportant in our case. It should however be noted that the model uses

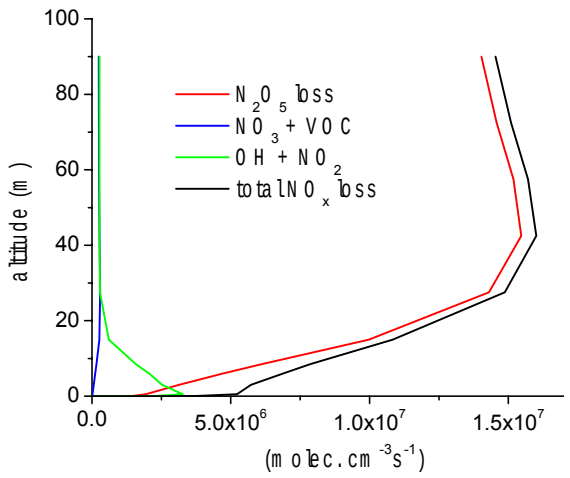

Figure 4: Modeled NO_x removal processes for an urban case (see also figure 3)

the geometrical surface of the ground and this effect is therefore underestimated.

The reactions of NO_3 radicals with VOCs lead to a removal of NO_x. Since we only included α-pinene and isoprene this pathway may also be underestimated in our calculations. One also has to consider that only a part of the nitrogen involved in the reaction is permanently removed. The oxidation of α-pinene by NO_3, for example, releases 80% of the NO_3 back into NO_2 [*Wangberg et al.*, 1997a]. To simplify our calculations we assumed that only ~30% of the NO_3 lost by VOC reactions leads to a removal of NO_x.

The OH + NO_2 reaction is the most important loss process during the day. It appears to be clear today that OH radicals are also present in the NBL and that this pathway can lead to a NO_x removal. Using the OH radical concentration predicted by our model, we found that this mechanism can be important in the lowest part of the atmosphere (figure 4).

The most important NO_x loss mechanism in our model is the hydrolysis of N_2O_5 (figure 4). In our model the homogeneous reaction of N_2O_5 with water was considered according to [*DeMore et al.*, 1997]. The heterogeneous uptake of N_2O_5 was determined by assuming a reactive uptake coefficient of 0.05 [*DeMore et al.*, 1997; *Sander et al.*, 2000] and a height independent aerosol surface-to volume ratio of $400 \mu m^2 cm^{-3}$. Figure 4 shows that the N_2O_5 hydrolysis is by far the most important loss mechanism and that it is very height dependent. The model also clearly shows that the majority of the removal occurs above 10m height, where the NO_3 and N_2O_5 levels are higher. The total NO_x removal in the lowest 100m calculated by our model is 1.5×10^{11} molec. s^{-1}, which is equivalent to ~30% of the emitted NO_x during the night.

4. Conclusions

Both our field observations and our modeling study show that the chemistry in the NBL is strongly altitude dependent. We have shown that the removal of NO_x occurs predominately in the upper part of the NBL. This yields a picture of nocturnal NO_x chemistry, where NO emitted at the ground is mixed upwards and converted to NO_2 by its reaction with ozone. After further upwards transport it is converted into N_2O_5 and removed through hydrolysis, predominately on surfaces. Our model also shows that the concentrations as well as the chemistry of radicals change with height. We have identified a number of reservoir species that lead to a net downward transport of radicals.

It is clear from our results that a description of nocturnal chemistry omitting vertical mixing is insufficient.

5. References

Bey, I., B. Aumont, and G. Toupance, The nighttime production of OH radicals in the continental troposphere, *Geophys Res Lett*, *24* (9), 1067-1070, 1997.

DeMore, W.B., S.P. Sander, D.M. Golden, R.F. Hampson, M.J. Kurylo, C.J. Howard, A.R. Ravishankara, C.E. Colc, and M.J. Molina, *Chemical kinetics and photochemical data for use in stratospheric modeling*, 1997.

Geyer, A., B. Alicke, S. Konrad, T. Schmitz, J. Stutz, and U. Platt, Chemistry and oxidation capacity of the nitrate radical in the continental boundary layer near Berlin, *J Geophys Res-Atmos*, *106* (D8), 8013-8025, 2001.

Platt, U., Differential optical absorption spectroscopy (DOAS), *Chem. Anal. Series*, *127*, 27 - 83, 1994.

Platt, U., and F. Heintz, Nitrate Radicals in Tropospheric Chemistry, *Isr J Chem*, *34* (3-4), 289-300, 1994.

Sander, S.P., R.R. Friedl, W.B. DeMore, A.R. Ravishankara, D.M. Golden, C.E. Kolb, M.J. Kurylo, R.F. Hampson, R.E. Huie, M.J. Molina, and G.K. Moortgat, Chemical Kinetics and Photochemical Data for Use in Stratospheric Modeling, Supplement to Evaluation 12: Update of Key Reactions, Evaluation Number 13, JPL, Pasadena, CA, 2000.

Wangberg, I., I. Barnes, and K.H. Becker, Product and mechanistic study of the reaction of NO3 radicals with alpha-pinene, *Environ Sci Technol*, *31* (7), 2130-2135, 1997a.

Wangberg, I., T. Etzkorn, I. Barnes, U. Platt, and K.H. Becker, Absolute determination of the temperature behavior of the $NO_2+NO_3+(M)<->N_2O_5+(M)$ equilibrium, *J Phys Chem A*, *101* (50), 9694-9698, 1997b.

Wayne, R.P., I. Barnes, P. Biggs, J.P. Burrows, C.E. Canosa-Mas, J. Hjorth, G. LeBras, G.K. Moortgat, D. Perner, G. Poulet, H. Sidebottom, The nitrate radical: Physics, chemistry, and the atmosphere, *Atmos. Environm.*, *25A*, 1-203, 1991.

P1.1

VERTICAL VARIATION OF NOCTURNAL NO_X CHEMISTRY IN THE URBAN ENVIRONMENT OF PHOENIX

Shuhui Wang[1*], Ralf Ackermann[1], Andreas Geyer[1], J. Christopher Doran[2], William J Shaw[2], Jerome D. Fast[2], Chester W. Spicer[3], Jochen Stutz[1]
[1] Department of Atmospheric Sciences, University of California at Los Angeles, Los Angeles, CA
[2] Pacific Northwest National Laboratory, Richland, WA
[3] Battelle Columbus Operations, Columbus, OH

ABSTRACT

During the Phoenix Sunrise Experiment in June-July, 2001, the vertical distributions of NO_2, HONO, NO_3 and several other trace gases were measured with a long-path differential optical absorption spectroscopy system in the downtown area. Strong vertical gradients of all observed species were observed during the night, clearly showing that nocturnal chemistry in this urban environment is height dependent. The disappearance of the gradients in the morning shows the onset of vertical mixing during the transition of a stable boundary layer to a well-mixed layer. During very stable nights, when NO and VOCs emissions were trapped near the ground, mixing ratios of NO_3 up to 200 ppt were found at 110-140m above the ground. Using this information together with the measurements of NO_2, vertical profiles of N_2O_5 can be derived. In addition, the vertical distribution of HONO and NO_2 allows the investigation of heterogeneous HONO formation process on surfaces and the impact of relative humidity on this process. Clear gradients of HCHO were also observed during most nights with high vertical stabilities, suggesting important direct sources of HCHO. The observations will be compared to results from a 1D chemical box model.

1. INTROCUCTION

Nocturnal chemistry in the urban boundary layer is dominated by reactions of NO_x and their products, such as NO_3 radicals and N_2O_5. Due to the high stability of the nocturnal boundary layer (NBL), surface emissions of NO and VOCs are trapped close to the ground, leading to unique vertical profiles of various chemical species throughout the night. These profiles provide rich information about the complex interaction of chemistry and vertical transport. To study this interaction, the Phoenix Sunrise Experiment was performed in June-July, 2001, during which the vertical distributions of O_3 and nitrogen containing trace gases such as NO_2, HONO and NO_3 were measured continuously with a long-path Differential Optical Absorption Spectroscopy (DOAS) system in the downtown area. In-situ measurements of NO and meteorological parameters were also made during the same period of time. We report here the measurement results and discuss their implications for the vertical variations of nocturnal NO_x chemistry with respect to NO titration, the NO_3-N_2O_5 system, and the HONO formation.

* *Corresponding author address:* Shuhui Wang, Univ. of California at Los Angeles, Los Angeles, CA 90095; e-mail: shw@atmos.ucla.edu.

2. OVERVIEW OF THE MEASUREMENTS

DOAS is a technique that identifies and quantifies trace gases by their distinctive UV-visible narrow band absorption structures in the open atmosphere. The main advantage of DOAS is the absolute quantification of trace species without disturbing the composition of the observed air mass. The quantification is solely based on the measured optical density and the known absorption cross section of the trace gases. In recent years we have expanded the classical long-path DOAS method to allow us to measure vertical distributions of trace gases.

During the 2001 Phoenix Sunrise Experiment, our DOAS instrument was set up on the 39th floor of the BankOne building, the highest skyscraper in downtown Phoenix. The instrument has been described elsewhere [Alicke et al., 2000] and only a short description is given here. Light from a 500W Xe-arc lamp was fed into a 1.5 m double Newtonian telescope which was used to send a highly collimated light beam onto an array of cubecorner prisms (retroreflectors) and to collect the reflected light. The retroreflectors were mounted on the roofs of three buildings at ~ 3.3 km distance (see figure 1). Since the three retroreflector arrays were located at different heights (see table 1), the average concentrations of trace gases along each light path were monitored by alternating the aiming direction of the telescope periodically. The schematic diagram of the light paths is shown in figure 1.

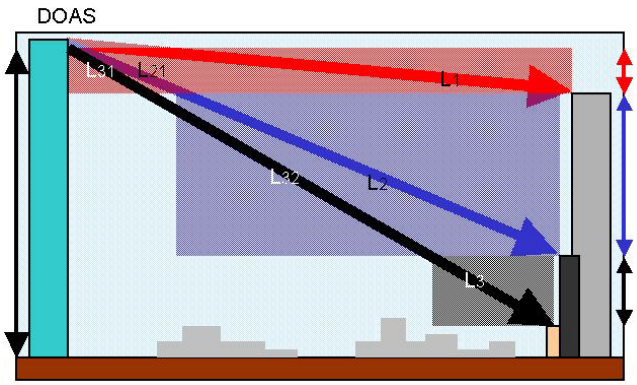

Figure 1. Schematics of the DOAS light paths and the definition of air boxes

In order to determine vertical profiles, the mixing ratio of each species at different altitudes must be derived. For this purpose, the concept of an "air box" was introduced, as shown in figure 1. Using the following equations the average mixing ratio in each air box (C_i) was calculated from the average mixing ratio along each light path (S_i). All the parameters needed for the calculation are listed in table 1. Due to the error propagation in this calculation, the lower level has larger errors and higher detection limits (table 2).

$$C_1 = S_1$$

$$C_2 = (S_2*L_2 + S_2*L_{21} - C_1*L_{21}) / L_2$$

$$C_3 = (S_3*L_3 + S_3*L_{31} + S_3*L_{32} - C_1*L_{31} - C_2*L_{32}) / L_3$$

Building Heights		Light Path Length (km)	
DOAS setup BankOne 39th	~140m		
Upper Retro DEQ Building	~ 110m	Upper	L_1= 3.51
Middle Retro HIL Building	~45m	Middle	L_2+L_{21} =3.29
Lower Retro MLT Building	~10m	Lower	$L_{31}+L_{32}+L_3$ =3.23

Table 1. Light paths and building heights at Phoenix site

	Absorption Structure (nm)	Average Detection Limit (2σ)		
		Upper	Middle	Lower
NO_2	336~371	0.11ppb	0.18 ppb	0.65 ppb
HONO	336~371	0.04 ppb	0.07 ppb	0.25 ppb
HCHO	303~326	0.23 ppb	0.38 ppb	1.4 ppb
SO_2	303~326	0.06 ppb	0.09 ppb	0.34 ppb
O_3	303~326	1.7 ppb	2.8 ppb	10 ppb
NO_3	617~668	3.8ppt	6.5 ppt	20 ppt

Table 2. Detection limits for each measured trace gas

In order to provide detailed meteorological information of the nocturnal boundary layer during the experiment, a number of in-situ measurements of meteorological parameters were performed. Relative humidities and temperatures at different altitudes were measured on top of the DEQ, HIL and MLT buildings. Mixing ratios of NO, as well as the meteorological parameters, were measured at two different floors (16th and 39th) on the BankOne building. Balloon sounding data during most of the nights was also provided.

3. RESULTS AND DISCUSSION

3.1 Vertical Gradients of Trace Gases

In general, our measurements show strong nighttime vertical gradients of all observed trace gases during this two-week field campaign (see, for example, figure 2 and figure 3).

On very stable nights, when NO and VOCs emissions were trapped close to the ground, mixing ratios of up to 200 ppt NO_3 were found at 110-140m height while the mixing ratio in the lower box at 10-45 m level, never reached above 50 ppt.

The clear vertical gradient of HCHO up to 10 ppb/100 m during some of the nights demonstrates the importance of direct emissions from the ground. This shows that photochemical processes may not be the only important source of HCHO.

NO_2 and HONO vertical profiles suggest further investigation of the height dependence of NO_2-to-HONO conversion process.

The disappearance of gradients in the morning coincides with the onset of the vertical mixing during the transition of the stable nocturnal boundary layer to a well-mixed convective layer (figure 2).

3.2 Implications for the Vertical Variation of Nocturnal NOx Chemistry

3.2.1 NO titration

Figure 2 shows the vertical variations of NO_2 and O_3 during the night of June 28-29. In the absence of other major chemical reaction pathways of O_3 and NO_2, NO titration (reaction 1) should be the most important process in determining the gradients of both NO_2 and O_3. NO emissions originating near the ground lead to higher NO_2 and lower O_3 levels at lower altitudes compared to regions aloft. The total amount of O_x, e.g. the sum of NO_2 and O_3, should therefore have no vertical gradient if NO titration is the only major cause for the gradients. The results in figure 2 clearly show the dominant role of NO titration in nocturnal NO_x chemistry.

$$NO + O_3 \rightarrow NO_2 + O_2 \qquad (1)$$

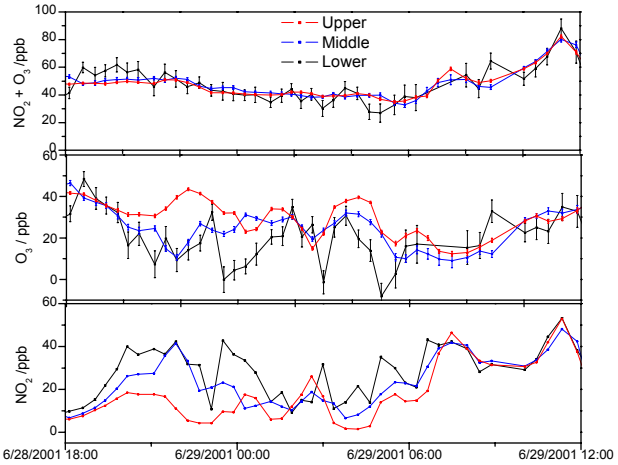

Fig 2. Vertical profiles of NO_2 and O_3 at Phoenix

3.2.2 Vertical profiles of NO_3 and its lifetime

The reaction of NO_2 with O_3 is responsible for the formation of the NO_3 radical (reaction 2), based on which the production rate and the steady state lifetime of NO_3 can be calculated as shown below:

$$NO_2 + O_3 \rightarrow NO_3 + O_2 \quad (2)$$

$k_2=1.2\times10^{-13}e^{-2450/T}$ cm^3s^{-1} [*DeMore et al.*, 1997]

NO_3 production rate = $k_2[NO_2][O_3]$

NO_3 steady state lifetime = $[NO_3]$ / ($k_2[NO_2][O_3]$)

Figure 3 shows the height profiles of the production rate, lifetime as well as the mixing ratio of NO_3 at the night of June 28-29, 2001 in downtown Phoenix. The NO_3 production rate calculated from our NO_2 and O_3 data was higher at lower altitudes. In contrast, the NO_3 lifetime was shorter near the ground. In many cases, both of the NO_3 mixing ratio and the NO_3 lifetime were below our detection limit in the lower air box. At the upper level the NO_3 radical lifetime was on the order of a few minutes.

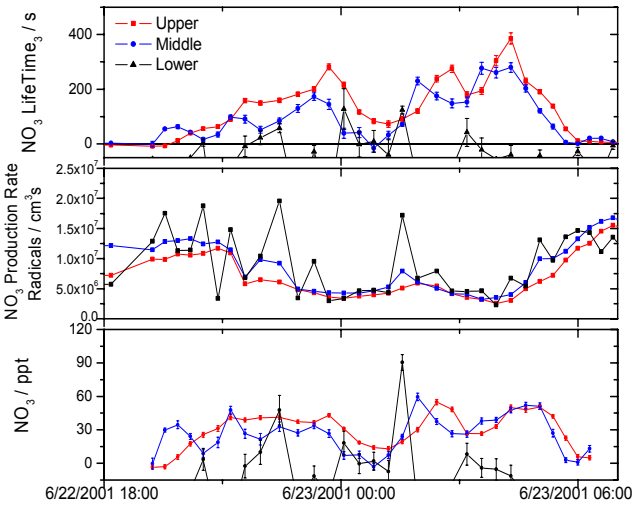

Figure 3. Vertical profiles of NO_3 mixing ratio, NO_3 production rate and NO_3 lifetime

One of the most possible reasons behind these vertical profiles is the direct loss process of NO_3 radical due to reactions with NO and VOCs (reaction 3, 4). Because of their ground based emissions and the limited vertical mixing in the nocturnal boundary layer, mixing ratios of NO and VOCs are generally higher near the ground. And thus a shorter NO_3 lifetime at lower altitude is expected.

$$NO_3 + NO \rightarrow NO_2 + NO_2 \quad (3)$$

$$NO_3 + VOCs \rightarrow HNO_3 + Products \quad (4)$$

The uptake of N_2O_5 on aerosols could be another important loss process of NO_3 radicals (reactions 5 followed by 6). The possible height profile of aerosol density could contribute to the gradients of NO_3 and its lifetime. In addition, temperature inversion, increasing temperature with height, could also lead to a positive gradient of NO_3 [Geyer et al., P1.16, AMS 2003].

$$NO_2 + NO_3 + M \rightarrow N_2O_5 + M \quad (5)$$

$$N_2O_5 + H_2O \rightarrow 2HNO_3 \quad (6)$$

3.2.3 HONO and NO_2

Unlike NO_3 which is only produced by chemical reactions, HONO originates from both direct emissions and heterogeneous formation processes. Laboratory studies [*Kirchstetter et al.*, 1996]) show that HONO-to-NO_x ratio of motor vehicle exhaust in the United States is 0.3% on average. By subtracting the direct emissions, the corrected secondary HONO can be calculated by the following equation.

$$[HONO]_{corr} = [HONO] - 0.003 \times [NO_x]$$

It is currently believed that the major pathway of chemical HONO formation is a heterogeneous reaction mechanism involving NO_2 and H_2O. Experiments and studies show that the formation of HONO is first order in NO_2 [*Kleffmann et al.*, 1998; *Svensson et al.*, 1987]. Thus the formation rate can be described by the following equation in which S and V are the surface area and reaction camber volume respectively [Svensson et al (1987)]. The ratio of corrected HONO to NO_2 acts as an important indicator of this NO_2 to HONO conversion process. During the Phoenix experiment, although both NO_2 and HONO had clear vertical variation (see figure 4), the $HONO_{corr}$ / NO_2 ratio shows no significant vertical gradient. The influence of relative humidity on this process will be further investigated.

$$(\frac{d[HONO]}{dt})_{het} = k_{het} \times \frac{S}{V} \times [NO_2] \times [H_2O] \propto [NO_2] \times R.H.$$

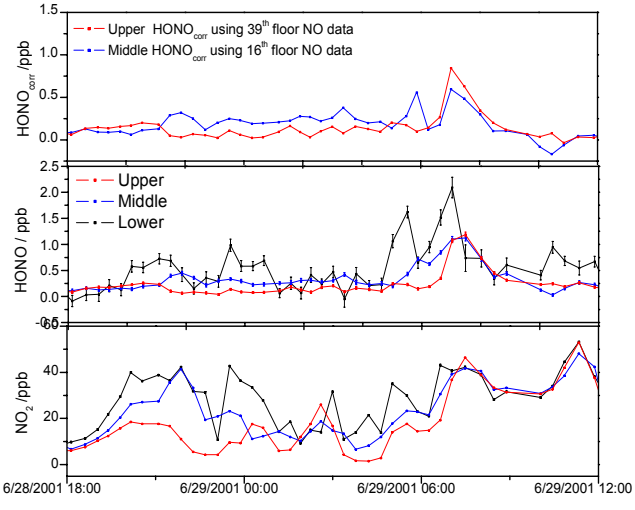

Figure 4. Vertical profiles of NO_2 and HONO

3.2.4 The derivation of N_2O_5 vertical profiles

With the measured mixing ratios of NO_2 and NO_3 as well as the temperature profile, unique vertical profiles of N_2O_5 can be developed.

Due to the formation reaction of N_2O_5 (reaction 5) and its thermal decay, a temperature dependent equilibrium is established between these three species. In the absence of vertical transport and N_2O_5 sinks other than thermal decay (i.e., reaction 6), the steady state mixing ratio of N_2O_5 can be simply determined by the following equation, in which $K_{eq}(T) = 5.5 \times 10^{-27} e^{10724/T}$ cm^3 [*Wangberg et al.*, 1997].

$$[N_2O_5] = K_{eq}(T)\,[NO_2][NO_3]$$

These simplifications are justified by model results by Geyer et al. (P1.16, AMS 2003), which show that vertical transport is only important for the N_2O_5 profile at altitudes below 10m. Neglecting the other sinks of N_2O_5 such as the reaction of N_2O_5 with H_2O and aerosol particles may cause less than 10% overestimation of N_2O_5 at the high temperatures at Phoenix.

In this study, the N_2O_5 vertical profile was calculated with the above mentioned simplified equilibrium and will be improved when the aerosol data becomes available in the future.

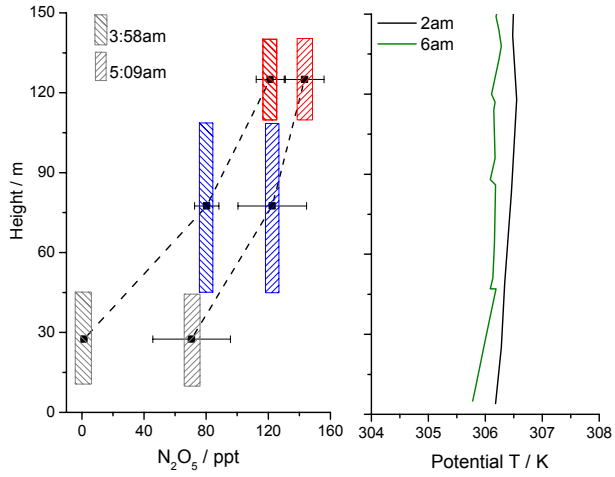

Figure 5. Calculated N_2O_5 profile and sounding data on June 22

Figure 5 shows the results of N_2O_5 profiles during the early morning hours of June 22. The colored bars indicate the height range of the three air boxes. The reported N_2O_5 mixing ratios are the averages in each box. Although this night had a relatively neutral boundary layer as shown in the potential temperature profile, clear vertical gradients of N_2O_5 were observed. During the same period of time, the observation also showed a vertical variation of NO_3 while NO_2 had no detectable gradient. The most likely reason is that surface emissions of NO and VOCs had an impact on the lower level NO_3 and thus also on N_2O_5. A vertical aerosol particle gradient could provide another explanation. This will be compared and discussed with the model results in the next section.

3.3 Comparison With 1D Chemical Transport Model

A 1-dimensional chemical transport model was developed to study the complex interaction of nocturnal NO_x chemistry and the vertical transport in boundary layer (see Geyer et al., P1.16, AMS2003). In general the model predicts distinct vertical profiles of NO_x, NO_3, N_2O_5, O_3 and VOCs under various atmospheric conditions. As observed in Phoenix, NO_3 and O_3 have generally higher mixing ratios at upper altitude while the other trace gases show higher mixing ratios close to the ground.

To learn more about the N_2O_5 profiles shown in figure 5, we performed model simulation of a night with very weak vertical stability assuming initially an even vertical distribution of NO_x and O_3 and allowing a continuous ground emissions of NO and VOCs. The detailed conditions are described by Geyer et al. (see descriptions of run5 in P1.16, AMS2003). After one hour, the NO_3 and N_2O_5 gradients were clearly developed while the vertical NO_2 remained nearly constant. After longer time, the gradient of N_2O_5 decreased. Although the conditions in this model are not exactly the same as the realistic situation in downtown Phoenix, the results, to a certain extent, support the observed N_2O_5 height profile in Phoenix.

4. CONCLUSIONS AND FUTURE WORK

Vertical distributions of various trace gases were measured with a long path DOAS system in downtown Phoenix in June-July, 2001. Strong gradients were observed for all the measured species on nights with a stable nocturnal boundary layer. The observations suggest that the nighttime NO_x chemistry in the urban environment is height dependent. The height profiles disappeared in the presence of vertical mixing after sunrise. The 1D model results are consistent with the measurements in the trend of the vertical variation of these nitrogen containing compounds and O_3.

O_x, the sum of NO_2 and O_3, shows no detectable vertical variation. The opposite vertical gradients of NO_2 and O_3 were therefore caused by titration by NO emitted at the ground.

Both NO_3 concentration and lifetime showed strong vertical gradients. Ground NO and VOCs emissions are believed to be the main reason for the small mixing ratio and short lifetime of NO_3 at low altitude. On stable nights, NO_3 levels of up to 200ppt were observed at 110-140m height.

The HONO formation process by NO_2 conversion was investigated with Phoenix data. It appears that this process is independent of height.

The HCHO gradient suggests the existence of direct emission sources.

The measurement data were compared with model results. Observed N_2O_5 height profiles could be reproduced by the model.

We intend to use the in-situ data of NO, VOCs and aerosols to provide a more detailed picture of the nighttime losses of NO_3 and N_2O_5. The low relative humidities in Phoenix allow the study of the relative humidity dependence of HONO formation processes.

The sources of HCHO direct emission will be investigated in the future.

Acknowledgement

We gratefully acknowledge the support of the Arizona Department of Environmental Quality for establishing the measurement site at downtown Phoenix.

References

Alicke, B., U. Platt, and J. Stutz, Impact of nitrous acid photolysis on the total hydroxyl radical budget during the LOOP/PIPAPO study in Milan, *submitted to J. Geophys. Res.*, 2000.

DeMore, W.B., S.P. Sander, D.M. Golden, R.F. Hampson, M.J. Kurylo, C.J. Howard, A.R. Ravishankara, C.E. Colc, and M.J. Molina, *Chemical kinetics and photochemical data for use in stratospheric modeling*, 1997.

Kirchstetter, T.W., R.A. Harley, and D. Littlejohn, Measurement of Nitrous Acid in Motor Vehicle Exhaust, *Environmental Science & Technology*, *30* (9), 2843-2849, 1996.

Kleffmann, J., K.H. Becker, and P. Wiesen, Heterogeneous NO_2 conversion processes on acid surfaces: possible atmospheric implications, *Atmos. Environm.*, *32*, 2721 - 2729, 1998.

Svensson, R., E. Ljungström, and O. Lindqvist, Kinetics of the reaction between nitrogen dioxide and water vapour, *Atmos. Environ.*, *21*, 1529-1539, 1987.

Wangberg, I., T. Etzkorn, I. Barnes, U. Platt, and K.H. Becker, Absolute determination of the temperature behavior of the $NO_2+NO_3+(M)<->N_2O_5+(M)$ equilibrium, *Journal of Physical Chemistry A*, *101* (50), 9694-9698, 1997.

P1.16 VERTICAL PROFILES OF FREE RADICALS IN THE POLLUTED NOCTURNAL BOUNDARY LAYER: A ONE-DIMENSIONAL MODEL STUDY

Andreas Geyer*, Shuihui Wang, and Jochen Stutz
Department of Atmospheric Sciences, University of Los Angeles, Los Angeles

Abstract. The oxidation of anthropogenic and biogenic VOCs and NO_x in the polluted nighttime boundary layer (NBL) is primarily controlled by NO_3 radicals. NO_3 oxidation can also lead to the formation of secondary peroxy and even hydroxyl radicals. Calculations of the oxidation capacity of the NBL from in-situ or long-path measurements of NO_3 and other radicals are, however, very difficult because the assumption of a well mixed boundary layer is often not valid during night. Since VOCs and NO_x are emitted near the ground while NO_3 radicals are formed at all altitudes, we can expect unique vertical profiles of these species. Recent measurements and model studies show in fact pronounced vertical profiles of NO_3 in the NBL. Here we present results from a 1D chemical box model of the nocturnal radical chemistry. The model includes vertical transport based on measured micrometeorological data, deposition and emission, and a simplified NO_3 and RO_x chemistry module. The model reproduced vertical profiles of NO_3, NO_2, and O_3 observed near Houston, where up to 180 ppt NO_3 at the top of the NBL and 40 ppt at the ground were found. It was found that vertical transport cannot be neglected at night. At certain altitudes, vertical transport of NO_3 even is a more important NO_3 source than its chemical production. The results also show that steady state calculations so far used in the investigation of NO_3 and N_2O_5 chemistry are not representative in all cases. The model predicts high values of OH radicals close to the ground which are caused by downward transport of RO_2, formed by the reaction of NO_3 + VOCs in heights above 10 m, towards the ground, where RO_2 is converted into HO_2 and OH by the emissions of NO. The dependence of the nocturnal radical chemistry on vertical stability, NO, and VOC emission fluxes will be discussed.

1 INTRODUCTION

Nocturnal atmospheric chemistry and physics play a crucial role in the conversion and removal of air pollutants such as nitrogen oxides and VOCs. Because of missing solar radiation, trace gases follow different pathways (both chemically and physically) in the nocturnal boundary layer (NBL) than during day in the convective boundary layer (CBL). The convective conditions are suppressed by radiative cooling of the surface generating stable vertical stratification. Consequently, vertical turbulent transport produced by wind shear is often reduced by negative buoyancy [*Arya*, 1988; *Rao and Snodgrass*, 1979]. Trace gases emitted near the surface will therefore accumulate close to the ground leading directly and indirectly to strong vertical gradients of a number of species. Because of higher vertical stability during night, vertical transport is a key component determining the concentration levels and height profiles of many trace gases. Recently it became clear that vertical transport and chemical conversion cannot be separated from each other in the NBL [*Galmarini et al.*, 1997].

**Corresponding author address*: Andreas Geyer, University of California Los Angeles, Dept. of Atmospheric Sciences, 7127 Math Sciences Bldg., Los Angeles, CA 90095-1565;
Email: andreas@atmos.ucla.edu

Photolytic reactions, which are the driving force of atmospheric chemistry during daytime hours, are unimportant during night. As a consequence the free radical pool is modified: the NO_3 radical, which is rapidly photolysed during day (e.g., [*Magnotta and Johnston*, 1980; *Wayne et al.*, 1991]), replaces the OH radical, which is mainly produced by the photolysis of ozone, HONO, or aldehydes (e.g., [*Alicke et al.*, 2002; *Finlayson-Pitts and Pitts*, 2000]). Recently, however, first evidences were found that significant amounts of OH radicals could also be formed during night (e.g., [*Faloona et al.*, 2001; *Geyer et al.*, 2002]). The coupled effects of nocturnal boundary layer chemistry and limited vertical transport suggest unique vertical profiles of a number of species such as NO_3, NO_2, NO, O_3, and OH during nighttime.

Our present knowledge about the origin and development of height profiles of nocturnal key compounds such as NO_3, RO_2, HO_2, and OH is, however, very poor:

Recently, first evidence was found that NO_3 has an unique vertical profile in the NBL [*Aliwell and Jones*, 1998; *Fish et al.*, 1999; *Friedeburg et al.*, 2002; *Povey et al.*, 1998; *Weaver et al.*, 1996]. First reasonably resolved profiles of NO_3 above urban areas were measured by [*Friedeburg et al.*, 2002] and Wang et al. (P1.1, AMS2003) showing a strong increase of the NO_3 concentration up to the height of the NBL followed by a sudden decrease above the NBL. [*Friedeburg et al.*, 2002] found near ground values ($\approx$ 2 ppt) to be up to a factor 60 lower than at the top of the NBL, where 130 ppt were detected..

Height profiles of nocturnal RO_x radicals were not measured up to now. Although there are a number of RO_x models, e.g., [*Bey et al.*, 1997; *Bey et al.*, 2001; *Geyer et al.*, 2002; *Gölz et al.*, 2001; *Harrison et al.*, 1998], to our knowledge vertical transport was not considered in a nighttime RO_x model study so far.

In our poster, we present results from a 1D model to calculate vertical profiles of reactive traces gases (e.g., NO_3, O_3, RO_2, HO_2, OH) in the polluted nocturnal boundary layer. The model includes vertical transport, deposition and emission, and a simplified NO_3 and RO_x chemistry set. The origin of the NO_3 and RO_x profiles was investigated. The role of vertical transport for the vertical profiles of NO_3 and other reactive gases (especially RO_2, HO_2, OH) was quantified.

2 DESCRIPTION OF THE 1D - MODEL

The model is based on a system of one-dimensional transport-kinetics equations (eq. 1), where the rate of

change of the concentration $c(z, t)$ of a trace gas is expressed as the sum of the rate of change by vertical transport ($\frac{\partial}{\partial z}(\mathrm{Diff}(z)\cdot\frac{\partial c}{\partial z})$, based on Fick's second law), the rate of change by chemical reactions (total chemical production rate $P(z,t)$ and loss rate $L(z,t)$), and the emission rate $\Phi(z,t)$:

$$\frac{dc}{dt}=\frac{\partial}{\partial z}(\mathrm{Diff}(z)\cdot\frac{\partial c}{\partial z})+P(z,t)-L(z,t)+\Phi(z,t) \quad (1)$$

Concentration changes by advection are neglected in our model.

The model spans altitudes from the ground up to 100 m subdivided in 14 layers with a log-linear spacing between the layers. It includes an explicit calculation of the vertical exchange of all compounds between neighboring boxes, calculation of the temperature profile, a simplified chemical mechanism of nocturnal NO_x, NO_3, RO_x, O_3, and VOC chemistry, heterogeneous reactions on aerosols, emission of NO from the soil and cars, emission of monoterpenes from the biosphere, and dry deposition on the ground. Because the model is restricted to nighttime conditions, photolysis is not included. Key parameters of the model are its variable vertical mixing strength and the NO and VOC emission rates (as well as emission heights).

2.1 Vertical transport

The concentration change of a trace gas in a box by vertical exchange is calculated using Ficks' second law from the height depending sum of the laminar diffusion coefficient D, which is of the order of 0.1 cm^2/s, and the turbulent (eddy) diffusion coefficients $K(z)$. The calculation of the turbulent diffusion coefficient $K(z)$ is based on an interpolation formula suggested by [*Reichardt*, 1951]. $K(z)$ can reach values of several 10^4 cm^2/s:

$$K(z)=10^4\cdot\kappa\cdot u^*\cdot\frac{zi}{\Phi(\frac{z}{L})}(\frac{z}{zi}-\tanh(\frac{z}{zi})) \quad (cm^2/s), (2)$$

where κ is the von-Karman constant ≈ 0.4, u^* is the surface friction velocity, and z is the height above ground. Thereby, zi is an empiric constant (representing approximately the height, where laminar and turbulent diffusion are of the same value) given by [*Reichardt*, 1951] as $zi=10^{-5}\frac{\sqrt{T}}{u^*}$. The dimensionless correction function $\Phi(\frac{z}{L})$ is a function of the stability parameter, z/L, given by [*Businger et al.*, 1971] (with L being the Monin-Obukhow length).

Because a constant surface friction velocity is assumed the calculation of $K(z)$ is limited to the Prandtl layer covering approximately the first 50 - 100 m of the atmosphere.

The gradient of the potential temperature Θ in the Prandtl layer is calculated from the heat flux H according to an equation presented for example by [*Roedel*, 1992] as:

$$\frac{d\Theta}{dz}=-\frac{H}{c_p\cdot\rho}\cdot\frac{1}{\kappa\cdot u^*\cdot z}\Phi_H(\frac{z}{L}) \quad (3)$$

Here, c_p represents the heat capacity of the air, ρ its density, and $\Phi_H(\frac{z}{L})$ the dimensionless correction function for heat transport published by [*Businger et al.*, 1971]. The actual temperature profile, which can easily be derived from $\frac{d\Theta}{dz}$, is used in the calculation of temperature-dependent kinetic rate-constants within the chemical mechanism.

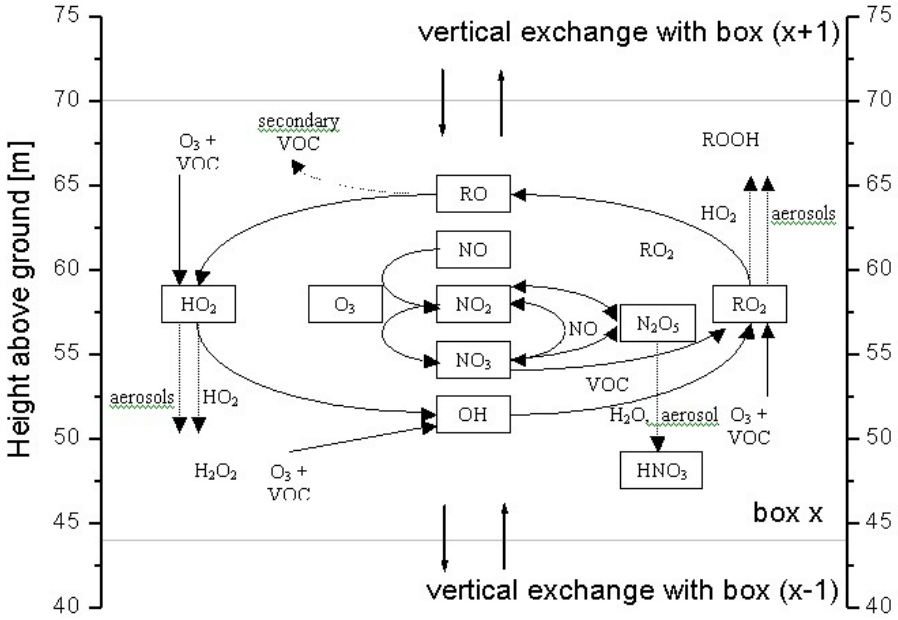

Figure 1. Chemistry and vertical transport of the 1D-boxmodel.

2.2 Chemical mechanism framework

The chemical reaction scheme of the model is shown in Figure 1. The inorganic reaction framework is taken from the Master Chemical Mechanism 3 (MCM3) published online under http://chmlin9.leeds.ac.uk/MCMframe.html. It is limited to three nocturnal key families: nitrogen oxides NO, NO_2, NO_3, N_2O_5, and HNO_3, ozone O_3, and the HO_x radical group OH and HO_2 (and the reservoir species HO_2NO_2) and reactions among each other. Updated rate constants are taken from [*DeMore et al.*, 1997; *Sander et al.*, 2000]. A key chain is the sequential oxidation of NO and NO_2 by O_3 into NO_3. The nitrate radical also reacts with NO back into NO_2. It also establishes a steady state with NO_2 and N_2O_5, which can react with water vapor or water adsorbed on aerosol surfaces. For this process an uptake coefficient of $\gamma(N_2O_5) = 0.05$ was chosen as suggested by the IUPAC subcommittee (June 2002)) for water droplets. Another reaction path of NO_3 is the reaction with unsaturated VOCs.

The oxidation mechanisms of three individual VOCs: α-pinene, isoprene, and propene are included in the model. The oxidation chains initiated by reactions with NO_3, OH, and O_3 generally follow the sequence VOC – RO_2 – RO – HO_2 – OH, which is discussed in detail by e.g., [*Geyer et al.*, 2002]. This sequence is carried by reactions of RO_2 and HO_2 with NO, NO_3, and RO_2. The alkoxy radical RO either reacts very fast with molecular oxygen to HO_2 or forms secondary VOCs by its thermal decay or isomerization. The self-reaction of HO_2 forms H_2O_2, which is an end product in the model. Peroxy radicals can also react on aerosol surfaces. Uptake coefficients of 0.01 and 0.015 were chosen for RO_2 and HO_2, respectively. In addition, ozonolysis can directly form HO_2 and OH radicals [*Paulson and Orlando*, 1996].

2.3 Deposition and emission

Dry deposition to the surface is calculated for reactive species in the lowest box, which is in contact with the ground. The number of molecules of each species in the this box colliding with the soil is calculated from kinetic gas theory and multiplied by the uptake coefficient γ to result in the loss on the ground. The following uptake coefficients were chosen:

$\gamma(O_3) = 0.002$, $\gamma(NO_2) = 0.0015$, $\gamma(NO_3) = 0.0005$, $\gamma(N_2O_5) = 0.05$, $\gamma(HNO_3) = 0.20$, $\gamma(RO_2) = 0.01$, $\gamma(HO_2) = 0.01$, and $\gamma(OH) = 0.005$.

These coefficients are based on the values suggested by the IUPAC subcommittee (June 2002)) for water droplets.

Nighttime emissions of NO and α-pinene are included in the model (see for example [*Fuentes et al.*, 2000; *Guenther et al.*, 2000] for more details about biogenic emissions). NO is emitted from the soil into the lowest box or by cars in 50 cm height. A homogeneous emission of α-pinene (for example from trees) was included between altitudes of 1 to 11 m.

2.4 Variation of input parameters

Height profiles were calculated for different scenarios, uncluding rural and urban environments, weak and strong atmospheric stability, and different temperatures (see Table 1).

3 Results

We discuss here first results of vertical profiles of O_3, NO_2, NO, NO_3, N_2O_5, and α-pinene for an urban case of high NO emissions at moderate vertical stability (typical urban situation, Run 20 from Table 1). Vertical profiles of RO_2, HO_2, and OH are discussed by Stutz et al. (4.2, AMS2003).

Figure 2 shows the vertical profiles of O_3, NO_2, NO, NO_3,

Run #	u* (m/s)	H (W/m^2)	T (K)	H_2O (cm^{-3})	p (mbar)	Aerosol surface ($\mu m^2/cm^3$)	NO_2 initial (ppb)	O_3 inital (ppb)	Isoprene initial (ppb)	Propene initial (ppb)	NO/α-pinene flux ($cm^{-2}s^{-1}$)
1	0.15	-7	290	2×10^{17}	1013	400	10	60	0.2	4	$10^{10}/3 \times 10^9$
2	**0.1**	**-15**	290	2×10^{17}	1013	400	10	60	0.2	4	$10^{10}/3 \times 10^9$
3	**0.25**	**0**	290	2×10^{17}	1013	400	10	60	0.2	4	$10^{10}/3 \times 10^9$
4	0.15	-7	**280**	2×10^{17}	1013	400	10	60	0.2	4	$10^{10}/3 \times 10^9$
5	0.15	-7	**300**	2×10^{17}	1013	400	10	60	0.2	4	$10^{10}/3 \times 10^9$
6	0.15	-7	290	2×10^{17}	1013	**100**	10	60	0.2	4	$10^{10}/3 \times 10^9$
7	0.15	-7	290	2×10^{17}	1013	**700**	10	60	0.2	4	$10^{10}/3 \times 10^9$
8	0.15	-7	290	2×10^{17}	1013	400	**1**	60	0.2	4	$10^{10}/3 \times 10^9$
9	0.15	-7	290	2×10^{17}	1013	400	**60**	60	0.2	4	$10^{10}/3 \times 10^9$
10	0.15	-7	290	2×10^{17}	1013	400	10	**10**	0.2	4	$10^{10}/3 \times 10^9$
11	0.15	-7	290	2×10^{17}	1013	400	10	**100**	0.2	4	$10^{10}/3 \times 10^9$
12	0.15	-7	290	2×10^{17}	1013	400	10	60	**0.05**	**0.4**	$10^{10}/3 \times 10^9$
13	0.15	-7	290	2×10^{17}	1013	400	10	60	**1**	**10**	$10^{10}/3 \times 10^9$
14	0.15	-7	290	2×10^{17}	1013	400	10	60	0.2	4	**$0/3 \times 10^9$**
15	0.15	-7	290	2×10^{17}	1013	400	10	60	0.2	4	**$10^{12}/3 \times 10^9$**
16	0.15	-7	290	2×10^{17}	1013	400	10	60	0.2	4	**$10^{10}/0$**
17	0.15	-7	290	2×10^{17}	1013	400	10	60	0.2	4	**$10^{10}/10^{11}$**
18	0.15	-7	290	2×10^{17}	1013	400	10	60	0.2	4	$10^{10} + 5 \times 10^{10} / 3 \times 10^9$
19	0.15	-7	290	2×10^{17}	1013	400	10	60	0.2	4	$10^{10} + 10^{11} / 3 \times 10^9$
20	0.15	-7	290	2×10^{17}	1013	400	10	60	0.2	4	$10^{10} + 5 \times 10^{11} / 3 \times 10^9$
21	**0.1**	**-15**	290	2×10^{17}	1013	400	10	60	0.2	4	$10^{10} + 5 \times 10^{10} / 3 \times 10^9$
22	**0.1**	**-15**	290	2×10^{17}	1013	400	10	60	0.2	4	$10^{10} + 10^{11} / 3 \times 10^9$
23	**0.1**	**-15**	290	2×10^{17}	1013	400	10	60	0.2	4	$10^{10} + 5 \times 10^{11} / 3 \times 10^9$

Table 1. Scenarios for 1D model.

N_2O_5, and α-pinene in the first 6 hours after model start. Throughout the night, NO, α-pinene, and NO_2 are increasing because of the NO and α-pinene emissions. As a consequence, O_3, NO_3, and N_2O_5 are decreasing. After 6h, O_3, NO_3, and N_2O_5 reached zero levels near the ground.

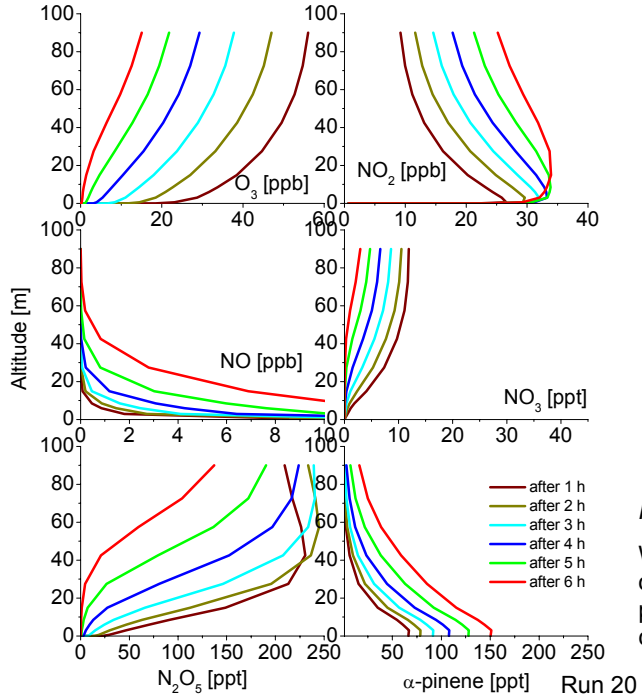

Figure 2. Vertical profiles of O_3, NO_2, NO, NO_3, N_2O_5, and α-pinene for urban scenario.

In short, the high NO emissions are the driving force for the chemistry of this scenario. Vertical mixing transports NO from the lowest 50 cm of the atmosphere to higher altitudes. In this scenario, NO reaches altitudes of 20 m after 1 h. In this NO enriched layer, NO reacts with O_3 to NO_2 resulting in a decrease of O_3 and an increase of NO_2 towards the ground. Vertical mixing transports a major part of the O_3 from altitudes above 20 m into the NO layer while NO_2 is transported out of this layer. This transport constitutes the main source of O_3 and the main sink of NO_2 below 20 m.

Vertical transport also plays a major role for the NO_3-N_2O_5 system (Figure 3): The chemical production rate of NO_3 is relatively constant with height. Its chemical sinks, however, are strongly depending on the altitude: The reaction with NO is the major sink of NO_3 below 15 m while loss of N_2O_5 on aerosols is the major (indirect) sink above this altitude. Reactions with VOCs or peroxy radicals play only a minor role in this scenario. Although direct vertical transport of NO_3 is negligible, a major part of N_2O_5 is transported from altitudes above 10 m towards the ground. There, its thermal decay forms about 25 - 50% of the NO_3 radicals (the path from N_2O_5 into NO_3 is favored because of the high loss frequency of NO_3).

Together, chemical processes and vertical transport result in a vertical profile of NO_3 with low, but not negligible, concentrations in the NO enriched surface layer (first 20 m) and higher but almost constant concentrations above this layer.

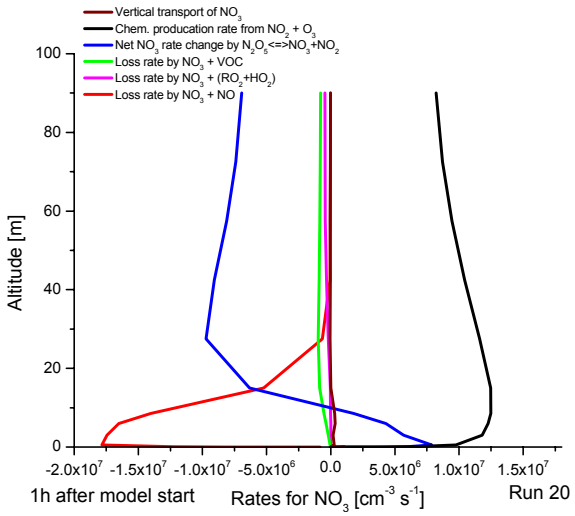

Figure 3. Rate analysis for NO_3 for urban scenario.

We can now quantify the contribution of vertical transport of NO_3 and N_2O_5 to the development of the NO_3 height profile. It was found in this study that the temporal change of N_2O_5 (dN_2O_5/dt) also has to be considered:

$$NO_3 = \frac{k_1\, NO_2\, O_3 + NO_3'v - \frac{dNO_3}{dt} + \frac{k_{2-}(N_2O_5'v - \frac{dN_2O_5}{dt})}{k_{2-} + k_3 Y}}{(k_{2+} - \frac{k_{2-}\, k_{2+}}{k_{2-} + k_3\, Y})\, NO_2 + k_4\, X} \qquad (4)$$

The constants k_1 – k_4 represent the rate constants of the reactions NO_2+O_3, NO_3+NO_2↔N_2O_5, of the sum of other N_2O_5 sinks Y, and other NO_3 sinks X, respectively.

It is apparent from Figure 4 and 5 that vertical transport of N_2O_5 and temporal change dN_2O_5/dt must be considered to calculate correct NO_3 height profiles.

4 The temperature profile and its impact on the NO_3 vertical profile

Because of surface cooling during night, modeled temperatures are generally increasing with height. In the case of very stable atmospheric conditions, our model predicts temperature differences of up to 10 K in the nocturnal boundary layer.

This vertical temperature profile impacts the NO_3 vertical profile significantly. Because of the strong temperature dependence of the thermal decay of N_2O_5, loss of N_2O_5 becomes more and more insignificant for the NO_3 concentration at increasing temperatures [*Geyer and Platt*, 2002] and the NO_3 levels increase. Therefore, the NO_3/N_2O_5 steady state shifts, leading to increasing NO_3 concentrations with altitude as a consequence of the increasing temperatures.

According to our calculations, the increasing temperature is the main cause of the NO_3 vertical profile above altitudes of 20 m.

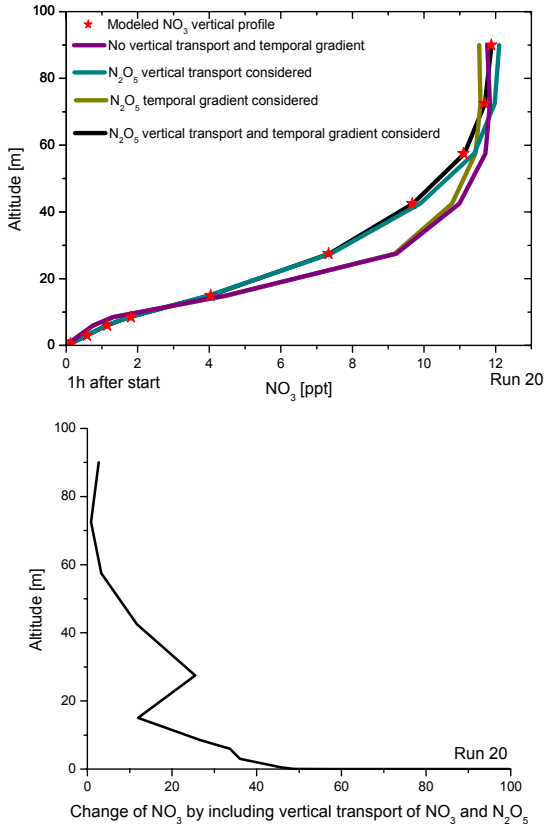

Figure 4 and 5. Contribution of vertical transport and temporal gradient of N_2O_5 to the development of the NO_3 height profile.

5 Conclusions

The following conclusions about the interaction of vertical transport and chemistry can be drawn from our model:

- The most important parameters determining the vertical distribution of all trace gases in the nocturnal boundary layer is the magnitude of vertical stability and the NO and VOC emissions.
- The model predicts NO_3 vertical profiles with increasing NO_3 with altitude. This is in agreement with measurements of the NO_3 profile (see Wang et al., P1.1, AMS2003).
- The vertical profile of NO_3 strongly depends on vertical transport and the temporal change of N_2O_5.
- The main reason for the NO_3 profile below 20 m are NO emissions from biosphere or traffic.
- The main cause for the NO_3 profile above 20 m is the temperature profile during nocturnal inversions.
- The model predicts clear vertical profiles of RO_2 and HO_2 with levels mostly increasing with height (see Stutz et al., 4.2, AMS2003).
- The Model predicts very high nocturnal OH concentrations of some 10^6 cm^{-3} in the first meter of the atmosphere (see Stutz et al., 4.2, AMS2003).

Literature:

Alicke, B., A. Geyer, A. Hofzumahaus, F. Holland, S. Konrad, H.-W. Pätz, J. Schäfer, J. Stutz, A. Volz-Thomas, and U. Platt, OH formation by HONO photolysis during the BERLIOZ experiment, *J. Geophys. Res.*, in press, 2002.

Aliwell, S.R., and R.L. Jones, Measurements of tropospheric NO_3 at midlatitude, *J. Geophys. Res.*, *103* (D5), 5719 - 5727, 1998.

Arya, S.P., *Introduction to Micrometeorology*, Academic Press, Inc., San Diego, 1988.

Bey, I., B. Aumont, and G. Toupance, The nighttime production of OH radicals in the continental troposphere, *Geophys. Res. Lett.*, *24* (9), 1067-70, 1997.

Bey, I., B. Aumont, and G. Toupance, A modelling study of the nighttime radical chemistry in the lower continental troposphere 2. Origin and evolution of HO_x, *J. Geophys. Res.*, *106* (D9), 9991 - 10001, 2001.

Businger, J.A., J.C. Wyngaard, Y. Izumi, and E.F. Bradley, Flux profile relationships in the atmospheric surface layer, *J. Atmos. Sci.*, *28*, 181-189, 1971.

DeMore, W.B., S.P. Sander, D.M. Golden, R.F. Hampson, M.J. Kurylo, C.J. Howard, A.R. Ravishankara, C.E. Colc, and M.J. Molina, Chemical kinetics and photochemical data for use in stratospheric modeling, JPL, Pasadena, 1997.

Faloona, I., D. Tan, W. Brune, J. Hurst, D. Barket, T.L. Couch, P. Shepson, E. Apel, D. Riemer, T. Thornberry, M.A. Carroll, S. Sillman, G.J. Keeler, J. Sagady, D. Hooper, and K. Paterson, Nighttime observations of anomalously high levels of hydroxyl radicals above a deciduous forest canopy, *J. Geophys. Res.*, *106* (D20), 24315-24333, 2001.

Finlayson-Pitts, B.J., and J.N. Pitts, *Chemistry of the upper and lower atmosphere: theory, experiments and applications*, xxii, 969 pp., Academic Press, San Diego, Calif. ; London, 2000.

Fish, D.J., D.E. Shallcross, and R.L. Jones, The vertical distribution of NO_3 in the atmospheric boundary layer, *Atmospheric environment*, *33* (5), 687 - 691, 1999.

Friedeburg, C., T. Wagner, A. Geyer, N. Kaiser, B. Vogel, H. Vogel, and U. Platt, Derivation of tropospheric NO_3 profiles using off-axis-DOAS measurements during sunrise and comparison with simulations, *J. Geophys. Res.*, *in press*, 2002.

Fuentes, J.D., M. Lerdau, R. Atkinson, D. Baldocchi, J.W. Bottenheim, P. Ciccioli, B. Lamb, C. Geron, L. Gu, A. Guenther, T.D. Sharkey, and W.R. Stockwell, Biogenic Hydrocarbons in the atmospheric boundary layer: A review, *Bulletin of the American Meteorological Society*, *81* (7), 1537 - 1575, 2000.

Galmarini, S., P.G. Duynkerke, and J. Vilà-Guerau de Arellano, Evolution of nitrogen oxide chemistry in the nocturnal boundary layer, *J. Appl. Meteo.*, *36* (7), 943 - 957, 1997.

Geyer, A., K. Bächmann, A. Hofzumahaus, F. Holland, S. Konrad, T. Klüpfel, H.W. Pätz, D. Perner, D. Mihelcic, H.J. Schäfer, A. Volz-Thomas, and U. Platt, Nighttime formation of peroxy and hydroxyl radicals during BERLIOZ - Observations and modeling studies, *J. Geophys. Res.*, in press, 2002.

Geyer, A., and U. Platt, The temperature dependence of the NO_3 degradation frequency - a new indicator forthe contribution of NO_3 to VOC oxidation and NO_x removal in the atmosphere, *J. Geophys. Res.*, doi: 10.1029/2001JD001215, 2002.

Gölz, C., J. Senzig, and U. Platt, NO_3-initiated oxidation of biogenic hydrocarbons, *Chemosphere - Global Change Science*, *3* (3), 339-352, 2001.

Guenther, A., C. Geron, T. Pierce, B. Lamb, P. Harley, and R. Fall, Natural emissions of non-methane volatile organic compounds, carbon monoxide, and oxides of nitrogen from North America, *Atmos. Environ.*, *34* (12-14), 2205-2230, 2000.

Harrison, R.M., J.P. Shi, and J.L. Grenfell, Novel nighttime free radical chemistry in severe nitrogen dioxide pollution episodes, *Atmos. Environ.*, *32* (16), 2769 - 2774, 1998.

Magnotta, F., and H.S. Johnston, Photodissociation quantum yields for the NO_3 free radical, *Geophys. Res. Lett.*, *7*, 769-772, 1980.

Paulson, S.E., and J.J. Orlando, The reactions of ozone with alkenes: an important source of HO_x in the boundary layer, *Geophys. Res. Lett.*, *23* (25), 3727-30, 1996.

Povey, I., A. South, A. Kint de Roodenbeke, C. Hill, R. Freshwater, and R. Jones, A broadband lidar for the measurement of tropospheric constituent profiles from the ground, *Journal of Geophysical Research*, *103* (D3), 3369 - 3380, 1998.

Rao, K.S., and H.F. Snodgrass, Some parametrizations of the nocturnal boundary layer, *Bound.-Layer Meteor.*, *17*, 15-28, 1979.

Reichardt, H., Vollstaendige Darstellung der turbulenten Geschwindigkeitsverteilung in glatten Leitungen, *Z. Angew. Math. Mech.*, *31*, 208-219, 1951.

Roedel, W., *Physik unserer Umwelt: Die Atmosphäre*, 457 pp., Springer Verlag, Berlin, 1992.

Sander, S.P., R.R. Friedl, W.B. DeMore, A.R. Ravishankara, D.M. Golden, C.E. Kolb, M.J. Kurylo, R.F. Hampson, R.E. Huie, M.J. Molina, and G.K. Moortgat, Chemical Kinetics and Photochemical Data for Use in Stratospheric Modeling, Supplement to Evaluation 12: Update of Key Reactions, Evaluation Number 13, JPL, Pasadena, CA, 2000.

Wayne, R.P., I. Barnes, P. Biggs, J.P. Burrows, C.E. Canosa-Mas, J. Hjorth, G. Le Bras, G. Moortgat, D. Perner, G. Poulet, G. Restelli, and H. Sidebottom, The nitrate radical: Physics, chemistry, and the atmosphere, *Atmos. Environ.*, *25A*, 1-203, 1991.

Weaver, A., S. Solomon, R.W. Sanders, K. Arpag, and J. Miller, H. L., Atmospheric NO_3 off-axis measurements at sunrise: Estimates of tropospheric NO_3 at 40°N, *J. Geophys. Res.*, *101* (D13), 18,605 - 18,612, 1996.

3.4 VERTICAL MIXING AND CHEMISTRY OVER AN ARID URBAN SITE: FIRST RESULTS FROM SKYSCRAPER OBSERVATIONS MADE DURING THE PHOENIX SUNRISE CAMPAIGN

Carl M. Berkowitz,*[1] Jochen Stutz,[2] Chester W. Spicer,[3] J. Christopher Doran,[1] Jerome D. Fast,[1] and Shuhui Wang[2]
[1]Pacific Northwest National Laboratory, Richland, Washington
[2]Department of Atmospheric Sciences, University of California at Los Angeles, Los Angeles, California
[3]Battelle Columbus Operations, Columbus, Ohio

1. INTRODUCTION

We report here on combined meteorological and chemical trace-gas observations made from two levels of a skyscraper in downtown Phoenix, Arizona. These observations were made as part the U.S. Department of Energy's Phoenix Sunrise Campaign in June 2001. The focus of this campaign was to study the early morning chemical and meteorological transition period as an urban atmosphere develops from a stable to a convective state. The measurements to be presented here were designed to evaluate changes to the concentration of NO_x, VOCs, PAN and other photochemically active species at sunrise concurrent with the onset of mixing and chemistry. The Bank One observations were one component of an extensive set of meteorological observations and supporting air chemistry measurements designed to characterize the vertical structure of the lower urban atmosphere (Figure 1), as described in Doran, et al. (2002). Additional measurements were available above the surface through a series of aircraft observations taken at approximately 300, 500, and 700 m AGL. Thus, the Bank One building provided two intermediate sampling levels within a much larger network of observations.

The motivation for this campaign developed from studies in other urban areas that found peak ozone values above the surface layer appeared to play an important role in governing the surface ozone concentrations in the early morning. The conceptual model for the design of our field campaign hinged on the development of a nocturnal stable layer via cooling at night. Phoenix was selected as a study site because of its heavy pre-dawn traffic, which is a common occurrence as workers schedule their days to avoid high daytime temperatures. As a result of this traffic we expected to find a rich mixture of emissions trapped close to the ground (below 200 m AGL) at sunrise. This rich mixture would be decoupled from air aloft at sunrise, which was expected to have its own unique chemical mix. With the

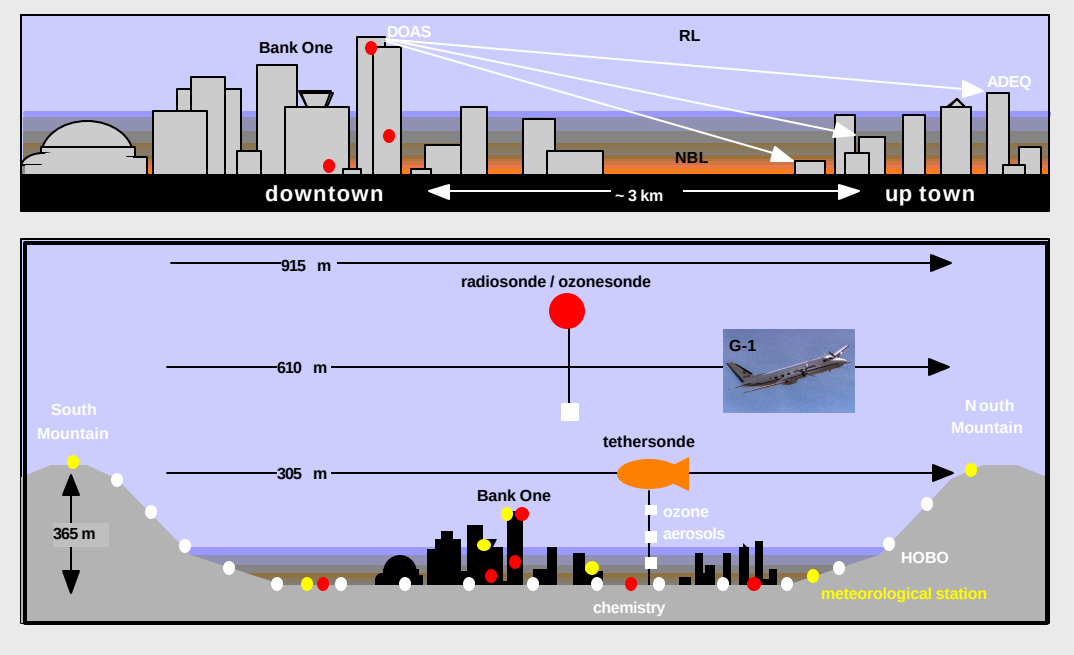

Figure 1. Experimental design of the Phoenix Sunrise Experiment.

*Corresponding author address: Carl M. Berkowitz, Pacific Northwest National Laboratory, Richland, WA 99352; e-mail: carl.berkowitz@pnl.gov

onset of sunrise and surface warming, these two layers would mix together, diluting surface pollutants into a deeper layer, and bringing air aloft down to the surface.

Sampling at two levels of a skyscraper was an ideal way to quantify this process. Measurements were made 24 hours a day, 7 days a week during the period from June 16-30. Observations made during the early morning hours at the 39th floor (~139 m AGL) were expected to be made above the nocturnal stable layer, while measurements made at the 16th floor (at ~73m AGL) would be within this layer at sunrise. We decided not to sample directly at street level so as to avoid contamination from idling vehicles or other very localized sources. As the day developed, we anticipated that observations from the 16th floor would measure changes associated with dilution as the mixed layer became deeper. In contrast, observations from the 39th floor were anticipated to characterize the chemistry above the nocturnal stable layer and the chemistry associated with the subsequent upward mixing of surface emissions.

2. OVERVIEW OF MEASUREMENTS

The observations made from the Bank One Building, and the organizations making these observations, are listed in Table 1.

One instrument unique to this field campaign was a differential optical absorption spectroscopy (DOAS) system. This system uses a technique that identifies and quantifies trace gases with narrow band absorption structures in the near UV and visible wavelength region in the open atmosphere. The advantages of DOAS are the unequivocal and absolute identification of the trace gases, as well as the fact that trace gas concentrations are determined based solely on the absorption cross section. The DOAS system used in Phoenix consisted of a 500 W Xe-arc lamp as a broadband light source. The light from this lamp was fed into a double Newtonian telescope that sent and received a highly collimated light beam that was reflected back via a set of retroreflectors located on adjacent buildings. The spectral recording is made by a spectrograph-detector system connected to the telescope by a quartz fiber mode mixer. To study the vertical distribution of trace gases we mounted the telescope on the 39th floor of the Bank One. The three arrays of retroreflectors were mounted at a distance of 3.4 km at heights of 10 m, 40 m, and 120 m from the tops of other buildings in the uptown of Phoenix (Figure 1, upper panel). We alternated the direction of the telescope between the three arrays, resulting in a trace gas profile every 20 min. The following trace gases were measured (average detection limits, in parentheses, are given as 10^{10} molec. cm^{-3}): O_3 (5.5), NO_2 (0.35), SO_2 (0.18), HCHO (0.73), HONO (0.13), and NO_3 (0.01).

3. FIRST RESULTS

Figure 2 shows the time series of carbon monoxide, NO and ozone observed on the 16th and 39th floors of the Bank One Building, measured on the morning of June 26. The peaks observed between 0700 and 0800 LST were associated with the morning rush hour. Mixing ratios on both the lower and upper flow approached 1 ppm, although somewhat

Table 1. Observations from the Bank One Building

Instrument/Measurement	16th Floor	39th Floor
Aerosol light scattering (b_{scat}) TSI 3563, 3 wavelengths; MRI-1550	BCO	BCO
O_3 (TECO 49)	BCO	BCO
Temperature	BCO	BCO
Dewpoint temp. (GE 1011B)	BCO	BCO
Pressure	PNNL	PNNL
NO/NO_Y ThermoEnvironmental 42S	BCO	BCO
PAN	BCO	BCO
Nitric and nitrous acid (API 365 MS)	BCO	
CO NDIR	BCO	BCO
Formaldehyde	BCO	
VOCs: Automated Canister Sampling System	ANL	ANL
Aerosol Samplers	ASU	
Elemental Aerosols	LUC.	
DOAS		UCLA
NO_3		UAF

Note: ANL = Argonne National Laboratory; ASU = Arizona State University; BCO = Battelle Columbus Operations; LUC = Loyola University at Chicago; PNNL = Pacific Northwest National Laboratory; UAF = University of Alaska at Fairbanks; UCLA = University of California at Los Angeles.

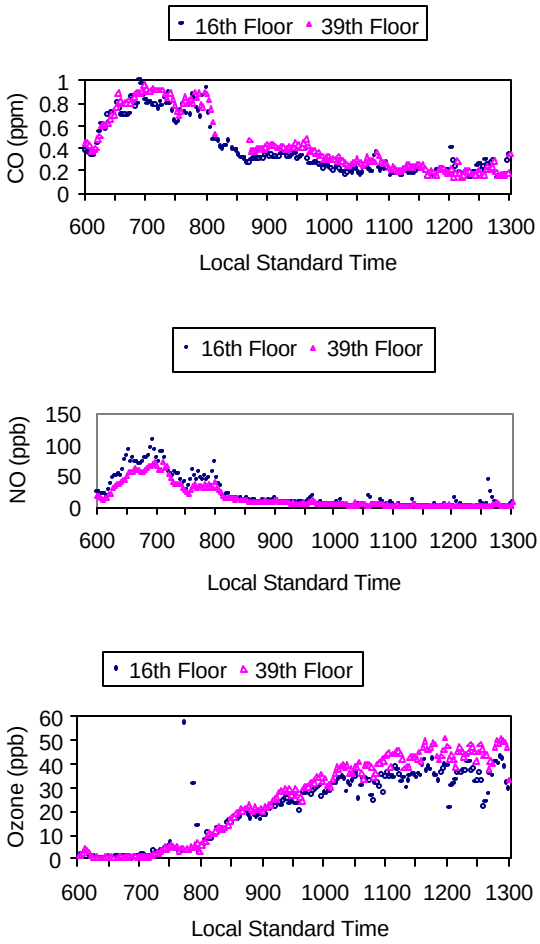

Figure 2. Time series of carbon monoxide, NO, and ozone on the 16th and 39th floor on June 26, 2001 between 0600 and 1300 LST.

surprisingly, the 39th floor detected higher values than those measured at the 16th floor. The greater value of CO aloft was found for both for the maximum value detected (at close to 1 ppm) and some hours after the maximum, between 0800 and 1100 LST. This gradient may be due to the horizontal transport of a CO-enriched air mass that did not mix down to the 16th floor.

NO is also associated with the morning rush hour of June 26. Following this morning spike the values quickly fell to lower levels. In contrast to the pattern previously noted for CO, greater values of NO were observed near the ground. This pattern is consistent with the emissions of NO at the ground by traffic and an upward mixing of these emissions. The maximum NO mixing ratios were observed at close to 0700 LST at both the lower and upper floors. Ozone at this time was measured to be less than 10 ppb, consistent with the reaction sequence $NO + O_3 \Rightarrow NO_2 + O$. We think this reaction, in addition to turbulent mixing, is also part of the explanation for the greater ozone values measured at the 39th floor between 1030 and 1300 LST (Figure 3). There is a significant difference between the mixing ratios at these two levels, with the values aloft typically more than 10 ppb greater than the values near the ground.

Figure 4 shows the mixing ratios measured on the three DOAS light paths before sunrise and during the daytime hours of June 17. All trace gases show strong gradients throughout the night. At around 0730 LST the gradients disappeared and the mixing ratios along the three light paths followed each other closely. The simultaneously measured temperature profiles (Figure 5) also

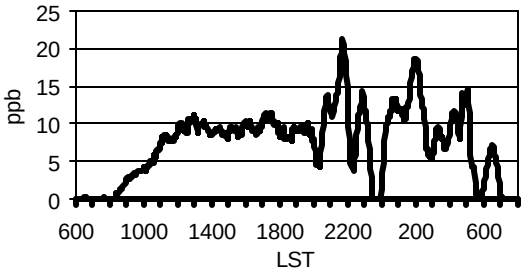

Figure 3. Time series of the difference in ozone at the 39th floors and the 16th floor, June 26, 2001. Positive values imply the values on the 39th floor were greater than those below. Note that the horizontal scale extends from 0600 LST on June 26 to 0800 LST on June 27.

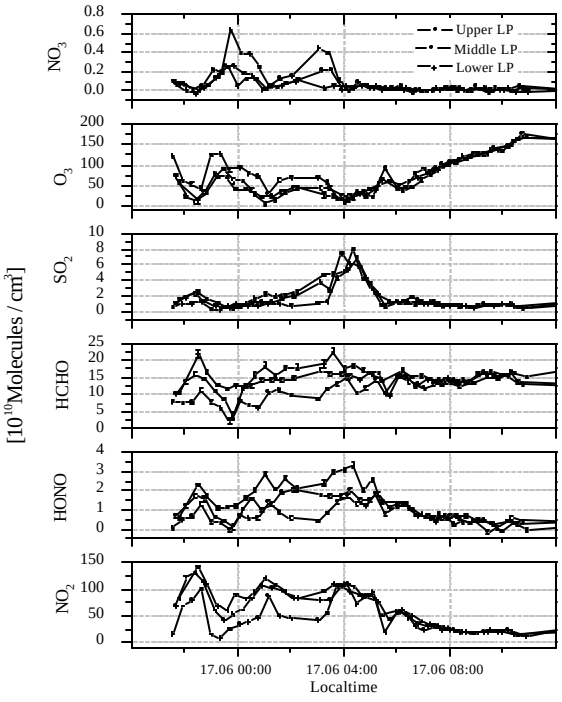

Figure 4. DOAS results for the morning of June 17. Time stamps are dd.mm hh:mm LST.

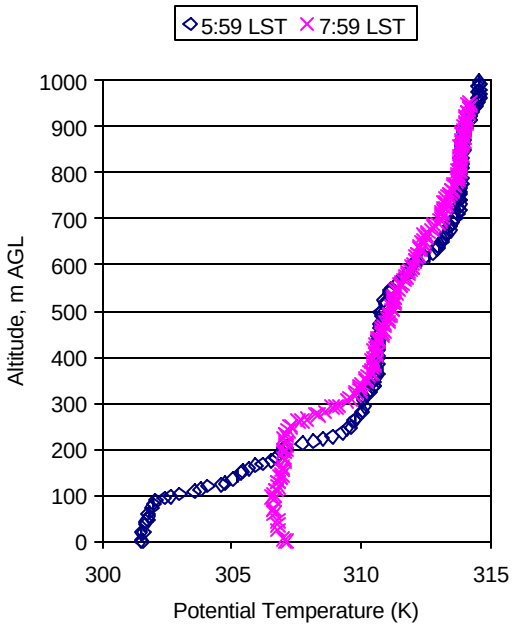

Figure 5. Temperature profile, showing the development of well-mixed layer during the morning of June 17, corresponding to the observations presented in Figure 4. Launch times are shown at the top of the figure.

detected a strong surface inversion before sunrise and then, with the onset of vertical mixing in the lowest 150 m of the atmosphere at 0730 LST, we measured the disappearance of the gradients. The simultaneous measurement of gradients of meteorological and chemical parameters is expected to greatly enhance our understanding of how chemical processes start at sunrise in an urban environment.

4. DISCUSSION AND FUTURE DIRECTIONS

Within the context of urban air quality, the buildup of ozone precursors in nocturnal boundary layers has been recognized for decades but relatively little attention has been given to quantifying how accumulations of ozone precursors in the nocturnal boundary layer affect chemical processes the next morning. Over flat, open terrain the effect on mid-afternoon chemistry may be relatively small but in basins and valleys the effect can be larger. Similarly, in the morning hours before the mixed layer has grown significantly, one can expect that the effects of the nocturnal buildup will be important. For a sufficient description of the vertical distribution of pollutants prior to sunrise, one needs not only the concentrations of the critical species but both their horizontal and vertical spatial distribution.

We have presented a small set of the observations recently made from the Bank One Building in Phoenix, Arizona, during a field campaign that took place last summer. While each day will likely pose its own unique features, the first examination of the data here suggests a) the vertical extent of the boundary layer before sunrise is below 200 m and the concentrations of trace gases are very sensitive to the stability of the atmosphere, as shown by the observed gradients. Capturing these processes with an air quality model will require a very high degree of vertical resolution. b) Typically at night, and sometimes during the day, we would see lower concentrations of ozone at the ground, as expected from the titration of O_3 with NO. On June 26 this difference throughout much of the day was of order 10 to 15 ppb. It is not clear if this is a local effect associated with street canyons, or representative of what actually occurs over the entire city and environs. c) DOAS observations highlight the relationship between the gradient structure of reactive trace gases and meteorology at night.

Much work remains to be done with this data including simply examining the daily values. A much bigger task will be to synthesize the type of results, such as those presented here, with the associated meteorological observations and related chemical measurements made throughout the Phoenix area during this study.

5. REFERENCES

Doran, J. C., C. M. Berkowitz, and J. D. Fast. 2002. "The Phoenix 2001 Field Campaign: Evolution of Oxidants During the Morning Transition Period." To be presented at the Fourth Conference on Atmospheric Chemistry, January 2002, Orlando, Florida.

6. ACKNOWLEDGMENT

We gratefully acknowledge the support of the Arizona Department of Environmental Quality (AzDEQ) in establishment of the measurement site at the downtown Bank One Building. Pacific Northwest National Laboratory is operated for the U.S. Department of Energy by Battelle Memorial Institute under contract DE-AC06-76RLO 1830.

The vertical structure of OH-HO_2-RO_2 chemistry in the nocturnal boundary layer: A one-dimensional model study

Andreas Geyer and Jochen Stutz

Department of Atmospheric Sciences, University of California, Los Angeles, California, USA

Received 7 December 2003; revised 21 April 2004; accepted 21 May 2004; published 17 August 2004.

[1] Elevated OH and peroxy radical levels have recently been observed in the nocturnal boundary layer (NBL). Despite the possible importance of OH for the gas phase and particulate composition, the source of these RO_x radicals at night is currently unclear. To investigate the influence of vertical mixing on nocturnal RO_x chemistry, calculations with a one-dimensional chemical transport model were performed. The model predicts distinct vertical profiles for all RO_x radical species during the night, with a pronounced RO_2 maximum aloft and maxima of HO_2 and OH closer to the ground. We conceptualize our results by distinguishing three chemical regimes in the NBL: (1) In the unreactive ground layer, which only forms at high NO emissions and strong vertical stabilities, OH chemistry is suppressed by high NO levels. (2) The upper layer, located in the upper NBL, is decoupled from the NO emissions at the ground. Ozonolysis of volatile organic compounds (VOCs) leads to the formation of $\sim 10^5$ molecules cm^{-3} of OH. The RO_2 maximum develops in the lower part of the upper layer by the elevated O_3/NO_3 + VOC reaction rates. (3) In the reactive mixing layer, in the height interval between the upper layer and the ground layer, RO_2 and HNO_4 (as HO_2 reservoir) from the upper layer are mixed with NO from the ground layer. The active radical propagation chain leads to distinctive maxima of HO_2 and OH (up to several 10^6 molecules cm^{-3}) in this layer. The OH radicals in the reactive mixing layer can contribute up to 43% to the nocturnal VOC oxidation, illustrating that OH chemistry can be important even at night. Our model simulations show that vertical transport can redistribute RO_x radicals in the NBL, acting as an important radical source in the lowest few meters of the atmosphere. *INDEX TERMS:* 0322 Atmospheric Composition and Structure: Constituent sources and sinks; 0345 Atmospheric Composition and Structure: Pollution—urban and regional (0305); 0365 Atmospheric Composition and Structure: Troposphere—composition and chemistry; 0368 Atmospheric Composition and Structure: Troposphere—constituent transport and chemistry; *KEYWORDS:* nocturnal chemistry, radical chemistry, chemical transport modeling

Citation: Geyer, A., and J. Stutz (2004), The vertical structure of OH-HO_2-RO_2 chemistry in the nocturnal boundary layer: A one-dimensional model study, *J. Geophys. Res.*, *109*, D16301, doi:10.1029/2003JD004425.

1. Introduction

[2] For many years it was accepted that elevated levels of OH and peroxy radicals are present only in the daytime atmosphere. However, recent field experiments have found elevated levels of RO_x radicals (the term RO_x comprises organic peroxy radicals, RO_2, HO_2, and OH) at night in both urban and rural areas [*Mihelcic et al.*, 1993; *Hu and Stedman*, 1995; *Tanner and Eisele*, 1995; *Cantrell et al.*, 1996a, 1996b, 1997; *Monks et al.*, 1996; *Carslaw et al.*, 1997; *George et al.*, 1999; *Kanaya et al.*, 1999; *Faloona et al.*, 2001; *Geyer et al.*, 2003; *Holland et al.*, 2003; *Mihelcic et al.*, 2003; *Ren et al.*, 2003]. Nocturnal OH concentrations exceeding 2×10^6 molecules cm^{-3} have been observed. It is now believed that OH radicals are formed during the night by two major mechanisms: a reaction chain initiated by reactions of NO_3 with volatile organic compounds (VOCs) and the ozonolysis of alkenes [*Daele et al.*, 1995; *Paulson et al.*, 1999; *Paulson and Orlando*, 1996; *Platt et al.*, 1990].

[3] RO_2, produced by the NO_3 + VOC reactions, acts as a precursor to OH through its subsequent oxidation to HO_2 and OH by reactions with NO (and, to a minor extent, NO_3 and RO_2):

$$\mathrm{VOC} \xrightarrow{NO_3} \underset{\text{+stable products}}{RO_2} \xrightarrow{NO(NO_3,RO_2)} \underset{\text{+stable products}}{HO_2} \xrightarrow{NO(RO_2)} \underset{\text{+stable products}}{OH}\ . \quad (1)$$

Positive correlations between $[RO_2]$ and $[NO_3]$ suggest that NO_3 + VOC reactions are the main source for peroxy

0148-0227/04/2003JD004425$09.00

radicals at night [*Cantrell et al.*, 1997; *Geyer et al.*, 2003; *Mihelcic et al.*, 1993]. In the presence of 40 parts per trillion (ppt) of RO_2, as observed by *Mihelcic et al.* [1993], reaction chain (1) could indeed lead to a significant formation of OH. Efficient generation of OH through reaction (1) can occur in the simultaneous presence of NO_3, as a VOC oxidant, and NO, as a fast chain carrier, converting RO_2 into OH [*Geyer et al.*, 2003]. However, the presence of NO_3 and NO in one air mass is unlikely from a purely chemical standpoint, since the two molecules undergo a very fast reaction, forming 2 NO_2 molecules [*Geyer et al.*, 2003]. It is thus often assumed that reaction chain (1) propagates through the much slower RO_2 + NO_3 and RO_2 + RO_2 reactions, and it is therefore less efficient as an OH source. Ozonolysis of unsaturated hydrocarbons is another production path for OH and peroxy radicals at night [*Paulson et al.*, 1997, 1999; *Donahue et al.*, 1998; *Neeb and Moortgat*, 1999]. *Paulson and Orlando* [1996] state that this mechanism can be the dominant OH source at night in forested and suburban areas. In contrast to propagation chain (1), NO is not necessary for the efficient production of OH in this case.

[4] In recent years, nocturnal OH chemistry has been investigated in several box model studies [*Bey et al.*, 1997, 2001; *Harrison et al.*, 1998; *Gölz et al.*, 2001; *Geyer et al.*, 2003]. Most of these studies found that the majority of OH is directly formed by ozonolysis of VOCs. However, these box model calculations were unable to explain the high OH levels observed in several field experiments. The results also showed that reaction chain (1) proceeded slowly, since high NO levels lead to low NO_3 concentrations in the box models.

[5] Studies of nocturnal OH chemistry have thus far relied on a zero-dimensional approach, by either measuring the radicals at a single altitude or applying box models for the interpretation of the data. However, stable vertical stratification in the nocturnal boundary layer (NBL) and weak vertical mixing, combined with direct emissions of NO and VOCs near the ground, can lead to an altitude-dependent chemistry and to pronounced gradients of many trace gases [*Geyer and Stutz*, 2004; *Stutz et al.*, 2004]. The vertical transport caused by the trace gas gradients can have a strong influence on the concentrations of radical precursors and free radicals, including NO, O_3, NO_3, and N_2O_5 [*Geyer and Stutz*, 2004]. A zero-dimensional view of nocturnal chemistry that neglects vertical transport processes may therefore not be appropriate.

[6] In this paper we investigate the influence of vertical mixing on the development of vertical profiles of RO_2, HO_2, and OH and the altitude dependence of OH chemistry in the nocturnal boundary layer by means of a highly resolved one-dimensional chemistry transport model. The radical formation processes in various parts of the NBL will be discussed, and chemical transport mechanisms that lead to the formation of radicals at certain altitudes will be presented. To assess the importance of nocturnal OH, the oxidation of VOCs and NO_2 will be studied.

2. Model Description

[7] This study was performed using an expanded version of the vertically highly resolved one-dimensional (1-D) Nocturnal Chemistry and Transport model (NCAT) [*Geyer and Stutz*, 2004], which includes the Regional Atmospheric Chemistry Mechanism (RACM) [*Stockwell et al.*, 1997]. NCAT is based on a system of 1-D transport kinetics equations, which express the change of the concentration $c_i(z, t)$ of a trace gas i at an altitude z at the time t as

$$\frac{dc_i(z,t)}{dt} = \Psi_i(z,t) + P_i(z,t) - L_i(z,t) + E_i(z,t). \quad (2)$$

[8] Here $\Psi_i(z, t) = -[\partial j_i(z, t)/\partial z]$ is the rate of the concentration change caused by a vertical flux $j_i(z, t)$, $P_i(z, t)$ is the total chemical production rate, $L_i(z, t)$ is the total chemical loss rate, and $E_i(z, t)$ is the emission rate of a compound i. This equation system is solved with a Gear-type solver [*Curtis and Sweetenham*, 1987]. In this study, the model subdivides the lowest 250 m of the nocturnal atmosphere into 20 boxes. Box heights increase logarithmically below 1 m and linearly above 1 m. The variations of trace gas concentrations are calculated for 6 hours following model start. Because the intention of this study is to investigate general features of vertically resolved nocturnal OH-HO_2-RO_2 chemistry, rather than to realistically simulate the evolution of vertical profiles in the atmosphere during the night, the emission rates and meteorological parameters are kept constant throughout the model run.

[9] Vertical fluxes are calculated by a first-order flux-gradient relationship (K model). As discussed by several authors [*Brost et al.*, 1988; *Fitzjarrald and Lenschow*, 1983; *Galmarini et al.*, 1997; *Geyer and Stutz*, 2004; *Hamba*, 1993; *Vilà-Guerau de Arellano et al.*, 1995], chemistry can alter the vertical flux of a species if (1) the concentration of the species is far from the pseudo chemical steady state concentration and (2) the chemical timescale of a reaction of the species is on the order of the turbulence timescale. Under these conditions the net vertical flux of a compound can be calculated by a modified K model [*Geyer and Stutz*, 2004]. In our previous study of the NBL we found that it is sufficient to apply the modified K model for NO [*Geyer and Stutz*, 2004]. The effect of chemistry on the vertical fluxes of all other compounds was found to be small, and therefore the original K model (see K_{inert} of equation (3)) was used. The modified K model was applied to the calculation of the vertical flux of NO by using the following set of equations: Using the definition

$$K_{\text{inert}}(z,t) = \frac{\kappa u^*(t) z}{\Phi_S\left(\frac{z}{L^*}, t\right)}, \quad (3)$$

the flux of NO is expressed by

$$j_{\text{NO}}(z,t) = -K_{\text{inert}}(z,t)\left\{\frac{\partial c_{\text{NO}}(z,t)}{\partial z} + \frac{\partial[P_{\text{NO}}(z,t) - L_{\text{NO}}(z,t)]}{\partial z}\tau_{\text{NO eff}}(z,t)\right\}. \quad (4)$$

Table 1. Variable Parameters of the Model Scenarios

	Characterization	K at 10 m, $m^2\ s^{-1}$	T at 10 m, K	Emission Rate of NO From Cars at 0.1–1 m, molecules $cm^{-3}\ s^{-1}$
Urban base run and sensitivity studies				
1	weak stability/moderate emissions	0.30	290	4×10^9
2	weak stability/low emissions	0.30	290	1×10^9
3	weak stability/high emissions	0.30	290	12×10^9
4	weak stability/very high emissions	0.30	290	30×10^9
5	strong stability/moderate emissions	0.06	290	4×10^9
6	neutral conditions/moderate emissions	1.00	290	4×10^9
7	scenario 1 at low temperatures	0.30	275	4×10^9
8	scenario 1 at high temperatures	0.30	305	4×10^9
Urban case with high stability and traffic emissions				
9	strong stability/high emissions	0.06	290	12×10^9
Rural case				
10	weak stability/moderate emissions	0.30	290	10×10^6

[10] The effective time τ_{ieff} was approximated according to *Hamba* [1987], who used the two-scale direct interaction approximation theory [*Yoshizawa*, 1982]:

$$\tau_{\mathrm{NO\ eff}}(z,t) = \frac{1}{\tau^{-1}_{\mathrm{turbulent}}(z,t) + \sum_{l,m} \left| k_{\mathrm{NO},lm}(c_l + c_m) \right|}. \quad (5)$$

In equation (5), $k_{\mathrm{NO},lm}$ represents the rate constant of a bimolecular reaction with NO. The turbulence timescale $\tau_{\mathrm{turbulent}}(z, t) = z/\kappa u^*(t)$ is on the order of 100 s in the NBL [*Fitzjarrald and Lenschow*, 1983; *Lenschow*, 1981].

[11] The gas phase chemical mechanism RACM contains 77 model species and considers a total of 237 reactions [*Stockwell et al.*, 1997]. The RACM mechanism aggregates the hundreds of VOCs in the real atmosphere into 23 model classes (four alkanes, four alkenes, three biogenics, three aromatics, and nine carbonyls). RACM distinguishes 24 different types of organic peroxy radicals, which are formed by the oxidation of VOCs initiated by NO_3, O_3, and OH. The RO_2 radicals can react with NO, NO_3, and other RO_2 radicals, forming a wide variety of secondary VOCs (mostly carbonyls) as well as HO_2. The hydroperoxy radical is further converted into OH, for example, by reactions with NO. It is important to note that in the case of the OH + VOC reactions, one peroxy radical is formed in RACM; that is, these reactions are neutral in [OH] [*Stockwell et al.*, 1997]. The direct formation of peroxy and OH radicals by ozonolysis [*Paulson and Orlando*, 1996] is also part of the RACM mechanism. In addition to the reactions in RACM we included the gas phase reaction of N_2O_5 with water vapor (first and second order in H_2O) in the NCAT model [*Wahner et al.*, 1998].

[12] In addition to gas phase chemistry, several gases can undergo heterogeneous reactions. Uptake rates on aerosols are calculated for a number of gases, including O_3 ($\gamma = 5 \times 10^{-5}$), NO_2 ($\gamma = 10^{-5}$), HONO ($\gamma = 10^{-4}$), N_2O_5 ($\gamma = 0.044$), HO_2 ($\gamma = 0.1$), NO_3 ($\gamma = 0.0013$), HNO_4 ($\gamma = 0.01$), and HNO_3 ($\gamma = 0.2$), according to the mass transfer equation given by *Fuchs and Sutugin* [1971], assuming a particle diameter of 150 nm. Dry deposition fluxes are calculated from the number of collisions with the ground surface and the appropriate uptake coefficients. Since we assume a flat surface and do not consider the surface of buildings and vegetation, NCAT probably underestimates deposition fluxes.

[13] NO is emitted from the soil (at 10^{10} molecules cm^{-2} in all scenarios) as well as from traffic between 0.1 and 1 m in urban scenarios (Table 1). The traffic NO emission rate of 4×10^9 molecules cm^{-3} in the base run is varied from 1×10^9 to 30×10^9 molecules cm^{-3} in scenarios 2–4. Using the emission ratios measured by *Kurtenbach et al.* [2001, 2002], anthropogenic emissions of VOCs ((alkanes)/[NO] = 0.18, (alkenes)/[NO] = 0.44, (aromatics)/[NO] = 0.13, (carbonyls)/[NO] = 0.06), CO ([CO]/[NO] = 6), NO_2 ($[NO_2]/[NO] = 0.058$), and HONO ([HONO]/[NO] = 0.008) are also considered. Biogenic emissions of monoterpenes (RACM classes API: α-pinene and other cyclic terpenes with one double bond and LIM: *d*-limonene and other cyclic diene-terpenes), at an emission ratio of API/LIM = 2, are included in the model between 1 and 10 m altitude. The API emission rate at 290 K was set to 3×10^6 molecules cm^{-3} in the urban scenarios. In the rural scenario a representative value of 10×10^6 molecules cm^{-3} was chosen (Table 1). Emissions of isoprene are negligible at night [*Guenther et al.*, 1996] and were thus not included in the model runs. Note that the monoterpene emission rate exponentially increases with temperature [*Guenther et al.*, 1993].

[14] The temperature T at 10 m altitude is set to 290 K in most cases, with the exception of scenario 7 (275 K) and scenario 8 (305 K). The eddy diffusivity K at 10 m altitude varied from 0.06 $m^2\ s^{-1}$ in scenario 5 to 1 $m^2\ s^{-1}$ in scenario 6. In all other cases, K is set to 0.3 $m^2\ s^{-1}$ (Table 1). The gradients of K are calculated from micrometeorological parameters (equation (3)). The temperature gradients were calculated according to $d\Theta(z, t)/dz = -[H(z, t)/c_p\rho](1/\kappa u^*(t)z)\Phi_H(z/L^*, t)$ [*Arya*, 1988; *Haugen*, 1973]. Here c_p represents the mass heat capacity of air, ρ represents its density, and $\Phi_H(z/L^*, t)$ is the dimensionless correction factor for heat transport suggested by *Businger et al.* [1971]. In the very stable case of scenario 5 the temperature gradient is $\sim$0.08 K m^{-1} over the lowest 100 m, while the gradient is -0.01 K m^{-1} in the neutrally stable scenario 6. In all other cases a slightly positive temperature gradient of +0.01 K m^{-1} in the lowest 100 m is found.

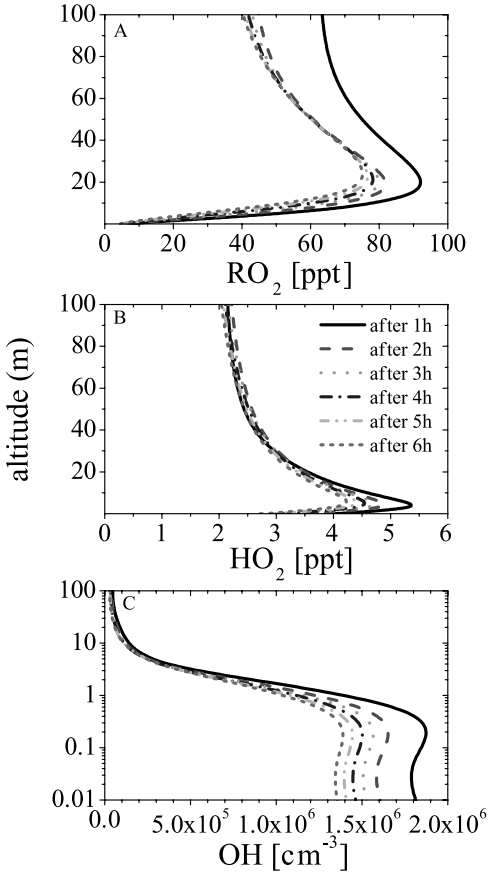

Figure 1. Hourly snapshots of the modeled vertical profiles of [RO_2], [HO_2], and [OH] in the first 6 hours after model start for an urban scenario with moderate NO emission and weak nocturnal stability (scenario 1 in Table 1). Note the logarithmic scale for the vertical profile of [OH].

[15] In the urban scenarios the summertime mixing ratios of trace gases measured by *Kurtenbach et al.* [2002] above the city of Wuppertal, Germany, in the later afternoon are used to initialize the model: CH_4, 1.8 ppm; H_2, 0.5 ppm; CO, 200 ppb; O_3, 100 ppb; NO_2, 10 ppb; alkanes, 22 ppb; alkenes, 4 ppb; aromatics, 35 ppb; carbonyls, 5 ppb; biogenic VOCs, 0.12 ppb; and peroxyacetyl nitrates (PANs), 2 ppb. All other short-lived compounds start at 1 ppt (OH and HO_2 at 10^4 molecules cm^{-3}). For the rural scenarios, data measured by *Konrad et al.* [2003] and *Volz-Thomas et al.* [2003] 50 km NW of Berlin, Germany, were used as initial values: CH_4, 1.8 ppm; H_2, 0.5 ppm; CO, 130 ppb; O_3, 40 ppb; NO_2, 2 ppb; alkanes, 3 ppb; alkenes, 1 ppb aromatics, 0.5 ppb; carbonyls, 4 ppb; biogenic VOCs, 0.3 ppb; and PANs, 0.4 ppb.

3. Vertical Structure of Nocturnal OH-HO_2-RO_2 Chemistry

[16] To provide a detailed analysis of the vertical variation of OH chemistry and its precursors, RO_2 and HO_2, we have chosen an urban scenario with moderate NO emission and weak temperature inversion (scenario 1 in Table 1) as a base case. The model results for this scenario will be discussed in detail in sections 3.1–3.2. In section 3.3 we introduce a description of NBL chemistry based on three vertical layers with distinct characteristics. This three-layer model simplifies the discussion of the sensitivity studies in section 3.5. Equations for the pseudo steady state concentrations of peroxy radicals and OH are derived in section 3.4. Finally, we discuss nocturnal chemistry in a highly polluted urban and a rural environment in sections 3.6 and 3.7. In sections 3.1–3.7 we focus on the lowest 100 m of the NBL.

3.1. Vertical Profiles in a Weakly Stable Urban Case

[17] Figure 1 shows snapshots of the modeled vertical profiles of [RO_2], [HO_2], and [OH] for the first 6 hours after model start of scenario 1. All RO_x radicals show a distinct vertical distribution in the NBL, with pronounced concentration maxima developing at specific altitudes. While the RO_2 maximum is located at ~15 m, OH shows a maximum close to the ground. HO_2 develops a maximum at an altitude of ~5 m, between the maxima of RO_2 and OH. The vertical extents of the maxima decrease from ~20 m in the case of RO_2, to ~1 m in the case of OH. Note that NCAT does not consider the effects of buildings and vegetation on chemistry and vertical transport. This idealization may affect the RO_x levels near the ground and may displace the RO_x maxima.

[18] In scenario 1 the shapes of the RO_x profiles do not change during the night. However, the overall levels of RO_2, HO_2, and OH decrease. After 1 hour a mixing ratio of 90 ppt is predicted for the RO_2 maximum. Close to the ground, RO_2 decreases to 10 ppt. At 100 m altitude the RO_2 mixing ratio reaches 70 ppt. After 2 hours, when isoprene and other substances produced during the previous day have been destroyed and the high mixing ratio of O_3 has decreased, the RO_2 levels drop by roughly 20 ppt. In the following 4 hours the RO_2 concentration slowly continues to decrease. In scenario 1, NO_3-alkene adducts and peroxy radicals formed from the oxidation of ethane and toluene are the most abundant RO_2 species. At the altitude of the HO_2 maximum, HO_2 levels are as high as 5.4 ppt after the first hour. They decrease to <3 ppt directly above the ground. At 100 m, [HO_2] is ~2 ppt. After 6 hours the HO_2 maximum has decreased to 4.5 ppt. While after 1 hour OH levels are 5×10^4 molecules cm^{-3}above 20 m, [OH] reaches a maximum concentration of 1.8×10^6 molecules cm^{-3} in the lowest meter of the NBL. After 6 hours the OH maximum has decreased to $<1.4 \times 10^6$ molecules cm^{-3}.

[19] The interpretation of the vertical profiles of the peroxy radicals and OH requires the analysis of the vertical distribution of their individual production and loss paths. These rates depend on the vertical concentration profiles of NO, O_3, NO_2, NO_3, and VOCs. Figure 2 shows hourly snapshots of the vertical profiles of [NO], [O_3], [NO_2], [NO_3], and the two RACM VOC classes, OLI (internal alkenes) and API (α-pinene and other cyclic terpenes with one double bond).

[20] After 1 hour, NO reveals a strong negative gradient, with levels of 2.5 ppb in the lowest meter and <1 ppt above 10 m. The extent of the layer with high [NO] slowly grows throughout the night, and the level of NO at the ground increases. The NO profile is caused by its fast reaction with O_3 during the upward transport from its emission height. [O_3] shows a weak positive gradient. After 1 hour the

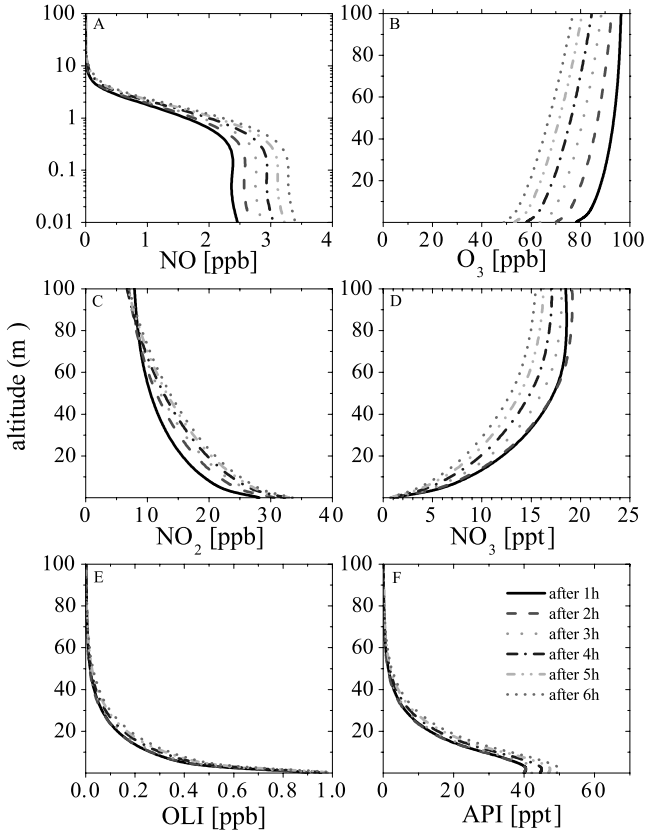

Figure 2. Hourly snapshots of the modeled vertical profiles of [NO], [O_3], [NO_2], [NO_3], and the RACM VOC classes OLI and API in the first 6 hours after nightfall for scenario 1. Note the logarithmic scale for the vertical profile of [NO].

initially uniform O_3 mixing ratio of 100 ppb is reduced to 96 ppb at 100 m altitude, while <80 ppb remain directly above the ground. O_3 levels are reduced by 20–30 ppb after 6 hours. The ozone loss is predominantly caused by titration with NO. Deposition and reactions with VOCs play a minor role. Because of the fast reaction rate of NO and O_3 near the ground, NO_2 develops a negative gradient in the NBL. After 1 hour the mixing ratio of NO_2 is 28 ppb in the lowest meter, while the initial 10 ppb are still present at 100 m altitude. During the night the NO_2 levels slowly increase. The model also predicts a strong positive gradient of [NO_3], with 1 hour NO_3 mixing ratios decreasing from 18 ppt above 50 m to <2 ppt in the lowest meter. After 6 hours NO_3 levels are reduced by ~25%. The NO_3 profile is caused by the reaction of NO_3 with NO in the lower part of the NBL.

[21] In summary, the slow upward transport of NO emitted near the ground and the simultaneously occurring chemistry, in particular, the reactions of NO with O_3 and NO_3, control the vertical structure of the chemistry of NO_x, NO_3, and VOCs. In the case of NO_2 and O_3, dry deposition is also significant. Vertical transport of N_2O_5 can play an important role and is often the main source of NO_3 radicals near the ground [*Geyer and Stutz*, 2004]. The two parameters controlling the shape of the various profiles are the NO emission rate and the vertical stability. In general, higher emissions and stronger stabilities will lead to stronger gradients. For a more detailed discussion of the development of the vertical profiles of nitrogen oxides and O_3, refer to *Geyer and Stutz* [2004].

[22] The different VOC classes included in RACM develop specific vertical profiles in the NBL depending on their lifetime and the dominant oxidant and its vertical profile. All VOCs show a negative concentration gradient because they are emitted or are predominantly chemically formed in the lowest 10 m. Alkanes and aromatics, which have a long lifetime and can be well mixed, show only a very weak negative gradient during the night. Similarly, carbonyls develop a very weak negative gradient. The concentrations of these long-lived species slowly increase during the night because their emission rate is higher than their oxidation rate. Alkenes and monoterpenes have a relatively short lifetime because of their reactions with NO_3 and O_3. Consequently, this group develops strong negative gradients and can reach steady state during the night. Figure 2 shows the vertical profiles of the RACM classes OLI and API as examples for these VOC groups. While [OLI] is as high as 1 ppb in the lowest meter, its concentration is negligible above ~80 m. Similarly, [API] is ~50 ppt at its emission heights (1–10 m) but does not reach altitudes above 70 m. Other compounds, such as CO, H_2O_2, and HNO_3, develop weak negative gradients because they are either emitted (CO) or are chemically produced near the ground and only slowly transported upward. [CO] in the lowest meter increases from 300 to 500 ppb in the first 6 hours of the night. Similarly, [H_2O_2] levels grow from 20 to 50 ppt, and [HNO_3] increases from 0.5 to 3 ppb near the ground. HNO_4 develops a vertical profile similar to that of HO_2. Its mixing ratio is as high as 130 ppt a few meters above the ground.

3.2. Altitude Dependence of RO_x Chemistry in the NBL

[23] In this section we investigate the origin of the nocturnal RO_x profiles shown in Figure 1 for the weakly stable urban case. In particular, the cause of the pronounced concentration maxima at specific altitudes is discussed.

[24] Figure 3 shows the vertical profiles of the various formation, destruction, and vertical transport rates of RO_2, HO_2, and OH in scenario 1, 3 hours after model start. The nomenclature of the rates follows that used in equation (2): P_{A-B+C} is a production rate of compound A due to the reaction $B + C$, L_{A-D} is a loss rate of compound A due to reaction with D, and Ψ_A is the rate of concentration change of compound A due to vertical transport.

3.2.1. RO_2 Radicals

[25] The main chemical source for RO_2 radicals during the early night is the reaction of unsaturated VOCs with NO_3 followed by O_2 addition, forming nitratoalkylperoxy radicals. The reaction of NO_3 with internal alkenes dominates in scenario 1 (60%), followed by the reaction with monoterpenes (20%). Terminal alkenes and dienes contribute another 15%. The product of the positive NO_3 and negative VOC gradients (Figures 2d–2f) causes a broad maximum of $P_{RO2-NO3+VOCs}$ of $\sim 10^7$ molecules cm^{-3} s^{-1} in the lowest 30 m. The production rate slowly decreases with altitude to 2×10^6 molecules cm^{-3} s^{-1} at 100 m and 5×10^6 molecules cm^{-3} s^{-1} at the ground. Ozonolysis of alkenes (with a contribution of internal alkenes of 75%) is another important source for peroxy radicals in the NBL. $P_{RO2-O3+VOCs}$ shows

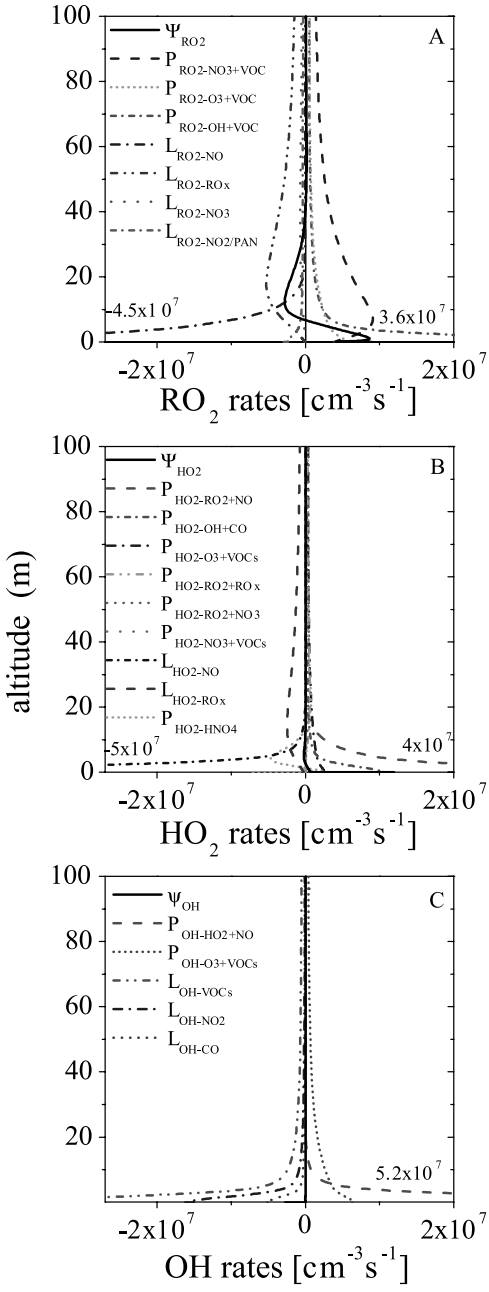

Figure 3. Vertical profiles of chemical rates and the rate of change by vertical transport of RO_2, HO_2, and OH 3 hours after model start for scenario 1. See color version of this figure at back of this issue.

a weak negative gradient and peaks at 5×10^6 molecules cm^{-3} s^{-1} at the ground. At 100 m, $P_{RO2-O3+VOCs}$ has decreased to 6×10^5 molecules cm^{-3} s^{-1}. Organic peroxy radicals are also formed by reactions of OH radicals with VOCs. $P_{RO2-OH+VOCs}$ strongly increases toward the ground, peaking at 3.6×10^7 molecules cm^{-3} s^{-1} in the lowest meter. However, because one OH radical is also destroyed in RACM by this reaction, $P_{RO2-OH+VOCs}$ is ultimately not a net source of RO_x radicals in the NBL.

[26] Two major loss paths for RO_2 are active in the NBL: reaction with NO and reactions with other RO_x radicals. Reaction with NO, which is negligible above 15 m because of low [NO], is the dominating RO_2 loss path in the lowest 10 m, peaking at 4.5×10^7 molecules cm^{-3} s^{-1} at the ground. L_{RO2-NO} has a strong negative gradient caused by the negative gradient of [NO] (Figure 2f). $L_{RO2-ROx}$ has a maximum of 6×10^6 molecules cm^{-3} s^{-1} at ~15 m. The $L_{RO2-ROx}$ profile is similar to the vertical profile of RO_2. RO_2 radicals can also be destroyed by reaction with NO_3 and, in the case of alkyl radicals, by reaction with NO_2 forming PANs. Note that $L_{RO2-NO2/PAN}$ in Figure 3a is corrected for the thermal decay of PANs back to RO_2 and NO_2. In scenario 1, $L_{RO2-NO3}$ and $L_{RO2-NO2/PAN}$ are less important.

[27] The RO_2 maximum at ~20 m shown in Figure 1a is caused by the broad peak of $P_{RO2-NO3+VOCs}$ in the lowest 30 m and the strong negative gradient of L_{RO2-NO}. From this maximum, RO_2 is transported downward and, to a minor extent, upward. Considering that Ψ_{RO2} is proportional to the gradient of the vertical RO_2 flux (see section 2), vertical mixing acts as a sink of RO_2 between 7 and 30 m and as a source of RO_2 in the lowest 7 m. Vertical transport strongly influences the RO_2 concentration in the lower part of the NBL (Figure 3a). At 10 m, for example, the contribution of vertical transport to the total RO_2 loss is ~25%. In the lowest meter, Ψ_{RO2} is the main net source for organic peroxy radicals.

3.2.2. HO_2 Radicals

[28] The reaction of RO_2 radicals with NO is by far the most important HO_2 source in the lower NBL. Similar to L_{RO2-NO}, $P_{HO2-RO2+NO}$ increases toward the ground, peaking at almost 4×10^7 molecules cm^{-3} s^{-1}. Other important HO_2 production paths include the conversion of OH into HO_2 by reaction with CO and the ozonolysis of alkenes. $P_{HO2-OH+CO}$ is highest close to the ground, where it reaches 10^7 molecules cm^{-3} s^{-1}. $P_{HO2-O3+VOCs}$ has a negative gradient in the lower NBL, with a maximum of 2×10^6 molecules cm^{-3} s^{-1} close to the ground. Other HO_2 sources, for example, the conversion of RO_2 into HO_2 by reaction with NO_3 and other RO_x radicals or direct formation by NO_3 + VOC reactions, are unimportant in scenario 1.

[29] The dominant sink of HO_2 in the lowest ~5 m is its reaction with NO, forming OH radicals. L_{HO2-NO}, which is as high as 5×10^7 molecules cm^{-3} s^{-1} in the lowest meter, shows a negative gradient because of the strong negative gradient of [NO]. Because of the strong negative gradient of L_{HO2-NO}, HO_2 develops its concentration maximum at ~5 m, as shown in Figure 1b. Another important sink of HO_2 is its reaction with other RO_x radicals ($L_{HO2-ROx}$). This loss path is dominant above 6 m, with a broad maximum at 15 m (3×10^6 molecules cm^{-3} s^{-1}). Other loss paths of HO_2 such as uptake on aerosols or the reactions with NO_3 and O_3 are unimportant in scenario 1.

[30] While RO_2 can be vertically transported, the lifetime of HO_2 is too short to allow significant transport rates (Ψ_{HO2} in Figure 3b). However, HO_2 can be transported indirectly via transport of its reservoir species HNO_4, which is formed by reaction of HO_2 radicals with NO_2 (lifetime ~30 s at 290 K). We define the net production rate of HO_2 from HNO_4 decay as

$$P_{HO2-HNO4} = f_{HNO4}[HNO_4] - k_{HO2+NO2}[HO_2][NO_2]. \quad (6)$$

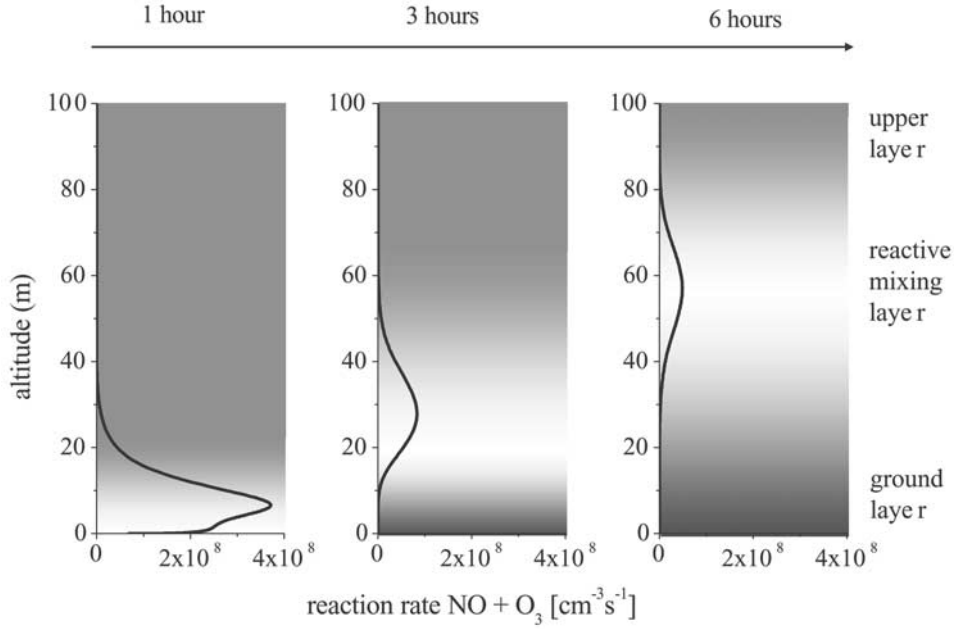

Figure 4. Illustration of the three-layer concept of the NBL. The evolution of the unreactive ground layer, the reactive mixing layer, and the upper layer during the night is exemplified by the NO + O_3 reaction rate for an urban case with high traffic emissions and stability (scenario 9).

[31] In equation (6), and in the remainder of the paper, f_X and k_{Y+Z} represent the unimolecular rate constant for thermal dissociation of a gas X and the rate constant of the reaction $Y + Z$, respectively. As shown in Figure 3b, $P_{HO2-HNO4}$ is negative between 2 and 12 m (down to -9×10^6 molecules cm^{-3} s^{-1}), while it is positive in the lowest 2 m and between 12 and 40 m. The positive $P_{HO2-HNO4}$ near the ground is caused by the high HO_2 loss rate L_{HO2-NO}, which leads to low HO_2 mixing ratios at this height. Consequently, less HNO_4 can be produced by the $HO_2 + NO_2$ reaction near the ground, and HNO_4 develops a positive gradient. Therefore HNO_4 is transported toward the ground, where its thermal decay acts as a net HO_2 source. As shown in section 3.6, $P_{HO2-HNO4}$ is an important source of HO_x radicals near the ground during strong vertical stabilities and high traffic emissions.

3.2.3. OH Radicals

[32] Only two paths are efficient in the formation of OH radicals in the nighttime atmosphere: reaction of HO_2 with NO and ozonolysis of unsaturated VOCs. Other OH sources, such as the reaction of HO_2 with NO_3, are negligible in scenario 1. $P_{OH-HO2+NO}$ increases toward the ground because of the strong negative gradient of [NO]. The rate exceeds $P_{OH-O3+VOCs}$ below ~7 m and reaches a maximum level of 5.2×10^7 molecules cm^{-3} s^{-1} in the lowest meter. At higher altitudes, OH is predominantly formed by the ozonolysis of alkenes. $P_{OH-O3+VOCs}$ shows a weak negative gradient and decreases to 5×10^5 molecules cm^{-3} s^{-1} at 100 m altitude.

[33] Because of the negative vertical profile of [OH], all its loss rates show a negative gradient, although the individual loss frequencies are only weakly altitude-dependent. In scenario 1 the highest OH loss rates result from the reaction of OH with VOCs, NO_2, and CO. The strong peak of $P_{OH-HO2+NO}$ close to the ground and the weak altitude dependence of the OH sinks cause the maximum of the OH concentration shown in Figure 1c. Vertical transport of OH is unimportant (Ψ_{OH} in Figure 3c).

3.3. Layer Concept of the NBL

[34] To conceptualize the vertical change in the OH-HO_2-RO_2 chemistry at night, we introduce a three-layer view of the NBL. We distinguish three chemical regimes that occupy different height intervals in the NBL on the basis of the mechanism and efficiency of the OH production. OH is produced at night by the ozonolysis of alkenes and by reactions of peroxy radicals with NO (section 3.2.3). For the latter mechanism (equation (1)) to be efficient, O_3 or NO_3 radicals must be present to produce RO_2 radicals by the oxidation of VOCs, and NO concentrations must be high enough to convert these peroxy radicals into HO_2 and OH. We have therefore chosen the reaction rate of NO with O_3 as an indicator for the vertical extent of these layers. This rate is easy to determine, both experimentally in the atmosphere and in models. Note that the nitrate radical is linked to O_3 by its production from the $O_3 + NO_2$ reaction.

[35] Figure 4 shows the vertical profile of the O_3 + NO reaction rate 1, 3, and 6 hours after nightfall for an urban scenario with elevated NO emissions and strong stability (scenario 9 in Table 1). We have chosen this case because it clearly illustrates the properties of the layers and their temporal behavior throughout the night (a more detailed discussion of the radical chemistry of scenario 9 will be given in section 3.6). After 1 hour a clear maximum of the reaction rate of up to 1.6×10^9 molecules cm^{-3} s^{-1} develops in the lowest 20 m. As the night advances, this layer with enhanced reaction rate of NO + O_3 moves upward, reaching a height between 5 and 40 m after 3 hours and between 10 and 70 m after 6 hours. Note that the overall rate decreases as the night proceeds (because [O_3] rapidly

decreases in scenario 9). As will become clear later, the temporal behavior and the extent of the three layers depend predominantly on the vertical stability and the magnitude of the NO emissions.

[36] The vertical profile of the NO + O_3 reaction rate allows us to distinguish the three chemical regimes in the NBL. The three layers are marked by different shades of gray in Figure 4.

[37] The unreactive ground layer, which occupies the lowest part of the NBL, is dominated by high concentrations of NO, which suppress significant levels of NO_3 and O_3. OH production is negligible because ozonolysis is unimportant, and RO_2 is not formed in the absence of NO_3 and O_3. The ground layer is not always present in the NBL. At low NO emissions and weak stabilities, ozone destroyed by the freshly emitted NO near the ground is continuously replenished from aloft, and the ground layer does not form. This is, for example, the case in scenario 1, where ozone and NO are both present at the ground throughout the model run (Figure 2). At higher NO emission rates and stronger stabilities, as, for example, in scenario 9, the ground layer slowly grows in height after the continuously emitted NO has destroyed all O_3 and NO_3 near the ground. Ground layers can therefore frequently be observed in cities. In Figure 4 the ground layer is characterized by the near-zero NO + O_3 reaction rate in the lower part of the NBL (dark gray zone). While it has not yet developed after 1 hour, the ground layer is ~3 m high after 3 hours and extends over the lowest 10 m after 6 hours.

[38] The upper layer is characterized by very low NO levels and is typically located at the upper end of the NBL. NO cannot reach this part of the NBL because it is converted to NO_2 during its upward transport by the fast NO + O_3 reaction. In the upper layer, OH is only produced by the ozonolysis of alkenes. Although RO_2 is efficiently produced by NO_3/O_3 + VOC reactions, in particular in the lower part of the upper layer, it is only slowly converted into HO_2 and OH in the absence of NO. Therefore the RO_2 maximum discussed in section 3.2.1 is typically located in the lower part of the upper layer. The extent of the upper layer is controlled by the NO emission rate, stability, and time of night. In Figure 4 the upper layer is determined by the very low NO + O_3 reaction rates at the top of the NBL (medium gray zone). Its lower boundary is at ~30 m after 1 hour. Because of the continuously emitted NO, the lower boundary of this layer increases to 70 m after 6 hours. In scenario 1 the upper layer extends from ~15 m upward throughout the night (Figure 2).

[39] The reactive mixing layer is characterized by elevated levels of both O_3/NO_3 and NO and is located between the upper layer and the ground layer. In the case in which the ground layer does not form, the reactive layer is bound by the ground. The reactive layer is always formed in the presence of ground NO emissions. The unique feature of the reactive layer is the simultaneous presence of NO_3, O_3, RO_2, and NO, which is maintained by the continuous downward mixing of O_3, the NO_3 precursor N_2O_5 [*Geyer and Stutz*, 2004], and RO_2 from the upper layer and by the upward transport of NO from the ground or the ground layer. As explained above, the simultaneous presence of RO_2 radicals (because of vertical transport and NO_3/O_3 + VOC reactions) and NO leads to an efficient HO_2 and OH production through the fast propagation chain (1). In addition, OH can be produced by the ozonolysis of VOCs, which are also mixed upward from their emission height. The HO_2 maximum discussed in section 3.2.2 is typically located in the upper part of the reactive mixing layer. The OH maximum (section 3.2.3) can be typically found in the lower part of this layer. In Figure 4 the reactive mixing layer can be determined by the elevated NO + O_3 reaction rates (light gray zone) and extends over the lowest 20 m after 1 hour. The growing ground layer pushes the reactive mixing layer to 10–70 m after 6 hours. In scenario 1 the ground layer extends from the ground to an altitude of ~15 m.

3.4. Steady State of RO_x Radicals in the Reactive Mixing Layer

[40] Because of their short lifetimes, we can establish equations for the pseudo steady state concentrations of RO_2, HO_2, and OH in the reactive mixing layer, which help in the interpretation of the various radical processes. We assume that the reaction with NO is the dominant loss path for RO_2 and HO_2 in the reactive mixing layer (Figure 3). This assumption is typically fulfilled for [NO] > ~100 ppt. The equations derived in this section are thus not valid in the upper layer or in very clean environments.

[41] The main sources of RO_2 in the reactive mixing layer are (1) oxidation of VOCs by OH radicals ($P_{RO2-OH+VOCs}$), (2) downward transport of RO_2 from the upper layer (ψ_{RO2}), and (3) in situ production by reactions of O_3 and NO_3 with VOCs ($P_{RO2-O3+VOCs}$ and $P_{RO2-NO3+VOCs}$) (section 3.2.1). The pseudo steady state of RO_2 can be expressed as

$$[RO_2] = \frac{\Psi_{RO2} + P_{RO2-NO3+VOCs} + P_{RO2-O3+VOCs} + P_{RO2-OH+VOCs}}{k_{RO2+NO}[NO]}. \quad (7)$$

[42] The main chemical sources of HO_2 in the reactive mixing layer include reactions of RO_2 radicals with NO ($P_{HO2-RO2+NO} = k_{RO2+NO}[RO_2][NO]$) and the reaction of OH with CO ($P_{HO2-OH+CO} = k_{OH+CO}[OH][CO]$) (section 3.2.2) Another source of HO_2 in the reactive mixing layer is in situ production by the reaction of O_3 with VOCs ($P_{HO2-O3+VOCs}$). The HO_2-NO_2-HNO_4 steady state ($P_{HO2-HNO4}$) also plays an important role as a source of HO_2 in the reactive mixing layer, in particular at high traffic emissions and strong stabilities (see sections 3.5.1 and 3.5.2). The pseudo steady state of HO_2 is therefore

$$[HO_2] = \frac{P_{HO2-RO2+NO} + P_{HO2-O3+VOCs} + P_{HO2-OH+CO} + P_{HO2-HNO4}}{k_{HO2+NO}[NO]}. \quad (8)$$

[43] The only sources of OH in the reactive mixing layer are the reaction of HO_2 with NO ($P_{OH-HO2+NO} = k_{HO2+NO}[HO_2][NO]$) and the ozonolysis of VOCs ($P_{OH-O3+VOCs}$) (section 3.2.3). Sinks of OH in the lower NBL include its reaction with VOCs, NO_2, and CO. The pseudo steady state concentration of OH in the reactive mixing layer can therefore be expressed as

$$[OH] = \frac{P_{OH-HO2+NO} + P_{OH-O3+VOCs}}{k_{OH+VOCs}[VOCs] + k_{OH+NO2}[NO_2] + k_{OH+CO}[CO]}. \quad (9)$$

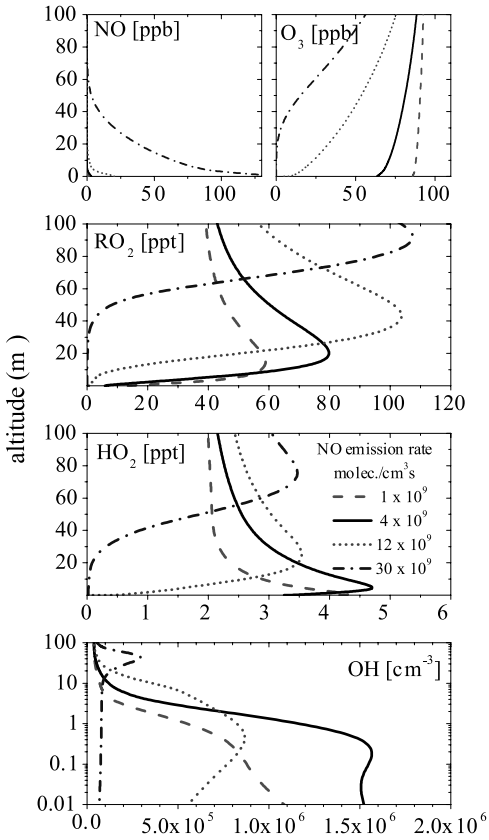

Figure 5. RO_x profiles at different traffic emission rates in a weakly stable urban case 3 hours after model start (scenarios 1–4) and the respective mixing ratios of NO and ozone.

[44] Assuming that one RO_2 is produced in each OH + VOC reaction, equations (7)–(9) can be combined to a new steady state equation for [OH] in the reactive mixing layer (with $P_{ROx-O3+VOCs} = P_{RO2-O3+VOCs} + P_{HO2-O3+VOCs} + P_{OH-O3+VOCs}$),

$$[OH] = \frac{P_{RO2-NO3+VOCs} + P_{ROx-O3+VOCs} + \Psi_{RO2} + P_{HO2-HNO4}}{k_{OH+NO2}[NO_2]}. \quad (10)$$

Equation (10) includes two known OH formation processes. First, the production of RO_2 radicals by reactions of NO_3 with VOCs leads to the formation of OH due to radical propagation chain (1). In addition, the ozonolysis of VOCs forms OH radicals both directly and indirectly via RO_2 and HO_2. In scenario 1, ozonolysis is the main source of OH near the ground: $P_{ROx-O3+VOCs}$ (2 m, 1 hour) = 1.4×10^7 molecules cm^{-3}. The NO_3 + VOC reaction is also important: $P_{RO2-NO3+VOCs}$ (2 m, 1 hour) = 5×10^6 molecules cm^{-3}. Two new and previously unrecognized contributions to the OH formation in the reactive mixing layer also enter equation (10): vertical transport of RO_2 and HNO_4. Under the conditions of scenario 1, downward mixing of RO_2 is comparable to the purely chemical mechanisms in the lowest 7 m (Ψ_{RO2} (2 m, 1 hour) = 8×10^6 molecules cm^{-3}). Note that the majority of RO_2 radicals in the upper layer are formed by reactions of NO_3 with VOCs. Transport of HNO_4 is also important in scenario 1: $P_{HO2-HNO4}$ (2 m, 1 hour) = 3×10^6 molecules cm^{-3}. The contribution of these two processes to the formation of OH varies for different conditions, as will be discussed in sections 3.5 and 3.6. It should be noted here that equation (10) is only an approximation for [OH], since the loss of RO_2 and HO_2 from reactions with RO_x and HO_2 (Figure 3) was omitted in our calculation. In scenario 1 at 2 m, for example, the inclusion of these reactions reduces the numerator in equation 10 by ~8%. [OH] is thus overestimated by this amount.

3.5. Sensitivity Analysis

[45] To determine the role of the various mechanisms influencing nocturnal RO_x chemistry, we performed a number of sensitivity studies. In particular, we investigated how the nocturnal RO_x systems react to changes in the emission rates of NO and VOCs, atmospheric stability, and ambient temperature. The parameters of the different scenarios are listed in Table 1. The variations of the vertical profiles of [RO_2], [HO_2], and [OH] and their the most important production and loss rate changes under different conditions will be discussed with the help of equations (7)–(10) and the three-layer concept introduced in section 3.3.

3.5.1. Variation of the Traffic Emission Rate

[46] Figure 5 shows the variation of the vertical profiles of [RO_2], [HO_2], and [OH] at NO traffic emission rates ranging from 1×10^9 to 30×10^9 molecules cm^{-3} s^{-1} 3 hours after model start (scenarios 1–4 in Table 1). Together with NO, other anthropogenic pollutants are also emitted at a different rate (see section 2 for the emission ratios). Also shown in Figure 5 are the profiles of NO and O_3, which provide a link to our definition of the three-layer model.

[47] The vertical extent of the three layers introduced in section 3.3 strongly changes with the traffic emission rate. The ground layer is only formed in scenario 4 at high NO emissions, where it reaches an altitude of ~10 m (Figure 5). The reactive mixing layer occupies the lowest 5 m at low emissions (scenario 2) and increases to almost 30 m at medium-high emissions (scenario 3). Once the ground layer is formed, as in the high-emission scenario 4, the reactive mixing layer detaches from the ground, extending, for example, from ~10 to 100 m. In general, both the altitude and the vertical extent of the reactive mixing layer increase with increasing traffic emissions. Consequently, the lower boundary of the upper layer is displaced upward with increasing emission rates. In the case of high emissions (scenario 4) the upper layer starts at ~100 m. It is interesting to note that the small change in the traffic emission rates between scenario 3 and scenario 4 causes a drastic change in the behavior of the altitude dependence of nocturnal radical chemistry. This behavior can be explained by reaching a compensation point, at which downward transport cannot replenish ozone that is destroyed by NO emitted at the ground. Once this point is reached, a ground layer will rapidly form and will grow throughout the night, influencing the vertical distribution of all trace gases in the NBL.

[48] The variations of the three RO_x profiles shown in Figure 5 follow the change of the vertical extent of the three layers with the traffic emission rate. As the altitude of the reactive mixing layer increases with increasing NO emission rates, the RO_2 maximum, which is located in the lower

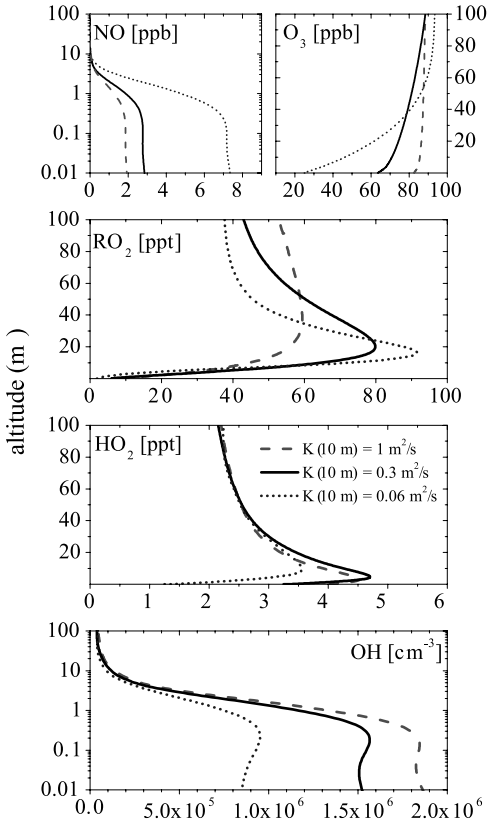

Figure 6. Vertical profiles of $[RO_2]$, $[HO_2]$, [OH], [NO], and $[O_3]$ at different atmospheric stabilities in an urban case with moderate traffic emissions 3 hours after model start (scenarios 1, 5, and 6).

part of the upper layer (sections 3.2.1 and 3.3), is pushed upward, moving from ~10 m in scenario 2 to 90 m in scenario 4. The concentration of RO_2 at the altitude of this maximum increases at higher traffic emissions because of the higher VOC levels, and thus $P_{RO2-NO3+VOCs}$ and $P_{RO2-O3+VOCs}$ increase.

[49] Likewise, the altitudes of the HO_2 concentration maximum in the upper part of the reactive mixing layer (sections 3.2.2 and 3.3) and the maximum of [OH] in the lower part of the reactive mixing layer (sections 3.2.3 and 3.3) increase with increasing traffic emissions. The extents of both maxima increase at higher emissions because the height of the reactive mixing layer increases. The behavior of $[HO_2]$ at the altitude of the HO_2 maximum is dominated by two counteracting effects: an increasing loss rate L_{HO2-NO} and an increasing production rate $P_{HO2-RO2+NO}$ at higher NO emissions (equation (8)). The magnitude of the HO_2 maximum therefore changes little. OH concentrations at the height of the OH maximum decrease with increasing traffic emissions because $[NO_2]$ increases while $[O_3]$ and $[NO_3]$ decrease in the reactive mixing layer (equation (10)).

3.5.2. Variation of Atmospheric Stability

[50] Figure 6 shows the vertical profiles of $[RO_2]$, $[HO_2]$, [OH], [NO], and $[O_3]$ 3 hours after model start at different atmospheric stabilities (scenario 6: neutral NBL, K (10 m) = 1.0 m^2 s^{-1}; scenario 1: weak inversion, K (10 m) = 0.3 m^2 s^{-1}; and scenario 5: strong inversion, K (10 m) = 0.06 m^2 s^{-1}; see Table 1). In all three scenarios the reactive mixing layer extends over the lowest ~10 m of the NBL. A ground layer does not develop because of the low traffic emission rates, as can be seen by the high O_3 levels at the ground (Figure 6).

[51] The differences of the RO_x profiles are caused by the increasing efficiency of vertical mixing at weaker stabilities. The RO_2 maximum in the upper layer broadens and becomes less pronounced at weaker stabilities. While, for example, the RO_2 maximum is limited to 15 ± 5 m in the strong inversion scenario 5, peaking at ~90 ppt, $[RO_2]$ is elevated between 20 and ~100 m under the neutral conditions of scenario 6. This behavior can be explained by the weaker vertical gradients of VOCs at weaker stabilities (see section 3.1). Consequently, $P_{RO2-NO3+VOCs}$ decreases in the lower part of the upper layer, while it increases at higher altitudes for weaker stabilities. In the reactive mixing layer, $[RO_2]$ increases at weaker stabilities because the downward flux of RO_2 from the upper layer (and thus Ψ_{RO2} in equation (7)) is larger.

[52] The vertical profiles of HO_2 and OH do not significantly change with stability because the extent of the NO layer is similar in scenarios 1, 5, and 6. In the upper layer, $[HO_2]$ is only weakly dependent on stability because both $P_{HO2-RO2+ROx}$ and $L_{HO2-ROx}$ increase at weaker stabilities. Likewise, [OH] in the upper layer does not significantly change with stability because the changes in $P_{OH-O3+VOCs}$ and $L_{OH-VOCs}$ partly compensate each other. However, the peak concentrations of HO_2 and OH in the reactive mixing layer increase at weaker stabilities (up to 1.9 × 10^6 molecules cm^{-3} s^{-1} in the neutral case) because of the higher downward flux of RO_2 (and thus Ψ_{RO2} in equation (7)). In addition, the steady state concentration of OH in the reactive mixing layer is higher at weaker stabilities because $[NO_2]$ is decreasing (equation (10)). It is interesting to note that $P_{HO2-HNO4}$ in the lower part of the reactive mixing layer decreases at weaker stabilities. The lower $P_{HO2-HNO4}$ partly compensates the higher Ψ_{RO2} and the lower OH loss rate by reaction with NO_2. Overall, the reactivity of the reactive layer increases at weaker stabilities.

3.5.3. Variation of Temperature

[53] Figure 7 compares the 3 hour vertical profiles of $[RO_2]$, $[HO_2]$, [OH], [NO], and $[O_3]$ for temperatures at 10 m ranging from 275 to 305 K. In all three cases the reactive mixing layer extends over the lowest ~10 m of the NBL, and a ground layer does not develop. The temperature change has little effect on [NO] and $[O_3]$. At increasing temperatures the concentrations of both NO_3 (because of a shift in the N_2O_5-NO_3 equilibrium [*Geyer and Stutz*, 2004]) and monoterpenes (because their emission rate increases) increase. The resulting increase of $P_{RO2-NO3+VOCs}$ has a significant impact on the levels of RO_x radicals in the NBL. With $P_{RO2-NO3+VOCs}$ the magnitude of the RO_2 maximum in the lower part of the upper layer increases at higher temperatures. While the RO_2 mixing ratio at 15 m in the 275 K scenario is 60 ppt, it exceeds 110 ppt in the 305 K scenario. The RO_2 maximum is also closer to the ground at higher temperatures, leading to higher RO_2 levels in the reactive mixing layer (because Ψ_{RO2} and $P_{RO2-NO3+VOCs}$ increase). In the upper layer the increase of $P_{RO2-NO3+VOCs}$ is mostly compensated by the simultaneous increase of $L_{RO2-NO3}$, which is a dominant sink at this height. $[RO_2]$ is thus only weakly temperature-dependent.

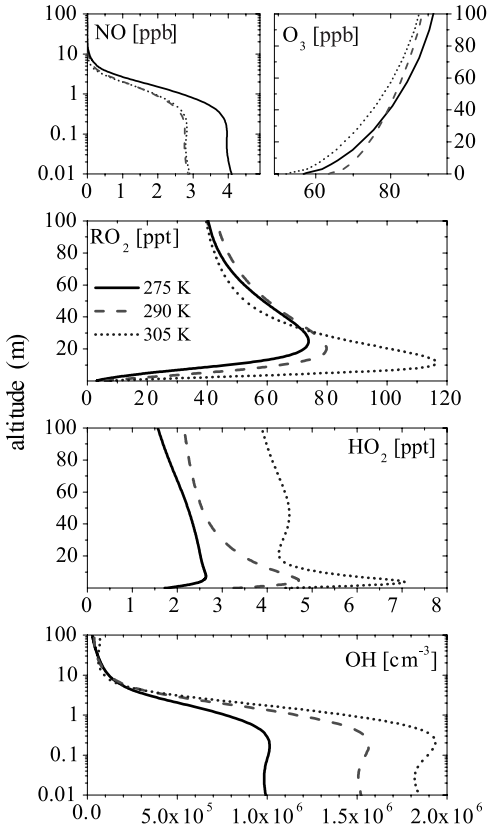

Figure 7. Vertical profiles of $[RO_2]$, $[HO_2]$, [OH], [NO], and $[O_3]$ at different ambient temperatures in a weakly stable urban case with moderate traffic emissions 3 hours after model start (scenarios 1, 7, and 8).

[54] The concentration of HO_2 increases with temperature in both the upper layer and the reactive mixing layer. The HO_2 peak in the upper part of the reactive mixing layer is more pronounced at high temperatures. While the HO_2 mixing ratio at 5 m is as high as 7 ppt at 305 K, it only reaches 2.5 ppt at 275 K. In the upper layer the higher $[HO_2]$ at higher temperatures is caused by the higher NO_3 levels, which lead to an enhanced $P_{HO2-RO2+NO3}$. The $[HO_2]$ increases in the reactive mixing layer at higher temperatures are due to the higher HO_2 production rate $P_{HO2-RO2+NO}$ (equation (8)).

[55] No significant dependence of OH on temperature was found in the upper layer, since OH is predominantly produced by the weakly temperature-dependent ozonolysis of anthropogenic alkenes $P_{OH-O3+VOCs}$. However, the peak OH concentration in the lower part of the reactive mixing layer is as high as 1.9×10^6 molecules cm^{-3} at 305 K, while [OH] only reaches 1.0×10^6 molecules cm^{-3} at 275 K (Figure 7). In the lower part of the reactive mixing layer, [OH] increases with temperature because both $P_{RO2-NO3+VOCs}$ and Ψ_{RO2} increase (equation (10)).

3.6. High-Emission Stable Urban Case

[56] In polluted urban areas a fast and complete destruction of ozone at the ground is often observed during the night [e.g., *Lee et al.*, 2003]. This O_3 depletion can be interpreted as the fast formation of the unreactive ground layer. It occurs if two conditions are met: (1) a strong atmospheric stability, which prevents ozone from being transported from aloft and replenishing lost O_3 at the ground, and (2) high traffic emissions of NO, which lead to a high loss rate of O_3 by its reaction with NO (section 3.3). In this section we investigate the vertical profiles of RO_x radicals in such a high-emission stable urban case (scenario 9 in Table 1). This scenario was also used in section 3.3 to explain the three-layer concept of the NBL.

[57] In the high-emission/high-stability case the levels of NO, NO_2, and anthropogenically emitted VOCs are considerably higher than in scenario 1. After 3 hours, for example, both [NO] (Figure 8) and $[NO_2]$ (not shown) reach ~120 ppb close to the ground. In contrast, ozone and NO_3 levels rapidly decrease during the night. Consequently, a ground layer begins to form after 1 hour, increasing in height as the night proceeds and covering the lowest ~15 m after 6 hours (see also Figure 4). This ground layer is characterized by very low O_3 levels, as can be seen in Figure 8. The growing ground layer slowly pushes the reactive mixing layer upward. While the reactive mixing layer is located in the lowest 20 m after 1 hour, it spans from 15 to 60 m after 6 hours.

[58] Figure 8 shows vertical profiles of $[RO_2]$, $[HO_2]$, and [OH] during the first 6 hours of the night in this scenario. Similar to the weakly stable urban case discussed in sections 3.1–3.5, a layer with elevated RO_2 levels develops in the lower part of the upper layer. As already discussed in

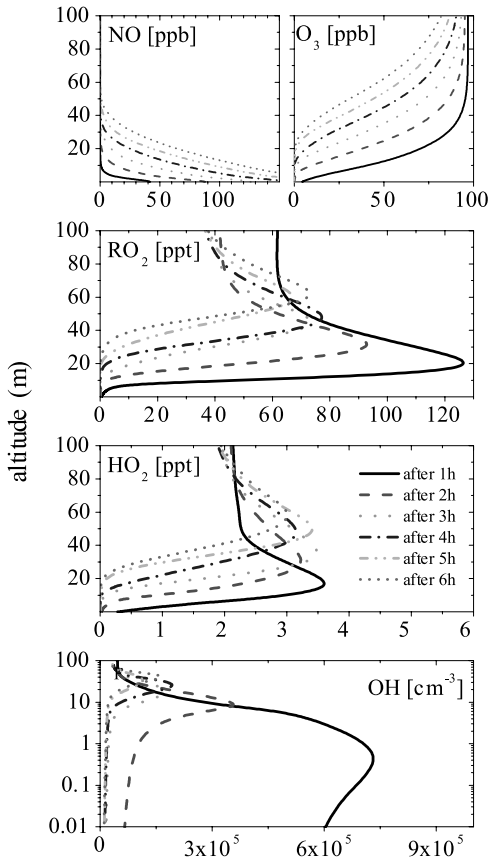

Figure 8. RO_x profiles in the first 6 hours after nightfall in an urban case with high stability and high traffic emission rates and the respective mixing ratios of NO and ozone.

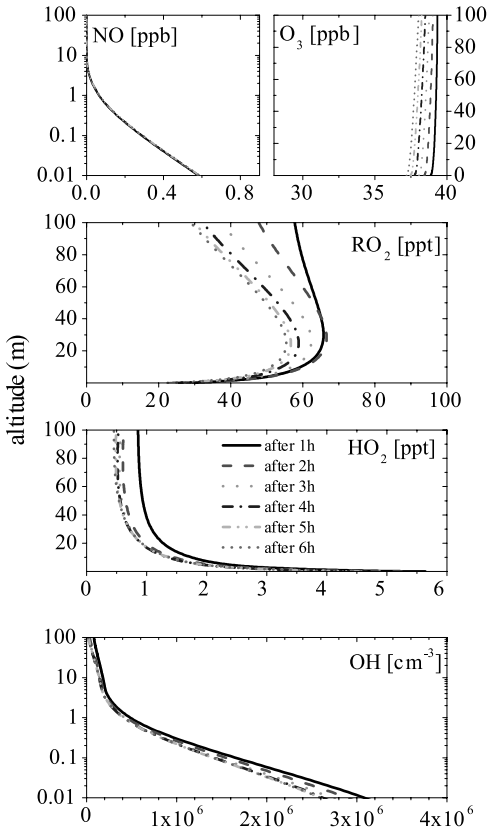

Figure 9. Hourly snapshots of the RO_2, HO_2, and OH profiles during the first 6 hours after model start in a weakly stable rural case (scenario 10) and the respective mixing ratios of NO and ozone.

section 3.2, this layer, in which [RO_2] mixing ratios can exceed 120 ppt, is caused by the elevated RO_2 production rate by NO_3 + VOC reactions at this height. The altitude of the RO_2 maximum increases as the night proceeds, and the lower boundary of the upper layer is pushed upward by the growing ground layer. After 6 hours the RO_2 maximum can be found at ~70 m. From this maximum, RO_2 radicals are transported into the reactive mixing layer. Because of the higher stability, Ψ_{RO2} is ~50% lower in the reactive mixing layer than in scenario 1. The main sources of RO_2 in the reactive mixing layer are therefore NO_3/O_3 + VOC reactions. Throughout the night, [RO_2] slowly decreases in the NBL because of the decrease of [O_3] and [NO_3].

[59] The development of a HO_2 maximum in the upper part of the reactive mixing layer, discussed in section 3.2.2, can also be observed in the high-emission stable case. With the growing ground layer pushing the reactive mixing layer upward, the altitude of the HO_2 layer increases throughout the night. Vertical mixing of HNO_4, formed by $HO_2 + NO_2$ reactions in the HO_2 layer, is the main source of HO_2 in the lower part of the reactive mixing layer in scenario 9. $P_{HO2-HNO4}$ exceeds 2.5×10^7 molecules cm^{-3} s^{-1} in the lowest meter after 1 hour and is by far the most important source of OH at this height (equation (10)). The high transport rate of HNO_4 under high-stability and high-traffic emissions is caused by the strong gradient of HO_2 in the reactive mixing layer.

[60] Similar to the weakly stable urban case, a peak of the OH concentration develops in the lower part of the reactive mixing layer. After 1 hour, $\sim 6 \times 10^5$ molecules cm^{-3} s^{-1} of OH are present in this layer. With the reactive mixing layer the altitude of the OH maximum increases during the night. As the extent of the reactive mixing layer increases, the OH maximum broadens as it moves upward through the NBL. In addition, the increasing NO_2 concentrations during the night lead to a decrease of [OH] at the height of its maximum.

3.7. Rural Low-Emission Case

[61] In this section the vertical profiles of RO_x radicals in a rural low-emission case (scenario 10 in Table 1) are investigated. The rural conditions are characterized by the absence of anthropogenic emissions; low initial levels of NO_2, O_3, and anthropogenic VOCs but high initial levels of biogenic VOCs; and high emission rates of monoterpenes. Our discussion in section 3.4, including equations (7)–(10), is therefore not always applicable. We used an average emission rate of monoterpenes of 10×10^6 molecules cm^{-3} s^{-1} (for class API at 290 K) in this scenario.

[62] In the rural case the concentrations of NO and NO_2 are considerably lower than in the urban cases (NO is <1 ppb at the ground; NO_2 is 2 ppb). In addition, NO is only emitted from the ground and not, as in the urban cases, between 0.1 and 1 m. The missing traffic NO sources have an influence on the trace gas gradients in the lowest meter of the atmosphere. NO, for example, shows a strong gradient in the lowest meter, which is caused by the slow transport and the simultaneous reaction with O_3, which is not observed in urban scenarios (Figure 9). In the rural scenario, NO does not reach altitudes above 5 m. The initial ozone level of ~40 ppb does not significantly change during the night, and [O_3] develops a weak positive gradient, mostly due to dry deposition. NO_3 and N_2O_5 develop positive gradients, which are caused by the high monoterpene levels in the lower NBL. Both NO_3 and N_2O_5 are lower in the rural case than in the urban scenarios ([NO_3] is around 5 ppt). Monoterpenes develop negative gradients, which are caused by their reactions with NO_3 and O_3 [*Geyer and Stutz*, 2004]. Throughout the night the reactive mixing layer is located in the lowest meter of the NBL. A ground layer does not develop.

[63] Vertical profiles of [RO_2], [HO_2], and [OH] for a rural case (scenario 10) are shown in Figure 9. The RO_x profiles change very little throughout the night. Only at the beginning of the night, when VOCs emitted during the day are still oxidized, are [RO_2] and [HO_2] slightly elevated. Similar to the urban cases, all three RO_x radicals develop pronounced concentration maxima at a specific altitude. The RO_2 concentration is highest at 20 m altitude. Below this altitude, [RO_2] decreases toward the ground because of the elevated L_{RO2-NO} rate in the lowest meter. Above 20 m, [RO_2] decreases with increasing altitude because of the decreasing concentrations of monoterpenes, which are oxidized during their upward transport. The maximum RO_2 mixing ratio decreases from 65 ppt after 1 hour to 55 ppt 5 hours later. In general, the RO_2 levels in the NBL depend on the monoterpene emission rate (not shown here), because $P_{RO2-O3+VOCs}$ increases with the monoterpene levels. In addition, the initial levels of isoprene at night

play a role. For example, a fivefold increase of initial isoprene increases RO_2 mixing ratios by ~20%. $P_{RO2-NO3+VOCs}$ depends less on the monoterpene emission rate and initial isoprene levels because $[NO_3]$ simultaneously decreases at higher monoterpene and isoprene concentrations. Downward transport acts as the main source of RO_2 in the reactive mixing layer.

[64] Both HO_2 and OH have a strong maximum in the reactive mixing layer, which occupies the lowest meter of the NBL. Close to the ground, [OH] can reach levels of several million molecules per cubic centimeter. These maxima are formed by the elevated reaction rates of RO_2 and HO_2 with NO, which is emitted from the ground. The strong vertical [OH] gradient in the lowest meter (Figure 9) is not observed in urban cases, which also include emission between 0.1 and 1 m. Because $[RO_2]$ increases in the reactive mixing layer at higher monoterpene emission rates and higher initial isoprene concentrations, $[HO_2]$ and [OH] also increase because of the increase of $P_{HO2-RO2+NO}$ and $P_{OH-HO2+NO}$. In the upper layer, $[HO_2]$ changes little with altitude and is predominantly produced by ozonolysis of monoterpenes and isoprene and self reactions of RO_2 radicals. The HO_2 mixing ratio in the upper layer depends little on monoterpene emissions and isoprene concentrations because the increase of $P_{HO2-O3+VOCs}$ and $P_{HO2-ROx}$ is compensated by the simultaneous increase of $L_{HO2-RO2}$. An OH concentration of $\sim 10^5$ molecules cm^{-3} is maintained by the ozonolysis of monoterpenes and isoprene in the upper layer. The OH concentration in the upper layer increases at higher monoterpene emission rates and initial isoprene because of higher $P_{OH-O3+VOCs}$.

[65] Our model is based on the original RACM mechanism by *Stockwell et al.* [1997]. However, we also performed model calculations with an updated RACM version that includes the isoprene oxidation scheme proposed by *Geiger et al.* [2003]. For the initial isoprene levels used in our rural scenario (case 10), differences in the concentrations of O_3, NO, and NO_3 are negligible between the schemes. NO_2 concentrations change near the ground by <5%. The shape of the vertical profiles of all three RO_x radicals is similar in both cases (Figure 9). However, the mixing ratios of RO_2 are higher by ~20% with the new isoprene oxidation scheme. HO_2 levels above 3 m altitude are lower with the updated RACM mechanism, while the OH concentration changes are small. The higher RO_2 concentrations lead to an increase of both HO_2 and OH of ~20% below 3 m, where RO_2 is mixed with NO. The new scheme by *Geiger et al.* [2003] changes the radical levels in our model slightly. However, the general behavior and the various chemical transport mechanisms are reproduced with the new isoprene oxidation scheme.

[66] Our investigation of the nocturnal chemistry in rural areas illustrated that similar mechanisms found in urban areas are active. However, the lack of NO emissions restricts the reactive mixing layer to the lowest few meters above the ground, where NO is still elevated. Our sensitivity analysis regarding the emissions of monoterpenes and the concentration of isoprene shows that nocturnal rural radical chemistry is dependent on the concentration of these species. Thus factors such as type of vegetation and temperature that influence the concentration of the biogenic VOCs have to be considered for more specific model calculations.

3.8. Comparison of the Model Results With Field Data

[67] It is difficult to compare the modeled vertical profiles of $[RO_2]$, $[HO_2]$, and [OH] with measured data at night because no measurements of the vertical profiles of RO_x radicals have been performed thus far. Most reported measurements were taken at 3–10 m height. The model results show that, in particular, the RO_2 mixing ratios develop a strong gradient in the lowest ~20 m of the atmosphere, and small changes in stability and emission rates can lead to considerable changes in $[RO_2]$ at 10 m. Therefore we can only compare the general levels predicted by the model in the lower NBL with the field observations.

[68] Measurements of RO_2 in the atmosphere were thus far almost exclusively performed in rural areas [*Cantrell et al.*, 1996a, 1996b, 1997; *Carslaw et al.*, 1997; *Geyer et al.*, 2003; *Holland et al.*, 2003; *Hu and Stedman*, 1995; *Kanaya et al.*, 1999; *Mihelcic et al.*, 1993, 2003; *Monks et al.*, 1996]. The one-dimensional model predicts ~50 ppt of RO_2 at 10 m altitude in the rural case in Figure 9. However, this level strongly depends on the monoterpene emission rate. While <30 ppt of RO_2 are modeled for an API emission rate of 3×10^6 molecules cm^{-3} s^{-1}, up to 90 ppt can be present at a rate of 30×10^6 molecules cm^{-3} s^{-1}. These modeled RO_2 levels are in the range of observed data, for example, by *Mihelcic et al.* [1993], who measured up to 40 ppt RO_2 on a mountain in Germany. In a rural area near Berlin, Germany, *Geyer et al.* [2003] observed 6 ppt of RO_2 at night. The monoterpene levels of 15–25 ppt measured at this site were, however, considerably lower than the levels modeled in scenario 10, thus causing the lower RO_2 concentration.

[69] The general levels of HO_2 and OH radicals predicted by the NCAT model for the various cases are in good agreement with the few observations in the NBL. For example, measurements near Berlin shortly before sunrise found that HO_2 was often on the order of 4 ppt, while OH peaked at 1.9×10^5 molecules cm^{-3} [*Geyer et al.*, 2003]. These values are on the order of the model results of scenario 10 at 10 m altitude (Figure 9).

[70] Although a layer of elevated OH concentrations near the ground is predicted for all scenarios discussed in this study, we cannot assess whether the recent observations of $\sim 10^6$ molecules cm^{-3} of OH at night above a forest and in New York City [*Faloona et al.*, 2001; *Ren et al.*, 2003] could be reproduced by our model without explicit calculations for the conditions encountered during these measurements.

[71] The OH levels modeled in our rural scenario above 3 m are lower than the concentrations of $\sim 2 \times 10^5$ molecules/cm^{-3} and $\sim 2 \times 10^5$ to 10×10^5 molecules cm^{-3} found by *Makar et al.* [1999] and *Sillman et al.* [2002], respectively. In addition, our HO_2 levels in this case are also lower. This discrepancy is most likely caused by a different choice in emission scenarios, since the studies of *Makar et al.* [1999] and *Sillman et al.* [2002] were both performed for forested areas with very high biogenic hydrocarbon emissions. It should be noted that the shape of vertical OH and HO_2 profiles by *Makar et al.* [1999]

Table 2. Contribution of Nocturnal OH to the VOC and NO_2 Removal in the Lowest 100 m of the NBL (3 Hours After Model Start) and the Relative Contribution of OH Compared With That of NO_3

Scenario	Characterization	VOC Oxidation by OH, ppt h^{-1}	NO_2 Oxidation by OH, ppt h^{-1}
1	urban, weak inversion/moderate emissions	280 (23%)	110 (7%)
2	urban, weak inversion/low emissions	132 (21%)	22 (3%)
3	urban, weak inversion/high emissions	620 (27%)	338 (13%)
4	urban, weak inversion/very high emissions	1095 (46%)	585 (44%)
5	urban, strong inversion/moderate emissions	296 (26%)	141 (9%)
6	urban, neutral conditions/moderate emissions	262 (25%)	58 (6%)
7	urban, scenario 1 at low temperatures	274 (30%)	111 (7%)
8	urban, scenario 1 at high temperatures	336 (17%)	117 (7%)
9	urban, strong inversion/high emissions	628 (43%)	344 (21%)
10	rural, weak inversion/moderate emissions	35 (13%)	9 (23%)

shows only weak altitude dependence above 5 m altitude, in agreement with our results. Below 5 m the assumption of a flat surface in our case leads to a different behavior than in the case of *Makar et al.* [1999].

4. Oxidation of VOCs and NO_2 by OH at Night

[72] The hydroxyl radical is known to be the main oxidant of VOCs and NO_2 during the day. At night, oxidation of pollutants by OH has thus far been mostly neglected. In this section we investigate the role of nocturnal OH in the removal of VOCs and NO_2.

[73] Table 2 summarizes the oxidation rates of VOCs and NO_2 by nighttime OH, averaged over the lowest 100 m of the NBL for the cases discussed in section 3, 3 hours after model start. In addition to the oxidation rates the relative contributions of nighttime OH compared with NO_3 and O_3 are shown. Reaction rates of OH + VOCs between 35 ppt h^{-1} in the rural case (scenario 10) and 1095 ppt h^{-1} in the weakly stable/high-emission scenario 4 were found. Nighttime OH contributes 13–46% to the total VOC oxidation at night. Compared with the oxidation rates of VOCs by OH during the day, which often exceed 1 ppb h^{-1} [*Crosley*, 1997; *Eisele et al.*, 1997; *Geyer et al.*, 2001; *Goldan et al.*, 1997; *Stroud et al.*, 2001; *Tan et al.*, 2001], the oxidation rates by OH during the night are low but not negligible.

[74] The single most important parameter controlling the contribution of the OH oxidation to the VOC removal is the emission rate of NO and other anthropogenic pollutants. The OH-induced VOC oxidation rate increases by a factor of 7 between low-emission scenario 2 and high-emission scenario 4. The relative contribution of nighttime OH to the nocturnal oxidation does, however, only change by a few percent, since the NO_3 + VOC and O_3 + VOC reaction rates also increase. Higher temperatures lead to a slightly higher OH + VOC reaction rate because the emission rates of biogenic VOCs increase. The relative contribution of OH is highest at cold temperatures (30%) because the contribution of NO_3 decreases with temperature. The degree of atmospheric stability has no strong influence on the role of nighttime OH as a VOC oxidant. In the rural cases the contribution of OH to the nocturnal VOC oxidation is considerably lower. The reaction rates are more than 1 order of magnitude below the rates in the urban cases. The low contribution can be explained by the fact that nighttime OH predominantly oxidizes anthropogenic VOCs, while the most abundant VOC species in the rural cases are biogenic monoterpenes, which are also oxidized by NO_3 and O_3.

[75] The results show that the contribution of nighttime OH to the VOC oxidation strongly depends on the VOC mix. In particular, in a case with high levels of alkanes or aldehydes, the hydroxyl radical can play a key role as an oxidant at night.

[76] Nighttime OH can also contribute to NO_x removal from the atmosphere by the oxidation of NO_2 into HNO_3 (followed by deposition of HNO_3). An oxidation rate of NO_2 by reaction with OH in the range of 22–585 ppt h^{-1} is predicted by the model in the urban scenarios (Table 2). Compared with other reactions, in particular, the hydrolysis and aerosol uptake of N_2O_5 [*Geyer and Stutz*, 2004], nighttime OH contributes only a few percent to the NO_2 loss in the NBL under normal conditions. Compared with the OH + NO_2 reaction rate during the day, which can be as high as 7 ppb h^{-1} at [OH] = 10^7 molecules cm^{-3} and [NO_2] = 20 ppb [*Donahue et al.*, 1997], NO_2 oxidation by nighttime OH is less important. The reaction rate of OH + NO_2 shows a clear dependence on the NO emission rate and is more than an order of magnitude larger in high-emission scenario 4 than in scenario 2. Temperature and atmospheric stability have a minor influence on this reaction. In the rural cases, lower reaction rates of OH + NO_2 were found ($\sim$9 ppt h^{-1}). The relative contribution of nighttime OH to the NO_2 removal increases with the monoterpene emission rate because the levels of NO_3 and N_2O_5 decrease simultaneously.

5. Conclusions

[77] A vertically highly resolved one-dimensional chemical transport model based on the RACM gas phase chemistry mechanism was applied to investigate the development of vertical profiles of peroxy radicals and OH in the nocturnal boundary layer. Our model results show that the vertical profiles of organic peroxy radicals, RO_2, show a maximum in the lower part of the NBL in all scenarios we investigated. The strong positive gradient below the maximum is caused by the high loss rate of RO_2 through its reaction with NO close to the ground. Above the maximum, [RO_2] slowly decreases with altitude because the RO_2 production by reactions of NO_3 and O_3 with unsaturated VOCs decreases. In all scenarios the reaction of NO_3 with monoterpenes is the most important net RO_2 source at

night. Hydroperoxy radicals, HO_2, develop a similar profile to RO_2. The maximum is, however, located closer to the ground. The positive gradient of HO_2 below this maximum is caused by the fast removal of HO_2 by reaction with NO. Above the maximum, [HO_2] decreases mostly because the HO_2 production by RO_2 + NO reactions decreases. The concentration of the hydroxyl radical, OH, is $\sim 10^5$ molecules cm^{-3} in the upper part of the NBL. However, in a layer close to the ground a high concentration maximum of $\sim 10^6$ molecules cm^{-3} can develop. These high nighttime levels of OH are caused by the maximum of the reaction rate of HO_2 and NO in this layer. Nighttime OH can significantly contribute to the removal of VOCs. In the cases discussed in this paper, 17–43% of the VOC oxidation is caused by OH at night. The conversion of NO_2 into HNO_3 by nighttime OH is negligible.

[78] To simplify the description of the altitude-dependent RO_x chemistry in the NBL, we propose to distinguish three chemical regimes on the basis of their RO_x chemistry and OH production rates. The regimes can be easily distinguished by using the NO + O_3 formation rate as an indicator.

[79] 1. The ground layer near the surface is defined by high levels of NO, which suppress the presence of NO_3 and O_3, reducing the NO + O_3 formation to near zero. All radical levels in this layer are low, and radical chemistry is basically inactive. The ground layer only forms when the destruction of O_3 by NO emissions at the ground surpasses the replenishment of ozone through downward transport.

[80] 2. The upper layer at the top of the NBL is characterized by high levels of NO_3, O_3, and organic peroxy radicals but negligible NO concentrations. Here VOCs are oxidized by NO_3 and O_3, but the peroxy radicals are only slowly converted into OH radicals. OH is mostly produced by the ozonolysis of alkenes. Again, the NO + O_3 rate is very low because of the low NO levels. The nocturnal RO_2 maximum typically develops in the lower part of the upper layer.

[81] 3. The reactive mixing layer is located between the ground layer and the upper layer. In this height interval, NO from the ground layer and NO_3, O_3, and RO_2 from the upper layer are mixed together. It is important to realize that in this layer the otherwise chemically unlikely simultaneous presence of RO_2, NO_3, and NO is maintained by vertical mixing. In addition to their downward transport, organic peroxy radicals are produced by NO_3 + VOC and O_3 + VOC reactions. RO_2 is rapidly converted into HO_2 and OH by reactions with NO. This fast radical propagation chain leads to high HO_2 and OH production. The concentration maxima of HO_2 and OH are located in the reactive layer. The reactive mixing layer is thus the height interval with the most active radical chemistry in the NBL.

[82] Our results illustrate a number of unique chemical transport mechanisms in the NBL that have thus far not been discussed in the literature:

[83] 1. Vertical transport of RO_2 radicals can play a crucial role for nocturnal chemistry. This transport is driven by the RO_2 concentration gradient, which is formed by high RO_2 production rates through the NO_3/O_3 + VOC reactions in the lower part of the upper layer, and destruction of RO_2 through its reaction with NO in the reactive mixing layer. Downward mixing of RO_2 acts as a sink for RO_2 above the NO-rich layer and as an important source close to the ground. This mechanism is important in all scenarios we investigated but in particular in scenarios with high monoterpene concentrations and weak stability.

[84] 2. Vertical transport of HNO_4, followed by its thermal decay, also often acts as an important source of HO_2, and thus indirectly of OH, near the ground. A positive vertical gradient of HNO_4 is formed through the destruction of HO_2 by NO near the ground that reduces [HNO_4] compared with its much higher pseudo steady state value aloft. This gradient leads to a downward transport of HNO_4, which then acts as an HO_2 source near the ground. This mechanism increases in importance with the degree of pollution and the vertical stability in the atmosphere. It is particularly important in urban environments.

[85] These two chemical transport mechanisms, in combination with purely chemical OH formation mechanisms, such as the ozonolysis of VOCs, can lead to significant amounts of OH in the reactive mixing layer. Further studies are necessary to expand our somewhat idealized model calculations to more realistic conditions. In addition, it would be desirable to test our results with field experiments that study the vertical distribution of radical species. The results of this paper and of previous work [*Geyer and Stutz*, 2004] clearly demonstrate the necessity of a one-dimensional approach with sufficient vertical resolution for both experimental and modeling studies of nocturnal chemistry.

[86] **Acknowledgments.** We would like to thank S. C. Hurlock, S. Wang, and Y. Stutz for helpful comments on the manuscript. This study was supported by the Department of Energy (grant DE-FG03-01ER63094).

References

Arya, S. P. (1988), *Introduction to Micrometeorology*, Academic, San Diego, Calif.

Bey, I., B. Aumont, and G. Toupance (1997), The nighttime production of OH radicals in the continental troposphere, *Geophys. Res. Lett.*, *24*, 1067–1070.

Bey, I., B. Aumont, and G. Toupance (2001), A modeling study of the nighttime radical chemistry in the lower continental troposphere: 2. Origin and evolution of HO_x, *J. Geophys. Res.*, *106*, 9991–10,001.

Brost, R. A., A. C. Delany, and B. J. Huebert (1988), Numerical modeling of concentrations and fluxes of HNO_3, NH_3, and NH_4NO_3 near the surface, *J. Geophys. Res.*, *93*, 7137–7152.

Businger, J. A., J. C. Wyngaard, Y. Izumi, and E. F. Bradley (1971), Flux profile relationships in the atmospheric surface layer, *J. Atmos. Sci.*, *28*, 181–189.

Cantrell, C. A., R. E. Shetter, T. M. Gilpin, and J. G. Calvert (1996a), Peroxy radicals measured during Mauna Loa Observatory Photochemistry Experiment: 2. The data and first analysis, *J. Geophys. Res.*, *101*, 14,643–14,652.

Cantrell, C. A., R. S. Shetter, and J. Calvert (1996b), Peroxy radical chemistry during FIELDVOC 1993 in Brittany, France, *Atmos. Environ.*, *30*, 3947–3957.

Cantrell, C. A., R. A. Shetter, J. G. Calvert, F. L. Eisele, and D. J. Tanner (1997), Some considerations of the origin of nighttime peroxy radicals observed in MLOPEX 2c, *J. Geophys. Res.*, *102*, 15,899–15,913.

Carslaw, N., L. J. Carpenter, J. M. C. Plane, B. J. Allan, R. A. Burgess, K. C. Clemitshaw, H. Coe, and S. A. Penkett (1997), Simultaneous observations of nitrate and peroxy radicals in the marine boundary layer, *J. Geophys. Res.*, *102*, 18,917–18,933.

Crosley, D. R. (1997), Tropospheric OH photochemistry experiment: A summary and perspective, *J. Geophys. Res.*, *102*, 6495–6510.

Curtis, A. R., and W. P. Sweetenham (1987), FACSIMILE release H user's manual, London.

Daele, V., G. Laverdet, G. Le Bras, and G. Poulet (1995), Kinetics of the reactions CH_3O + NO, CH_3O + NO_3, and CH_3O_2 + NO_3, *J. Phys. Chem.*, *99*, 1470–1477.

Donahue, N. M., M. K. Dubey, R. Mohrschladt, K. L. Demerjian, and J. G. Anderson (1997), High-pressure flow study of the reactions OH +

$NO_x \rightarrow HONO_x$: Errors in the falloff region, *J. Geophys. Res.*, *102*, 6159–6168.

Donahue, N. M., J. H. Kroll, J. G. Anderson, and K. L. Demerjian (1998), Direct observation of OH production from the ozonolysis of olefins, *Geophys. Res. Lett.*, *25*, 59–62.

Eisele, F. L., G. H. Mount, D. Tanner, A. Jefferson, R. Shetter, J. W. Harder, and E. J. Williams (1997), Understanding the production and interconversion of the hydroxyl radical during the Tropospheric OH Photochemistry Experiment, *J. Geophys. Res.*, *102*, 6457–6465.

Faloona, I., et al. (2001), Nighttime observations of anomalously high levels of hydroxyl radicals above a deciduous forest canopy, *J. Geophys. Res.*, *106*, 24,315–24,333.

Fitzjarrald, D. R., and D. Lenschow (1983), Mean concentration and flux profiles for chemically reactive species in the atmospheric surface layer, *Atmos. Environ.*, *17*, 2505–2512.

Fuchs, N. A., and A. G. Sutugin (1971), *Highly Dispersed Aerosols*, Butterworth-Heinemann, Woburn, Mass.

Galmarini, S., P. G. Duynkerke, and J. Vilà-Guerau de Arellano (1997), Evolution of nitrogen oxide chemistry in the nocturnal boundary layer, *J. Appl. Meteorol.*, *36*(7), 943–957.

Geiger, H., I. Barnes, I. Bejan, T. Benter, and M. Spittler (2003), The tropospheric degradation of isoprene: An updated module for the regional atmospheric chemistry mechanism, *Atmos. Environ.*, *37*, 1503–1519.

George, L. A., T. M. Hard, and R. J. O'Brien (1999), Measurement of free radicals OH and HO_2 in Los Angeles smog, *J. Geophys. Res.*, *104*, 1643–1655.

Geyer, A., and J. Stutz (2004), Vertical profiles of NO_3, N_2O_5, O_3, and NO_x in the nocturnal boundary layer: 2. Model studies on the altitude dependence of composition and chemistry, *J. Geophys. Res.*, *109*, D12307, doi:10.1029/2003JD004211.

Geyer, A., B. Alicke, S. Konrad, T. Schmitz, J. Stutz, and U. Platt (2001), Chemistry and oxidation capacity of the nitrate radical in the continental boundary layer near Berlin, *J. Geophys. Res.*, *106*, 8013–8025.

Geyer, A., et al. (2003), Nighttime formation of peroxy and hydroxyl radicals during the BERLIOZ campaign: Observations and modeling studies, *J. Geophys. Res.*, *108*(D4), 8249, doi:10.1029/2001JD000656.

Goldan, P. D., W. C. Kuster, and F. C. Fehsenfeld (1997), Nonmethane hydrocarbon measurements during the Tropospheric OH Photochemistry Experiment, *J. Geophys. Res.*, *102*, 6315–6324.

Gölz, C., J. Senzig, and U. Platt (2001), NO_3-initiated oxidation of biogenic hydrocarbons, *Chemosphere Global Change Sci.*, *3*(3), 339–352.

Guenther, A. B., P. R. Zimmerman, P. C. Harley, R. K. Monson, and R. Fall (1993), Isoprene and monoterpene emission rate variability: Model evaluations and sensitivity analyses, *J. Geophys. Res.*, *98*, 12,609–12,617.

Guenther, A., et al. (1996), Isoprene fluxes measured by enclosure, relaxed eddy accumulation, surface layer gradient, mixed layer gradient, and mixed layer mass balance techniques, *J. Geophys. Res.*, *101*, 18,555–18,567.

Hamba, F. (1987), Statistical analysis of chemically reacting passive scalars in turbulent flows, *J. Phys. Soc. Jpn.*, *56*, 79–96.

Hamba, F. (1993), A modified *K* model for chemically reactive species in the planetary boundary layer, *J. Geophys. Res.*, *98*, 5173–5182.

Harrison, R. M., J. P. Shi, and J. L. Grenfell (1998), Novel nighttime free radical chemistry in severe nitrogen dioxide pollution episodes, *Atmos. Environ.*, *32*, 2769–2774.

Haugen, D. A., (Ed.) (1973), *Workshop on Micrometeorology*, Am. Meterol. Soc., Boston, Mass.

Holland, F., A. Hofzumahaus, J. Schäfer, A. Kraus, and H.-W. Pätz (2003), Measurements of OH and HO_2 radical concentrations and photolysis frequencies during BERLIOZ, *J. Geophys. Res.*, *108*(D4), 8246, doi:10.1029/2001JD001393.

Hu, J., and D. H. Stedman (1995), Atmospheric RO_x radicals at an urban site: Comparison to a simple theoretical model, *Environ. Sci. Technol.*, *29*, 1655–1659.

Kanaya, Y., Y. Sadanaga, J. Matsumoto, U. K. Sharma, J. Hirokawa, Y. Kajii, and H. Akimoto (1999), Nighttime observation of the HO_2 radical by an LIF instrument at Oki island, Japan, and its possible origins, *Geophys. Res. Lett.*, *26*, 2179–2182.

Konrad, S., et al. (2003), Hydrocarbon measurements at Pabstthum during the BERLIOZ campaign and modeling of free radicals, *J. Geophys. Res.*, *108*, 8251, doi:10.1029/2001JD000866.

Kurtenbach, R., K. H. Becker, J. A. G. Gomes, J. Kleffmann, J. C. Lorzer, M. Spittler, P. Wiesen, R. Ackermann, A. Geyer, and U. Platt (2001), Investigations of emissions and heterogeneous formation of HONO in a road traffic tunnel, *Atmos. Environ.*, *35*, 3385–3394.

Kurtenbach, R., R. Ackermann, K. H. Becker, A. Geyer, J. A. G. Gomes, J. C. Lörzer, U. Platt, and P. Wiesen (2002), Verification of the contribution of vehicular traffic to the total NMVOC emissions in Germany and the importance of the NO_3 chemistry in the city air, *J. Atmos. Chem.*, *42*, 395–411.

Lee, S.-M., H. J. S. Fernando, M. Princevac, D. Zajic, M. Sinesi, J. L. McCulley, and J. Anderson (2003), Transport and diffusion of ozone in the nocturnal and morning planetary boundary layer of the Phoenix Valley, *Environ. Fluid Mech.*, *3*, 331–362.

Lenschow, D. (1981), Reactive trace species in the boundary layer from a micrometeorological perspective, *J. Phys. Soc. Jpn.*, *60*, 472–480.

Makar, P. A., J. D. Fuentes, D. Wang, R. M. Staebler, and H. A. Wiebe (1999), Chemical processing of biogenic hydrocarbons within and above a temperate deciduous forest, *J. Geophys. Res.*, *104*, 3581–3603.

Mihelcic, D., D. Klemp, P. Musgen, H. W. Paetz, and A. Volz-Thomas (1993), Simultaneous measurements of peroxy and nitrate radicals at Schauinsland, *J. Atmos. Chem.*, *16*, 313–335.

Mihelcic, D., et al. (2003), Peroxy radicals during BERLIOZ at Pabstthum: Measurements, radical budgets and ozone production, *J. Geophys. Res.*, *108*, 8254, doi:10.1029/2001JD001014.

Monks, P. S., L. J. Carpenter, S. A. Penkett, and G. P. Ayers (1996), Nighttime peroxy radical chemistry in the remote marine boundary layer over the Southern Ocean, *Geophys. Res. Lett.*, *23*, 535–538.

Neeb, P., and G. K. Moortgat (1999), Formation of OH radicals in the gas-phase reaction of propene, isobutene, and isoprene with O_3: Yields and mechanistic implications, *J. Phys. Chem. A*, *103*(45), 9003–9012.

Paulson, S. E., and J. J. Orlando (1996), The reactions of ozone with alkenes: An important source of HO_x in the boundary layer, *Geophys. Res. Lett.*, *23*, 3727–3730.

Paulson, S. E., A. D. Sen, L. Ping, J. D. Fenske, and M. J. Fox (1997), Evidence for formation of OH radicals from the reaction of O_3 with alkenes in the gas phase, *Geophys. Res. Lett.*, *24*, 3193–3196.

Paulson, S. E., M. Y. Chung, and A. S. Hasson (1999), OH radical formation from the gas-phase reaction of ozone with terminal alkenes and the relationship between structure and mechanism, *J. Phys. Chem. A*, *103*(41), 8125–8138.

Platt, U., G. LeBras, G. Poulet, J. P. Burrows, and G. Moortgat (1990), Peroxy radicals from night-time reaction of NO_3 with organic compounds, *Nature*, *348*(6297), 147–149.

Ren, X., H. Harder, M. Martinez, R. L. Lesher, A. Oliger, T. Shirley, J. Adams, J. B. Simpas, and W. H. Brune (2003), HO_x concentrations and OH reactivity observations in New York City during PMTACS-NY2001, *Atmos. Environ.*, *37*, 3627–3637.

Sillman, S., et al. (2002), Loss of isoprene and sources of nighttime OH radicals at a rural site in the United States: Results from photochemical models, *J. Geophys. Res.*, *107*(D5), 4043, doi:10.1029/2001JD000449.

Stockwell, W. R., F. Kirchner, M. Kuhn, and S. Seefeld (1997), A new mechanism for regional atmospheric chemistry modeling, *J. Geophys. Res.*, *102*(D22), 25,847–25,879.

Stroud, C. A., et al. (2001), Isoprene and its oxidation products, methacrolein and methylvinyl ketone, at an urban forested site during the 1999 Southern Oxidants Study, *J. Geophys. Res.*, *106*, 8035–8046.

Stutz, J., B. Alicke, R. Ackermann, A. Geyer, A. White, and E. Williams (2004), Vertical profiles of NO_3, N_2O_5, O_3, and NO_x in the nocturnal boundary layer: 1. Observations during the Texas Air Quality Study 2000, *J. Geophys. Res.*, D12306, doi:10.1029/2003JD004209.

Tan, D., et al. (2001), HO_x budgets in a deciduous forest: Results from the PROPHET summer 1998 campaign, *J. Geophys. Res.*, *106*, 24,407–24,427.

Tanner, D. J., and F. L. Eisele (1995), Present OH measurement limits and associated uncertainties, *J. Geophys. Res.*, *100*, 2883–2892.

Vilà-Guerau de Arellano, J., P. G. Duynkerke, and K. F. Zeller (1995), Atmospheric surface layer similarity theory applied to chemically reactive species, *J. Geophys. Res.*, *100*, 1397–1408.

Volz-Thomas, A., H. W. Paetz, N. Houben, S. Konrad, D. Mihelcic, T. Kluepfel, and D. Perner (2003), Inorganic trace gases and peroxy radicals during BERLIOZ at Pabstthum: An investigation of the photostationary state of NO_x and O_3, *J. Geophys. Res.*, *108*(D4), 8248, doi:10.1029/2001JD001255.

Wahner, A., T. F. Mentel, and M. Sohn (1998), Gas-phase reaction of N_2O_5 with water vapor: Importance of heterogeneous hydrolysis of N_2O_5 and surface desorption of HNO_3 in a large Teflon chamber, *Geophys. Res. Lett.*, *25*, 2169–2172.

Yoshizawa, A. (1982), A statistical investigation of shear turbulence: The Reynolds-stress transport equation, *J. Phys. Soc. Jpn.*, *51*, 658–666.

A. Geyer and J. Stutz, Department of Atmospheric Sciences, University of California, 7127 Math Sciences, Los Angeles, CA 90095-1565, USA. (andreas@atmos.ucla.edu; jochen@atmos.ucla.edu)

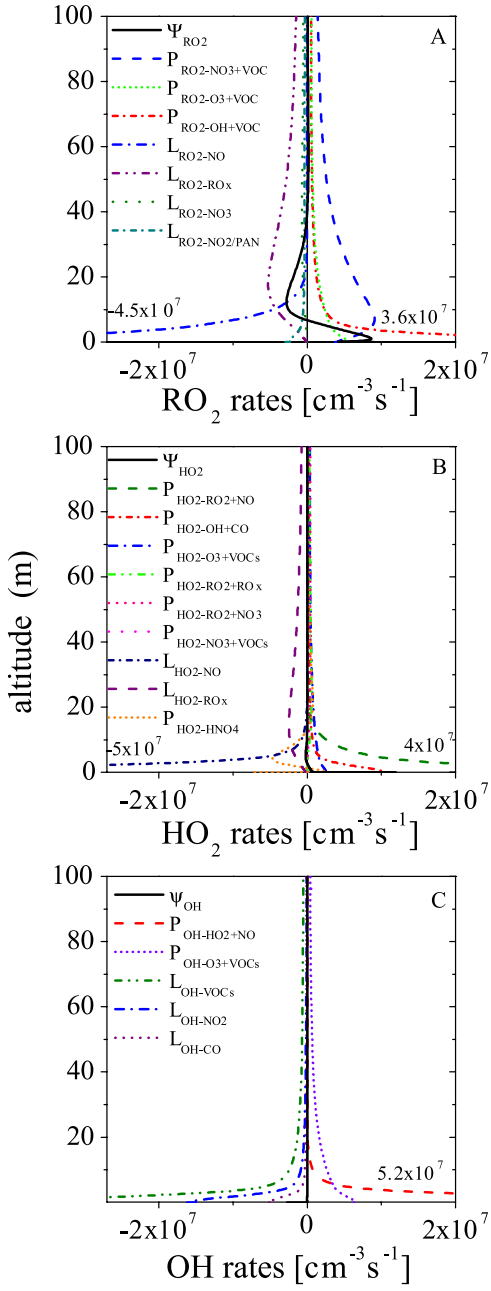

Figure 3. Vertical profiles of chemical rates and the rate of change by vertical transport of RO_2, HO_2, and OH 3 hours after model start for scenario 1.

Vertical profiles of NO_3, N_2O_5, O_3, and NO_x in the nocturnal boundary layer: 2. Model studies on the altitude dependence of composition and chemistry

Andreas Geyer and Jochen Stutz

Department of Atmospheric Sciences, University of California, Los Angeles, California, USA

Received 2 October 2003; revised 8 March 2004; accepted 31 March 2004; published 30 June 2004.

[1] Recent field observations in urban areas have shown that trace gases, such as O_3, NO_2, and NO_3, develop distinct vertical concentration profiles at night. Because nocturnal chemistry can change the gas-phase and particulate composition in the urban boundary layer considerably, it is important to understand the mechanisms that lead to the change of trace gas levels with altitude. The quantification of the altitude dependence of chemical processes leading to the removal of volatile organic carbons (VOC) and NO_x are crucial to assess the influence of nocturnal chemistry on ozone formation during the following day. We present a one-dimensional chemical transport model developed to study the interaction between chemistry and vertical transport in the nocturnal boundary layer. The model reproduces the general features found in field observations, such as positive O_3 and NO_3 gradients. The slow upward transport of NO and VOC emitted near the ground and the simultaneously occurring chemistry, in particular the reactions of NO with O_3 and NO_3, are found to control the vertical structure of the chemistry of NO_x, NO_3, N_2O_5, and VOC. In the case of NO_2 and O_3, dry deposition is also significant. The model results show that vertical transport of N_2O_5 plays an important role, and is often the main source of NO_3 radicals near the ground. Chemical steady state calculations of the concentrations of NO_3 and N_2O_5, as they have been used in the past, are therefore not representative in cases with significant vertical fluxes of N_2O_5. The vertical gradient of the oxidation rate of NO_2 implies that the removal of NO_x occurs predominately in the upper nocturnal boundary layer (NBL). Our study shows that observations at one altitude and chemical box models are often insufficient to accurately describe the chemistry in NBL. *INDEX TERMS:* 0345 Atmospheric Composition and Structure: Pollution—urban and regional (0305); 0365 Atmospheric Composition and Structure: Troposphere—composition and chemistry; 0368 Atmospheric Composition and Structure: Troposphere—constituent transport and chemistry; *KEYWORDS:* nocturnal chemistry, nitrate radical, vertical transport

Citation: Geyer, A., and J. Stutz (2004), Vertical profiles of NO_3, N_2O_5, O_3, and NO_x in the nocturnal boundary layer: 2. Model studies on the altitude dependence of composition and chemistry, *J. Geophys. Res.*, *109*, D12307, doi:10.1029/2003JD004211.

1. Introduction

[2] Nocturnal chemistry and physics play a crucial role in the conversion and removal of air pollutants such as nitrogen oxides and volatile organic carbons (VOC), which would otherwise be available for daytime ozone formation [*Allan et al.*, 2000; *Geyer et al.*, 2001a, 2001b; *Heintz et al.*, 1996; *Martinez et al.*, 2000; *Mihelcic et al.*, 1993; *Paulson and Orlando*, 1996; *Platt et al.*, 2002; *Smith et al.*, 1995; *Wayne et al.*, 1991]. Photolytic reactions, which are the driving force of atmospheric chemistry during the day, are absent at night. As a consequence, the NO_3 radical, which is rapidly photolyzed during the day [*Geyer et al.*, 2003a; *Magnotta and Johnston*, 1980; *Wayne et al.*, 1991], becomes the dominant radical species. Besides NO_3, ozone plays an important role as an oxidant of NO and unsaturated VOC.

[3] During the night convection is suppressed by radiative cooling of the surface, often generating stable vertical stratification. Consequently, vertical turbulent transport produced by wind shear is reduced by negative buoyancy [*Arya*, 1988; *Businger et al.*, 1971; *Rao and Snodgrass*, 1979]. Trace gases emitted near the surface can accumulate close to the ground influencing the vertical profiles of reactive species. Zero-dimensional approaches such as measuring trace gases at only one altitude, or applying box models, which assume vertically evenly distributed concen-

0148-0227/04/2003JD004211$09.00

trations [*Allan et al.*, 2000; *Bey et al.*, 1997; *Faloona et al.*, 2001; *Geyer et al.*, 2003b; *Gölz et al.*, 2001; *Mihelcic et al.*, 1993; *Platt et al.*, 1990], may therefore not be applicable in the nocturnal boundary layer (NBL).

[4] This is the second of two papers proposing a one-dimensional view of the NBL. The first paper by *Stutz et al.* [2004] concentrates on the observation and interpretation of vertical profiles of the NO-O_3-NO_2 system, NO_3, and N_2O_5 during the TEXAQS 2000 study in La Porte near Houston, TX. Here we describe one-dimensional modeling studies of the mechanisms influencing the development of vertical profiles of trace gas concentrations in the urban and rural NBL. The role of vertical transport in nocturnal chemistry, and the influence of chemistry on the vertical fluxes of reactive gases in the NBL are analyzed.

[5] The following section gives a short overview of previous work about the vertical distribution of trace gases in the planetary boundary layer.

1.1. The Vertical Distribution of Trace Gases in the NBL

[6] During recent years a number of studies were performed to investigate the vertical profiles of trace gases in the NBL. Generally, a reduction of O_3 toward the ground was observed in both rural and urban areas [*Cros et al.*, 1992; *Glaser et al.*, 2003; *Guesten et al.*, 1998; *Pisano et al.*, 1997; *Stutz et al.*, 2004; *Wang et al.*, 2003; *Zhang and Rao*, 1999]. The positive O_3 gradient is attributed to dry deposition of O_3, and titration of O_3 with NO emitted close to the ground. Often, ozone is completely destroyed in the NBL at the end of the night, while it is present at a mixing ratio of more than 40 ppb above 400 m altitude [*Guesten et al.*, 1998]. Contrary to O_3, NO_2 often develops a negative gradient, with highest values in the lowest part of the nocturnal atmosphere due to its production from the reaction of NO and O_3 [*Glaser et al.*, 2003; *Guesten et al.*, 1998; *Stutz et al.*, 2004; *Wang et al.*, 2003].

[7] Several groups have applied one-dimensional models to study the vertical structures of the NO-O_3-NO_2 system in the boundary layer [*Fitzjarrald and Lenschow*, 1983; *Gao and Wesely*, 1994; *Gao et al.*, 1991; *Hov*, 1983; *Kramm et al.*, 1991; *Lenschow and Delany*, 1987; *Thompson and Lenschow*, 1984]. These studies predict that the fast titration of NO in polluted air can lead to the development of negative gradients of [NO] and [NO_2] and a positive gradient of [O_3] in the lower boundary layer. The absence of NO_2 photolysis and weaker vertical mixing seems to intensify the vertical gradients during night [*Galmarini et al.*, 1997; *Hov*, 1983; *Riemer et al.*, 2003].

[8] Recently, several studies have focused on the investigation of the NO_3 gradient in the NBL [*Aliwell and Jones*, 1998; *Allan et al.*, 2002; *Fish et al.*, 1999; *von Friedeburg et al.*, 2002; *Galmarini et al.*, 1997; *Povey et al.*, 1998; *Riemer et al.*, 2003; *Wang et al.*, 2003; *Weaver et al.*, 1996]. Generally, urban NO_3 levels are higher at the top of the NBL than near the surface, due to NO emission near the surface and the suppressed mixing during the night [*Aliwell and Jones*, 1998; *von Friedeburg et al.*, 2002]. Close to the ground, NO_3 is often completely depleted, while up to ~120 ppt were detected at 300 m altitude. The observations by *Stutz et al.* [2004] confirm that in urban areas NO_3 has a positive gradient during most nights. While the NO_3 concentration was often below the detection limit of 10–20 ppt 2 m above the ground, more than 100 ppt were measured at a height of 99–115 m.

[9] Model studies of the vertical profile of [NO_3] in the lowest 2 km performed by *Fish et al.* [1999] also show that NO_3 levels are significantly lower near the ground than at the top of the NBL. Using 1D model calculations for an urban plume case, *Riemer et al.* [2003] derive a strong positive gradient of [NO_3] in the lowest ~150 m of the NBL ranging from near-zero levels at the ground to several hundred ppt at 150 m for both high and low NO_x regimes.

2. Model Description

[10] The one-dimensional nocturnal chemical and transport model (NCAT) is based on a system of 1D transport kinetics equations, which express the change of the concentration $c_i(z, t)$ of a trace gas i at an altitude z at the time t as follows:

$$\frac{dc_i(z,t)}{dt} = \Psi_i(z,t) + P_i(z,t) - L_i(z,t) + E_i(z,t). \quad (1)$$

[11] Here, $\Psi_i(z, t) = -\frac{\partial j_i(z,t)}{\partial z}$ is the rate of the concentration change caused by the net vertical flux $j_i(z, t)$, $P_i(z, t)$ the total chemical production rate, $L_i(z, t)$ the total chemical loss rate, and $E_i(z, t)$ the emission rate of compound i. The equation system is solved with a Gear-type solver (Facsimile [*Curtis and Sweetenham*, 1987]). Concentration changes by advection are neglected.

[12] The model spans altitudes from the ground up to 1 km. For this study we subdivided the lowest 250 m into 20 boxes (sensitivity tests show that the results are identical to that of model runs using more than 100 grid points). An additional box between 250 m and 1000 m is used to provide an upper boundary for the model. Considering the reduced vertical transport efficiency near the ground, a logarithmic scale was chosen below 1 m.

[13] The model includes an explicit computation of vertical exchange and the temperature profile, gas-phase and heterogeneous nocturnal NO_x-NO_3-HO_x-O_3 chemistry, a simplified VOC oxidation scheme, emission of NO from soil and cars, CO emission from cars, emission of monoterpenes from the biosphere, and dry deposition on the ground. Because the model is restricted to nighttime conditions, photolytic reactions are not included.

2.1. Vertical Transport Calculation

2.1.1. Vertical Flux of an Inert Gas

[14] The vertical flux, $j_i(z, t)$, of an inert or slow reacting trace gas, for example CO and CH_4, is calculated in the model using a linear flux-gradient relationship (K model, we implicitly assume that atmospheric density does not change over the height of the NBL):

$$j_i(z,t) = -K_{inert}(z,t) \cdot \frac{\partial c_i(z,t)}{\partial z} \quad (2)$$

[15] In this first-order model, the vertical flux $j_i(z, t)$ only depends on the vertical concentration gradient of a gas i, $\frac{\partial c_i(z,t)}{\partial z}$, and on the altitude dependent eddy diffu-

sivity $K_{inert}(z, t)$ (laminar diffusion is considered only close to the ground surface). The eddy diffusivity is identical for all inert gases, and is calculated by Monin-Obukhov similarity theory for an aerodynamically plane terrain using the empirical equations for the dimensionless stability correction factor, $\Phi_S\left(\frac{z}{L*}, t\right)$, for turbulent molecular transport given by *Businger et al.* [1971] for the lowest 50 m.

$$K_{inert}(z,t) = \frac{\kappa \cdot u^*(t) \cdot z}{\Phi_S\left(\frac{z}{L^*}, t\right)} \quad (3)$$

[16] In equation (3), $\kappa \approx 0.4$ is the von-Karman constant, and $u^*(t)$ the Prandtl layer friction velocity. Above 50 m the inert eddy diffusivity is set to its value at 50 m altitude. The correction factor $\Phi_S\left(\frac{z}{L*}, t\right)$ is a function of altitude and atmospheric stability, which is described by the Monin-Obukhov length $L^*(t)$.

2.1.2. Vertical Flux of a Reactive Gas

[17] As pointed out by several studies [*Brost et al.*, 1988; *Fitzjarrald and Lenschow*, 1983; *Galmarini et al.*, 1997; *Gao et al.*, 1991; *Hamba*, 1993; *Lenschow*, 1982; *McDonald-Buller et al.*, 1999; *Schumann*, 1989; *Thompson and Lenschow*, 1984; *Vila-Guerau de Arellano*, 2003; *Vila-Guerau de Arellano et al.*, 1995], the unmodified K model is restricted to inert or slow reacting gases because the effect of chemistry on the vertical flux of a trace gas is not considered. Since second order closure models, as applied for example by *Galmarini et al.* [1997] and *Vila-Guerau de Arellano et al.* [1995] for reactive gases, are difficult to use with complex chemical frameworks, we included a modified K model in NCAT, which considers the effects of both vertical mixing and chemistry on the vertical flux of a trace gas.

[18] The vertical net flux of a reactive species i can therefore be approximated by

$$j_i(z,t) = \overline{w'(z,t)\cdot z'} \cdot \frac{\partial c_i(z,t)}{\partial z} + \overline{w'(z,t)\cdot z'} \cdot \frac{\partial\left(P_{ij}(z,t) - L_{ij}(z,t)\right)}{\partial z} \cdot \tau_{ieff}(z,t), \quad (4)$$

where $w'(z, t)$ is the fluctuations the vertical component of the wind speed, z' the turbulent mixing length, and $\tau_{i\ eff}(z, t)$ an effective timescale for the transport. Using the definition $K_{inert}(z, t) = \overline{w' \cdot z'}$, the flux of a reactive species can be expressed by

$$j_i(z,t) = -K_{inert}(z,t) \cdot \left(\frac{\partial c_i(z,t)}{\partial z} + \frac{\partial(P_i(z,t) - L_i(z,t))}{\partial z} \cdot \tau_{ieff}(z,t)\right) \quad (5)$$

[19] Equation (5) is similar to the modified K model discussed by *Hamba* [1993] [also *Hamba*, 1994; *Verver*, 1994]. The effective time $\tau_{i\ eff}$ was approximated by *Hamba* [1987] using the Two Scale Direct Interaction Approximation (TSDIA) theory [*Yoshizawa*, 1982].

$$\tau_{ieff}(z,t) = \frac{1}{\tau^{-1}_{i\,turbulent}(z,t) + \sum_l |j_{il}| + \sum_{l,m} |k_{ilm}(c_l + c_m)|} \quad (6)$$

[20] In equation (6), j_{il} represent the reaction rate constant of an unimolecular reaction, k_{ilm} the rate constant of a bimolecular reaction involving the gas i. The turbulence timescale $\tau_{i\ turbulent}(z, t) = \frac{z}{\kappa \cdot u^*(t)}$ is on the order of 100 s in the NBL [*Fitzjarrald and Lenschow*, 1983; *Lenschow*, 1981].

[21] By introducing the modified K model (equation (5)), vertical transport of a gas is no longer only a function of its concentration profile, but also of the concentration profiles of other gases that react or are educts of this gas (cross-diffusion). Equation (5) is particularly useful if turbulent transport and chemistry occur on comparative timescales. If the chemical timescale of a gas is very short, its vertical flux is influenced little by chemistry, either because it is in a steady state or because τ_{ieff} is small. At the other extreme, vertical transport of a gas is hardly influenced by chemistry if its chemical timescale is very long, and equation (2) can be used to calculate $j_i(z, t)$.

2.1.3. Calculation of the Temperature Profile

[22] The profile of the potential temperature $\Theta(z, t)$ in the lowest 50 m is calculated from the heat flux $H(t)$ according to $\frac{d\Theta(z,t)}{dz} = -\frac{H(z,t)}{c_p \cdot \rho} \cdot \frac{1}{\kappa \cdot u^*(t) \cdot z} \Phi_H\left(\frac{z}{L*}, t\right)$ [*Arya*, 1988; *Haugen*, 1973]. Here, c_p represents the mass heat capacity of air, ρ its density, and $\Phi_H\left(\frac{z}{L*}, t\right)$ the dimensionless correction factor for heat transport suggested by *Businger et al.* [1971]. Above 50 m the potential temperature is set to its value at 50 m altitude. The temperature profile is explicitly used to calculate temperature dependent rate constants and the profile of $[H_2O]$.

2.2. Chemical Mechanism

[23] A simplified version of the chemical reaction scheme of the model is shown in Figure 1. The reaction framework, as well as most reaction rate constants, are adopted from the Master Chemical Mechanism 3 [*Jenkin et al.*, 2003; *Saunders et al.*, 2003]. The reaction rates for the NO_3 self-reaction and gas-phase hydrolysis of N_2O_5 are taken from *Sander et al.* [2003] and *Atkinson et al.* [2002], respectively. The gas-phase chemistry module is limited to the nocturnal key species NO, NO_2, NO_3, N_2O_5, HONO, O_3, CO, the HO_x radical group OH and HO_2 (with the reservoir species HO_2NO_2), α-pinene, isoprene, propene, propane, CH_4, various RO_2 radicals, and PAN. The chemistry of reaction products, such as HNO_3, aldehydes, and H_2O_2, which show slow chemistry at night, is not further considered in NCAT.

[24] A key chain is the sequential oxidation of NO into NO_2 and NO_3 by ozone. The nitrate radical can react with NO back into NO_2. Another reaction path of NO_3 is the reaction with unsaturated VOC. The reaction of NO_3 with NO_2 can lead to the formation of the reservoir species N_2O_5, which rapidly decays again into NO_3 and NO_2. N_2O_5 can also react with water vapor or water adsorbed on aerosol surfaces (see section 2.3). For more details on NO_3 chemistry refer to *Geyer et al.* [2001b] and *Wayne et al.* [1991].

[25] The complex VOC reaction system in the atmosphere is simplified in the NCAT model by including the explicit oxidation mechanisms of four VOC representing different classes of VOC. This obvious simplification of the VOC chemistry should not affect the analysis of the chemical transport mechanisms in this study. Biogenic VOC are represented by α-pinene and isoprene. These species often account for a major part of the nocturnal VOC reactivity toward NO_3 and O_3, even in urban environments [*Berndt and Boge*, 1997; *Fuentes et al.*, 2000; *Geyer et al.*,

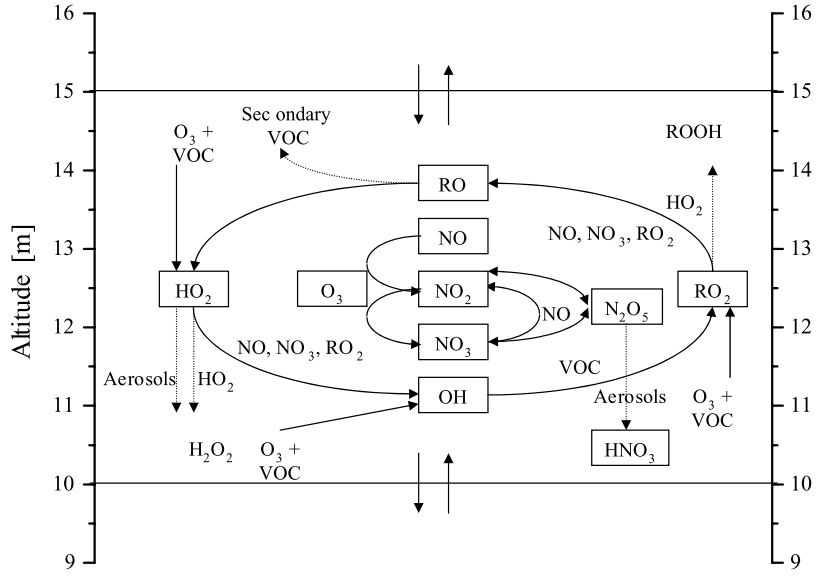

Figure 1. Setup of the one-dimensional model: Nocturnal NO_3 and RO_x cycles in a box between the altitudes of 10 and 15 m (as an example), with simultaneous exchange of molecules with the upper and lower boxes.

2001b; *Guenther et al.*, 2000; *Kesselmeier and Staudt*, 1999; *Paulson et al.*, 1998]. Alkanes and alkenes are represented by propane and propene, respectively. The VOC oxidation chains initiated by reactions with NO_3 and OH generally follow the sequence VOC-RO_2-(RO)-HO_2-OH, which is discussed in detail by *Geyer et al.* [2003b]. The direct formation of HO_2 and OH radicals by ozonolysis is also included in the NCAT model [*Paulson and Orlando*, 1996]. Another source of peroxy radicals is the thermal decay of photochemically produced peroxyacetyl nitrate (PAN), which can persist into the night.

2.3. Deposition, Aerosol Uptake, and Emission

[26] Dry deposition and uptake onto aerosols is calculated for a number of species including O_3, NO_2, NO_3, N_2O_5, HONO, and HO_2. The range of uptake coefficients for the various aerosol and ground surfaces is large (see the IUPAC recommendation under http://www.iupac-kinetic.ch.cam.ac.uk). We have therefore chosen uptake coefficients that are in the middle of the range of measured data (see Table 1).

[27] Dry deposition is calculated from the number of molecules of a gas in the lowest box colliding with the surface and the respective uptake coefficient. We assume a flat ground surface for the calculation of the deposition rate, which may lead to an underestimation of the dry deposition. The uptake rate of a gas onto aerosols is calculated from the aerosol surface area (assuming a particle diameter of 150 nm) and the uptake coefficient according to the mass transfer equation given by *Fuchs and Sutugin* [1971].

[28] Biogenic emissions of NO from the soil and α-pinene from vegetation (uniformly in altitudes between 1 and 10 m) are included in the model. Additionally, traffic emissions of NO and CO between 0.1 and 1 m altitude are considered in the urban case scenarios, with a [CO]/[NO] emission ratio of 6 [*Klemp et al.*, 2002].

2.4. Initialization of the Model

[29] The model is initialized with meteorological parameters, emission rates, and concentrations of O_3, NO_2, PAN, and VOC typical for the early part of the night [e.g., *Atkinson*, 2000; *Finlayson-Pitts and Pitts*, 2000]. All other compounds start at near-zero concentration. Because of the convective conditions during the day, all trace gases start with uniform concentrations in the NBL. The initial parameters of the scenarios discussed in this paper are summarized in Table 2.

[30] The variations of trace gas concentrations are calculated for six hours following model start. Since the intent of this paper is to study the mechanisms of the interaction of chemistry and transport in the NBL rather than to simulate the evolution of vertical profiles during the night, meteorological parameters (including the inert eddy diffusivity and temperature profile) and emission rates are kept at their initial values. This simplification has no impact on the conclusions of this paper.

[31] In this study, three different nocturnal stabilities, neutral (K_{inert}(10 m) = 1.0 m^2/s), weak inversion (K_{inert}(10 m) = 0.3 m^2/s), and strong inversion (K_{inert}(10 m) = 0.06 m^2/s)),

Table 1. Uptake Coefficients Used in the NCAT Model

Species	Substrate	Temp, K	Uptake Coefficient γ	Reference
O_3	sand	296	6×10^{-5}	*Michel et al.* [2002]
NO_2	typical value	298	10^{-4}	*Jacob* [2000]
NO_3	water (KI = 10^{-5} M)	273	1.3×10^{-3}	*Rudich et al.* [1996]
N_2O_5	80% $(NH_4)_2SO_4$ aerosol, rH = 50%	297	0.044	*Hu and Abbatt* [1997]
HONO	liquid jet	299	5×10^{-3}	*Kirchner et al.* [1990]
HO_2	typical value	298	0.2	*Jacob* [2000]

Table 2. Start Parameters of the Model Scenarios

Scenario	K_{inert} in 10 m, m^2/s	T in 50 m, K	Aerosol Surface, $\mu m^2/cm^3$	NO_2 Initial, ppb	O_3 Initial, ppb	Isoprene Initial, ppb	Propene Initial, ppb	Propane Initial, ppb	PAN Initial, ppb	Emission Rates NO From Cars in 0.1–1 m/ α-Pinene in 1–10 m, molecules/cm^3s
Urban Scenarios										
1	0.3	290	200	10	60	0.2	4	20	1	2×10^9/ 3×10^6
2	0.06	290	200	10	60	0.2	4	20	1	2×10^9/ 3×10^6
3	1.0	290	200	10	60	0.2	4	20	1	2×10^9/ 3×10^6
4	0.3	290	200	10	60	0.2	4	20	1	0.5×10^9/ 3×10^6
5	0.3	290	200	10	60	0.2	4	20	1	10×10^9/ 3×10^6
6	0.3	290	200	30	120	0.2	4	20	1	2×10^9/ 3×10^6
7	0.3	290	200	3	40	0.2	4	20	1	2×10^9/ 3×10^6
8	0.3	290	50	10	60	0.2	4	20	1	2×10^9/ 3×10^6
9	0.3	290	200–800	10	60	0.2	4	20	1	2×10^9/ 3×10^6
Rural Scenarios										
10	0.3	290	200	3	60	0.6	1	4	0.2	0/ 3×10^6
11	0.3	290	200	3	60	0.6	1	4	0.2	0/ 6×10^6
12	0.3	290	200	3	60	0.6	1	4	0.2	0/ 15×10^6
Temperature Scenarios										
13	0.3	275	200	10	60	0.2	4	20	1	2×10^9/ 3×10^6
14	0.3	305	200	10	60	0.2	4	20	1	2×10^9/ 3×10^6

were used [*Businger et al.*, 1971]. While in the neutral case an adiabatic temperature gradient is calculated, the model predicts a temperature inversion in the very stable case (dT/dz = 0.13 K/m in the lowest 50 m). The ambient temperature at 50 m altitude was varied between 275 K and 305 K in the different model runs. The atmospheric pressure at the ground was fixed at 1013 mbar. The relative humidity was set to 50% at all heights. A uniform aerosol surface area of 200 $\mu m^2/cm^3$, a level which is typical for urban areas [*McMurry*, 2000; *Seinfeld and Pandis*, 1997], was used in most scenarios. In addition, the effect of a lower uniform surface area of 50 $\mu m^2/cm^3$ was calculated. The influence of a negative aerosol surface gradient (exponential decrease from 800 $\mu m^2/cm^3$ at the ground to 200 $\mu m^2/cm^3$ at 100 m) as suggested for the PLUME1 case by *Kuhn et al.* [1998] was also studied. The flux of NO from soil was set to a value of 10^{10} molecules/cm^2s in all scenarios. Additionally, emission of NO and CO from cars between 0.1 and 1 m was considered in the urban scenarios, ranging from $0.5–10 \times 10^9$ and $3–60 \times 10^9$ molecules/cm^3s, respectively (see *Sawyer et al.* [2000] for a review on mobile sources in the US). Emission rates of α-pinene from vegetation in 1–10 m were set to 3×10^6 molecules/cm^3s in the urban cases, and were varied between 3 and 15×10^6 molecules/cm^3s in the rural scenarios (see *Fuentes et al.* [2000], *Ganzeveld et al.* [2002], *Guenther et al.* [2000], and *Stohl et al.* [1996] for data on biogenic emissions). Nocturnal emissions of other VOC are not considered in the model.

3. Results

[32] We applied the model to various urban and rural scenarios as described in Table 2. The mechanisms behind the development of the vertical distributions of the NO-O_3-NO_2 system, [NO_3], [N_2O_5], and [α-pinene] are identical in all scenarios. The detailed behavior and the magnitude of the effects, however, depend in particular on vertical stability and the NO and VOC emission rates. To provide a detailed analysis of the model results, we have chosen an urban scenario with moderate NO emission and weak temperature inversion (scenario 1 in Table 2) as a base run. The influence of variations from these conditions is discussed. We focus our analysis on the lowest 100 m of the NBL.

3.1. Development of Vertical Profiles in the Urban Nocturnal Boundary Layer (NBL)

[33] Figure 2 shows hourly snapshots of the vertical distributions of [NO], [O_3], [NO_2], [α-pinene], [NO_3], and [N_2O_5] for scenario 1. Owing to the assumption of constant meteorology and emission rates we restrict the analysis of the profiles to the first 6 hours of the night. For all species, distinctive vertical profiles in the lowest 100 m of the NBL were found. We exemplarily extracted the individual reaction rates and the rates of concentration change by vertical transport and emission (see equation (1)) one hour after model start in Figure 3.

3.1.1. The NO-O_3-NO_2 System

[34] The vertical structure of the NO-O_3-NO_2 system is controlled by the NO emission between 0.1 and 1 m and the conversion of NO and O_3 into NO_2 and oxygen (Figures 3a–3c).

$$NO + O_3 \rightarrow NO_2 + O_2 \quad (7)$$

[35] The emission of NO close to the ground is the primary cause of the negative gradient of [NO] (Figure 2a). After 1 hour, NO levels reach 4 ppb in the lowest meter, but less than 0.1 ppt above 20 m. Consequently, turbulent diffusion leads to a net upward flux of NO (positive $\Psi_{NO}(z, t)$). However, the effective upward flux is strongly reduced by the fast reaction (7) (peak reaction rate of 8×10^8 molecules/cm^3s), which also limits the height of the NO rich layer. The temporal behavior in Figure 2a shows that this NO layer slowly grows during the night because the chemical loss cannot fully compensate for the NO emissions. At the top of the NBL the influence of the NO emissions is negligible, and a chemical pseudo steady state of NO

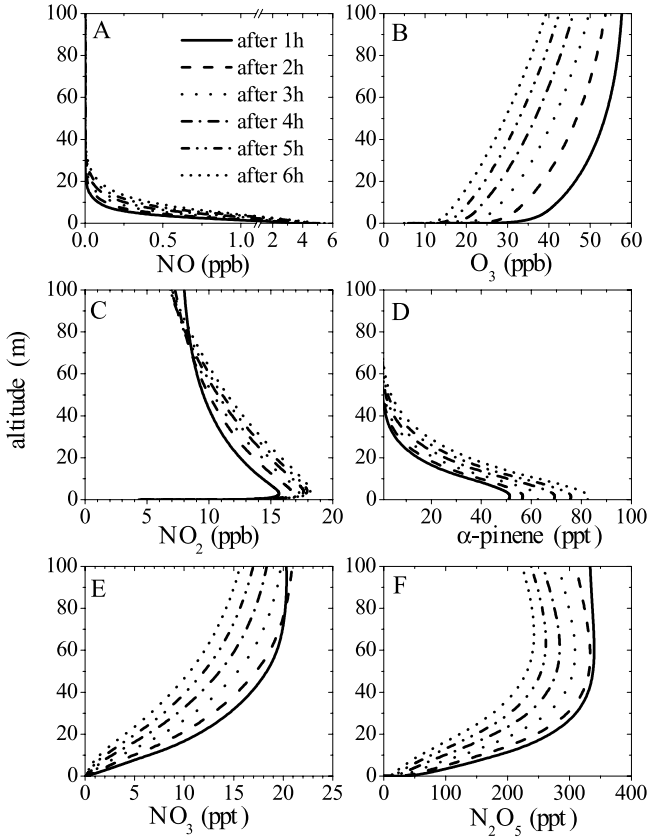

Figure 2. Hourly snapshots of the modeled vertical profiles of [NO], [O_3], [NO_2], [α-pinene], [NO_3], and [N_2O_5] in the first 6 hours after model start for an urban scenario with weak nocturnal inversion (scenario 1).

between its production by the reaction of NO_3 with NO_2 and its destruction by reactions with O_3, NO_3, and peroxy radicals can develop (Figure 3a).

[36] The concentration of O_3 shows the opposite vertical distribution than NO (Figure 2b). After 1 hour, the initially uniform O_3 mixing ratio of 60 ppb is reduced to 57 ppb between 80 and 100 m, while only 33 ppb of [O_3] remain between 0.1 and 1 m. Ozone levels are less than 13 ppb near the ground and 38 ppb at 90 m after 6 hours. The positive gradient of [O_3] is fairly constant with altitude, with the exception of the lowest meters. The fast destruction of ozone near the ground is mainly caused by reaction (7). Dry deposition on the ground surface is another notable O_3 loss during night in scenario 1, and further amplifies the positive O_3 gradient. The strong reduction of [O_3] close to the surface is caused by dry deposition. The loss of O_3 near the ground is replenished by the downward transport of O_3, which acts as the dominant sink for O_3 in the upper NBL (Figure 3b) and the residual layer. Note that without vertical mixing, O_3 would vanish near the ground within less than an hour (chemical lifetime of O_3 at [NO] = 5 ppb is ~8 min), and the NO-to-NO_2 conversion and most other chemical reactions would effectively stop. Other O_3 sinks, such as reaction with unsaturated VOC or NO_2 are negligible in scenario 1.

$$NO_2 + O_3 \rightarrow NO_3 + O_2 \quad (8)$$

[37] As a consequence of reaction (7), NO_2 exhibits a negative gradient above 1 m, with a maximum of 16 ppb in 0.5–5 m altitude and 9 ppb above 50 m after one hour (Figure 2c). As NO titration continues, the average concentration of NO_2 slowly increases during the night. After 6 hours a [NO_2] maximum of 18 ppb is found between 3 and 4 m. Compared to reaction (7), other NO_2 sources, such as the reactions of NO with NO_3, RO_2, and HO_2, as well as HO_2NO_2 and N_2O_5 chemistry, play no role in scenario 1. Vertical transport of NO_2 from the NO rich ground layer into higher altitudes is the main sink below ~12 m (after one hour), and the main source for NO_2 above this altitude. There, $\Psi_{NO2}(z, t)$ is partly compensated by the reactions of NO_2 with O_3 (reaction (8)) and NO_3. In the lowest 2–5 m, NO_2 develops a strong positive gradient because, close to the ground, NO_2 loss by dry deposition is larger than the formation of NO_2 by other processes (Figure 2c). Dry deposition acts as a major loss path for NO_2 in scenario 1.

3.1.2. α-Pinene

[38] α-Pinene shows a strong negative vertical gradient throughout the night (Figure 2d). While after 1 hour its mixing ratio is, for example, 50 ppt in the lowest 5 m, α-pinene is negligible above 45 m. The ground level of α-pinene increases to 80 ppt after 6 hours, when α-pinene reaches a height of 65 m. Analysis of the α-pinene source and loss rates in Figure 3d shows that vertical transport of α-pinene, which is emitted between 1 and 10 m, is responsible for its elevated levels above 10 m. The loss of α-pinene is dominated by oxidation by NO_3 (Figure 3d). After one hour, the reaction rate of α-pinene and NO_3 is highest at 10 m altitude (8×10^6 molecules/cm^{3}s). Loss through ozonolysis, which is in general less important than NO_3 oxidation, shows a similar behavior with a maximum at 3 m after 1 hour (1.5×10^6 molecules/cm^{3}s). In scenario 1, reactions with OH radicals contribute to the removal of α-pinene only in the lowest 5 m (see also section 3.1.4). Throughout the night the maximum of the total α-pinene oxidation rate moves to higher altitudes as the NO rich ground layer grows, and ozone and NO_3 levels near the ground decrease.

3.1.3. NO_3 and N_2O_5

[39] The model predicts a strong positive gradient of [NO_3] (Figure 2e). While the NO_3 mixing ratio after 1 hour is 20 ppt above 50 m, [NO_3] decreases to 3 ppt at 5 m. During the night the overall NO_3 level in the NBL slowly decreases because of its increased loss frequency by the reaction with NO, and the declining production by reaction of O_3 with NO_2. The vertical profile of [N_2O_5], which is strongly coupled to NO_3 by the reaction system (9a)–(9b), depends on both the vertical profiles of [NO_3] and [NO_2] and on the temperature profile.

$$NO_2 + NO_3 \rightarrow N_2O_5 \quad (9a)$$

$$N_2O_5 \rightarrow NO_2 + NO_3 \quad (9b)$$

[40] In scenario 1, N_2O_5 reveals a positive gradient below 30 m, and a constant level of 340 ppt above this altitude after one hour. Ground levels of N_2O_5 are less than 50 ppt (Figure 2f). Note that the negative NO_2 gradient and the positive NO_3 gradient may not compensate for each other, and the N_2O_5 profile at the top of the NBL may be different

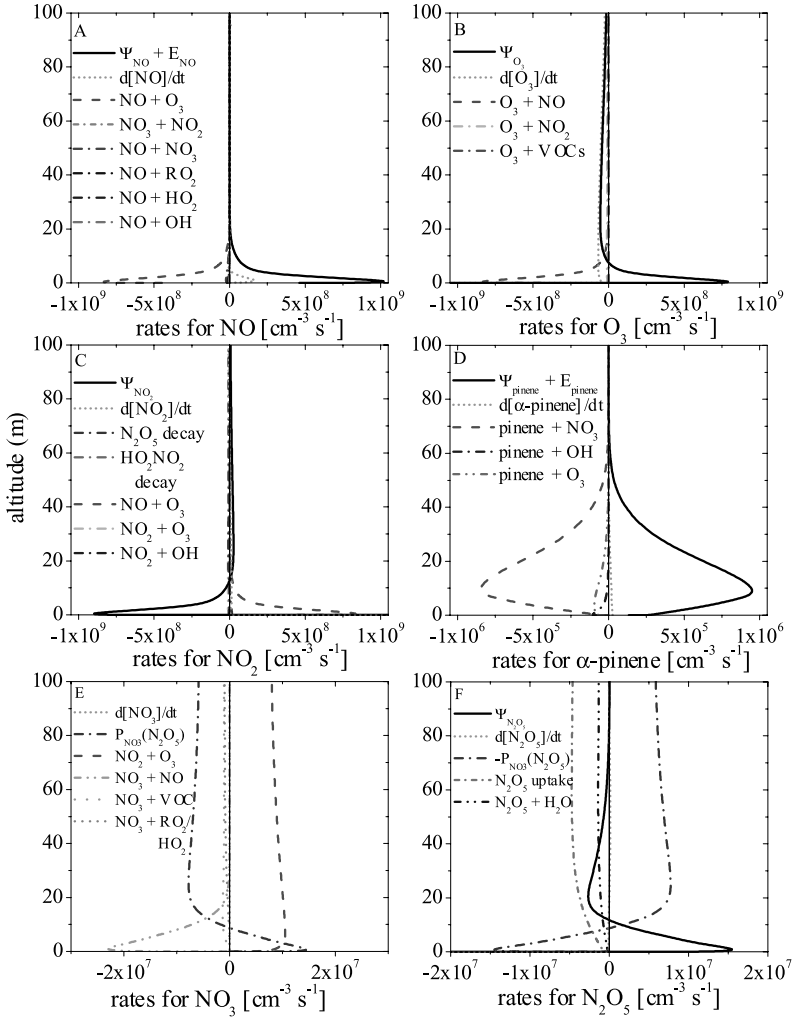

Figure 3. Vertical distribution of chemical rates and the rate of change by vertical transport and emission of NO, O_3, NO_2, α-pinene, NO_3, and N_2O_5, one hour after model start of scenario 1. See color version of this figure at back of this issue.

in other scenarios. After 6 hours, the N_2O_5 level has decreased to 220 ppt at top of the NBL and 10 ppt near the ground.

[41] The chemical production rate of NO_3 by reaction (8) is relatively constant over the NBL ($\sim 10^7$ molecules/cm^{3}s, see Figure 3e). The chemical sinks for NO_3, however, show a strong variation with altitude: In the lowest 10 m the reaction with NO (reaction (10)) clearly dominates, destroying up to 2.3×10^7 molecules/cm^{3}s of NO_3 one hour after model start.

$$NO_3 + NO \rightarrow NO_2 + NO_2 \qquad (10)$$

[42] This large sink of NO_3 near the ground is the main cause for the profiles of $[NO_3]$ and $[N_2O_5]$ in scenario 1. The reactions of NO_3 with VOC and peroxy radicals, the reduction of NO_3 to NO by reaction with NO_2, as well as dry deposition and aerosol uptake of NO_3, are unimportant for the development of the NO_3 and N_2O_5 profiles in the urban environment. Vertical transport of NO_3 is also insignificant for the profiles of $[NO_3]$ and $[N_2O_5]$ (Figures 3e–3f).

[43] The NO_3-NO_2-N_2O_5 reaction system (9a)–(9b) plays another important role for the development of the NO_3 profile. Although both reactions (9a) and (9b) are fast (the lifetime of NO_3 is ~2 s at a NO_2 mixing ratio of 20 ppb (290 K), the lifetime of N_2O_5 is ~60 s at 290 K), other reactions, as well as vertical mixing (see also section 4.4), can alter the pure chemical steady state between N_2O_5 and NO_3 and lead to a net production or loss of NO_3 by reaction system (9a)–(9b). We therefore define the net production rate of NO_3 through N_2O_5 as

$$P_{NO_3}(N_2O_5) = k_{9b} \cdot [N_2O_5] - k_{9a} \cdot [NO_3] \cdot [NO_2]. \qquad (11)$$

[44] Figure 3e shows that $P_{NO3}(N_2O_5)$ is negative (sink for NO_3) above 7 m, while it is positive (source for NO_3) below this altitude. Consequently, vertical transport of N_2O_5 from higher altitudes toward the ground, and subsequent thermal decay of N_2O_5, forms up to 70% of the NO_3 radicals in the lowest 5 m, and is therefore an important formation pathway of NO_3 in the lower NBL. Downward transport of N_2O_5 also plays a role as N_2O_5 sink between 10 and 60 m. Above 10 m N_2O_5 is destroyed by its

conversion to HNO_3 (including both reaction with water vapor and uptake onto aerosols).

$$N_2O_5 + H_2O \xrightarrow{H_2O,aerosols} 2HNO_3 \quad (12)$$

[45] Because of equation (11) this loss path also acts indirectly as main sink for NO_3 at the top of the NBL.

3.1.4. Other Trace Gases

[46] Distinctive vertical profiles were modeled for several other traces gases, including the peroxy radicals RO_2 and HO_2, as well as OH. While peroxy radicals generally showed a positive gradient in the NBL, a distinctive layer of elevated OH levels ($\sim 10^6$ molecules/cm^3) was found close to the ground in various scenarios. The development of the vertical profiles of [RO_2], [HO_2], and [OH] in the NBL is investigated by *Geyer and Stutz* [2004].

3.2. Variations of the Urban Scenario

[47] Stability, emission rates, pollution, and aerosol levels in the NBL can vary considerably from our arbitrarily chosen scenario 1. We have therefore performed a number of sensitivity studies. The different scenarios, together with their respective parameters, are listed in Table 2.

3.2.1. Variations of Atmospheric Stability

[48] Figure 4 compares the vertical profiles of the NO-O_3-NO_2 system, [α-pinene], [NO_3], and [N_2O_5] in the weakly stable case of section 3.1 with the profiles in the strong inversion scenario 2 and in the neutral scenario 3. The NO-O_3–NO_2 system reveals the most obvious response to the change in vertical stability. In the neutral case the high downward flux of O_3 from aloft leads to relatively low NO levels near the ground through reaction (7). Above the NO layer, which is limited to the lowest 15 m of the NBL throughout the night, O_3 and NO_2 are uniformly distributed. In the lowest meters dry deposition and in the case of O_3 reaction (7) lead to positive gradients of O_3 and NO_2. As the stability increases the downward flux of O_3 decreases leading to higher NO levels near the ground. In the lowest part of the NBL O_3 can be completely destroyed by reaction (7). Under stable conditions the build up of the NO rich layer can accelerate significantly because its emission rate is no longer balanced by reaction (7). Vertical profiles of O_3 and NO_2 are therefore more pronounced at higher stabilities.

[49] The accelerated growth of the NO layer at higher nocturnal stabilities has a strong impact on the vertical profiles of [NO_3] and [N_2O_5]. Under neutral conditions, [NO_3] increases from the ground upward, and shows only weak gradients above 25 m throughout the night. Under strong inversion conditions, however, NO_3 basically disappears in the lowest 20 m after 6 hours because of the high concentrations of NO. The level of NO_3 in the upper NBL increases with stability, because downward transport of N_2O_5 is reduced. Because [N_2O_5] is a function of the profiles of [NO_3], [NO_2], and temperature (reactions (9a)–(9b)), the change of the N_2O_5 profile throughout the night is more complex than that of other trace gases. Similar to NO_3, the N_2O_5 gradient in the weak inversion case is more pronounced in the lower part of the NBL. Under strong inversion conditions, a region with maximum N_2O_5 levels develops at the height where the rate of reaction (9a) has its maximum. In the case of a fairly uniform distributed aerosol, the uptake of N_2O_5 would be enhanced at this altitude (section 3.2.3).

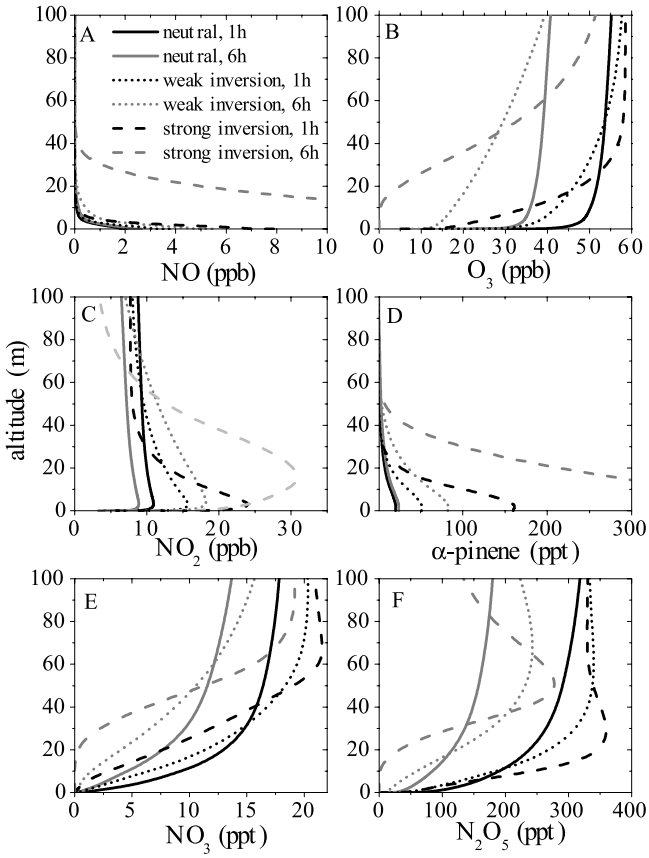

Figure 4. Variation of the vertical profiles of [NO], [O_3], [NO_2], [α-pinene], [NO_3], and [N_2O_5] 1 and 6 hours after model start under urban conditions with atmospheric stability (scenarios 1–3).

3.2.2. Variations of the NO Emission Rate

[50] We performed model runs for two scenarios besides scenario 1 ($E_{NO} = 2 \times 10^9$ molecules/cm^{3}s). Scenario 4 has smaller NO emissions ($E_{NO} = 0.5 \times 10^9$ molecules/cm^{3}s), while we assumed a high NO emission rate of $E_{NO} = 10^{10}$ molecules/cm^{3}s in scenario 5 (Table 2). Figure 5 shows the resulting vertical profiles one and six hours after model start. The effect of an elevated NO emission on nocturnal chemistry is already apparent after one hour. The increase of [NO] close to the ground at a high NO emission rate leads to a faster removal of O_3 and NO_3 by reactions (7) and (10). In the beginning of the night the concentration of NO_2 increases faster because of reaction (7). The N_2O_5 level is only weakly dependent on the NO emission rate due to the counterbalancing effects of lower [NO_3] and higher [NO_2]. This picture changes considerably after 6 hours: while NO is limited to the lowest 5 m in the low emission scenario, it fills out the whole NBL and reaches a level of 90 ppb in the high emission case. Similar to our discussion in section 3.2.1, the cause of the strong NO buildup at higher NO emission is the complete destruction of O_3 by reaction (7) in the lower NBL. Because of the high NO levels, NO_3, and N_2O_5 have completely disappeared after 6 hours. With its main scavengers

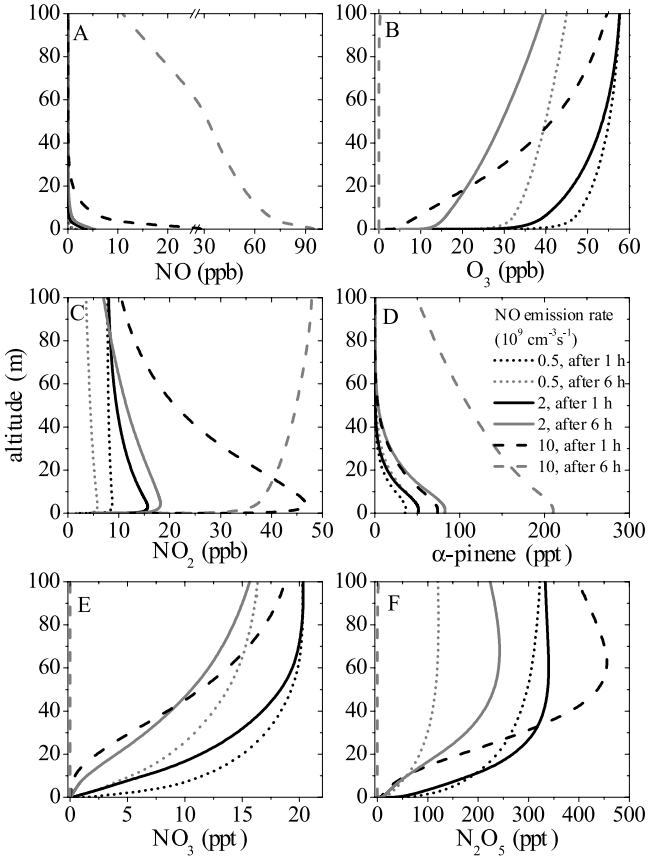

Figure 5. Variation of the vertical profiles of [NO], [O_3], [NO_2], [α-pinene], [NO_3], and [N_2O_5] 1 and 6 hours after model start under urban conditions with the NO emission rate (scenarios 1, 4, and 5).

destroyed, α-pinene can develop a higher level in the NBL.

3.2.3. Variations of the Initial Concentrations of O_3 and NO_2

[51] The initial levels of O_3 and NO_2 were varied in scenarios 6 (high [O_3] and [NO_2]) and 7 (low [O_3] and [NO_2], see Table 2). A higher O_3 concentration and thus higher NO loss frequency delays the buildup of elevated levels of NO. Because of the higher NO_3 production rate (equation (8)) and lower loss frequency through its reaction with NO (reaction (10)), NO_3 levels in scenario 6 are considerably higher than in scenario 1. The NO_3 increase is partly compensated by the reaction rate of NO_3 with the elevated NO_2 into N_2O_5. The N_2O_5 levels are therefore also higher in scenario 6.

3.2.4. Variations of the Aerosol Surface Area

[52] To study the influence of the aerosol surface area on our results, we performed model calculations with a reduced uniform aerosol surface area of 50 $\mu m^2/cm^3$ (scenario 8 in Table 2), and a vertical gradient of the aerosol surface area similar to the PLUME1 case used by *Kuhn et al.* [1998] and *Riemer et al.* [2003], which decreases exponentially from 800 $\mu m^2/cm^3$ at the ground to 200 $\mu m^2/cm^3$ at 100 m altitude (scenario 9).

[53] The aerosol surface area has little effect on [NO], [O_3], and [NO_2]. Because of the lower loss frequency of N_2O_5 by reaction (12) in the reduced surface case, both NO_3 and N_2O_5 levels are, however, considerably higher than in scenario 1 and the importance of vertical transport of N_2O_5 as a source for NO_3 in the lower NBL increases. A negative gradient of the aerosol surface area leads to an increase of the rate of reaction (12) toward the ground. However, near the ground the reaction of NO_3 and NO is the dominant sink for the NO_3-NO_2-N_2O_5 system, and the higher rate of reaction (12) has only a weak influence on NO_3 chemistry. The higher aerosol surface area in 20–80 m altitude can, however, lead to a reduction of the levels of N_2O_5 at the height of the nocturnal N_2O_5 maximum (see Figure 2). As a consequence the N_2O_5 gradient toward the ground decreases (in scenario 9 by ~30% after 1 hour, compared to scenario 1), leading to a reduced vertical transport rate of N_2O_5.

3.3. Vertical Profiles in Rural Air

[54] We applied the NCAT model to three rural scenarios, with α-pinene emission rates ranging from 3 to 15 × 10^6 molecules/cm^3s (scenarios 10–12 in Table 2). The rural conditions are characterized by a very low NO emission flux from the soil, low initial levels of NO_2, propene, propane, and PAN, but a relatively high initial mixing ratio of isoprene. Figure 6 shows the vertical profiles of the NO-O_3-NO_2 system, [α-pinene], [NO_3], and [N_2O_5] one and six hours after model start for the rural scenarios. The vertical profiles of [NO], [O_3], and [NO_2] are independent of the monoterpene emission rate. The NO level in all rural scenarios is much lower (less than 200 ppt) than in the urban cases, and NO does not reach altitudes above 10 m in the first six hours of the night. Ozone always has a weak positive gradient and slowly decreases during the night, mainly because of dry deposition (see also section 4.5). Except for the lowest few meters, where NO_2 has a positive gradient because of dry deposition, the NO_2 concentration is constant with altitude. α-Pinene has a negative gradient and a higher level at higher emission rates. As in the urban scenarios, NO_3 and N_2O_5 generally develop positive gradients. The decreasing concentrations of NO_3 and N_2O_5 toward the ground are caused by the high α-pinene levels in the lowest 10 m. NO plays a minor role in the development of the NO_3 and N_2O_5 profiles.

[55] A number of differences in NO_3 chemistry can be observed between the rural and urban cases. The production rate of NO_3 is lower because of the lower NO_2 levels in a rural area. Loss of N_2O_5 by aerosol uptake has less effect on [NO_3] because [NO_2] is lower. While the loss frequency of NO_3 due to the NO_3 + NO reaction (reaction (10)) is significantly lower because of the reduced NO levels, the loss frequency due to the reaction with α-pinene can increase. Since in rural air the loss frequency of NO_3 from reactions with terpenes is lower than the loss frequency from reactions with NO in urban air, the gradients of [NO_3] and [N_2O_5] are generally weaker under rural conditions.

4. Discussion

4.1. Comparison of Model Results With Field Data and Other Model Studies

[56] Although we did not intend to accurately simulate field data, a comparison of the model results with profile measurements in the NBL reveals that the model reproduces

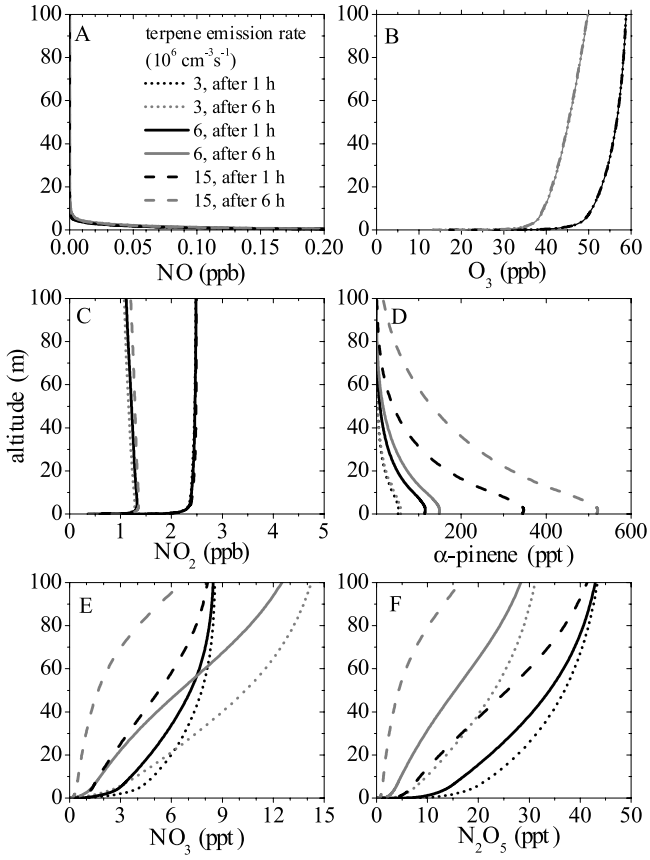

Figure 6. Variation of the vertical profiles of [NO], [O_3], [NO_2], [α-pinene], [NO_3], and [N_2O_5] 1 and 6 hours after model start under rural conditions with the terpene emission rate (scenarios 10–12).

the general features of the vertical distribution of the NO-O_3-NO_2 system, [NO_3], and [N_2O_5] well. The NCAT model predicts, for example, that in an urban environment O_3 often develops a positive gradient in the NBL, while NO_2 levels are highest near the ground. As discussed in section 1, several field studies confirm this feature of nocturnal chemistry [e.g., *Cros et al.*, 1992; *Glaser et al.*, 2003; *Guesten et al.*, 1998; *Pisano et al.*, 1997; *Stutz et al.*, 2004; *Wang et al.*, 2003; *Zhang and Rao*, 1999]. The prediction of the model that NO_3 generally develops a positive gradient during the night is also found by field observations [*von Friedeburg et al.*, 2002; *Stutz et al.*, 2004; *Wang et al.*, 2003]. *Stutz et al.* [2004] applied the NCAT model in their accompanying paper for the conditions near Houston, TX. The model reproduced the trace gas profiles well (see Figures 6 and 7 of *Stutz et al.* [2004]). In particular, the gradients of the observed and modeled O_3, NO_2, NO_3, and N_2O_5 profiles are in good agreement.

[57] It is interesting to compare the model results to profiles of the NO-O_3-NO_2 system, [NO_3], and [N_2O_5] modeled in other studies. For a case with a low NO emission similar to scenario 10, the model by *Galmarini et al.* [1997], for example, predicts a strong negative gradient of [NO] close to the ground. However, we can not compare the temporal behavior of the NO profile because [NO] was fixed to 0.25 ppb at the ground by *Galmarini et al.* [1997]. Positive gradients of [O_3] and [NO_2] were also calculated by *Galmarini et al.* [1997]. In a recent model study, *Riemer et al.* [2003] compared the vertical profiles of [O_3] and [NO_2] for a low and high NO_x case. Under both conditions a positive O_3 gradient was found. Similar to our results, a positive NO_2 gradient caused by dry deposition was predicted close to the ground, while NO_2 decreased with altitude above 10–20 m.

[58] Although the scenarios differ between this work and the model studies by *Riemer et al.* [2003] and *Fish et al.* [1999], the modeled NO_3 and N_2O_5 profiles show similar features. A strong positive NO_3 gradient in the lowest 100 m of the NBL was found in all studies. *Fish et al.* [1999] concluded that in an urban case the reactions of NO_3 with NO emitted near the ground is the cause of the low NO_3 levels near the ground. In the rural plume case calculated by *Riemer et al.* [2003], reactions with terpenes emitted from trees were the reason behind the positive NO_3 gradient. Similar to our results, both studies found distinctive maxima of the concentrations of NO_2 and N_2O_5 at certain altitudes.

4.2. Effect of Chemistry on the Eddy Diffusivities of Reactive Gases

[59] The effective eddy diffusivity of a gas, $K_i(z, t)$, is defined as the negative ratio of its vertical flux and concentration gradient:

$$K_i(z,t) = -\frac{j_i(z,t)}{\frac{\partial c_i(z,t)}{\partial z}}. \quad (13)$$

[60] Because chemical reactions alter the vertical flux of a reactive trace gas (section 2.1), the effective eddy diffusivity of a reactive gas can be different from that of an inert gas. Applying equation (5), $K_i(z, t)$ can be expressed as product of the eddy diffusivity of an inert gas and a chemistry correction factor.

$$K_i(z,t) = K_{inert}(z) \cdot \left[1 + \frac{\frac{\partial (P_i(z,t) - L_i(z,t))}{\partial z} \cdot \tau_{ieff}(z,t)}{\frac{\partial c_i(z,t)}{\partial z}} \right]. \quad (14)$$

[61] The chemistry correction factor is closer to unity if a gas a) has a strong concentration gradient, b) is in chemical steady state (because $\frac{\partial (P_i(z,t) - L_i(z,t))}{\partial z}$ is negligible), and c) has a short chemical lifetime. $K_i(z, t)$ is larger than $K_{inert}(z)$ if $\frac{\partial (P_i(z,t) - L_i(z,t))}{\partial z}$ has the same trend as its concentration gradient. Likewise, $K_i(z, t)$ is smaller than $K_{inert}(z)$ if both gradients have opposite directions.

[62] In Figure 7 the vertical profiles of the concentration gradients, vertical fluxes, and effective eddy diffusivities of NO, O_3, NO_2, NO_3, and N_2O_5 are shown using the data of scenario 1 one hour after model start. Note that we did not calculate effective diffusivities for NO, NO_3, and N_2O_5 above 50 m since equation (14) is no longer applicable at very weak concentration gradients. The vertical profile of $K_{NO}(z, t)$ in Figure 7 reveals three layers with different chemistry correction factors. Below 10 m the chemistry correction term in equation (14) is, in principle, negligible because the effective time, $\tau_{NOeff}(z, t)$, is very short (e.g., ~1 s in 3–4 m). The causes of the short effective time close

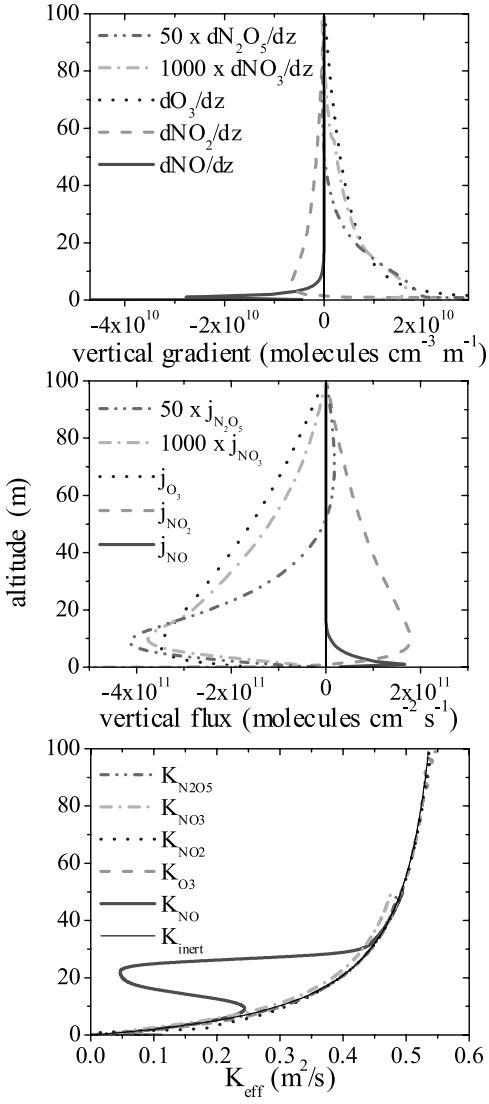

Figure 7. Vertical profiles of concentration gradients, vertical fluxes, and effective eddy diffusivities for the reactive trace gases NO, O_3, NO_2, NO_3, and N_2O_5 (scenario 1, one hour after start). Additionally, the eddy diffusivity of an inert gas is shown. Note that because of the very weak concentration gradients the effective eddy diffusivities of NO_3 and N_2O_5 cannot be calculated by equation (14) above 50 m.

to the ground are the short turbulent timescale, which increases linearly with altitude, and the fast reaction frequency of NO (equation (6)). In a layer between 10 and 30 m, the effective eddy diffusivity of NO is, however, strongly reduced. In the example in Figure 7, $K_{NO}(z, t)$ is as low as 0.05 m^2/s at an altitude of 20 m. This value is almost an order of magnitude lower than the eddy diffusivity of an inert gas of 0.40 m^2/s. The strong reduction of $K_{NO}(z, t)$ in this height interval is mainly caused by the long effective timescale $\tau_{NOeff}(z, t)$ of ~30 s. In addition, the ratio of $\frac{\partial L_{NO-O3}(z,t)}{\partial z}$ and $\frac{\partial [NO](z,t)}{\partial z}$ in equation (14) is a factor of 2–3 higher in this layer than it is near the ground. Since both gradients have the same trend, $K_{NO}(z, t)$ is smaller than $K_{inert}(z, t)$. The chemistry correction factor for $K_{NO}(z, t)$ again becomes negligible above 30 m because NO establishes a chemical pseudo steady state at higher altitudes.

[63] While we found that a chemistry correction of the eddy diffusivity is necessary for NO, no important changes of the vertical fluxes by chemical reactions were calculated for O_3, NO_2, NO_3, and N_2O_5. In the case of O_3 and NO_2, the eddy diffusivities are only weakly changed by chemistry because for both gases the gradient of the total reaction rate is small compared to its concentration gradient. In the case of NO_3 and N_2O_5, the fast interconversion of both gases (reaction system (9a)–(9b)) leads to very short effective times $\tau_{NO_3eff}(z, t)$ and $\tau_{N_2O_5eff}(z, t)$ on the order of a few seconds at all altitudes. In addition, the gradients of the total reaction rate are weak compared to the concentration gradients for both gases.

[64] It is interesting to compare our results to other studies on the influence of chemistry on eddy diffusion. *Hamba* [1993] applied the chemistry correction of equation (5) to a simple NO-O_3-NO_2 triad during the day. He found a strong reduction of the vertical flux of NO between 100 and 1000 m. The NO gradient seemed to be less influenced by the chemistry correction factor. According to equation (13), this behavior corresponds to a reduction of $K_{NO}(z, t)$. The influence of chemistry on the eddy diffusivities of NO_2 and O_3 was small. Although these model calculations were done for daytime conditions (stronger mixing) and with a very simple chemistry framework, the results seem to confirm that a chemistry correction of the eddy diffusivity should be applied for NO. *Galmarini et al.* [1997] also observed a decrease of $K_{NO}(z, t)$ compared to the eddy diffusivity of an inert gas for a rural nighttime scenario. Similar to our results, the effect of chemistry on the eddy diffusivity of NO was highest at ~10 m altitude, but negligible very close to the ground surface and above 40 m. As in our case only a minor influence of chemistry on the eddy diffusivities of O_3, NO_2, NO_3, and N_2O_5 was calculated.

[65] *Vila-Guerau de Arellano et al.* [1995] derived a reduction of $K_{NO}(z, t)$ over the diffusivity of an inert gas by ~50% at 60 m altitude under labile conditions. At higher stabilities no effect of chemistry on the eddy diffusivity of NO was found at this altitude. This result could be ascribed to the variation of the height of the layer, in which $K_{NO}(z, t)$ is reduced, with atmospheric stabilities.

[66] Our results show that it is important to consider a chemistry correction for the eddy diffusivity of NO to correctly calculate vertically resolved chemistry in the NBL. The reduced effective eddy diffusivity of NO around 20 m results in a suppression of the mixing of NO from the ground into higher altitudes, thus forming a sharper borderline between the chemistry in the NO filled ground layer and in higher altitudes. Since NO is important for a number of chemical transformations, its suppressed mixing can have various secondary effects, for example for the vertical profiles of [NO_3], [RO_2], [HO_2], and [OH].

4.3. Influence of the Temperature Profile on [NO_3] and [N_2O_5]

[67] The strong temperature dependence of the NO_3-N_2O_5 reaction system (9a)–(9b) implies that the vertical gradients of [NO_3] and [N_2O_5] are influenced by the ambient temperature profile. It is well known that at lower temperatures T the ratio of $\frac{[N_2O_5]}{[NO_3]} \propto e^{\frac{10724}{T}}$ is higher and N_2O_5

becomes a more important reservoir for NO_3 [*Wängberg et al.*, 1997]. Consequently, at colder temperatures more NO_3 molecules are indirectly destroyed if one N_2O_5 molecule is removed from the atmosphere. For example, removal of NO_3 by reaction (12) is 46 times more effective at 275 K than at 305 K [*Geyer and Platt*, 2002].

[68] Figure 8 shows the variation of the NO_3 and N_2O_5 profiles of the urban scenario 1 with ambient temperature (scenario 13: 275 K, scenario 1: 290 K, and scenario 14: 305 K, Table 2). Note that the vertical gradient of temperature is very weak in these scenarios. As expected, NO_3 levels are considerably lower at colder temperatures because N_2O_5 loss is a more effective NO_3 destruction path. At 50 m altitude for example, the NO_3 mixing ratio is 2.5 ppt at 275 K, compared to 16 ppt at 290 K and 79 ppt at 305 K. The factor of 33 between $[NO_3]$ at 305 K and 275 K is lower than the factor 46 calculated from reaction system (9a)–(9b) because of other reactions involved in NO_3 chemistry. Although the overall level of NO_3 is different, the shapes of the profile of $[NO_3]$ in scenarios 13 and 14 are similar (Figure 8). However, the shape of the NO_3 profile can change if a temperature gradient is established, for example in nights with a temperature inversion. Then, the strong positive dependence of $[NO_3]$ on temperature can lead to the development of a positive NO_3 gradient even in the absence of NO and terpene emissions.

[69] The concentration of N_2O_5 is less influenced by temperature (Figure 8). It is, however, important to note that the N_2O_5 gradient is weakest in the 275 K case. This is caused by the reduced importance of the NO_3 + NO reaction near the ground at low temperatures. Consequently, downward mixing of N_2O_5 is a less important ground source of NO_3 in a colder NBL.

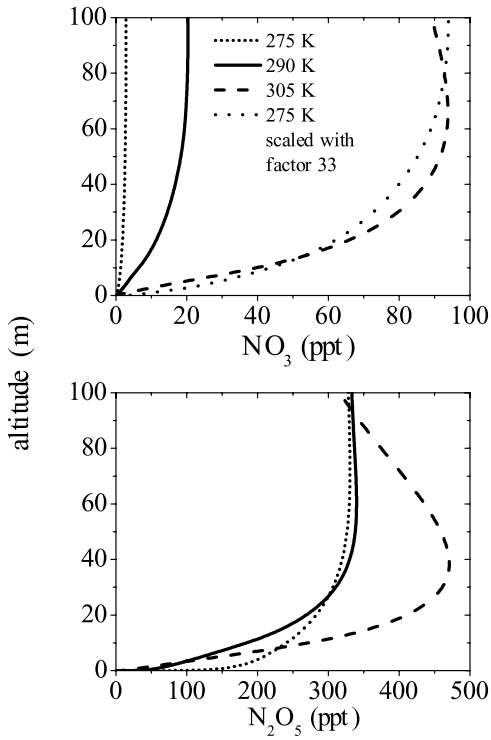

Figure 8. Variation of the vertical profiles of $[NO_3]$ and $[N_2O_5]$ under urban conditions with ambient temperature. To compare the relative vertical gradient of scenario 13 (275 K) to scenario 14 (305 K), the NO_3 profile of scenario 13 is scaled by a factor 33 (data 1 hour after model start).

4.4. Influence of Vertical Mixing on the Steady State of NO_3 and N_2O_5

[70] Our discussion of the vertical profiles in section 3 reveals that vertical mixing plays a crucial role in nocturnal chemistry. In particular, vertical transport of N_2O_5 from the upper NBL downward acts as a major source of N_2O_5 and NO_3 near the ground and a sink of both species in the upper layer (see vertical profile of $P_{NO3}(N_2O_5)$ in Figure 3e). It is interesting to discuss how representative chemical pseudo steady state calculations of $[NO_3]$ and $[N_2O_5]$, which are frequently used in the interpretation of field data, are if vertical transport of N_2O_5 is considered. For this purpose we compare chemical pseudo steady state concentrations of N_2O_5 and NO_3 in the NBL with and without vertical transport terms based on the model results for scenario 1.

4.4.1. The N_2O_5 Steady State in the NBL

[71] Vertical transport of N_2O_5 (leading to a rate of concentration change $\psi(N_2O_5)$) and loss of N_2O_5 by reaction (12), (at a loss frequency f_{N2O5}) can alter the NO_3-NO_2-N_2O_5 equilibrium of reaction system (9a)–(9b). Assuming a purely chemical pseudo steady state, the N_2O_5 concentration at an altitude z and a time t can be expressed as:

$$[N_2O_5](z,t) = \frac{k_{9a} \cdot [NO_3](z,t) \cdot [NO_2](z,t)}{k_{9b} + f_{N2O5}(z,t)} \qquad (15)$$

[72] $[N_2O_5](z, t)$ is often used to derive N_2O_5 levels from field measurements of NO_2, NO_3, and aerosol [see, e.g., *Stutz et al.*, 2004]. Figure 9a compares $[N_2O_5]$ calculated based on equation (15) from the modeled NO_2 and NO_3 profiles, with the model output for $[N_2O_5]$ of scenario 1. Over most of the NBL the difference between N_2O_5 from equation (15) and the model output is small (Figure 9b). However, below 10 m vertical transport leads to higher N_2O_5, thus shifting the concentrations away from the chemical steady state. Below 1 m the modeled N_2O_5 levels are higher by a factor of 3 due to downward transport.

[73] To determine whether $[N_2O_5]$ is in a combined chemical-transport pseudo steady state, we also calculated the concentration including the vertical transport term $\psi(N_2O_5)$, which could, for example, be derived from measurements of the N_2O_5 profile:

$$[N_2O_5](z,t) = \frac{k_{9a} \cdot [NO_3](z,t) \cdot [NO_2](z,t) + \psi(N_2O_5)(z,t)}{k_{9b} + f_{N2O5}(z,t)} \qquad (16)$$

[74] The negligible difference between N_2O_5 from equation (16) and the model output (Figure 9b) shows that, in our scenario, N_2O_5 is in a pseudo steady state if vertical transport is considered. As pointed out by *Brown et al.* [2003], this may not be true at very cold temperatures, low $[H_2O]$ and aerosol surfaces areas, and high NO_2 levels.

4.4.2. The NO_3 Equation in the NBL

[75] Calculations of NO_3 concentrations in the NBL were thus far generally based on the assumption of a pure chemical pseudo steady state equation, which does not consider vertical transport [*Allan et al.*, 2000; *Geyer et*

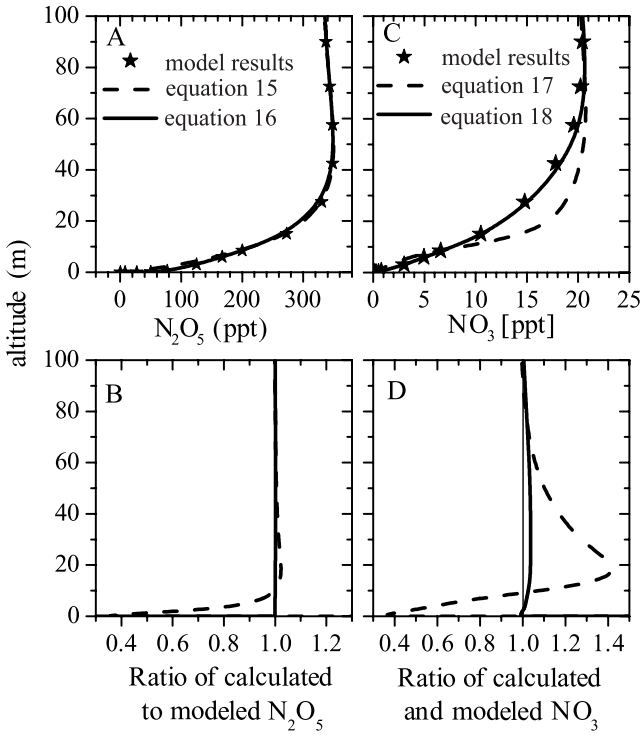

Figure 9. (a, c) Vertical profiles of N_2O_5 and NO_3 calculated with the chemical steady state equations and the chemical-transport steady state equation, in comparison with modeled data (scenario 1, one hour after start). (b, d) Vertical profiles of the ratios of calculated and modeled N_2O_5 and NO_3 concentrations.

al., 2001a; *Geyer et al.*, 2001b; *Heintz et al.*, 1996; *Martinez et al.*, 2000]:

$$[NO_3](z,t) = k_8(z) \cdot [NO_2](z,t) \cdot [O_3](z,t) \cdot \tau_{NO3}(z,t), \quad (17)$$

with

$$\tau_{NO3}(z,t) = \frac{1}{\left(k_{9a}(z) - \frac{k_{9b}(z) \cdot k_{9a}(z)}{k_{9b}(z) + f_{N2O5}(z,t)}\right) \cdot [NO_2](z,t) + f_{NO3}(z,t)}.$$

[76] Here, f_{N2O5} and f_{NO3} represent the total loss frequencies of N_2O_5 from reaction (12) and of NO_3 from reactions with NO, VOC, and RO_x, respectively. Figures 9c and 9d compare the modeled profile of $[NO_3]$ with the profile calculated according to equation (17). Equation (17) severely underestimates $[NO_3]$ near the ground (up to 60%), but overestimates $[NO_3]$ at higher altitudes (for example by 40% at 20 m). That these large differences arise mostly from NO_3 concentration changes due to vertical transport of N_2O_5 can be illustrated by expanding equation (17), including $\Psi(N_2O_5)$.

$$[NO_3](z,t) = \left[k_8(z) \cdot [NO_2](z,t) \cdot [O_3](z,t) + \frac{k_{9b}(z) \cdot \psi(N_2O_5)(z,t)}{k_{9b}(z) + f_{N2O5}(z,t)}\right] \cdot \tau_{NO3}(z,t) \quad (18)$$

[77] The NO_3 chemical-transport steady state equation (18) simulates the NO_3 profile well (Figures 9c and 9d). The difference of ~3% between the calculated and modeled NO_3 levels is caused by the fact that the N_2O_5 concentration is slowly changing in time. This temporal change, which constitutes a deviation from the steady state, is more pronounced in the NO_3 than in the N_2O_5 concentrations.

[78] Our analysis shows that, in cases where N_2O_5 has a strong vertical gradient, which is often the case in urban areas, it is essential to include the vertical transport rate of N_2O_5 in the steady state equation of NO_3 to correctly describe the chemistry of NO_3. In rural cases, where the N_2O_5 gradient is often less pronounced (section 3.3), chemical steady state calculations may be sufficient to describe the NO_3 profile [*Allan et al.*, 2000; *Carslaw et al.*, 1997; *Geyer et al.*, 2001a; *Heintz et al.*, 1996; *Martinez et al.*, 2000].

4.5. Implications for the Removal of O_3 and Its Precursors

[79] One of the most important aspects of nocturnal chemistry is the removal of ozone and its precursors NO_2 and VOC from the boundary layer. We used our model results to study the vertical variation of the removal processes of O_3, NO_2, and VOC in the different scenarios. As an example, the vertical dependence of the different removal processes for scenario 1 after one hour are shown in Figure 10. We also investigated how well the removal rates of these pollutants can be determined from observation at one single altitude (3 m and 10 m, respectively), i.e., assuming that these rates are representative for the entire NBL, by comparing them to the model results column-averaged over the lowest 100 m of the NBL (Table 3). Table 3 also shows the deposition rates for O_3 and NO_2 (integrated for the 100 m deep NBL) derived from the modeled dry deposition flux for each scenario.

4.5.1. O_3 Loss

[80] Figure 10 illustrates that the O_3 oxidation rate changes considerably with altitude in the NBL. For scenario 1, for example, the loss rate is over two orders of magnitude larger near the ground than in the upper NBL (Figure 10). This general behavior was found in all scenarios we investigated, and can also be seen by comparing the 3 m and 10 m values in Table 3. This strong altitude variation leads to considerably higher (typically a factor 2–10) loss rates at 3 m than those averaged over the NBL in all cases (Table 3). The O_3 oxidation rate at 10 m can be lower or higher than the average value for the NBL, depending on the shape of the vertical O_3 profile, but is in general closer to the averaged value than the 3 m value.

[81] Three major processes are responsible for the removal of O_3 from the NBL. (1) Loss of O_3 through the NO + O_3 reaction: In urban scenarios most of the ozone at night is destroyed by its reaction with NO (reaction (7)) near the ground. At the top of the NBL this O_3 loss path is negligible. One can argue that this destruction is not permanent, since the photolysis of NO_2 during the following morning will reform part of the destroyed O_3. However, only part of the NO_2 formed by NO + O_3 will be available during the next morning. The loss of ozone during the night will therefore proceed indirectly through the loss of NO_2. With these complications in mind we have included the

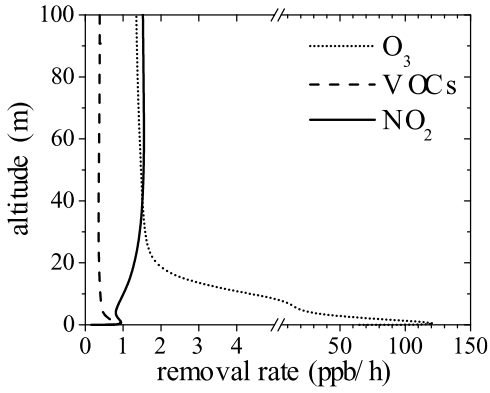

Figure 10. Vertical profiles of the removal rates of O_3, NO_2, and volatile organic carbons in the nocturnal boundary layer (NBL) (scenario 1, one hour after start). While in this urban case most of the ozone is destroyed near the ground by reaction with NO, NO_2 is primarily lost at the top of the NBL.

$NO + O_3$ reaction as an O_3 destruction pathway in this discussion. (2) Loss of O_3 through $NO_2 + O_3$: Reaction (8) is, in all scenarios, the most important destruction path in the upper NBL. The rate of the reaction $NO_2 + O_3$ often has no significant vertical variation because the opposite gradients of $[NO_2]$ and $[O_3]$ counterbalance each other. The fate of the NO_3 formed in reaction (8) is loss by reactions with NO, VOC, or via N_2O_5 destruction. It should be noted here that the reaction of NO_3 with NO and VOC can lead to NO_2 formation, and the same arguments as above regarding the effectivity of the O_3 destruction apply. (3) Dry deposition of O_3: Dry deposition is the main loss path for O_3 in the rural cases (Table 3), and can also play an important role in urban environments (scenario 3). The dry deposition rate of O_3 is a strong function of the vertical profile of $[O_3]$, and thus of atmospheric stability and NO emission rate. Under highly polluted conditions (scenario 5), where most of the O_3 near the ground is destroyed, dry deposition has effectively shut down. Approaches to estimate dry deposition fluxes, which assume a fairly uniform distribution of a gas and use data at a single reference altitude (as often used for the convective mixing layer [*Wesely and Hicks*, 2000]) may therefore not be applicable in a stable NBL with high NO emissions. (4) Other O_3 losses: A number of other processes, such as the $O_3 + HO_2$ reaction or the ozonolysis of alkenes, destroy ozone. In all modeled scenarios their impact is negligible compared to the pathways described above.

4.5.2. NO_2 Loss

[82] The oxidation rate of NO_2 in scenario 1 shows only a weak positive gradient. It decreases slightly between 5 and 30 m, and increases again below 5 m toward the ground (Figure 10). In all cases the altitude dependence of NO_2 oxidation was less developed than for ozone. In all scenarios (Table 3) measurements at 3 and 10 m altitude underestimate the average NO_2 oxidation rate in the NBL. The underestimation is larger at stronger stability and higher NO emission rates. In the high NO emission scenario 5, for example, measurements at 3 m would underrate the average NO_2 loss rate in the NBL by a factor of 5. In rural cases the vertical gradient of the NO_2 oxidation rate is very weak and in situ measurements of the NO_2 loss rate at night are appropriate.

[83] Two major processes remove NO_2 from the NBL. (1) Dry deposition of NO_2: In all cases dry deposition is an effective NO_2 sink in the NBL, destroying typically half of the NO_2 in the 100 m high NBL (Table 3). It is interesting that the dry deposition rate of NO_2 is only weakly dependent on atmospheric stability because the effects of reduced NO_2 levels near the ground and faster transport toward the surface balance each other. However, NO_2 deposition is a strong function of the NO emission rate (scenarios 4 and 5 in Table 3). (2) Indirect NO_2 destruction by NO_3 loss: The reactions of NO_3 with VOC, and the conversion of N_2O_5 into HNO_3 account for roughly half of the nocturnal NO_2 loss in most model runs. The contributions of NO_3/N_2O_5 sinks to NO_2 removal are highest in the upper part of the boundary layer. A strong negative aerosol gradient may reduce the positive gradient of the NO_2 loss rate by N_2O_5 uptake. Because of the low NO_3 and N_2O_5 levels in the lower NBL, measurements at 3 and 10 m will, however,

Table 3. Comparison of the Oxidation Rates of O_3, NO_2, and Volatile Organic Carbon in the Lowest 100 m of the NBL Determined From Rates at One Single Altitude (3 m and 10 m) With the Altitude Integrated Modeled Rates (avg)[a]

	O_3 Oxidation Rate, ppb/h			O_3 Deposition Rate, ppb/h	NO_2 Oxidation Rate, ppb/h			NO_2 Deposition Rate, ppb/h	VOC Oxidation Rate, ppb/h		
Scenario	3 m	10 m	avg	avg	3 m	10 m	avg	avg	3 m	10 m	avg
1	46	6.4	5.5	2.7	0.82	1.0	1.4	1.5	0.53	0.40	0.38
2	50	5.4	5.5	1.1	0.64	1.2	1.4	1.7	0.26	0.32	0.37
3	38	6.6	5.0	4.7	1.1	1.0	1.3	1.5	0.80	0.45	0.41
4	12	1.7	2.3	3.4	0.88	1.0	1.3	0.83	0.60	0.47	0.41
5	108	62	18	0.36	0.32	0.54	1.5	4.4	0.10	0.15	0.25
6	48	7.0	10	6.3	8.2	7.6	8.6	2.5	1.4	0.70	0.70
7	46	8.6	4.7	1.7	0.34	0.32	0.37	1.1	0.40	0.29	0.26
8	47	5.7	5.6	2.9	0.70	0.60	0.74	1.5	0.58	0.43	0.41
9	48	6.5	5.8	2.8	1.4	1.8	1.8	1.4	0.45	0.35	0.34
10	1.5	0.4	0.6	3.6	0.28	0.32	0.34	0.2	0.32	0.32	0.27
11	1.5	0.4	0.6	3.6	0.30	0.34	0.34	0.2	0.38	0.38	0.30
12	1.5	0.4	0.6	3.6	0.32	0.34	0.34	0.2	0.56	0.54	0.37
13	48	8.0	5.4	2.8	0.98	1.1	1.2	1.5	0.28	0.23	0.20
14	48	4.4	6.2	2.8	0.80	1.0	1.3	1.5	0.68	0.54	0.58

[a]The dry deposition rate averaged over the NBL is also shown (1 hour after model start).

mostly underrate the contribution of NO_3/N_2O_5 to the total NO_2 removal at night.

4.5.3. VOC Loss

[84] The VOC oxidation rate is defined as the sum of all reaction rates of α-pinene, isoprene, propene, and propane with NO_3, O_3, and OH. The model predicts that, in most cases, the VOC oxidation rate is only weakly altitude dependent (see also Figure 10). Close to the ground the rate increases slightly, for example in scenario 1 from 0.40 ppb/h at 10 m to 0.53 ppb/h at 3 m (Table 3). This increase is caused by the elevated OH levels predicted by the model in a layer close to the ground (section 3.1.4). In many cases, measurements at 3 m alone may therefore lead to an overestimation of the VOC oxidation rate. In the high NO emission case, the average oxidation rate in the NBL is higher than the rates at 3 m and 10 m because close to the ground radicals have been effectively destroyed by the high NO levels.

[85] Although the gradient of the VOC oxidation rate is very weak above 10 m, the rates of individual reactions may vary with altitude: The reaction rate of NO_3 with VOC, especially with monoterpenes, is highest in the middle of the NBL. This maximum arises from the opposite gradients of $[NO_3]$ and [α-pinene]. Since ozone reacts mostly with alkenes, which do not develop a strong vertical variation in the first six hours of the night in the NCAT model, the oxidation rate of VOC by O_3 reactions is highest at the top of the NBL (where O_3 levels are highest).

5. Conclusions

[86] A one-dimensional chemical transport model was developed to investigate the influence of vertical mixing on the chemistry of the $NO\text{-}O_3\text{-}NO_2$ system, NO_3, N_2O_5, and other trace gases in the nocturnal boundary layer. The model includes explicit calculation of vertical transport rates, deposition and emission of several species, and nocturnal chemistry. We applied the model to various urban and rural scenarios. The calculated vertical profiles are in good agreement with field observations [*Stutz et al.*, 2004]. From the results of this study we can draw the following conclusions about the development of vertical profiles at night:

[87] 1. In urban areas the $NO\text{-}O_3\text{-}NO_2$ system is generally characterized by negative NO and NO_2 gradients, and a positive O_3 gradient caused by the reaction of O_3 with NO, which is emitted from traffic near the ground. During the night a ground-based layer of elevated [NO] can build up, in which O_3 is completely destroyed. Because of negative feedbacks between NO and the vertical transport rate of O_3, and between O_3 and the NO emission rate, the buildup of [NO] accelerates at strong stabilities and high NO emissions. In rural areas, dry deposition of O_3 and NO_2 often leads to positive gradients of both gases.

[88] 2. Biogenic VOC such as α-pinene generally have a negative gradient because of their emission in the lower NBL. In addition, the loss frequency of biogenic VOC is often highest at the top of the NBL because of the elevated levels of NO_3 and O_3 in this height. In rural areas the buildup of α-pinene in the NBL accelerates at high α-pinene emission rates because of the negative feedback between α-pinene and NO_3.

[89] 3. Both NO_3 and N_2O_5 have positive gradients in the NBL, which are caused by the reaction of NO_3 with NO and α-pinene close to the ground. An additional mechanism for a positive NO_3 gradient is a temperature inversion during night. The NO_3 gradient increases at strong vertical stabilities and high emission rates of NO and α-pinene. The profile of the aerosol surface area has minor influence on the NO_3 profile in urban areas.

[90] 4. The vertical structure of chemistry in the NBL can have a significant effect on the effective eddy diffusivities of reactive trace gases. In a layer near the ground, the eddy diffusivity of NO is significantly reduced by the reaction of NO with O_3. A chemistry correction factor for NO should be considered in *K* models.

[91] 5. Downward transport of N_2O_5, followed by its thermal decay, often acts as main source for NO_3 near the ground. Vertical transport rates of N_2O_5 increase at high temperatures and weak vertical stabilities. They also depend on the gradient of the aerosol surface area. In most situations, vertical transport of N_2O_5 has to be considered in steady state calculations of $[NO_3]$ and $[N_2O_5]$.

[92] 6. The oxidation rates of O_3, NO_2, and VOC often develop strong vertical profiles at night. Measuring trace gases at one single altitude (for example 3 m) generally leads to an overestimation of the O_3 oxidation rate and an underestimation of the NO_2 loss rate, and are not sufficient to calculate the nocturnal loss of these gases.

[93] Our results show that nocturnal chemistry is extremely altitude dependent. A correct description is only possible if the vertical distributions of trace gas concentrations and vertical transport rates are considered. Further studies on the altitude dependence of nocturnal chemistry and the influence of vertical mixing are therefore needed to better quantify the influence of nocturnal chemistry on the air quality in urban and suburban areas.

[94] **Acknowledgments.** We would like to thank S. C. Hurlock, S. Wang, and Y. Stutz for helpful comments on the manuscript. This study was supported by the Department of Energy (grant DE-FG03-01ER63094).

References

Aliwell, S. R., and R. L. Jones (1998), Measurements of tropospheric NO_3 at midlatitude, *J. Geophys. Res.*, *103*(D5), 5719–5727.

Allan, B. J., G. McFiggans, J. M. C. Plane, H. Coe, and G. G. McFadyen (2000), The nitrate radical in the remote marine boundary layer, *J. Geophys. Res.*, *105*(D19), 24,191–24,204.

Allan, B. J., J. M. C. Plane, H. Coe, and J. Shillito (2002), Observations of NO_3 concentration profiles in the troposphere, *J. Geophys. Res.*, *107*(D21), 4588, doi:10.1029/2002JD002112.

Arya, S. P. (1988), *Introduction to Micrometeorology*, Academic, San Diego, Calif.

Atkinson, R. (2000), Atmospheric chemistry of VOCs and NO_x, *Atmos. Environ.*, *34*(12–14), 2063–2101.

Atkinson, R., D. L. Baulch, R. A. Cox, R. F. Hampson, J. A. Kerr, M. J. Rossi, and J. Troe (2002), Evaluated kinetic and photochemical data for atmospheric chemistry, paper presented to Subcommittee on Gas Kinetic Data Evaluation for Atmospheric Chemistry, Int. Union of Pure and Appl. Chem., Cambridge, UK.

Berndt, T., and O. Boge (1997), Gas-phase reaction of NO_3 radicals with isoprene: A kinetic and mechanistic study, *Int. J. Chem. Kinet.*, *29*(10), 755–765.

Bey, I., B. Aumont, and G. Toupance (1997), The nighttime production of OH radicals in the continental troposphere, *Geophys. Res. Lett.*, *24*(9), 1067–1070.

Brost, R. A., A. C. Delany, and B. J. Huebert (1988), Numerical modeling of concentrations and fluxes of HNO_3, NH_3 and NH_4NO_3 near the surface, *J. Geophys. Res.*, *93*(D6), 7137–7152.

Brown, S. S., H. Stark, and A. R. Ravishankara (2003), Applicability of the steady state approximation to the interpretation of atmospheric

observations of NO_3 and N_2O_5, *J. Geophys. Res.*, *108*(D17), 4539, doi:10.1029/2003JD003407.
Businger, J. A., J. C. Wyngaard, Y. Izumi, and E. F. Bradley (1971), Flux profile relationships in the atmospheric surface layer, *J. Atmos. Sci.*, *28*, 181–189.
Carslaw, N., J. M. C. Plane, H. Coe, and E. Cuevas (1997), Observations of the nitrate radical in the free troposphere at Izana de Tenerife, *J. Geophys. Res.*, *102*(D9), 10,613–10,622.
Cros, B., J. Fontan, A. Minga, G. Helas, D. Nganga, R. Delmas, A. Chapuis, B. Benech, A. Druilhet, and M. O. Andreae (1992), Vertical profiles of ozone between 0 meters and 400 meters in and above the African equatorial forest, *J. Geophys. Res.*, *97*, 12,877–12,887.
Curtis, A. R., and W. P. Sweetenham (1987), FACSIMILE release H user's manual, London.
Faloona, I., et al. (2001), Nighttime observations of anomalously high levels of hydroxyl radicals above a deciduous forest canopy, *J. Geophys. Res.*, *106*(D20), 24,315–24,333.
Finlayson-Pitts, B. J., and J. N. Pitts (2000), *Chemistry of the Upper and Lower Atmosphere: Theory, Experiments and Applications*, Academic, San Diego, Calif.
Fish, D. J., D. E. Shallcross, and R. L. Jones (1999), The vertical distribution of NO_3 in the atmospheric boundary layer, *Atmos. Environ.*, *33*(5), 687–691.
Fitzjarrald, D. R., and D. Lenschow (1983), Mean concentration and flux profiles for chemically reactive species in the atmospheric surface layer, *Atmos. Environ.*, *17*(12), 2505–2512.
Fuchs, N. A., and A. G. Sutugin (1971), *Highly Dispersed Aerosols*, Butterworth-Heinemann, Woburn, Mass.
Fuentes, J. D., et al. (2000), Biogenic Hydrocarbons in the atmospheric boundary layer: A review, *Bull. Am. Meteorol. Soc.*, *81*(7), 1537–1575.
Galmarini, S., P. G. Duynkerke, and J. Vilà-Guerau de Arellano (1997), Evolution of nitrogen oxide chemistry in the nocturnal boundary layer, *J. Appl. Meteorol.*, *36*(7), 943–957.
Ganzeveld, L. N., J. Lelieveld, F. J. Dentener, M. C. Krol, A. J. Bouwman, and G. J. Roelofs (2002), Global soil-biogenic NO_x emissions and the role of canopy processes, *J. Geophys. Res.*, *107*(D16), 4298, doi:10.1029/2001JD001289.
Gao, W., and M. L. Wesely (1994), Numerical modeling of the turbulent fluxes of chemically reactive trace gases in the atmospheric boundary layer, *J. Appl. Meteorol.*, *33*(7), 835–847.
Gao, W., M. L. Wesely, and I. Y. Lee (1991), A numerical study of the effects of air chemistry on fluxes of NO, NO_2, and O_3 near the surface, *J. Geophys. Res.*, *96*, 18,761–18,770.
Geyer, A., and U. Platt (2002), Temperature dependence of the NO_3 loss frequency: A new indicator for the contribution of NO_3 to the oxidation of monoterpenes and NO_x removal in the atmosphere, *J. Geophys. Res.*, *107*(D20), 4431, doi:10.1029/2001JD001215.
Geyer, A., and J. Stutz (2004), The vertical structure of OH-HO_2-RO_2 chemistry in the nocturnal boundary layer: A one-dimensional model study, *J. Geophys. Res.*, *109*, doi:10.1029/2003JD004425, in press.
Geyer, A., R. Ackermann, R. Dubois, B. Lohrmann, T. Müller, and U. Platt (2001a), Long-term observation of nitrate radicals in the continental boundary layer near Berlin, *Atmos. Environ.*, *35*(21), 3619–3631.
Geyer, A., B. Alicke, S. Konrad, T. Schmitz, J. Stutz, and U. Platt (2001b), Chemistry and oxidation capacity of the nitrate radical in the continental boundary layer near Berlin, *J. Geophys. Res.*, *106*(D8), 8013–8025.
Geyer, A., et al. (2003a), Direct observations of daytime NO_3: Implications for urban boundary layer chemistry, *J. Geophys. Res.*, *108*(D12), 4368, doi:10.1029/2002JD002967.
Geyer, A., et al. (2003b), Nighttime formation of peroxy and hydroxyl radicals during the BERLIOZ campaign: Observations and modeling studies, *J. Geophys. Res.*, *108*(D4), 8249, doi:10.1029/2001JD000656.
Glaser, K., U. Vogt, G. Baumbach, A. Volz-Thomas, and H. Geiss (2003), Vertical profiles of O_3, NO_2, NO_x, VOC, and meteorological parameters during the Berlin Ozone Experiment (BERLIOZ) campaign, *J. Geophys. Res.*, *108*(D4), 8253, doi:10.1029/2002JD002475.
Gölz, C., J. Senzig, and U. Platt (2001), NO_3–initiated oxidation of biogenic hydrocarbons, *Chem. Global Change Sci.*, *3*(3), 339–352.
Guenther, A., C. Geron, T. Pierce, B. Lamb, P. Harley, and R. Fall (2000), Natural emissions of non-methane volatile organic compounds, carbon monoxide, and oxides of nitrogen from North America, *Atmos. Environ.*, *34*(12–14), 2205–2230.
Guesten, H., G. Heinrich, and D. Sprung (1998), Nocturnal depletion of ozone in the Upper Rhine Valley, *Atmos. Environ.*, *32*(7), 1195–1202.
Hamba, F. (1987), Statistical analysis of chemically reacting passive scalars in turbulent flows, *J. Phys. Soc. Jpn.*, *56*, 79–96.
Hamba, F. (1993), A modified K model for chemically reactive species in the planetary boundary layer, *J. Geophys. Res.*, *98*(D3), 5173–5182.
Hamba, F. (1994), Reply, *J. Geophys. Res.*, *98*(D3), 5173–5182.
Haugen, D. A. (1973), *Workshop on Micrometeorology*, edited by D. A. Haugen, 392 pp., Am. Meteorol. Soc., Boston, Mass.
Heintz, F., U. Platt, H. Flentje, and R. Dubois (1996), Long-term observation of nitrate radicals at the Tor Starion, Kap Arkona (Rügen), *J. Geophys. Res.*, *101*(D17), 22,891–22,910.
Hov, O. (1983), One-dimensional vertical model for ozone and other gases in the atmosphere boundary layer, *Atmos. Environ.*, *17*, 535–550.
Hu, J. H., and J. P. D. Abbatt (1997), Reaction probabilities for N_2O_5 hydrolysis on sulfuric acid and ammonium sulfate aerosols at room temperature, *J. Phys. Chem. A*, *101*(5), 871–878.
Jacob, D. J. (2000), Heterogeneous chemistry and tropospheric ozone, *Atmos. Environ.*, *34*(12–14), 2131–2159.
Jenkin, M. E., S. M. Saunders, V. Wagner, and M. J. Pilling (2003), Protocol for the development of the Master Chemical Mechanism, MCM v3 (Part B): Tropospheric degradation of aromatic volatile organic compounds, *Atmos. Chem. Phys.*, *3*, 181–193.
Kesselmeier, J., and M. Staudt (1999), Biogenic volatile organic compounds (VOC): An overview on emission, physiology, and ecology, *J. Atmos. Chem.*, *33*, 23–88.
Kirchner, W., F. Welter, A. Bongartz, J. Kames, S. Schweighofer, and U. Schurath (1990), Trace gas exchange at the air/water interface: Measurements of mass accommodation coefficients, *J. Atmos. Chem.*, *10*, 427–449.
Klemp, D., K. Mannschreck, H. W. Paetz, M. Habram, P. Matuska, and F. Slemr (2002), Determination of anthropogenic emission ratios in the Augsburh area from concentration ratios: Results from long-term measurements, *Atmos. Environ.*, *36*, suppl. 1, 61–80.
Kramm, G., H. Mueller, D. Fowler, K. D. Hoefken, F. X. Meixner, and E. Schaller (1991), A modified profile method for determining the vertical fluxes of NO, NO_2, ozone, and HNO_3 in the atmospheric surface layer, *J. Atmos. Chem.*, *13*, 265–288.
Kuhn, M., et al. (1998), Intercomparison of the gas-phase chemistry in several chemistry and transport models, *Atmos. Environ.*, *32*(4), 693–709.
Lenschow, D. (1981), Reactive trace species in the boundary layer from a micrometeorological perspective, *J. Phys. Soc. Jpn.*, *60*, 472–480.
Lenschow, D. H. (1982), Reactive trace species in the boundary layer from a micrometeorological perspective, *J. Meteorol. Soc. Jpn.*, *1*, 60.
Lenschow, D. H., and A. C. Delany (1987), An analytic formulation for NO and NO_2 flux profiles in the atmospheric surface layer, *J. Atmos. Chem.*, *5*, 301–309.
Magnotta, F., and H. S. Johnston (1980), Photodissociation quantum yields for the NO_3 free radical, *Geophys. Res. Lett.*, *7*, 769–772.
Martinez, M., D. Perner, E.-M. Hackenthal, S. Külzer, and L. Schütz (2000), NO_3 at Helgoland during the NORDEX campaign in October 1996, *J. Geophys. Res.*, *105*(D18), 22,685–22,695.
McDonald-Buller, E. C., H. M. Liljestrand, and K. Sepehrnoori (1999), Numerical modeling of dry deposition coupled to 22 photochemical reactions, *Atmos. Environ.*, *33*(10), 1491–1502.
McMurry, P. H. (2000), A review of atmospheric aerosol measurements, *Atmos. Environ.*, *34*(12–14), 1959–1999.
Michel, A. E., C. R. Usher, and V. H. Grassian (2002), Heterogeneous and catalytic uptake of ozone on mineral oxides and dusts: A Knudsen cell investigation, *Geophys. Res. Lett.*, *29*(14), 1665, doi:10.1029/2002GL014896.
Mihelcic, D., D. Klemp, P. Musgen, H. W. Paetz, and A. Volz-Thomas (1993), Simultaneous measurements of peroxy and nitrate radicals at schauinsland, *J. Atmos. Chem.*, *16*(4), 313–335.
Paulson, S. E., and J. J. Orlando (1996), The reactions of ozone with alkenes: An important source of HO_x in the boundary layer, *Geophys. Res. Lett.*, *23*(25), 3727–3730.
Paulson, S. E., C. Myeong, A. D. Sen, and G. Orzechowska (1998), Measurement of OH radical formation from the reaction of ozone with several biogenic alkenes, *J. Geophys. Res.*, *103*(D19), 25,533–25,539.
Pisano, J. T., I. McKendry, D. G. Steyn, and D. R. Hastie (1997), Vertical nitrogen dioxide and ozone concentrations measured from a tethered balloon in the Lower Fraser Valley, *Atmos. Environ.*, *31*(14), 2071–2078.
Platt, U., G. LeBras, G. Poulet, J. P. Burrows, and G. Moortgat (1990), Peroxy radicals from nighttime reaction of NO_3 with organic compounds, *Nature*, *348*(6297), 147–149.
Platt, U., et al. (2002), Free radicals and fast photochemistry during BERLIOZ, *J. Atmos. Chem.*, *42*, 359–394.
Povey, I., A. South, A. Kint de Roodenbeke, C. Hill, R. Freshwater, and R. Jones (1998), A broadband lidar for the measurement of tropospheric constituent profiles from the ground, *J. Geophys. Res.*, *103*(D3), 3369–3380.
Rao, K. S., and H. F. Snodgrass (1979), Some parameterizations of the nocturnal boundary layer, *Boundary Layer Meteorol.*, *17*, 15–28.
Riemer, N., H. Vogel, B. Vogel, B. Schell, I. Ackermann, C. Kessler, and H. Hass (2003), Impact of the heterogeneous hydrolysis of N_2O_5 on chemistry and nitrate aerosol formation in the lower troposphere under

photosmog conditions, *J. Geophys. Res.*, *108*(D4), 4144, doi:10.1029/2002JD002436.

Rudich, Y., R. K. Talukdar, A. R. Ravishankara, and R. W. Fox (1996), Reactive uptake of NO_3 on pure water and ionic solutions, *J. Geophys. Res.*, *101*(D15), 21,023–21,031.

Sander, S. P., et al. (2003), Chemical kinetics and photochemical data for use in atmospheric studies, *Eval. 14*, NASA-JPL, Pasadena, Calif.

Saunders, S. M., M. E. Jenkin, R. G. Derwent, and M. J. Pilling (2003), Protocol for the development of the Master Chemical Mechanism, MCM vol. 3, part A, Tropospheric degradation of non-aromatic volatile organic compounds, *Atmos. Chem. Phys.*, *3*, 161–180.

Sawyer, R. F., R. A. Harley, S. H. Cadle, J. M. Norbeck, R. Slott, and H. A. Bravo (2000), Mobile sources critical review: 1998 NARSTO assessment, *Atmos. Environ.*, *34*(12–14), 2161–2181.

Schumann, U. (1989), Large-eddy simulation of turbulent diffusion with chemical reactions in the convective boundary layer, *Atmos. Environ.*, *23*(8), 1713–1727.

Seinfeld, J. H., and S. N. Pandis (1997), *Atmospheric Chemistry and Physics: From Air Pollution to Climate Change*, John Wiley, Hoboken, N. J.

Smith, N., J. M. C. Plane, C. Nien, and O. A. Solomon (1995), Nighttime radical chemistry in the San Joaquin Valley, *Atmos. Environ.*, *29*, 2887–2897.

Stohl, A., E. Williams, G. Wotawa, and H. Krompkolb (1996), A European inventory of soil nitric oxide emissions and the effect of these emissions on the photochemical formation of ozone, *Atmos. Environ.*, *30*(22), 3741–3755.

Stutz, J., B. Alicke, R. Ackermann, A. Geyer, A. White, and E. Williams (2004), Vertical profiles of NO_3, N_2O_5, O_3, and NO_x in the nocturnal boundary layer: 1. Observations during the Texas Air Quality Study 2000, *J. Geophys. Res.*, *109*, D12107, doi:10.1029/2003JD004209.

Thompson, A. M., and D. Lenschow (1984), Mean profiles of trace reactive species in the unpolluted marine surface layer, *J. Geophys. Res.*, *89*(D3), 4788–4796.

Verver, G. (1994), Comment on "A modified K model for chemically reactive species in the planetary boundary layer" by Fujihiro Hamba, *J. Geophys. Res.*, *99*(D9), 19,021–19,023.

Vila-Guerau de Arellano, J. (2003), Bridging the gap between atmospheric physics and chemistry in studies of small-scale turbulence, *Bull. Am. Meteorol. Soc.*, *84*(1), 51–56.

Vila-Guerau de Arellano, J., P. G. Duynkerke, and K. F. Zeller (1995), Atmospheric surface layer similarity theory applied to chemically reactive species, *J. Geophys. Res.*, *100*(D1), 1397–1408.

von Friedeburg, C., T. Wagner, A. Geyer, N. Kaiser, B. Vogel, H. Vogel, and U. Platt (2002), Derivation of tropospheric NO_3 profiles using off-axis differential optical absorption spectroscopy measurements during sunrise and comparison with simulations, *J. Geophys. Res.*, *107*(D13), 4168, doi:10.1029/2001JD000481.

Wang, S., R. Ackermann, A. Geyer, J. C. Doran, W. J. Shaw, J. D. Fast, C. W. Spicer, and J. Stutz (2003), *Vertical Variation of Nocturnal NOx Chemistry in the Urban Environment of Phoenix*, *Proc. 83rd AMS Ann. Meet.*, CD-ROM, P1.1, Am. Meteorol. Soc., Long Beach, Calif.

Wängberg, I., T. Etzkorn, I. Barnes, U. Platt, and K. H. Becker (1997), Absolute determination of the temperature behavior of the $NO_2 + NO_3 +$ (M) $\langle - \rangle$ N_2O_5 + (M) equilibrium, *J. Phys. Chem. A*, *101*(50), 9694–9698.

Wayne, R. P., et al. (1991), The nitrate radical: Physics, chemistry, and the atmosphere, *Atmos. Environ.*, *25A*, 1–203.

Weaver, A., S. Solomon, R. W. Sanders, K. Arpag, and J. Miller (1996), Atmospheric NO_3 off-axis measurements at sunrise: Estimates of tropospheric NO_3 at 40°N, *J. Geophys. Res.*, *101*(D13), 18,605–18,612.

Wesely, M. L., and B. B. Hicks (2000), A review of the current status of knowledge on dry deposition, *Atmos. Environ.*, *34*(12–14), 2261–2282.

Yoshizawa, A. (1982), A statistical investigation of shear turbulence: The Reynolds-stress transport equation, *J. Phys. Soc. Jpn.*, *51*, 658–666.

Zhang, J., and S. T. Rao (1999), The role of vertical mixing in the temporal evolution of ground-level ozone concentrations, *J. Appl. Meteorol.*, *38*, 1674–1691.

A. Geyer and J. Stutz, Department of Atmospheric Sciences, UCLA, Los Angeles, CA 90095-1565, USA. (jochen@atmos.ucla.edu)

Vertical profiles of NO_3, N_2O_5, O_3, and NO_x in the nocturnal boundary layer: 1. Observations during the Texas Air Quality Study 2000

Jochen Stutz, Björn Alicke, Ralf Ackermann, and Andreas Geyer
Department of Atmospheric Sciences, University of California, Los Angeles, California, USA

Allen White
Environmental Technology Laboratory, NOAA, Boulder, Colorado, USA

Eric Williams
NOAA Aeronomy Laboratory and Cooperative Institute for Research in Environmental Sciences, University of Colorado, Boulder, Colorado, USA

Received 2 October 2003; revised 30 January 2004; accepted 27 March 2004; published 30 June 2004.

[1] Nocturnal chemistry in urban areas can considerably influence the composition of the boundary layer by removing nitrogen oxides and hydrocarbons, as well as changing the size and composition of aerosol particles. Although these processes can have a severe impact on pollution levels at night and during the following day, little quantitative information is available. In particular, the vertical variation of trace gas concentrations and chemistry at night has received little attention and is thus poorly understood. Here we present differential optical absorption spectroscopy (DOAS) measurements of the vertical distributions of O_3, NO_2, and NO_3 during the Texas Air Quality Study 2000 near Houston, TX. Distinct vertical profiles, with lower mixing ratios of O_3 and NO_3 near the ground than above 100 m altitude, were observed. Mixing ratios of NO_3 aloft reached 50 ppt and above, and steady state N_2O_5 levels were calculated to be 100–300 ppt. A one-dimensional chemical transport model reveals that the formation of the vertical trace gas distributions is driven by deposition, surface emissions of NO, reactions of O_3 and NO_3, and vertical mixing. The removal of O_3 in Houston is found to proceed by dry deposition, while NO_x is primarily lost above 10 m altitude by N_2O_5 chemistry. The study shows that chemistry in polluted areas is strongly altitude dependent in the lowest 100 m of the nocturnal atmosphere. This altitude dependence should be considered in future field and model studies of urban air pollution. *INDEX TERMS:* 0345 Atmospheric Composition and Structure: Pollution—urban and regional (0305); 0365 Atmospheric Composition and Structure: Troposphere—composition and chemistry; 0368 Atmospheric Composition and Structure: Troposphere—constituent transport and chemistry; 0394 Atmospheric Composition and Structure: Instruments and techniques; *KEYWORDS:* nocturnal chemistry, nitrate radical, vertical transport

Citation: Stutz, J., B. Alicke, R. Ackermann, A. Geyer, A. White, and E. Williams (2004), Vertical profiles of NO_3, N_2O_5, O_3, and NO_x in the nocturnal boundary layer: 1. Observations during the Texas Air Quality Study 2000, *J. Geophys. Res.*, *109*, D12306, doi:10.1029/2003JD004209.

1. Introduction

[2] The study of air pollution in urban areas has, for many decades, focused on the daytime processes responsible for the formation of ozone and particles. The chemical reactions and transport processes modifying the composition of the urban nocturnal boundary layer (NBL) have, on the other hand, received surprisingly little attention. This lack of information is partially explained by the absence of reliable means to study this subject and the difficulty in performing field experiments. From experimental and modeling studies in remote and marine regions, we know that nocturnal chemistry can efficiently transform and remove O_3, NO_x, and VOC, and influence the size and composition of particles [*Dentener and Crutzen*, 1993; *Dimitroulopoulou and Marsh*, 1997; *Li et al.*, 1993; *Makar et al.*, 1998; *Riemer et al.*, 2003]. The importance of these mechanisms in urban environments, however, remains uncertain.

[3] A number of unique characteristics distinguish the NBL from the well mixed daytime boundary layer in urban areas:

[4] 1. Negative buoyancy inhibits turbulent mixing, thus vertical transport is slower at night than during the day

0148-0227/04/2003JD004209$09.00

[*Mahrt et al.*, 1998; *Stull*, 1988]. Trace gases that are emitted near the surface, such as NO_x and CO from traffic, therefore accumulate near the ground at night.

[5] 2. Trace gases emitted at the ground can be chemically converted as they are slowly transported upwards [*Galmarini et al.*, 1997], and develop strong vertical gradients. Compounds reacting with the emitted gases, such as O_3 with NO, will also show distinct vertical profiles [*Beyrich et al.*, 1996; *Gusten et al.*, 1998; *Pisano et al.*, 1997].

[6] 3. Radical chemistry is slower and less efficient at night, since OH concentrations are small due to the lack of photochemical OH sources [*Finlayson-Pitts and Pitts*, 2000]. In general, the nitrate radical, NO_3, is considered the most important oxidant in the urban NBL [*Finlayson-Pitts and Pitts*, 2000; *Geyer et al.*, 2001; *Platt et al.*, 2002; *Wayne et al.*, 1991]. For example, observations downwind of Los Angeles in the beginning of the 1980s found NO_3 mixing ratios exceeding 300 ppt [*Harris et al.*, 1983; *Platt et al.*, 1980, 1984]. *Smith et al.* [1995] and *Geyer et al.* [2001, 1999] report 80–100 ppt NO_3 in polluted suburban areas.

[7] 4. A number of unique heterogeneous reactions, such as the uptake of N_2O_5, play an important role at night [*Jacob*, 2000].

[8] 5. Due to the lower boundary layer height the ground plays a more important role for heterogeneous chemistry in the boundary layer at night than during the day.

[9] Because the NBL behaves differently than the daytime boundary layer, the scientific approach developed to study daytime chemistry needs to be adapted for experiments and models at night. Observations are often performed by local in-situ measurements near the ground, without considering the vertical change in composition and chemistry. This approach may be successful in the well mixed daytime boundary layer. However, it excludes large portions of the NBL, and often also the nocturnal residual layer from the observations.

[10] This is the first of two papers adopting a one-dimensional view of the nocturnal boundary layer. Here we will concentrate on the observation and interpretation of the vertical trace gas profiles of O_3, NO_2, and NO_3 during the TEXAQS 2000 field experiment in La Porte near Houston, TX. The vertical distribution of trace gases, in particular NO_3, are discussed, and conclusions about the altitude dependence of the chemistry in the NBL are drawn with respect to the topics discussed above. An accompanying paper by *Geyer and Stutz* [2004] describes modeling studies of the various mechanisms influencing the chemistry of NO_3, N_2O_5, and the NO-O_3-NO_2 system in the NBL.

[11] The motivation for both studies is to improve our ability to assess the influence of nocturnal chemistry on the composition of the nocturnal atmosphere. In particular, we want to overcome the shortcomings posed by the poor understanding of the influence of vertical mixing in the nocturnal boundary layer, and the lack of altitude resolved measurements of the chemical composition in the NBL.

2. The Urban Nocturnal Boundary Layer

2.1. Chemistry

[12] Nocturnal chemistry is dominated by the reactions of ozone and the nitrogen oxides NO, NO_2, NO_3, and N_2O_5. In urban areas the most significant reaction is the titration of ozone by NO.

$$\mathrm{NO + O_3 \rightarrow NO_2 + O_2} \qquad \mathrm{k_1(296\ K) = 1.8 \times 10^{-14} cm^3 molec^{-1} s^{-1}} \tag{1}$$

[13] In cities this fast reaction can lead to a complete destruction of ozone at night, while simultaneously forming NO_2. This leads to vertical profiles of ozone, with lower concentrations near the surface [*Beyrich et al.*, 1996; *Gusten et al.*, 1998; *Pisano et al.*, 1997].

[14] The nitrate radical, NO_3, is in many cases the most important nocturnal radical species for the oxidation power of the atmosphere [*Platt et al.*, 2002; *Wayne et al.*, 1991]. It is formed in the presence of ozone and NO_2.

$$\mathrm{NO_2 + O_3 \rightarrow NO_3 + O_2} \qquad \mathrm{k_2(296\ K) = 3.5 \times 10^{-17} cm^3 molec^{-1} s^{-1}} \tag{2}$$

[15] Various loss pathways influence NO_3 levels in urban areas (for details refer to *Wayne et al.* [1991]). The fast reaction with NO often controls NO_3 concentrations at the ground in urban areas.

$$\mathrm{NO_3 + NO \rightarrow 2\ NO_2} \qquad \mathrm{k_3(296\ K) = 2.6 \times 10^{-11} cm^3 molec^{-1} s^{-1}} \tag{3}$$

[16] Because the NO_3 lifetime at NO mixing ratios above 0.1 ppb is less than 15 s, it is often assumed that, in areas with large NO emissions, NO_3 chemistry is relatively unimportant.

[17] NO_3 oxidizes larger alkenes, in particular isoprene and monoterpenes [*Atkinson*, 1991], forming, among other reaction products, various RO_2 radicals [*Geyer et al.*, 2003b; *Platt et al.*, 1990]. Reactions of NO_3 on organic aerosol, with uptake coefficients in the range from 0.0014 to 0.015, have also been reported [*Moise et al.*, 2002].

[18] Another significant process at night is the temperature dependent equilibrium of NO_2, NO_3, and N_2O_5 [*Wängberg et al.*, 1997]:

$$\mathrm{NO_2 + NO_3 \leftrightarrow N_2O_5} \qquad \mathrm{K(T) = \exp(-60.46 + 10724/T)} \tag{4}$$

[19] N_2O_5 can be taken up by surfaces with uptake coefficients in the range of 0.001 to 0.05 [*Hallquist et al.*, 2000; *Kane et al.*, 2001; *Mentel et al.*, 1996; *Wahner et al.*, 1998b]. Another possible pathway for N_2O_5 is its reaction with water vapor. *Mentel et al.* [1996], and *Wahner et al.* [1998a], suggest that this reaction is both first and a second order in water.

$$\mathrm{N_2O_5 + H_2O \rightarrow 2\ HNO_3} \qquad \mathrm{k_5 = 2.5 \times 10^{-22} cm^3 molec^{-1} s^{-1}} \tag{5}$$

$$\mathrm{N_2O_5 + 2\ H_2O \rightarrow 2\ HNO_3 + H_2O} \qquad \mathrm{k_6 = 1.8 \times 10^{-39} cm^6 molec^{-2} s^{-1}} \tag{6}$$

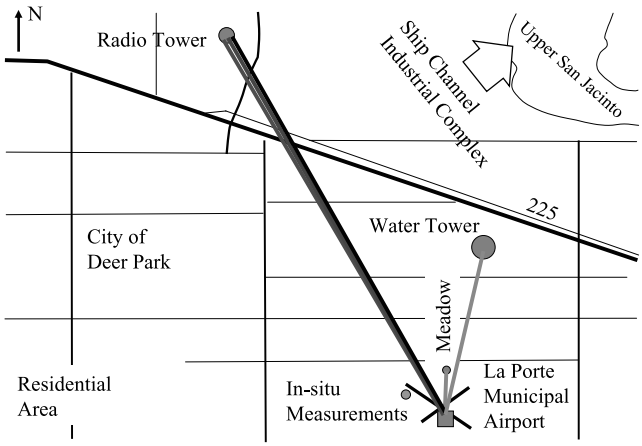

Figure 1. Map of the experimental setup at La Porte.

[20] There is currently some uncertainty connected with these values (http://www.iupac-kinetics.ch.cam.ac.uk) [*Voegele et al.*, 2003].

2.2. Vertical Mixing and Transport

[21] Vertical transport of trace gases plays an important role in cities, where most emissions occur close to the ground. Radiative surface cooling at night suppresses mechanically produced turbulence, leading to surface temperature inversions [*Stull*, 1988]. Under neutral and weakly stable conditions, trace gases are still efficiently mixed, and vertical transport can be described by Monin-Obukov similarity theory [*Mahrt et al.*, 1998; *Stull*, 1988]. Under strong stabilities, mixing is strongly inhibited, turbulence becomes intermittent, and non-turbulent motions become important [*Coulter and Doran*, 2002; *Mahrt et al.*, 1998]. The description of vertical exchange at night, for example in air quality modeling applications, is thus challenging. An additional problem is posed by the similarity between the timescale of turbulent mixing at night, which is in the range of ~100 s [*Fitzjarrald and Lenschow*, 1983; *Lenschow*, 1981], and the chemical lifetime of many reactive species. This similarity leads to differences in the vertical transport of unreactive and reactive trace gases [*Fitzjarrald and Lenschow*, 1983; *Galmarini et al.*, 1997; *Hamba*, 1993; *Kramm et al.*, 1991].

2.3. Vertical Trace Gas Profiles

[22] The influence of vertical transport on the distribution of trace gases in the NBL has primarily been studied with respect to vertical profiles of ozone, which were measured with in-situ instruments mounted on tethered balloons [*Beyrich et al.*, 1996; *Colbeck and Harrison*, 1985; *Galbally*, 1968, 1971; *Glaser et al.*, 2003; *Gusten et al.*, 1998; *Pisano et al.*, 1997]. In general, ozone concentrations increase from the ground upwards due to its deposition on the surface [*Wesely and Hicks*, 2000] and reactions with NO. Profiles of NO_2, measured with the help of tethered balloons, in the NBL have also been reported [*Glaser et al.*, 2003; *Pisano et al.*, 1997], and usually show a negative profile (higher concentrations at the ground than aloft) due to the conversion of NO emissions to NO_2.

[23] Measurements of vertical profiles of [NO_3] have been made by two groups [*Allan et al.*, 2002; *Coe et al.*, 2002; *von Friedeburg et al.*, 2002]. Both groups relied on the measurement of NO_3 absorption in scattered sunlight during sunrise to derive the vertical [NO_3] distribution. The general finding is that, shortly before sunrise, NO_3 mixing ratios increase from the ground up to a certain height, and then decrease again. Only the measurements of *von Friedeburg et al.* [2002], however, have the resolution to give information about the distribution in the boundary layer, and show a maximum of ~120 ppt at 300 m altitude. A number of modeling studies also find an increase of [NO_3] from the ground to heights of several hundred meters, which is caused by ozone deposition and NO emissions at the ground [*Fish et al.*, 1999; *Galmarini et al.*, 1997].

3. Experimental

3.1. Location

[24] Measurements were performed during the Texas Air Quality Study (TEXAQS) in August and September 2000, at the La Porte Municipal Airport (95°03′51.1″W, 29°40′09.3″N, height: 8 m asl) 30 km ENE of the city center of Houston, TX. The airport is located south-southwest of the heavy industrialized ship channel area, and is thus influenced by fresh emissions under northerly and easterly winds. The areas west and south of the airport are mostly residential, without larger industrial complexes. Freeway 225 runs 3 km north of the airport in ENE direction (Figure 1). While heavy traffic is common on the freeway during rush hour, it is only sparsely traveled at night. The immediate area around the airport is characterized by grassland, residential homes and low trees. The airport itself is open to small aircrafts with infrequent starts and landings. Nocturnal meteorological conditions at this site were dominated by mostly westerly winds with speeds of 1–4 ms^{-1}. Temperatures at night were between 25 and 30°C with high relative humidities of 60–90%.

3.2. Instrumentation

[25] We deployed Differential Optical Absorption Spectroscopy (DOAS) systems and a number of in-situ chemical and meteorological instruments at the La Porte Airport during the TEXAQS 2000 study.

3.2.1. Differential Optical Absorption Spectroscopy (DOAS) Instruments

[26] In short, DOAS is a technique that quantifies trace gases with narrow band absorption structures in the UV and visible wavelength region in the open atmosphere [*Platt*, 1994]. Two identical DOAS systems were set up at the southern end of the La Porte airport, at an altitude of 2 m above the ground during TEXAQS 2000 (see Figures 1 and 2). Each DOAS system consisted of a coaxial double

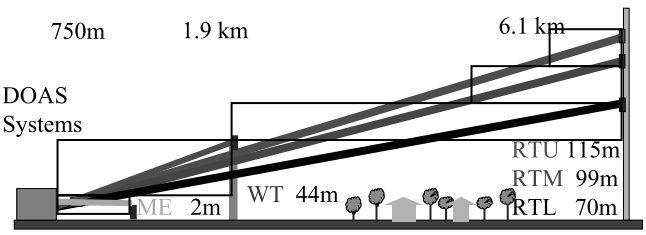

Figure 2. Setup of the differential optical absorption spectroscopic (DOAS) light path in a side view. See color version of this figure at back of this issue.

Newtonian telescope that sent a collimated beam of white light from a Xe short-arc lamp onto an array of quartz corner cube retroreflectors. The retroreflectors folded the beam back into the telescope, where it was focused and fed through a quartz fiber into a spectrometer [*Stutz and Platt*, 1997]. The spectral analysis of the path-averaged atmospheric absorption spectra was performed by a thermally stabilized 0.5 m focal length Czerny-Turner spectrograph (Acton Research, Spectra Pro 500) and a cooled photodiode array detector system (Hoffmann Messtechnik). A detailed description of the basic setup is given by *Alicke et al.* [2002] and *Stutz and Platt* [1997].

[27] We deployed five different retroreflector arrays, with the goal of measuring the vertical distribution of various trace gases. Three arrays were mounted at different altitudes on a radio tower at 6.1 km distance from the DOAS telescopes (see Figures 1 and 2). The mounting heights were 70 m, 99 m, and 115 m above the ground. These three light paths will be referred to as radio tower lower (RTL), middle (RTM), and upper (RTU). Another retroreflector array was mounted on a water tower at 1.9 km distance and an altitude of 44 m. This light path will be called water tower (WT). The last and shortest light path ran 2 m above the meadow inside the airport. The distance between telescope and the retroreflectors of this "meadow" (MD) light path was 750 m.

[28] From 25 August to 12 September 2000, we measured concentrations of NO_3, NO_2, O_3, and SO_2, along all five light paths. One DOAS instrument sequentially aimed at the three retroreflector arrays mounted on the radio tower. Typically, a complete set of measurements on all three light paths required 20 min. The second DOAS telescope sequentially aimed at the water tower and the meadow retroreflectors. A sequence of measurements on these two light paths took 10–15 min.

[29] Measurements of NO_2, O_3, and SO_2 were made in the spectral range of 300–380 nm with a spectral resolution of 0.5 nm, employing the MultiChannel-Scanning Technique [*Brauers et al.*, 1995] to correct the diode-to-diode variation in the detector sensitivity. The analysis procedure is described in detail by *Alicke et al.* [2002]. The method and analysis technique of the NO_3 measurements is described in detail by *Geyer et al.* [2003a]. As discussed by *Stutz and Platt* [1996], errors of the concentrations are calculated by the analysis procedure for each individual spectrum and trace gas. All errors of trace gas mixing ratios in this paper refer to the 1σ statistical uncertainties. The systematic errors of the reported trace gas mixing ratios are dominated by the uncertainties of the absorption cross sections. The uncertainty of the O_3, NO_2, and NO_3 absorption cross sections are ±3%, ±8%, and ±10%, respectively [*Bass and Paur*, 1984; *Harder et al.*, 1997; *Yokelson et al.*, 1994]. The systematic error of the DOAS spectrometer was determined to be <3% [*Stutz*, 1996].

[30] The average and best detection limits achieved on the different light paths are listed in Table 1. The average detection limits were calculated as twice the average of the individual 1σ random error of all measurements, including measurements that were taken during times of low visibility, instrument misalignment, and lamp failure. The detection limits achieved under optimum conditions are also listed in Table 1. Detection limits below 1 ppt for NO_3 and 50 ppt for NO_2 were achieved during TEXAQS 2000. In general, the detection limits on the shorter light paths were higher compared to the RT data by a factor determined by the ratio of the path lengths (Table 1). A comparison of the two DOAS instruments aiming at the WT retroreflector for a 12 hour period before 24 August showed an excellent agreement between the two systems.

Table 1. Summary of Data Coverage, Average, and Best Detection Limits for the Differential Optical Absorption Spectroscopy Results

	Lightpath "Meadow"	Lightpath "Water Tower"	Lightpaths "Radio Tower"
Distance, km	0.75	1.9	6.1
Data coverage	20 Aug. to 10 Sept.	18 Aug. to 10 Sept.	24 Aug. to 12 Sept.
	Detection Limit NO_3, ppt		
Average	23	8	2.6
Best	2	1.5	0.8
	Detection Limit NO_2, ppb		
Average	0.88	0.4	0.13
Best	0.24	0.2	0.05
	Detection Limit O_3, ppb		
Average	9	4	2.5
Best	4.7	1.5	0.9

3.2.2. Meteorological Instruments

[31] A number of meteorological measurements were made at La Porte. Temperature and R.H. were measured at 2 m altitude at the La Porte airport, as well as on top of the water tower 44 m above the ground (Vaisala HMP45C humidity probe, Campbell Scientific data logger). Wind speed and direction were measured at 10 m above ground by a prop-vane anemometer (RM Young model 5103). In addition, a sonic anemometer/thermometer (Applied Technologies K-probe) was mounted at 8 m above ground.

3.2.3. In Situ Chemical Instruments

[32] A large number of other chemical compounds were measured at La Porte during TEXAQS 2000. Particularly useful for our analysis are the measurements of NO, NO_2, and O_3, which were performed 600 m west-northwest of the DOAS telescopes. Air was sampled at 10 m altitude by glass manifold with a ~150 slpm flow rate, and thus a residence time of ~1 sec. O_3 was measured by UV-absorption. NO and NO_2 were detected by chemiluminescence and photolytic conversion [*Thornton et al.*, 2003].

3.3. Deconvolution of Spatial Trace Gas Distribution

[33] The spatial distributions of the various trace gases measured by the DOAS instruments were calculated from the data measured along the five light paths pointing from H = 2 m to altitudes h_i of 2, 44, 70, 99, and 115 m. Because the measurements were made sequentially we linearly interpolated all the data to the time of the RTU measurement. We will refer to the temporally interpolated concentrations averaged along the ith light path as S_i, and to the concentrations in a specific height interval as C_i. The numbering proceeds from the ground upwards, i.e., S_1 is the meadow, S_2 is the water tower data, etc. The data of the two lowest paths directly represent the concentrations at 2 m altitude and in the height interval (2–44) m. The other concentrations C_3, C_4, and C_5 in the height intervals (44 m–

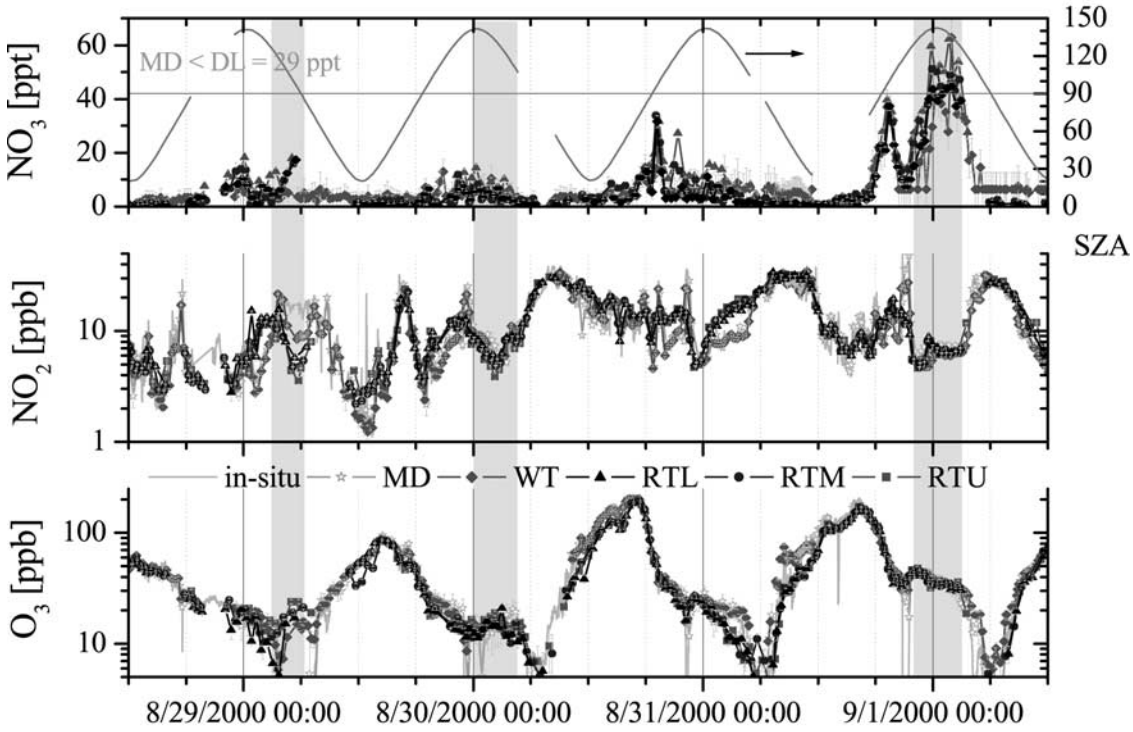

Figure 3. Overview of path averaged DOAS data from noon of 28 August to noon 2 September 2000. The data is color coded according to the colors in Figure 2. Please note the logarithmic scale for NO_2 and O_3. See color version of this figure at back of this issue.

70 m), (70 m–99 m), and (99 m–115 m) were calculated from the ground upwards with equation (7):

$$C_i = \frac{h_i - H}{h_i - h_{i-1}} S_i - \frac{h_{i-1} - H}{h_i - h_{i-1}} S_{i-1} \quad (7)$$

Errors for each individual C_i were calculated based on the propagation of the errors of the individual path-averaged concentrations S_i. Figure 2 illustrates the vertical extent of the volumes represented by the different C_i.

[34] As illustrated in Figures 1 and 2 the MD, WT, and radio tower light paths are not only separated in the vertical but to some extent also in the horizontal. We therefore have to ensure that the concentrations C_i, do indeed yield information about the vertical distribution of trace gases in the respective height intervals, and are not influenced by horizontal inhomogeneities.

3.4. Analysis of Horizontal Trace Gas Homogeneity

[35] In a first step, the degree of the horizontal trace gas homogeneity can be determined by a simple comparison between the RTL and the WT light path data. Geometric considerations reveal that the two light paths overlap by 62% in their vertical coverage, but by less than 32% in the horizontal coverage. Inhomogeneities in the horizontal trace gas distributions will thus be weighted more strongly than differences in the vertical distribution. In contrast, the vertical overlap between RTL and RTU is 60%, while the horizontal overlap is 100%. Horizontal inhomogeneities in trace gas concentrations should thus not lead to differences in the RTL and RTU observations, while vertical gradients can be observed. Figure 3 shows the time series of NO_3, NO_2, and O_3 mixing ratios measured along all five light paths from 28 August to 1 September. During a number of occasions, mixing ratio differences between RTL and WT, and similar values for RTL and RTU, can be clearly identified. For example, from 0000 to 0600 on 31 August, NO_2 data of RTL and WT differ by a factor 2, while RTL and RTU values are nearly identical. If the RTL/WT difference would be purely caused by a vertical NO_2 gradient, the mixing ratio above 44 m would be 26 ppb and thus 3 times higher than below this altitude. Such a strong gradient is clearly not reflected in the comparison between RTU and RTL. In addition, the vertical stability was weak during this period (wind speed $\sim$2 ms^{-1}, friction velocity u* $\sim$ 0.2 ms^{-1}) and such a strong vertical NO_2 gradient cannot be sustained. We therefore conclude that the behavior in this period was most likely caused by a horizontally inhomogeneous trace gas distribution. A number of other intervals such as the one just described were identified during the observational period. The criteria to identify horizontally mixed air masses based on these arguments was a similarity between WT and RTL data together with a difference between the other light paths, in particular between RTL, RTM, and RTU.

[36] Another method to study the horizontal mixing of an air mass is the comparison of the temporal behavior of trace gas concentrations from the DOAS and the in-situ measurements. Concentration changes due to the advection of air masses that are well-mixed on scales larger than the length of the DOAS light paths lead to similar concentrations in the DOAS and the in-situ observations. In contrast, plumes that are smaller than the extent of the DOAS light paths lead to a stronger response in the in-situ data. Figure 3 shows a

number of small scale plumes that passed over the La Porte airport causing a sudden increase in the concentration of the in-situ instruments and the shorter light path DOAS data, but are not reflected in the RT data. For example, on 31 August 2000 around 2000 CST the NO_2 mixing ratio increases from 7 ppb to 12–15 ppb on the two shorter light paths and the in-situ instrument for about 1 hour, while the radio tower data does not appear to change. Periods during which temporal concentration changes are reflected in all DOAS and the in-situ data are thus identified as horizontally well mixed.

[37] After performing the tests described above, we identified three periods where a comparison between the DOAS data on different light paths indicates that the air mass was horizontally well mixed. In addition, the temporal behavior of DOAS and in-situ measurements showed a very good agreement, strengthening this conclusion. The DOAS data during these periods thus clearly allow the derivation of vertical trace gas profiles. The periods are marked by gray bars in Figure 3. In particular, the period between 2200 on 31 August and 0600 on 1 September is well suited for the investigation of vertical trace gas profiles. We will thus focus on this night throughout most of this publication. The early morning of 29 August is also very interesting due to its strong vertical stability. Back-trajectories with the NOAA-HYSPLIT model for these periods show that the observed air originated from the Gulf of Mexico, and touched the coast four hours before the measurements. The air then continued to travel in north and northeastern direction toward La Porte. Only a few small NO_x sources were located along the trajectory (www.epa.gov/air/data), which is in agreement with the comparatively low NO_x mixing ratios at midnight.

[38] Finally, we would like to note that a comparison of DOAS data measured on different light paths, and the comparison with in-situ data as described above, offers a powerful tool to investigate the spatial distribution of trace gases. For example, this method allows the determination of how representative in-situ measurements are for a larger area, and thus helps in the extrapolation of point data to larger scales, such as those used in air pollution models.

4. Results

[39] We will focus here on the nocturnal observations during a four day period, 28 August 2000 to 1 September 2000 (see also section 3.4), which includes the days with the highest daytime ozone mixing ratios observed at La Porte during TEXAQS 2000 (Figure 3). We will begin by discussing the general behavior of the meteorology and trace gas data, and then focus on the vertical profiles of various trace gases. The night of 31 August to 1 September will be discussed in detail.

4.1. Meteorological Observations

[40] During most nights at La Porte the wind direction turned from ~220° at the beginning of the night to ~360° in the early morning (Figure 4), with wind speeds between 1 and 4 ms^{-1} (Figure 4). On two occasions we encountered very calm conditions. On 29 August between 0300 and 0600, wind speeds of 0–1 ms^{-1} are also reflected in the temperature gradient of ~2 K between 2 m and 44 m. Similarly, a temperature difference of 0.5 K was observed during the morning of 1 September. The temperature gradients allow us to infer that La Porte typically did not encounter strong ground inversions during the period shown in Figure 4. This is further emphasized in the friction velocity, u*, in the range of 0.1–0.3 ms^{-1}, (Figure 4) during most nights. The heat flux was slightly negative at night (Figure 4).

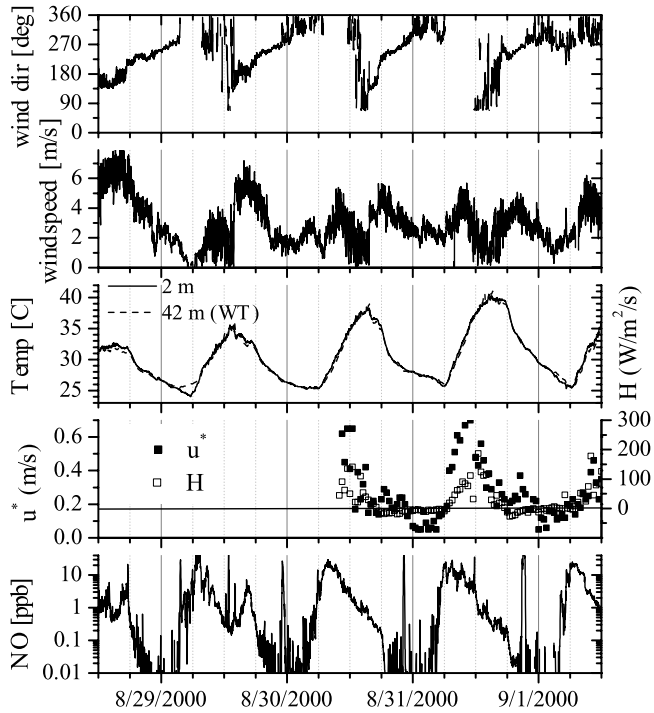

Figure 4. Meteorological data and NO mixing ratios from 28 August to 2 September 2000 at La Porte. Micrometeorological data for the first half of this period is missing due to instrumental problems.

4.2. Trace Gas Concentrations

4.2.1. NO

[41] Nocturnal NO mixing ratios typically varied between 0 and 0.1 ppb (Figure 4). However, under the stable conditions after 0300 on 29 August, NO mixing ratios increased to 2 ppb. These high NO levels, and the fact that mixing ratios of up to 0.1 ppb were observed during other nights, are indicative of a small local NO source, most likely ground emission and emissions from nearby traffic. NO mixing ratios generally increased in the early morning around 0500 at the beginning of the local rush hour. During several evenings between 2000 and 2300, NO mixing ratios exceed 10 ppb for about one hour. We explain this sudden NO increase by a local plume from a nearby NO source passing over the airport. The wind direction associated with this plume is 270 degrees.

4.2.2. O_3

[42] Figure 3 shows the highest daytime ozone levels of ~200 ppb observed at La Porte during TEXAQS 2000. Nocturnal O_3 is typically between 10 and 40 ppb from the beginning of the night to the onset of rush hour. After the onset of rush hour, O_3 mixing ratios drop below 5 ppb, except on 29 August. Low in-situ ozone is also found in the plumes of elevated NO described above. It should finally be noted that the agreement between the DOAS and the in-situ

O_3 mixing ratios is excellent, in particular with respect to the WT and MD light paths.

4.2.3. NO_2

[43] Nocturnal NO_2 mixing ratios displayed rapid fluctuation in the first part of all four nights (Figure 3), which are associated with local pollution plumes that are also reflected in the O_3 and NO data. During the second half of the nights of 29 August to 1 September NO_2 typically varied less strongly. The NO_2 mixing ratios during the night of 31 August to 1 September, for example, are around 5 ppb from 2200 to midnight, and then around 7 ppb from midnight to the time rush hour starts. Only during the stable period on the morning of 29 August large variations, in particular between the different light paths and the in-situ data, were observed. NO_2 increased rapidly after 0500 when NO emission from traffic begins.

4.2.4. NO_3

[44] As expected, the path-averaged NO_3 data measured during the four days at La Porte (Figure 3) show low mixing ratios during most of the day. NO_3 was, however, elevated during some of the late afternoons within 3 hours of sunset [*Geyer et al.*, 2003a]. During the first two nights in Figure 3, NO_3 mixing ratios remained below 20 ppt, but well above our detection limit on the WT and RT light paths. NO_3 mixing ratios during the night of 30–31 August reached ~20–30 ppt at 2000 and 2200. These peaks can also be seen in the NO_2 data and indicate that NO_3 is elevated in the pollution plumes observed at La Porte. The night of 31 August to 1 September had the highest path averaged data during this four day period. Maximum values reached 60 ppt on the RTU light path. Figure 3 clearly shows that RTU has the highest mixing ratio, followed by RTM, RTL, and WT. The NO_3 MD data were below the detection limit during the whole period. NO_3 disappeared during all nights at the onset of rush hour, when high NO concentrations titrated both O_3 and NO_3.

4.3. Vertical Trace Gas Profiles

[45] Figure 5 shows the spatial distribution of the mixing ratios of O_3, NO_2, and NO_3 during the four day period at La Porte, as calculated by equation (7). The mixing ratios of N_2O_5, which are also shown in Figure 5, will be explained in detail in section 4.3.4. The vertical trace gas profiles during the night of 31 August to 1 September are displayed in more detail in Figure 6. We chose four times, approximately separated by 2 hours each, beginning at 2032 for this graph. For the first time, 2032, horizontal inhomogeneities can not be excluded entirely. The later times are during periods where we found a horizontally well mixed air mass. The profiles in Figure 6 are therefore representative for the general form of the profiles during this night. In the following section we will discuss the different trace gas profiles in Figures 5 and 6.

4.3.1. O_3 and NO_2

[46] The logarithmic color coding in Figure 5 reveals the typical diurnal O_3 variation, with high mixing ratios during the afternoon and lower values at night. Vertical ozone profiles were typically weak during the four day period. As illustrated during the night of 30–31 August, O_3 mixing ratios were sometimes also highly variable, and no clear gradients can be observed. However, a closer look at Figure 6 reveals that ozone was generally higher in the upper altitude levels, with mixing ratios of 50–60 ppb during 31 August to 1 September. Ozone then decreases in the next two altitude

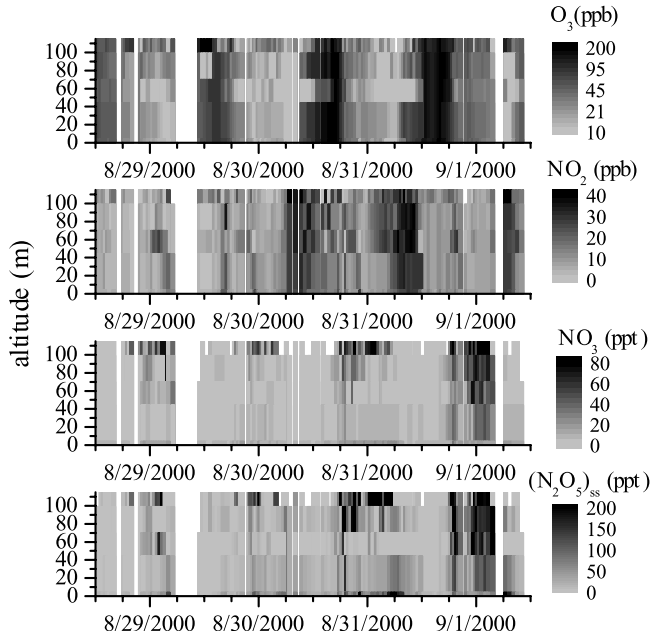

Figure 5. Overview of the vertical distribution of various trace gases at La Porte. NO_3 and steady state N_2O_5 clearly show elevated concentrations at higher altitudes during the night. The white areas in the graph, for example on 29 August from 0600 to 1030, indicate periods where DOAS light path data is missing. See color version of this figure at back of this issue.

levels to 30–40 ppb, and then increases again slightly at the 21 m level. The increase at 21 m altitude is typically in the range of 2–3 ppb, and is most likely statistically insignificant. The lowest altitude level is, within its error, not different from the 21 m level. In general, it appears that $[O_3]$ in the lowest three altitude intervals decreases from 2254 to 0240 by approximately 5 ppb. The concentration in the top interval, on the other hand, remains constant.

4.3.2. NO_2

[47] The mixing ratios of NO_2 in Figure 5 are, in general, very patchy. The only clear structures that can be identified are a plume above 50 m altitude around noon of 30 August, and a plume of NO_2 at 85 m altitude on the morning of 31 August. In both cases, NO_2 reached mixing ratios of up to 40 ppb. During the nights no distinct vertical profiles can be identified in Figure 5. For the night of 31 August to 1 September this is caused by the weak vertical profile, as can be seen in Figure 6. The NO_2 profile at 2032 varies between 7 and 17 ppb, without a clear vertical structure. During this time an interpretation of the deconvoluted mixing ratios as a vertical profile may be incorrect. The profiles at 2254, 0042, and 0240 display a much smoother behavior. In general, the vertical NO_2 gradient during this time is weak but distinct, with mixing ratios of ~7 ppb at the ground and ~5 ppb aloft.

4.3.3. NO_3

[48] In contrast to O_3 and NO_2, NO_3 is elevated at higher altitudes every night (Figure 5). During the first two nights, mixing ratios of NO_3 at the ground are negligible, while mixing ratios of 40–60 ppt are observed at the 107 m level. It may at first be surprising that mixing ratios at 107 m are higher than the mixing ratios in Figure 3. Because the RTU light path averages from 2 m to 115 m altitude, the elevated

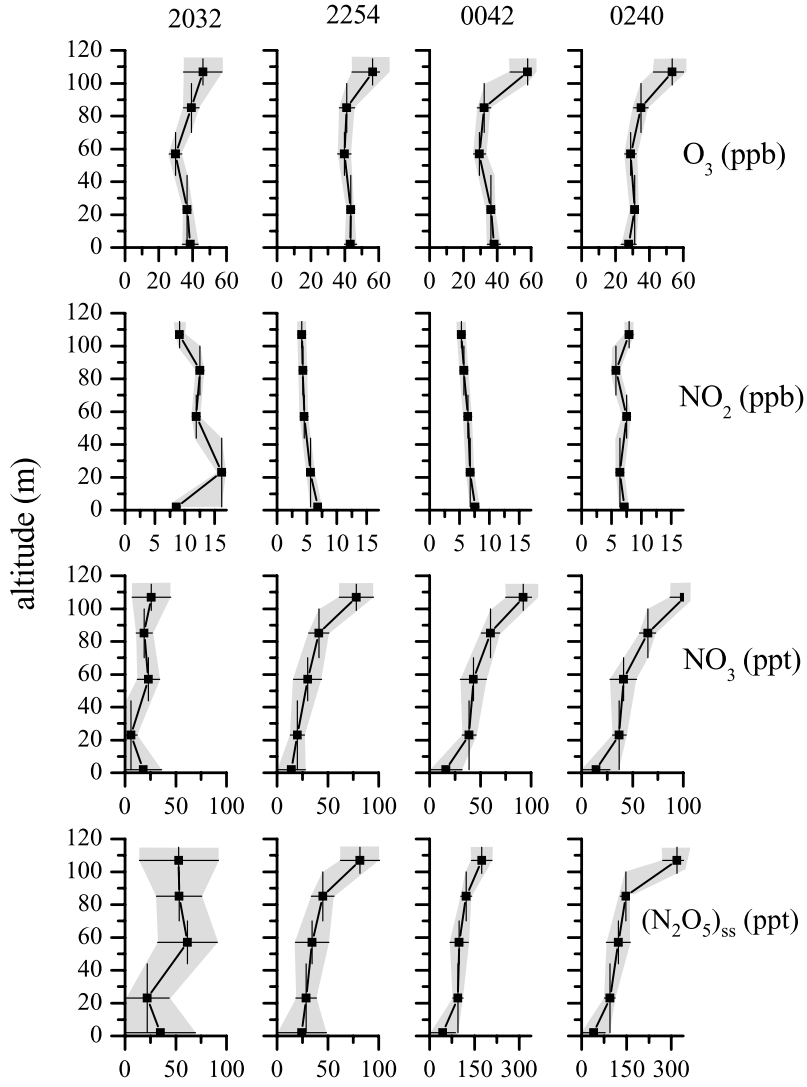

Figure 6. Vertical distributions of NO_2, O_3, NO_3, and steady state N_2O_5 during the night of 31 August to 1 September. The data points denote the average altitude levels of each altitude interval (2, 21, 57, 85, and 107 m). The vertical bars show the box height, while the horizontal bars, which are smaller than the symbol in the case of NO_2, show the 1σ statistical uncertainties after taking into account error propagation in the deconvolution of the vertical profiles.

NO_3 mixing ratios at 107 m contribute little to the path-averaged mixing ratio, which integrates over the entire altitude range. Although the interpretation of the observations during the night of 30–31 August as a vertical NO_3 gradient is uncertain, we also see elevated NO_3 in the upper part of the observed volume during this night. The clearest vertical NO_3 profile was observed during the night of 31 August to 1 September. Figure 6 shows that at 2254, 0042, and 0240, NO_3 mixing ratios at the ground are statistically indistinguishable from zero. The mixing ratios then continuously increase with altitude, reaching mixing ratios of up to 100 ppt at 107 m. These profiles were sustained throughout most of this night after 2200.

4.3.4. N_2O_5

[49] Based on our observation of NO_2 and NO_3 we calculated the steady state mixing ratio of N_2O_5 with $[N_2O_5] = K(T)\,[NO_2]\,[NO_3]$ (see equation (4)). Since no temperature gradient between 2 m and 44 m was observed during most nights we used the 8 m data for all altitudes to calculate the temperature dependent equilibrium constant K(T). During the morning of 29 August this will lead to a small error in the N_2O_5 mixing ratios. As will be explained in the accompanying paper by *Geyer and Stutz* [2004], our assumption of a pure chemical steady state can lead to an error in $[N_2O_5]$ of 10–30% due to vertical transport. Similar to NO_3, N_2O_5 mixing ratios are elevated aloft during every night (Figure 5). Mixing ratios frequently exceeded 100 ppt. The clearest vertical profiles were again observed on the night of 31 August to 1 September. Figure 6 shows that N_2O_5 mixing ratios at the ground were statistically indistinguishable from 0, and then steadily increased with increasing altitude, reaching up to 300 ppt at 0240. The N_2O_5 profiles follow the NO_3 profiles closely, since NO_2 is only weakly altitude dependent.

5. Discussion

[50] The interpretation of vertical profiles of reactive trace gases is challenging due to the simultaneous acting chem-

istry and vertical mixing. To facilitate the understanding of the processes acting in the NBL at La Porte, we used a 1-D chemical transport model [*Geyer and Stutz*, 2004] to provide a basic analysis of the processes responsible for the formation of the vertical trace gas profiles in Figure 6. We also want to determine how the loss rates of NO_x and O_3 vary with altitude at night.

5.1. Model Description

[51] The details of the 1D nocturnal chemistry and transport (NCAT) model are described in an accompanying paper by *Geyer and Stutz* [2004]. Here, only a short description of the model and the parameters of the model for the night of 31 August to 1 September at La Porte will be given. For the La Porte case the model spans altitudes from the ground up to 150 m, subdivided in 14 layers with a log linear spacing. An additional box between 150 m and 1000 m provides an upper boundary for the NBL. The vertical exchange of inert gases, K(z), is calculated based on similarity theory using values for the surface friction velocity, $u^* = 0.2$ ms^{-1}, and the heat flux, $H = -20$ W/m^2, and was in the range of 0 at the ground to 5×10^3 cm^{2}s^{-1} at 65 m and above. The vertical mixing was kept constant with time. The influence of chemical reactions on the vertical transport of reactive gases was explicitly taken into account (see *Geyer and Stutz* [2004] for more details). The temperature was set to 306 K at the beginning of the night, and decreased by 1 K per hour. The temperature profile showed only a very weak altitude dependence, as expected from the observation at 2 and 44 m. The chemical mechanism in NCAT includes reactions of the NO_x-O_3-NO_3 system, the HO_x/RO_2 reaction scheme, and a simplified mechanism of the oxidation of CO, propane, propene, isoprene, and α-pinene by OH, O_3, and NO_3 [*Jenkin et al.*, 2003; *Saunders et al.*, 2003]. Heterogeneous uptake of trace gases is calculated for an exponentially decaying aerosol surface area to air volume ratio (S/V) profile. According to the observations the S/V at 5 m was chosen to be 370 μm^{2}cm^{-3} and decreased to 100 μm^{2}cm^{-3} above 50 m. Dry deposition is simulated by assuming a heterogeneous loss of reactive species at the ground. The assumption of a flat surface may lead to an underestimation of the dry deposition. The heterogeneous loss is calculated with the following uptake coefficients: $\gamma(O_3) = 6 \times 10^{-5}$ [*Longfellow et al.*, 2000], $\gamma(NO_3) = 1.3 \times 10^{-3}$ [*Rudich et al.*, 1996], $\gamma\ (NO_2) = 1 \times 10^{-4}$, $\gamma\ (N_2O_5) = 0.044$ [*Jacob*, 2000].

[52] Nocturnal emissions of NO from the soil and traffic were included at a flux of 6×10^{10} molecules cm^{-2}s^{-1} from the ground and an emission rate of 6.7×10^8 molecules cm^{-3}s^{-1} between 0.1 and 0.9 m. CO traffic emissions were 3.3×10^9 molecules cm^{-3}s^{-1}. R.H. was 60%, in accordance with the observations. The model was initialized by vertically uniformly distributed mixing ratios of $[NO_2] = 12$ ppb, and $[O_3] = 70$ ppb. To represent a semi-realistic VOC chemistry, we used the reaction equivalent ($\sum k_i \times [VOC_i]/k_{model\ molecule}$) from the measured VOC and increased this value by 2 to account for unmeasured gases. The result of this procedure leads us to the following initial concentrations of propane, propene, and isoprene: 5×10^{11}molecules cm^{-3}, 10^{11} molecules cm^{-3}, and 10^{10} molecules cm^{-3}, respectively. An emission rate of α-pinene from trees of 1.1×10^6 molecules cm^{-3}s^{-1} was included between altitudes of 1 and 10 m [e.g., *Fuentes et al.*, 2000; *Guenther et al.*, 2000]. Modeled α-pinene mixing ratios (Figure 7) agree well with terpene concentrations observed at La Porte at 10 m altitude during the night of 31 August to 1 September.

5.2. Interpretation of Vertical Trace Gas Profiles

[53] A comparison of the model results after 3 hours (Figure 7) with the observations at 2254 on 31 August in Figure 6 illustrates that the model reproduces the general behavior of the trace gas gradients observed at La Porte. The model therefore appears to describe the general mechanisms that determine the vertical trace gas distributions and can be used to derive more information about the chemical transport processes during this night at LaPorte. However, we want to caution the reader to interpret the model results directly as an accurate reproduction of the observations, since NCAT is in many aspects highly idealized. On the other hand, the qualitative NCAT results offer valuable insight with respect to the interpretation of the observations.

5.2.1. Vertical Profile of NO

[54] Due to surface emissions the model shows that [NO] is highest close to the ground (Figure 7) with mixing ratios between 0.1 and 0.5 ppb. In contrast, [NO] is below 10 ppt at 10 m above the ground, which is in agreement with the averaged observations (Figure 4) for the night of 31 August to 1 September. Above 10 m [NO] is in the sub-ppt range. The mechanism responsible for the formation of the NO profile is the simultaneous titration of NO by ozone, and its slow upwards transport.

5.2.2. Vertical Profile of O_3

[55] After 3 hours the model calculates O_3 mixing ratios of 40 ppb close to the ground, which increase with altitude and reach ~60 ppb above 100 m (Figure 7). A careful comparison of the 2254 data in Figure 6 illustrates that the modeled ozone mixing ratios close to the ground and those at 110 m agree with the observations. However, even considering the uncertainties of the observations, the shape of the profile is quite different. The disagreement is not surprising since the vertical mixing and transport in our model is idealized. Ozone is lost by downward transport above 5 m, while transport is a net source of ozone below this altitude. At 10 m the model predicts an O_3 downward flux of 3×10^{11} cm^{-2}s^{-1}. Dry deposition is the main loss of O_3 below 5 m, accounting for ~85% of the loss. Only ~15% is destroyed by the NO reaction. The deposition velocity at 10 m caused by dry deposition is therefore ~0.23 cm s^{-1}. This value is very close to the typical values of 0.2 cm s^{-1} given by *Wesely and Hicks* [2000], and describes the overall loss of ozone during the night of 31 August to 1 September fairly well. The observed and modeled O_3 profiles, with lower values close to the ground and higher values aloft, agree in their general behavior with other observations [*Beyrich et al.*, 1996; *Colbeck and Harrison*, 1985; *Galbally*, 1968, 1971; *Glaser et al.*, 2003; *Gusten et al.*, 1998; *Pisano et al.*, 1997] and modeling studies [*Galmarini et al.*, 1997].

5.2.3. Vertical Profile of NO_2

[56] The modeled NO_2 profile (Figure 7) is in surprisingly good agreement with the observation at 2254 (Figure 6). Modeled and observed NO_2 mixing ratios decrease above 3 m. The model results also reveal a decrease of NO_2 from 3 m toward the ground (Figure 7), which could not be observed with the DOAS system due

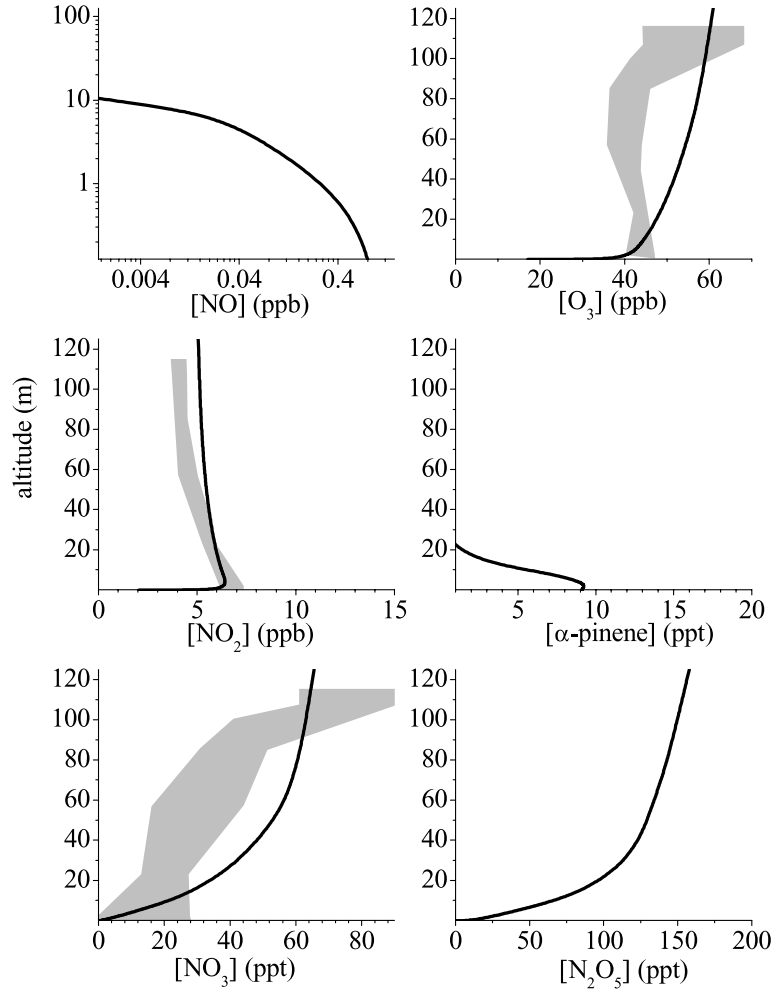

Figure 7. Vertical profiles of [NO], [O_3], [NO_2], [α-pinene], [NO_3], and [N_2O_5] modeled by NCAT for the La Porte conditions three hours after sunset (31 August 2254).

the light paths geometry. The overall shape of the NO_2 profile, with a mixing ratio maximum at 3 m, is caused by two competing effects. NO_2 is produced by the reaction of ozone with NO, which occurs predominantly below 5 m, leading to a negative vertical gradient of NO_2. This formation is counteracted by the dry deposition of NO_2, which by itself would lead to a positive gradient. The model predicts that the NO_2 profile remains fairly constant after 3 hours calculation time, because loss of NO_2 and formation by O_3 + NO counterbalance each other. Figure 6 shows that this also appears to be the case for the observations at LaPorte. At 10 m the model calculates an upward flux of NO_2 of -2.8×10^{10} $cm^{-2}s^{-1}$ for La Porte. Because NO_2 is both produced and destroyed, the vertical flux at 2 m is negligible in our case. Very few observations of urban NO_2 vertical profiles have been published. *Pisano et al.* [1997], and *Glaser et al.* [2003], report elevated nocturnal NO_2 at the ground, but no systematic profiles as in our case can be identified. Modeling studies of NO_2 profiles by *Hov* [1983] and *Galmarini et al.* [1997], are in agreement with our observations of a maximum of NO_2 close to the ground.

5.2.4. Vertical Profiles of NO_3 and N_2O_5

[57] The vertical distribution of NO_3 and N_2O_5 are closely linked through the NO_2-NO_3-N_2O_5 equilibrium. Our observations (Figure 6) show decreasing mixing ratios toward the ground, which is supported by the model calculations (Figure 7). Due to the large statistical error, our NO_3 and N_2O_5 observations 2 m above ground are indistinguishable from zero. Within the large statistical uncertainty the observations and the model result therefore agree. Modeled NO_3 and N_2O_5 mixing ratios (Figure 7) increase steadily with altitude, reaching mixing ratios of $\sim$65 ppt for NO_3 and $\sim$150 ppt for N_2O_5 at 120 m altitude. The comparison between model output and observations are in good agreement for the mixing ratios calculated in the lowest 4 altitude levels at 2254 (Figure 6). Above 100 m, however, the observed NO_3 and steady state N_2O_5 mixing ratios are higher than those in the model.

[58] To compare the chemical behavior of NO_3 in the model with the observations, we used the pseudo steady state lifetime of NO_3, τ_{NO3} [*Brown et al.*, 2003]:

$$\tau_{NO_3} = \frac{[NO_3]}{k_2[O_3][NO_2]} \tag{8}$$

[59] We calculated τ_{NO3} based on the observations at 2254 on 31 August (Figure 6) and compared it to the values

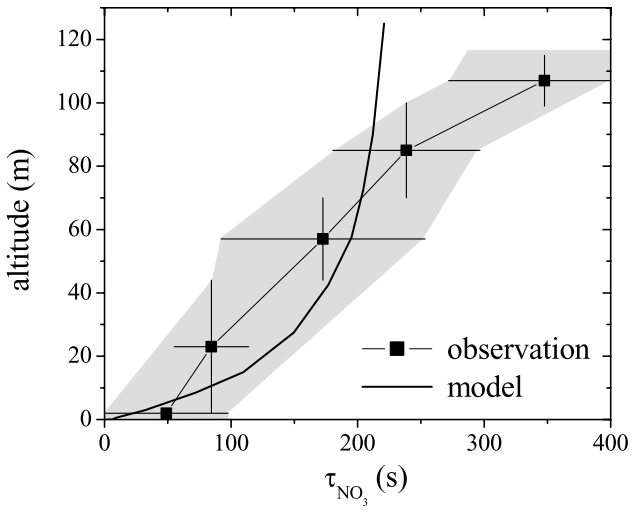

Figure 8. Comparison of the observed pseudo steady state lifetime profile of NO_3 on 31 August 2254 with the modeled values.

derived from the modeled $[O_3]$, $[NO_2]$, and $[NO_3]$ in Figure 8. The observed τ_{NO3} is near 0 at the ground due to the elevated NO levels, which destroy NO_3 through the fast NO + NO_3 reaction, and increases to ~350 s at 107 m. Considering the uncertainties in our observations the agreement between model and measurements is very good in the lowest 100 m. Above 100 m the modeled τ_{NO3} is, however, only half of the observed value. We can conclude from this comparison that the loss processes in the model are well quantified in the lower 100 m, but are too high aloft.

[60] The production rate of NO_3 through R2 at La Porte depends only weakly on altitude (Figure 9a), due to the counterbalance of the positive O_3 and negative NO_2 altitude dependence. In the upper part of the NBL, ~55% of the NO_3 loss, described by a negative $P_{NO3}(N_2O_5) = k_{4-}[N_2O_5] - k_{4+}[NO_2][NO_3]$, proceeds indirectly through the N_2O_5 equilibrium (Figure 9a). The reactions with VOC and RO_2 account for the other 45% of the NO_3 loss. The NO_3 + NO reaction becomes the dominant NO_3 loss process in the lowest 10 m and is responsible for the low NO_3 levels near the ground. Figure 9b shows that above 5 m equilibrium 4 is the sole source of N_2O_5, while it is a loss mechanism below 5 m. The dominant N_2O_5 loss processes above this altitude are the uptake of N_2O_5 on aerosol surfaces, and the reaction of N_2O_5 with water vapor. The aerosol uptake rate changes little with altitude due to our assumption of an exponentially decreasing aerosol surface area, which by coincidence balances the increase of N_2O_5 mixing ratio with altitude. It is surprising that the most important N_2O_5 loss pathway in the upper 70 m of the model is the gas-phase hydrolysis of N_2O_5 (reactions (5) and (6)). The reason for this dominance is the relatively high water vapor concentrations at La Porte at night. The N_2O_5 water vapor reaction contributes ~70% to the N_2O_5 loss, leading to a large formation of gaseous HNO_3 at night.

[61] We can only speculate about the reason for the discrepancy between observations and model above 100 m. It is possible that the actual mixing ratios of RO_2 and VOC may be lower than calculated in the model. The most likely cause, however, is an overestimate of the N_2O_5 loss frequency in the model. The aerosol uptake is inherently uncertain since it depends on the unknown composition and surface to volume area of the particles above 100 m. The aerosol uptake, however, only accounts for ~30% of the N_2O_5 loss. On the other hand, the rate constants for reactions (5) and (6) are based on only one direct measurement, and are thus highly uncertain (http://www.iupac-kinetics.ch.cam.ac.uk). Additional investigations of these two reactions would therefore be highly desirable.

[62] Figure 9b reveals that vertical transport of N_2O_5 plays an important role at La Porte. Between 10 and 60 m, downward transport is a net N_2O_5 loss mechanism, while it is a net source below 10 m. This behavior has two consequences, which are discussed in detail by *Geyer and Stutz* [2004]. The assumption of a purely chemical steady state for NO_3 can not be upheld below 60 m, where N_2O_5 transport processes influence NO_3 levels. The combination of vertical transport and equilibrium 4 leads to a mechanism that converts NO_3 into N_2O_5 between 10 and 60 m, transports N_2O_5 below 10 m, where it then converted back into NO_3 radicals.

5.3. NO_x and O_3 Loss in La Porte

[63] To investigate the altitude dependence of the different loss processes and to quantify their importance averaged over the lowest 100 m of the atmosphere at La Porte, we used the results of NCAT for the night of 31 August to 1 September. The main loss processes for O_3 are: a) reaction with NO, b) reaction with NO_2, c) reaction with VOC, and d) dry deposition (Figure 10a). Above 10 m the dominant loss is the NO_2 + O_3 reaction, followed by the loss through O_3 + VOC. Below 10 m the reaction with NO + O_3 dominates. This reaction will only destroy ozone if NO_2 is removed

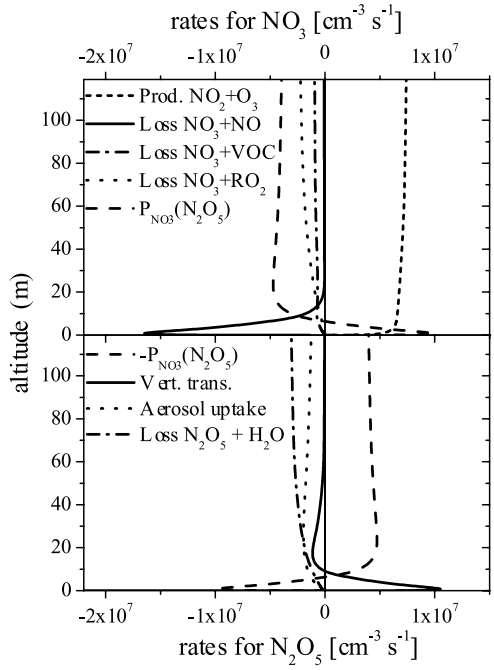

Figure 9. Vertical profiles of the production and loss rates of NO_3 and N_2O_5, as calculated by NCAT for the La Porte conditions (31 August 2254).

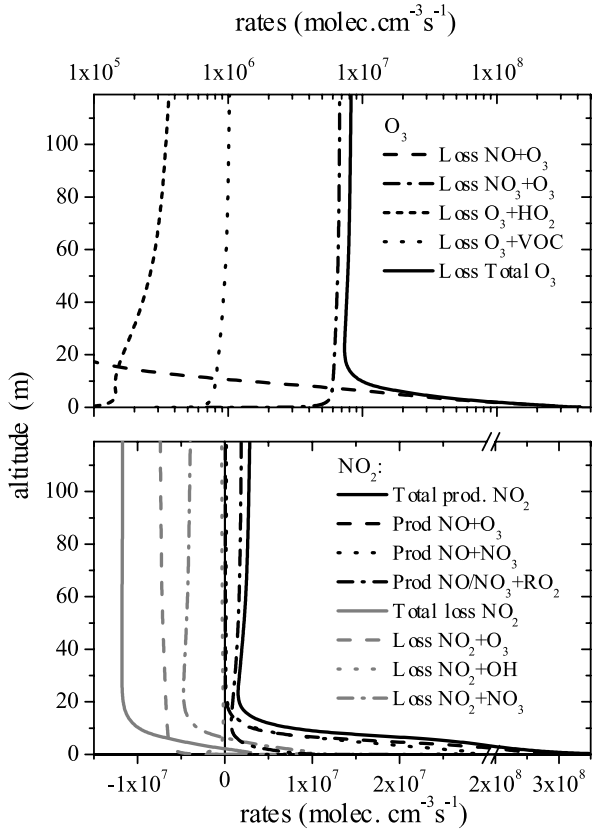

Figure 10. Vertical profiles of the loss and production rates of O_3 and NO_2 extracted from NCAT (La Porte, 31 August 2254).

before sunrise, thus not leading to O_3 production upon photolysis in the morning. Averaged over the lowest 100 m, dry deposition is the dominant O_3 loss process at La Porte, with a loss rate of 2.4 ppb h^{-1} (Table 2). The NO_2 + O_3 reaction contributes ~25% to the overall O_3 loss of 4.1 ppb h^{-1} calculated by the model. The analysis of the DOAS data reveals that the observed loss of O_3 from 2200 on 31 August and 0300 on 1 September is ~3 ± 1 ppb h^{-1}, close to the modeled value.

[64] In contrast to O_3, NO_2 is both destroyed and formed in the NBL. The dominant formation process is the reaction of O_3 + NO close to the ground, and its upward transport. Smaller amounts of NO_2 are also produced by the NO + NO_3 and NO/NO_3 + RO_2 reactions above 10 m (Figure 10b). NO_2 is lost in the NBL by a) reactions of NO_2 + O_3, b) net loss through the NO_2 − NO_3 − N_2O_5 equilibrium, and thus the loss processes of N_2O_5, and c) dry deposition (Figure 10b). The chemical loss processes show little altitude dependence above 10 m. Figure 10b shows that the chemical loss of NO_2 proceeds almost completely above 10 m. The loss rates averaged over the lowest 100 m of the atmosphere are listed in Table 2. In contrast to ozone, chemical loss dominates for NO_2, with a contribution of ~65%. NO_2 is converted both into surface adsorbed nitrate and gas phase HNO_3, through the N_2O_5 + H_2O reactions. The averaged NO_2 concentration in the model decreases at a rate of ~0.9 ppb h^{-1} due to the simultaneously acting NO_2 formation. This value is larger than the observed NO_2 loss rate, which was close to zero. The difference originates from an overestimate of the NO_2 loss, most likely because the N_2O_5 loss in the model is too high, as already discussed above.

6. Conclusions

[65] Our measurements of vertical concentration gradients of O_3, NO_2, and NO_3 during TEXAQS 2000 reveal that the composition and chemistry in the nocturnal boundary layer is strongly altitude dependent. The dominant nocturnal oxidant, NO_3, typically exhibits a positive gradient, with mixing ratios of up to 100 ppt above 100 m altitude. Similarly, calculated steady state N_2O_5 mixing ratios are higher aloft, reaching up to 300 ppt. The profiles of [O_3] and [NO_2] are less clear during most of the nights, most likely due to the relatively weak vertical stability at La Porte. During the night of 31 August to 1 September, however, we observed a positive O_3 and a negative NO_2 gradient.

[66] A one-dimensional chemical transport model, which is discussed in detail in *Geyer and Stutz* [2004], describes the general behavior of the observed trace gas profiles well, allowing us to draw conclusions about the different mechanisms that are responsible for the change of trace gas concentrations with altitude. In the case of ozone, the nocturnal vertical profile and the loss of O_3 in the suburban environment encountered at La Porte are dominated by dry deposition. The titration of ozone by NO, which is emitted near the ground, only played a secondary role for ozone, but is responsible for the positive NO_2 gradient. The profiles of [NO_3] and [N_2O_5] are dominated by the NO_3 + NO reaction, and the vertical transport of N_2O_5. Because N_2O_5 mixing ratios are elevated aloft, most of the NO_x loss at night proceeds above 10 m altitude. The model predicts that the dominant N_2O_5, and thus NO_x, loss proceeds through the homogeneous reaction of N_2O_5 with water, followed in importance by the uptake of N_2O_5 on the aerosol. The overprediction of the NO_3/N_2O_5 loss above 100 m altitude could be associated with the homogeneous N_2O_5 water reaction. More investigations of this reaction are needed to reduce the uncertainties connected with its rate constant.

[67] Based on our observations and the model results, we can distinguish two regimes in the NBL during the night of

Table 2. Comparison of O_3 and NO_2 Loss Rates Averaged Over the Lowest 100 m of the Nocturnal Boundary Layer During the Nights of 31 August to 1 September at La Porte

Sink	Loss Rates Averaged Over Lowest 100 m, ppb/h
Ozone	
NO + O_3	0.6
NO_2 + O_3	1.0
Dry deposition	2.4
VOC + O_3	0.1
Total	4.1
NO_2	
NO_2 + O_3	1.0
NO_2 + NO_3	0.5
Dry deposition	0.7
Total	2.3

31 August to 1 September at La Porte. Below 10 m altitude the atmosphere is dominated by the emissions of NO, which titrates O_3, and NO_3. Above 10 m altitude NO levels are small and chemistry is dominated by the reactions of NO_3, N_2O_5, and to a lesser extent O_3. The two height intervals are connected to each other by vertical transport, which determines the vertical extent of these two layers.

[68] Our measurements clearly illustrate that in-situ measurements at one altitude are not sufficient to describe the chemical processes occurring in the nocturnal boundary layer. Ground based measurements, for example, underestimate the loss of NO_x and VOC because NO_3 and O_3 levels are much higher aloft. In addition, vertical transport processes, which can lead to a net production of radicals in the lower part of the NBL through the transport of radical reservoir species such as N_2O_5 need to be considered. Further studies on the altitude dependence of nocturnal chemistry and the influence of vertical mixing are needed to better quantify the chemical processes occurring at night and their influence on air quality in urban and suburban areas.

[69] **Acknowledgments.** We would like to thank Vincent Torres, Jim Price, and Rainer Volkamer for their help in setting up in Houston; Ulrich Platt, Dieter Perner, Theo Brauers, and Rene Dubois for lending us equipment; and S. C. Hurlock and Y. Stutz for helpful comments on the manuscript. This study was supported by the EPA Southern Oxidant Study program (grant 1995-1786-09), the Texas Natural Resource Conservation Commission (grant 582-2-48650), and the Department of Energy (grant DE-FG03-01ER63094).

References

Alicke, B., U. Platt, and J. Stutz (2002), Impact of nitrous acid photolysis on the total hydroxyl radical budget during the Limitation of Oxidant Production/Pianura Padana Produzione di Ozono study in Milan, *J. Geophys. Res.*, *107*(D22), 8196, doi:10.1029/2000JD000075.

Allan, B. J., J. M. C. Plane, H. Coe, and J. Shillito (2002), Observations of NO_3 concentration profiles in the troposphere, *J. Geophys. Res.*, *107*(D21), 4588, doi:10.1029/2002JD002112.

Atkinson, R. (1991), Kinetics and mechanisms of the gas-phase reactions of the NO_3 radical with organic compounds, *J. Phys. Chem. Ref. Data*, *20*, 459–507.

Bass, A. M., and R. J. Paur (1984), The ultraviolet cross-section of ozone: I. The measurements/atmospheric ozone, in *Quadrennial Ozone Symposium 1984*, edited by C. Czerefos and A. Ghazi, pp. 606–616, D. Reidel, Norwell, Mass.

Beyrich, F., U. Weisensee, D. Sprung, and H. Gusten (1996), Comparative analysis of sodar and ozone profile measurements in a complex structured boundary layer and implications for mixing height estimation, *Boundary Layer Meteorol.*, *81*, 1–9.

Brauers, T., M. Hausmann, U. Brandenburger, and H.-P. Dorn (1995), Improvement of differential optical absorption spectroscopy with a multichannel scanning technique, *Appl. Opt.*, *34*, 4472–4479.

Brown, S. S., H. Stark, and A. R. Ravishankara (2003), Applicability of the steady state approximation to the interpretation of atmospheric observations of NO_3 and N_2O_5, *J. Geophys. Res.*, *108*(D17), 4539, doi:10.1029/2003JD003407.

Coe, H., B. J. Allan, and J. M. C. Plane (2002), Retrieval of vertical profiles of NO_3 from zenith sky measurements using an optimal estimation method, *J. Geophys. Res.*, *107*(D21), 4587, doi:10.1029/2002JD002111.

Colbeck, I., and R. M. Harrison (1985), Dry deposition of ozone: Some measurements of deposition velocity and of vertical profiles to 100 metres, *Atmos. Environ.*, *19*, 1807–1818.

Coulter, R. L., and J. C. Doran (2002), Spatial and temporal occurrences of intermittent turbulence during CASES-99, *Boundary Layer Meteorol.*, *105*, 329–349.

Dentener, F. J., and P. J. Crutzen (1993), Reaction of N_2O_5 on tropospheric aerosols: Impact on the global distributions of NO_x, O_3, and OH, *J. Geophys. Res.*, *98*, 7149–7163.

Dimitroulopoulou, C., and A. R. W. Marsh (1997), Modeling studies of NO_3 nighttime chemistry and its effects on subsequent ozone formation, *Atmos. Environ.*, *31*, 3041–3057.

Finlayson-Pitts, B. J., and J. N. Pitts (2000), *Chemistry of the Upper and Lower Atmosphere: Theory, Experiments and Applications*, vol. 22, 969 pp., Academic, San Diego, Calif.

Fish, D. J., D. E. Shallcross, and R. L. Jones (1999), The vertical distribution of NO_3 in the atmospheric boundary layer, *Atmos. Environ.*, *33*, 687–691.

Fitzjarrald, D. R., and D. Lenschow (1983), Mean concentration and flux profiles for chemically reactive species in the atmospheric surface layer, *Atmos. Environ.*, *17*, 2505–2512.

Fuentes, J. D., et al. (2000), Biogenic hydrocarbons in the atmospheric boundary layer: A review, *Bull. Am. Soc. Meteorol.*, *81*, 1537–1575.

Galbally, I. (1968), Some measurements of ozone variation and destruction in the atmospheric surface layer, *Nature*, *218*, 456–457.

Galbally, I. E. (1971), Ozone profiles and ozone fluxes in the atmospheric surface layer, *Q. J. R. Meteorol. Soc.*, *97*, 18–29.

Galmarini, S., P. G. Duynkerke, and J. Vilà-Guerau de Arellano (1997), Evolution of nitrogen oxide chemistry in the nocturnal boundary layer, *J. Appl. Meteorol.*, *36*, 943–957.

Geyer, A., and J. Stutz (2004), Vertical profiles of NO_3, N_2O_5, O_3, and NO_x in the nocturnal boundary layer: 2. Model studies of the interaction of chemistry and vertical mixing, *J. Geophys. Res.*, *109*, D12108, doi:10.1029/2003JD004211.

Geyer, A., B. Alicke, D. Mihelcic, J. Stutz, and U. Platt (1999), Comparison of tropospheric NO_3 radical measurements by differential optical absorption spectroscopy and matrix isolation spin resonance, *J. Geophys. Res.*, *104*, 26,097–26,105.

Geyer, A., B. Alicke, S. Konrad, T. Schmitz, J. Stutz, and U. Platt (2001), Chemistry and oxidation capacity of the nitrate radical in the continental boundary layer near Berlin, *J. Geophys. Res.*, *106*, 8013–8025.

Geyer, A., et al. (2003a), Direct observations of daytime NO_3: Implications for urban boundary layer chemistry, *J. Geophys. Res.*, *108*(D12), 4368, doi:10.1029/2002JD002967.

Geyer, A., et al. (2003b), Nighttime formation of peroxy and hydroxyl radicals during the BERLIOZ campaign: Observations and modeling studies, *J. Geophys. Res.*, *108*(D4), 8249, doi:10.1029/2001JD000656.

Glaser, K., U. Vogt, G. Baumbach, A. Volz-Thomas, and H. Geiss (2003), Vertical profiles of O_3, NO_2, NO_x, VOC, and meteorological parameters during the Berlin Ozone Experiment (BERLIOZ) campaign, *J. Geophys. Res.*, *108*(D4), 8253, doi:10.1029/2002JD002475.

Guenther, A., C. Geron, T. Pierce, B. Lamb, P. Harley, and R. Fall (2000), Natural emissions of non-methane volatile organic compounds, carbon monoxide, and oxides of nitrogen from North America, *Atmos. Environ.*, *34*, 2205–2230.

Gusten, H., G. Heinrich, and D. Sprung (1998), Nocturnal depletion of ozone in the Upper Rhine Valley, *Atmos. Environ.*, *32*, 1195–1202.

Hallquist, M., D. J. Stewart, J. Baker, and R. A. Cox (2000), Hydrolysis of N_2O_5 on submicron sulfuric acid aerosols, *J. Phys. Chem. A*, *104*, 3984–3990.

Hamba, F. (1993), A modified K model for chemically reactive species in the planetary boundary layer, *J. Geophys. Res.*, *98*(D3), 5173–5182.

Harder, J. W., J. W. Brault, P. V. Johnston, and G. H. Mount (1997), Temperature dependent NO_2 cross section at high spectral resolution, *J. Geophys. Res.*, *102*, 3861–3879.

Harris, G. W., et al. (1983), Measurement of HONO, NO_3 and NO_2 by long-path differential optical absorption spectroscopy in the Los Angeles basin, in *Optical and Laser Remote Sensing*, *Springer Ser. Opt. Sci.*, *39*, 106–113.

Hov, O. (1983), One-dimensional vertical model for ozone and other gases in the atmosphere boundary layer, *Atmos. Environ.*, *17*, 535–550.

Jacob, D. J. (2000), Heterogeneous chemistry and tropospheric ozone, *Atmos. Environ.*, *34*, 2131–2159.

Jenkin, M. E., S. M. Saunders, V. Wagner, and M. J. Pilling (2003), Protocol for the development of the Master Chemical Mechanism, MCM v3 (Part B): Tropospheric degradation of aromatic volatile organic compounds, *Atmos. Chem. Phys.*, *3*, 181–193.

Kane, S. M., F. Caloz, and M. T. Leu (2001), Heterogeneous uptake of gaseous N_2O_5 by $(NH_4)_2SO_4$, NH_4HSO_4, and H_2SO_4 aerosols, *J. Phys. Chem. A*, *105*, 6465–6470.

Kramm, G., H. Mueller, D. Fowler, K. D. Hoefken, F. X. Meixner, and E. Schaller (1991), A modified profile method for determining the vertical fluxes of NO, NO_2, ozone, and HNO_3 in the atmospheric surface layer, *J. Atmos. Chem.*, *13*, 265–288.

Lenschow, D. H. (1981), Reactive trace species in the boundary layer from a micrometeorological perspective, *J. Phys. Soc. Jpn.*, *60*, 472–480.

Li, S.-M., K. G. Anlauf, and H. A. Wiebe (1993), Heterogeneous nighttime production and deposition of particle nitrate at a rural site in North America during summer 1988, *J. Geophys. Res.*, *98*, 5139–5158.

Longfellow, C. A., A. R. Ravishankara, and D. R. Hanson (2000), Reactive and nonreactive uptake on hydrocarbon soot: HNO_3, O_3, and N_2O_5, *J. Geophys. Res.*, *105*, 24,345–24,350.

Mahrt, L., J. Sun, W. Blumen, T. Delany, and S. Oncley (1998), Nocturnal boundary-layer regimes, *Boundary Layer Meteorol.*, *88*(2), 255–278.

Makar, P. A., H. A. Wiebe, R. M. Staebler, S. M. Li, and K. Anlauf (1998), Measurement and modeling of particle nitrate formation, *J. Geophys. Res.*, *103*, 13,095–13,110.

Mentel, T. F., D. Bleilebens, and A. Wahner (1996), A study of nighttime nitrogen oxide oxidation in a large reaction chamber- the fate of NO_2, N_2O_5, HNO_3, and O_3 at different humidities, *Atmos. Environ.*, *30*, 4007–4020.

Moise, T., R. K. Talukdar, G. J. Frost, R. W. Fox, and Y. Rudich (2002), Reactive uptake of NO_3 by liquid and frozen organics, *J. Geophys. Res.*, *107*(D2), 4014, doi:10.1029/2001JD000334.

Pisano, J. T., I. McKendry, D. G. Steyn, and D. R. Hastie (1997), Vertical nitrogen dioxide and ozone concentrations measured from a tethered balloon in the Lower Fraser Valley, *Atmos. Environ.*, *31*, 2071–2078.

Platt, U. (1994), Differential Optical Absorption Spectroscopy (DOAS), in *Monitoring by Spectroscopic Techniques*, edited by M. W. Sigrist, pp. 27–85, John Wiley, Hoboken, N. J.

Platt, U., D. Perner, G. W. Harris, A. M. Winer, and J. N. Pitts (1980), Detection of NO_3 in the polluted troposphere by differential optical absorption, *Geophys. Res. Lett.*, *7*, 89–92.

Platt, U., A. Winer, H. Biermann, R. Atkinson, and J. Pitts (1984), Measurement of nitrate radical concentration in continental air, *Environ. Sci. Technol.*, *18*, 365–369.

Platt, U., G. LeBras, G. Poulet, J. P. Burrows, and G. Moortgat (1990), Peroxy radicals from night-time reaction of NO_3 with organic compounds, *Nature*, *348*, 147–149.

Platt, U., et al. (2002), Free radicals and fast photochemistry during BERLIOZ, *J. Atmos. Chem.*, *42*, 359–394.

Riemer, N., H. Vogel, B. Vogel, B. Schell, I. Ackermann, C. Kessler, and H. Hass (2003), Impact of the heterogeneous hydrolysis of N_2O_5 on chemistry and nitrate aerosol formation in the lower troposphere under photosmog conditions, *J. Geophys. Res.*, *108*(D4), 4144, doi:10.1029/2002JD002436.

Rudich, Y., R. Talukdar, and A. R. Ravishankara (1996), Reactive uptake of NO_3 on pure water and ionic solutions, *J. Geophys. Res.*, *101*, 21,023–21,031.

Saunders, S. M., M. E. Jenkin, R. G. Derwent, and M. J. Pilling (2003), Protocol for the development of the Master Chemical Mechanism, MCM v3: Part A. Tropospheric degradation of non-aromatic volatile organic compounds, *Atmos. Chem. Phys.*, *3*, 161–180.

Smith, N., J. M. C. Plane, C. Nien, and O. A. Solomon (1995), Nighttime radical chemistry in the San Joaquin Valley, *Atmos. Environ.*, *29*, 2887–2897.

Stull, R. B. (1988), *An Introduction to Boundary Layer Meteorology*, 670 pp., Kluwer Acad., Norwell, Mass.

Stutz, J. (1996), Messung der Konzentration troposphärischer Spurenstoffe mittels Differentieller Optischer Absorptionspektroskopie: Eine neue Gerneration von Geräten und Algorithmen, Ph.D. thesis, Univ. of Heidelberg, Heidelberg, Germany.

Stutz, J., and U. Platt (1996), Numerical analysis and estimation of the statistical error of differential optical absorption spectroscopy measurements with least-squares methods, *Appl. Opt.*, *35*(30), 6041–6053.

Stutz, J., and U. Platt (1997), Improving long-path differential optical absorption spectroscopy with a quartz-fiber mode mixer, *Appl. Opt.*, *36*, 1105–1115.

Thornton, J. A., P. J. Wooldridge, R. C. Cohen, E. J. Williams, D. Hereid, F. C. Fehsenfeld, J. Stutz, and B. Alicke (2003), Comparisons of in situ and long path measurements of NO_2 in urban plumes, *J. Geophys. Res.*, *108*(D3), 4496, doi:10.1029/2003JD003559.

Voegele, A. F., C. S. Tautermann, T. Loerting, and K. R. Liedl (2003), Toward elimination of discrepancies between theory and experiment: The gas-phase reaction of N_2O_5 with H_2O, *Phys. Chem. Chem. Phys.*, *5*, 487–495.

von Friedeburg, C., T. Wagner, A. Geyer, N. Kaiser, B. Vogel, H. Vogel, and U. Platt (2002), Derivation of tropospheric NO_3 profiles using off-axis differential optical absorption spectroscopy measurements during sunrise and comparison with simulations, *J. Geophys. Res.*, *107*(D13), 4168, doi:10.1029/2001JD000481.

Wahner, A., T. F. Mentel, and M. Sohn (1998a), Gas-phase reaction of N_2O_5 with water vapor: Importance of heterogeneous hydrolysis of N_2O_5 and surface desorption of HNO_3 in a large teflon chamber, *Geophys. Res. Lett.*, *25*, 2169–2172.

Wahner, A., T. F. Mentel, M. Sohn, and J. Stier (1998b), Heterogeneous reaction of N_2O_5 on sodium nitrate aerosol, *J. Geophys. Res.*, *103*, 31,103–31,112.

Wängberg, I., T. Etzkorn, I. Barnes, U. Platt, and K. H. Becker (1997), Absolute determination of the temperature behavior of the $NO_2 + NO_3 + (M) \langle - \rangle N_2O_5 + (M)$ equilibrium, *J. Phys. Chem. A*, *101*, 9694–9698.

Wayne, R. P., et al. (1991), The nitrate radical: Physics, chemistry, and the atmosphere, *Atmos. Environ., Part A*, *25*, 1–203.

Wesely, M. L., and B. B. Hicks (2000), A review of the current status of knowledge on dry deposition, *Atmos. Environ.*, *34*, 2261–2282.

Yokelson, R. J., J. B. Burkholder, R. W. Fox, R. K. Talukdar, and A. R. Ravishankara (1994), Temperature dependence of the NO_3 absorption, *J. Phys. Chem.*, *98*, 13,144–13,150.

J. Stutz, B. Alicke, R. Ackermann, and A. Geyer, Department of Atmospheric Sciences, UCLA, Los Angeles, CA 90095-1565, USA. (jochen@atmos.ucla.edu)

A. White, NOAA, Environmental Technology Laboratory, Boulder, CO 80309, USA.

E. Williams, NOAA Aeronomy Laboratory and Cooperative Institute for Research in Environmental Sciences, University of Colorado, Boulder, CO 80309, USA.

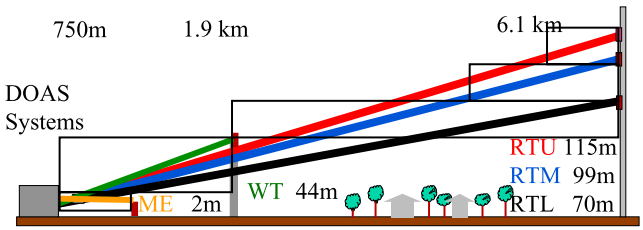

Figure 2. Setup of the differential optical absorption spectroscopic (DOAS) light path in a side view.

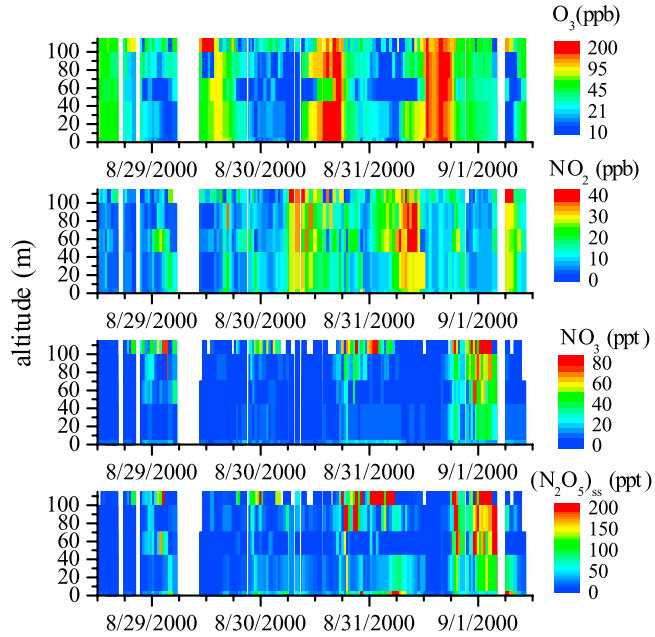

Figure 5. Overview of the vertical distribution of various trace gases at La Porte. NO_3 and steady state N_2O_5 clearly show elevated concentrations at higher altitudes during the night. The white areas in the graph, for example on 29 August from 0600 to 1030, indicate periods where DOAS light path data is missing.

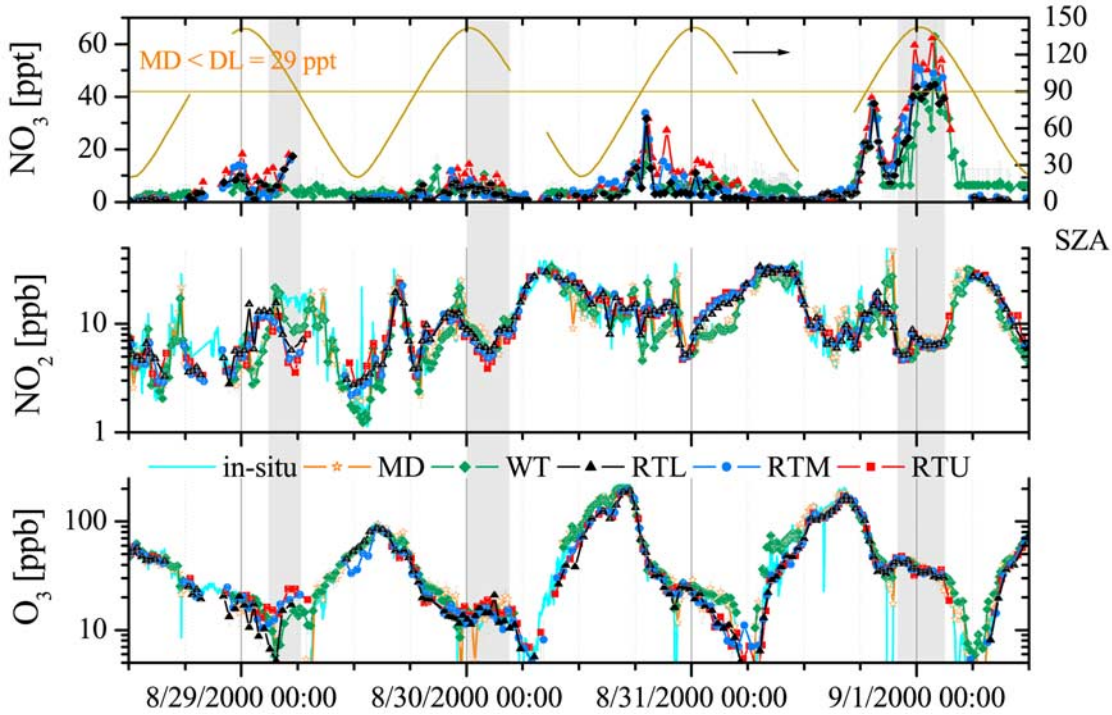

Figure 3. Overview of path averaged DOAS data from noon of 28 August to noon 2 September 2000. The data is color coded according to the colors in Figure 2. Please note the logarithmic scale for NO_2 and O_3.

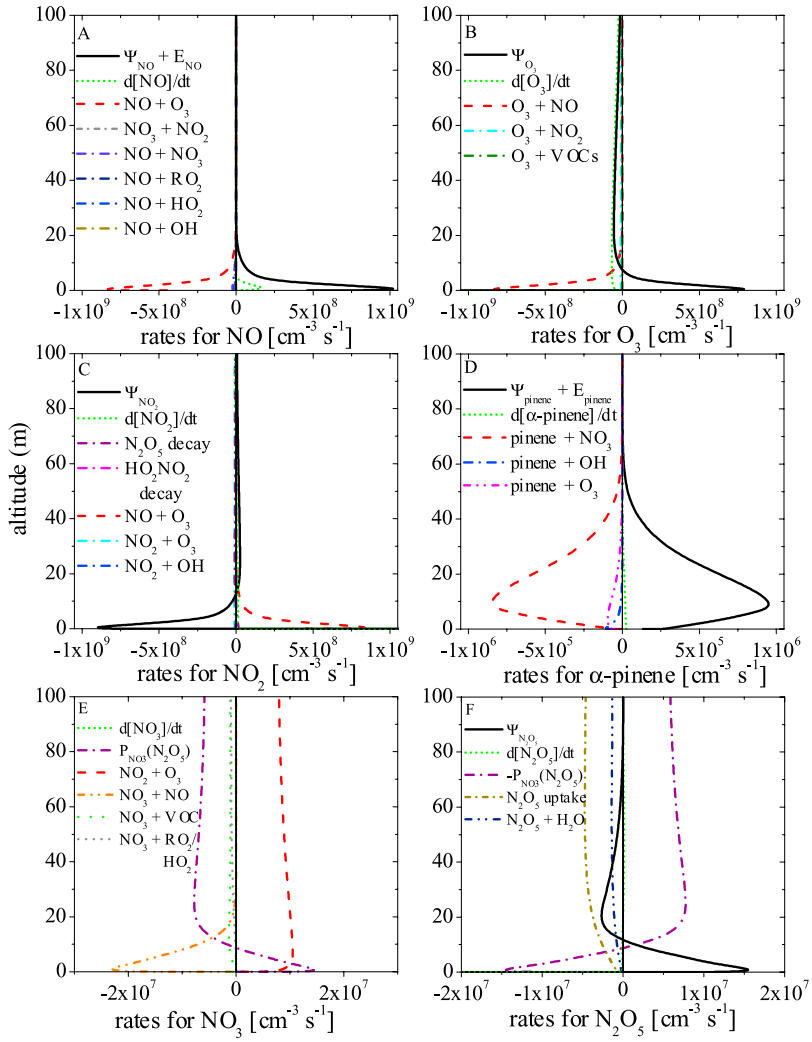

Figure 3. Vertical distribution of chemical rates and the rate of change by vertical transport and emission of NO, O_3, NO_2, α-pinene, NO_3, and N_2O_5, one hour after model start of scenario 1.

Relative humidity dependence of HONO chemistry in urban areas

Jochen Stutz,[1] Björn Alicke,[1] Ralf Ackermann,[1] Andreas Geyer,[1] Shuhui Wang,[1] Allen B. White,[2] Eric J. Williams,[3,6] Chester W. Spicer,[4] and Jerome D. Fast[5]

Received 4 September 2003; revised 1 December 2003; accepted 17 December 2003; published 13 February 2004.

[1] The role of nitrous acid, HONO, as a precursor for hydroxyl radicals in polluted urban air has been recognized for many years. The chemical processes leading to the formation of HONO are, however, still not well understood. Laboratory studies show that HONO formation occurs primarily on surfaces and is first order in NO_2. Water also plays an important role in the conversion process. While the latter has been shown in the laboratory, little information is available regarding the influence of water on the NO_2 and HONO chemistry in the real atmosphere. Here we present nocturnal DOAS measurements of HONO and NO_2 from three field experiments. The observations show that [HONO]/[NO_2] ratios between 10 and 30% relative humidity (RH) do not exceed 0.04, while values of up to 0.09 were observed at higher RH. These results are analyzed by interpreting the observed maximum [HONO]/[NO_2] ratio at a given relative humidity as the pseudo steady state (PSS) between the heterogeneous NO_2 to HONO conversion and the HONO loss on surfaces. Theoretical considerations show that the [HONO]/[NO_2] ratio at the PSS is equal to the ratio of the heterogeneous NO_2 to HONO conversion coefficient and the reactive HONO uptake coefficient, thus showing that these processes depend on the RH. This result implies that RH has to be considered in the parameterization of HONO formation in air pollution models. *INDEX TERMS:* 0322 Atmospheric Composition and Structure: Constituent sources and sinks; 0345 Atmospheric Composition and Structure: Pollution—urban and regional (0305); 0365 Atmospheric Composition and Structure: Troposphere—composition and chemistry; *KEYWORDS:* atmospheric chemistry, air pollution, HONO chemistry

Citation: Stutz, J., B. Alicke, R. Ackermann, A. Geyer, S. Wang, A. B. White, E. J. Williams, C. W. Spicer, and J. D. Fast (2004), Relative humidity dependence of HONO chemistry in urban areas, *J. Geophys. Res.*, *109*, D03307, doi:10.1029/2003JD004135.

1. Introduction

[2] The photolysis of nitrous acid, HONO, is often the dominant source of OH radicals in the morning boundary layer. Recent observations show that HONO photolysis can contribute up to 34% to the total daily OH formation in polluted environments [*Alicke et al.*, 2002; *Alicke et al.*, 2003]. HONO photolysis therefore changes the HO_x budget and can lead to increased ozone levels in polluted atmospheres [*Harris et al.*, 1982; *Jenkin et al.*, 1988]. A recent modeling study, for example, shows that HONO photolysis in a polluted winter atmosphere contributes up to 35% to the OH production and leads to an increase of ozone levels of up to 27% [*Aumont et al.*, 2003]. Despite the importance of HONO photolysis, many aspects of HONO formation are still a mystery.

[3] The basic properties of HONO formation have been studied in the laboratory and the atmosphere, and can be summarized as follows:

[4] 1. The conversion of NO_2 into HONO occurs on surfaces. The heterogeneous nature of the reaction was shown by an increase of the conversion frequency with the surface to volume ratio and a strong dependence on surface properties [*Kleffmann et al.*, 1998; *Svensson et al.*, 1987].

[5] 2. The kinetics of the heterogeneous conversion of NO_2 into HONO is first order in NO_2 [*Finlayson-Pitts et al.*, 2003; *Jenkin et al.*, 1988; *Kleffmann et al.*, 1998; *Pitts et al.*, 1984b; *Sakamaki et al.*, 1983; *Svensson et al.*, 1987].

[6] 3. HONO is observed with a yield of nearly 50% in various laboratory studies [*Goodman et al.*, 1999; *Kleffmann et al.*, 1998; *Svensson et al.*, 1987]. Minor products such as NO and N_2O from secondary reactions have also been reported. *Goodman et al.* [1999] and *Svensson et al.* [1987] found the remaining 50% of the nitrogen as surface adsorbed HNO_3.

[7] 4. Several studies have reported that the reaction is first order in water vapor [*Jenkin et al.*, 1988; *Pitts et al.*, 1984b; *Sakamaki et al.*, 1983; *Svensson et al.*, 1987]. Other studies, however, suggest that the amount of surface adsorbed water plays a more important role [*Finlayson-*

[1]Department of Atmospheric Sciences, University of California, Los Angeles, California, USA.
[2]Environmental Technology Laboratory, National Oceanic and Atmospheric Administration, Boulder, Colorado, USA.
[3]Aeronomy Laboratory, National Oceanic and Atmospheric Administration, Boulder, Colorado, USA.
[4]Battelle Science and Technology International, Columbus, Ohio, USA.
[5]Pacific Northwest National Laboratory, Richland, Washington, USA.
[6]Also at Cooperative Institute for Research in Environmental Sciences, University of Colorado, Boulder, Colorado, USA.

0148-0227/04/2003JD004135$09.00

Pitts et al., 2003; *Kleffmann et al.*, 1998]. Since water vapor and surface adsorbed water are closely related to each other, it is difficult to assess the role of water in the different laboratory experiments. Attempts to explain the formation of HONO typically assume that the dependence is on surface adsorbed water [*Finlayson-Pitts et al.*, 2003; *Jenkin et al.*, 1988].

[8] Based on these observations the following stochiometry for NO_2 to HONO conversion has been suggested:

$$\text{(R1)} \qquad NO_2 + NO_2 + H_2O \rightarrow HONO + HNO_3.$$

[9] Besides the phenomenological descriptions of the NO_2 to HONO conversion via reaction (R1), we know very little about the detailed molecular processes. *Jenkin et al.* [1988] proposed a reaction mechanism in which a $H_2O \cdot NO_2$ water complex on the surface reacts with a gas-phase NO_2 molecule. In a more recent publication, *Finlayson-Pitts et al.* [2003] proposed a mechanism that proceeds through N_2O_4 adsorbed on surface films where it isomerizes to the asymmetric form, $ONONO_2$. Whether the formation of the N_2O_4 occurs in the gas-phase, followed by an uptake onto the surface, or directly on the surface is currently unclear. The $ONONO_2$ autoionizes to $NO^+NO_3^-$, which reacts with surface adsorbed water to generate HONO and HNO_3. HONO can then escape into the gas phase or undergo secondary reactions. While evidence for certain steps of this mechanism has been observed in the laboratory [*Barney and Finlayson-Pitts*, 2000], most observations were made at NO_2 levels far above typical ambient concentrations. It remains to be seen whether this mechanism can explain the HONO levels observed in the atmosphere.

[10] A number of other HONO formation mechanisms have been suggested. Some researchers have suggested a reaction stochiometry according to reaction (R2) [*Andres-Hernandez et al.*, 1996; *Calvert et al.*, 1994; *Sjödin and Ferm*, 1985], but many laboratory and field studies have observed high formation rates of HONO in the absence of NO [*Alicke et al.*, 2002; *Kleffmann et al.*, 1998; *Platt*, 1986; *Svensson et al.*, 1987], thus making it unlikely that this mechanism plays a role in the atmosphere:

$$\text{(R2)} \qquad NO + NO_2 + H_2O \rightarrow 2\ HONO.$$

[11] *Saliba et al.* [2000, 2001] recently proposed that the reaction of NO with surface adsorbed HNO_3 releases gas-phase HONO, but the mechanism appears to play a role only under conditions with very high NO concentrations. Recent studies [*Ammann et al.*, 1998; *Gerecke et al.*, 1998; *Kalberer et al.*, 1999; *Kleffmann et al.*, 1999; *Longfellow et al.*, 2000] also point at soot particles as a possible surface for the formation of HONO. While the formation rate seems to be fast in the first minute of exposure with NO_2, a passivation of the surface rapidly slows down the formation afterwards.

[12] HONO is also produced directly in various combustion processes. Earlier studies [*Kessler*, 1984; *Pitts et al.*, 1984a] found that the [HONO]/[NO_x] emission ratio from automobiles varied between 0.1 and 1%. Recent traffic tunnel studies in the United States and Germany found average [HONO]/[NO_x] values ranging from 0.3% to 0.8% [*Ackermann*, 2000; *Kirchstetter et al.*, 1996; *Kurtenbach et al.*, 2001].

[13] A number of parameterizations of the NO_2 to HONO conversion rate have been presented. *Svensson et al.* [1987] propose a rate of formation based on their observations in a glass reactor that depends on NO_2 and gas-phase water concentrations, as well as the surface to volume ratio. *Lammel* [1999] introduced a similar parameterization of the formation of HONO, which is based on surface type and a relative humidity specific surface to volume ratio, thus expanding the concept introduced by *Svensson et al.* [1987] (see below for more details). *Kleffmann et al.* [1998] derived a reactive uptake coefficient for NO_2 of $\sim 10^{-6}$ on a surface with adsorbed water. In a recent study, *Kurtenbach et al.* [2001] determined the NO_2-HONO conversion frequency on a concrete traffic tunnel wall with a surface to volume ratio of 1 m^{-1} to be 5×10^{-5} s^{-1}.

[14] Only a few investigations have studied the water dependence of HONO formation in the atmosphere. While not analyzed in detail, the observations of *Harris et al.* [1982] appear to show a weak dependence of the nocturnal [HONO]/[NO_2] ratio on relative humidity (RH). *Sjödin and Ferm* [1985] found a correlation of their 12h integrated denuder measurements of HONO mixing ratios with the product of [NO][NO_2][H_2O], based on the mechanism in reaction (R2). It is difficult to assess the role of water, in particular since it is believed today that the mechanism in reaction (R2) does not play a major role in the formation of HONO under normal atmospheric conditions. A similar argument applies to the data shown by *Calvert et al.* [1994]. The most detailed information on the role of water can be found in the work of *Lammel* [1999], who parameterizes the formation of HONO by classifying surfaces as "dry," "wet," and "aqueous." For most surfaces, "dry" was defined as the surface state below a limiting RH, for example, 50% RH for urban surfaces. "Wet" surfaces of insoluble material, i.e., soil, occurred at a RH range that was limited by the transition to "dry" surfaces at the lower end and ~95% at the upper end. Insoluble surfaces above ~95% RH and soluble aerosol above their deliquescence point or crystallization point, depending on their history, were classified as "aqueous" surfaces. *Lammel* [1999] then parameterized the HONO formation rate, P_{HONO}, on all surfaces, with the exception of soot particles, with the following equation (here only given for nonsoot surfaces):

$$P_{HONO} = 0.5 \times [NO_2] \times \left\{ \left[\left(\frac{S_{dry}}{V} \right) + \left(\frac{S_{aqueous}}{V} \right) \right] \times k^{het(1)} + \left(\frac{S_{wet}}{V} \right) \times k^{het(2)} \times [H_2O] \right\}. \quad (3)$$

[15] The equation is based on a pseudo-first order behavior for "dry" and "aqueous" surfaces, which makes the HONO formation independent of [H_2O] with a first order rate coefficient $k^{het(1)}$. In the case of a "wet" surface, equation (3) becomes dependent on the water concentration with a second-order rate coefficient of $k^{het(2)}$. This parameterization is based on the argument that the amount of chemisorbed water at very dry conditions becomes approximately independent of the water vapor levels, while in a "wet" case (above 1 monolayer of H_2O) the amount of adsorbed water is dependent on water vapor.

[16] The nonphotolytic loss of HONO also plays an important role in the nocturnal atmosphere. A number of

atmospheric observations [*Harrison et al.*, 1996; *Kitto and Harrison*, 1992; *Spindler et al.*, 1999; *Stutz et al.*, 2002] and laboratory investigations [*Bongartz et al.*, 1994; *Kaiser and Wu*, 1977; *Mertes and Wahner*, 1995; *Pitts et al.*, 1984b; *Sakamaki et al.*, 1983; *Svensson et al.*, 1987; *TenBrink and Spoelstra*, 1998] have studied the fate of HONO in the dark. All studies report that the loss of HONO in the atmosphere proceeds via heterogeneous reactions or surface uptake. One proposed reaction mechanism has the stochiometry:

$$\text{(R4)} \qquad \text{HONO} + \text{HONO} \rightarrow \text{NO}_2 + \text{NO} + \text{H}_2\text{O}.$$

[17] Several studies have reported that reaction (R4) occurs as a second-order reaction on the surfaces of the respective reaction vessels [*Kaiser and Wu*, 1977; *Sakamaki et al.*, 1983; *Svensson et al.*, 1987; *TenBrink and Spoelstra*, 1998] with rate constants of 10^{-22} cm^3 molec^{-1} s^{-1} for a passivated surface [*Svensson et al.*, 1987] and 1.5×10^{-19}cm^3 molec^{-1} s^{-1} in a Teflon smog chamber [*TenBrink and Spoelstra*, 1998]. At these rates, destruction of HONO in the atmosphere would be too slow to be significant. Recently, *Syomin et al.* [2002] suggested, based on laboratory observations, a different mechanism in the presence of surface adsorbed HNO_3:

$$\text{(R5)} \quad \text{HONO}_{(\text{surface})} + \text{HNO}_{3(\text{surface})} \rightarrow 2\ \text{NO}_{2(\text{gas})} + \text{H}_2\text{O}_{(\text{surface})}.$$

The order of the HONO loss is, however, unclear.

[18] It is clear from the existing literature that a dependence of HONO chemistry on gas phase or adsorbed water can be expected. Most studies, however, have been made in laboratory environments on surfaces that may not be representative for atmospheric conditions. The water dependence in the real atmosphere has thus far not been extensively studied. Here we present nocturnal HONO and NO_2 data from three field experiments in environments with different RH. Humid data was obtained in Nashville during the Southern Oxidant Study in 1999 and during the Texas Air Quality Study in Houston, Texas in 2000. Much drier conditions were observed in Phoenix, Arizona during an experiment in 2001. The three data sets are analyzed with respect to the conversion of NO_2 to HONO in the nocturnal atmosphere using a pseudo steady state approach. Conclusions about the dependence of the net NO_2 to HONO conversion mechanism on the RH in the urban environment are drawn.

2. Experimental Procedure

[19] All NO_2 and HONO data presented here were measured by long-path differential optical absorption spectroscopy (DOAS) [*Platt*, 1994]. The University of California, Los Angeles DOAS system consists of a telescope that sends and receives a collimated light beam. The beam is folded once by an array of quartz corner cube retroreflectors. Spectroscopic detection is achieved by a spectrograph detector system coupled to the telescope. A detailed description of the basic setup and the analysis method can be found in the work of *Alicke et al.* [2003]. To achieve low detection limits, the telescope and the retroreflector array were separated by 1–5 km. In addition, the retroreflector array was mounted at a different altitude than the telescope. The DOAS light beam therefore integrated over a volume of air that extended both in the horizontal and the vertical. Measurements of RH were made by standard meteorological instruments in all cases. The NO data used in the analysis was determined by chemiluminescence instruments.

[20] We present here data from three field experiments at different locations in the United States. All three experiments were performed during summer, with relatively high temperatures.

2.1. SOS 1999

[21] In June and July 1999, during the Southern Oxidant Study experiment in Nashville, Tennessee, we deployed our DOAS system in a suburban area 8 km northeast of downtown Nashville. The main ground site, the Cornelia Fort airfield, was located in the 30 m deep and 1.5 km wide Cumberland River valley. The DOAS telescope was set up in the valley and aimed at a retroreflector array located at a building on the opposite valley ridge. The data were measured on a light path of 1.35 km single length, extending from 2 to 35 m altitude above the valley ground. The light path integrated over the entire cross section of the valley. The valley floor was a mixture of grass, trees, and concrete. No direct sources of NO_x and HONO were located in the valley. The airport was operated infrequently and was closed at night. Roads were located on both ridges of the valley. The nocturnal conditions in the valley were generally humid, often reaching RH of 100%. We also frequently observed ground fog. Measurements of RH were made with a Vaisala HMP45C humidity probe in 2 m altitude. NO was measured by a chemiluminescence instrument [*Williams et al.*, 1998] 10 m above the ground. Winds in the valley were typically slow at night, and vertical mixing was weak.

2.2. TEXAQS 2000

[22] During the Texas Air Quality Study in August and September 2000 our instrument was set up at the ground at the La Porte airport, 20 km southeast of downtown Houston. Although we measured on several different light paths, we will only use the data of the light path aiming at a retroreflector array placed on top of a water tower at 1.9 km distance. The path averaged over an altitude interval from 2 to 44 m. The area under the light path was a mixture of concrete, grass, trees, and house roofs. The immediate location around the airport had little traffic, and the airfield was only rarely used during the night. However, larger chemical refineries were located at a distance of 3–6 km, thus influencing the site at certain wind directions. RH and NO were measured in approximately 750 m distance from the light path by a Vaisala HMP45C humidity probe 2 m above ground and a chemiluminescence instrument [*Williams et al.*, 1998] at 10 m altitude, respectively. During this campaign, nocturnal RH was in the range from 50 to 100%. Winds were generally stronger than in Nashville, and the air at night was vertically better mixed.

2.3. Phoenix 2001

[23] The setup during the Phoenix Sunrise experiment in June 2001 was different from the first two campaigns. While the DOAS telescope was located on the ground in Nashville and Houston, it was placed on the top of the highest building in downtown Phoenix, at an altitude of 139 m above the ground. Retroreflectors were mounted at a

distance of 3.3 km on the roof of three buildings, at altitudes of 10, 45, and 110 m agl. The DOAS telescope was aimed consecutively onto the individual retroreflector arrays, measuring on all three light paths within 15–20 min.

[24] Because of the influence of vertical mixing on HONO levels [*Stutz et al.*, 2002], it is difficult to compare the path integrated data averaging from 10 m to 139 m height directly with the results from the other studies that integrated over much smaller height intervals. We have therefore used the data from the 45–139 m and 10–139 m light paths to calculate the trace gas concentrations in the 10–45 m height interval [*Wang et al.*, 2003b]. In short, we linearly interpolated the data of the 45–139 m light path to the time of the 10–139 m light path measurements. In this process, we filtered out periods where fast temporal concentration changes would have made a subtraction of the data on the two light paths unreliable. The 10–45 m interval concentration is then derived by scaling the 45–139 m concentrations with the length of the 10–139 m path between 45 and 139 m, followed by a subtraction of this value from the 10–139 m path trace gas levels. The result are the trace gas concentrations in the height interval of 10–45 m with a horizontal length of 0.9 km. Owing to the possible influence of temporal concentration changes between the two light paths that escaped the filtering procedure, the 10–45 m data can show larger temporal variations.

[25] The area under the light paths in Phoenix was covered by buildings, roads, and some vegetation. Most of the buildings were about 2–5 stories high with a few exceptions of higher structures. This mixture of ground and roofs leads to an average altitude of the reactive ground surface that is higher than the ground. Thus the retroreflector mounted on the roof of a three-story building at 10 m agl was closer to the reactive surface than the height above the ground suggests.

[26] The vegetation in Phoenix was sparser than at the other two locations. Another difference between Phoenix and the other experiments was the larger direct emissions due to traffic. In particular, after 0500 local time the morning rush hour introduced large amounts of NO_x and HONO into the boundary layer. The strongest nocturnal source was the I10 freeway, which crossed the light beam close to the location of the telescope. Because the 10–45 m interval was located at a distance of ~2 km from the freeway, direct emissions should not have a large impact on the data.

[27] Measurements of NO, which are later used to calculate the significance of direct emission as a HONO source, were performed at the 16th floor of the building hosting the DOAS telescope at 50 m agl. This altitude is above the 10–45 m interval of the DOAS data. We therefore have to consider that during the night the concentration measurements of NO, which is emitted at the ground, will most likely underestimate the NO levels between 10 and 45 m due to the weak vertical mixing and the reaction with ozone. The NO monitor was located at a distance of ~2.4 km from the DOAS measurement volume. Although the different locations of the probed volumes could introduce uncertainties in our analysis, a comparison of the DOAS and in situ O_3 data measured at the same location as NO shows that the agreement is, in general, good.

[28] Meteorological measurements were made at an altitude of 45 m agl at the rooftop of a building with a Campbell weather station. Comparison with other measurements close to the ground (not shown here) gives us confidence that the RH measurements at 45 m altitude are representative for the 10–45 m height interval. Our measurements show that the nights in Phoenix were very dry. With the exception of the night of 25–26 June, the RH never exceeded 50%. On 25 June the RH climbed up to 70%, comparable to the observations in Nashville and Houston. Details of the light path geometries during the three field experiments, as well as the various meteorological conditions, are summarized in Table 1.

Table 1. Time Frame and Measurement Characteristics of the Three Field Experiments

	Time Frame	Height Interval, m	Relative Humidity Range, %
SOS99 Nashville	6/18/99–7/12/99	2–35	50–100
TexAQS 2000	8/24/00–9/11/00	2–44	35–100
Phoenix 2001	6/17/01–6/30/01	10–45	10–70

[29] Since our study is focused on the chemical formation of HONO, it is necessary to separate direct HONO emissions from HONO that is formed through the conversion of NO_2. We estimated the concentration of HONO that is emitted from traffic from the observed NO_x levels and the emission ratio of 0.003 measured by *Kirchstetter et al.* [1996] for a typical U.S. car fleet in a traffic tunnel and subtracted this value from the observed HONO concentrations, $[HONO]_{obs}$,

$$[HONO] = [HONO]_{obs} - 0.003 \times [NO_x]. \quad (6)$$

[30] Equation (6) is based on the assumption that directly emitted HONO is not lost after emission. This is clearly incorrect for HONO emissions during the day, when photolysis will destroy HONO. Additionally, nocturnal NO_x levels emitted before sunset should, in principle, not be considered in equation (6). Since it is difficult to determine the time of the NO_x emissions, in particular later during the night, we will use $0.003 \times [NO_x]$ as an upper estimate of the contribution of direct HONO emissions. As mentioned above, HONO can also be lost heterogeneously during the night. This process will also reduce the contribution of direct HONO emissions in equation (6). We will thus interpret [HONO] as the lower limit of the amount of chemically formed HONO, while the uncorrected observation, $[HONO]_{obs}$, is the upper limit. To illustrate the possible effect of direct HONO emissions we will use both, $[HONO]_{obs}$ and [HONO] throughout most of this paper.

3. Results

[31] We chose four example nights from the three locations (Nashville, Houston, and Phoenix) to illustrate the behavior of $[NO_2]$ and [HONO] during the night (Figures 1–4). The figures also contain information about the relative humidity and [NO]. The latter is needed for the correction of direct HONO emissions by equation (6). We begin with discussing two humid nights from Nashville and Houston.

[32] The RH in Nashville (Figure 1) increased from a sunset value of ~60% to 95–100% in the second half of the night. The night of 12–13 July 1999 had very low NO

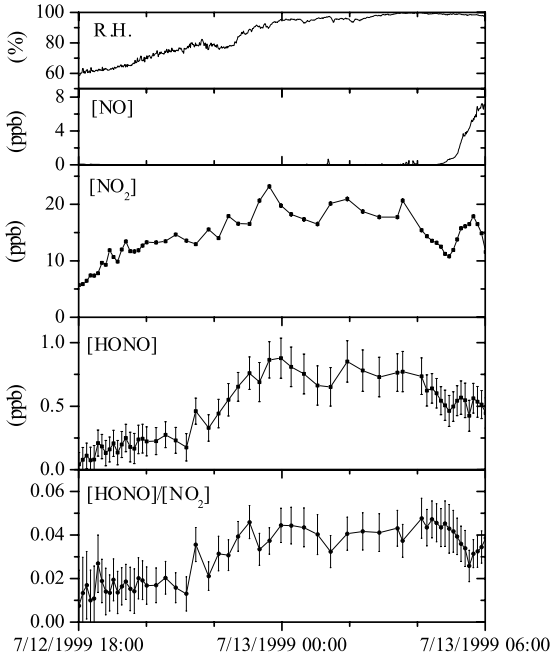

Figure 1. Behavior of [NO], [NO_2], [HONO], and relative humidity (RH) during one night in Nashville, Tennessee. Sunrise is around 0530. $[HONO]_{obs}$ was not statistically different from [HONO] and was thus omitted in the graph.

levels. The increase of [NO] in the morning was caused by the beginning photolysis of NO_2 at sunrise and the onset of the rush hour. The NO_2 levels in Nashville increased slightly from sunset to midnight but stayed constant at

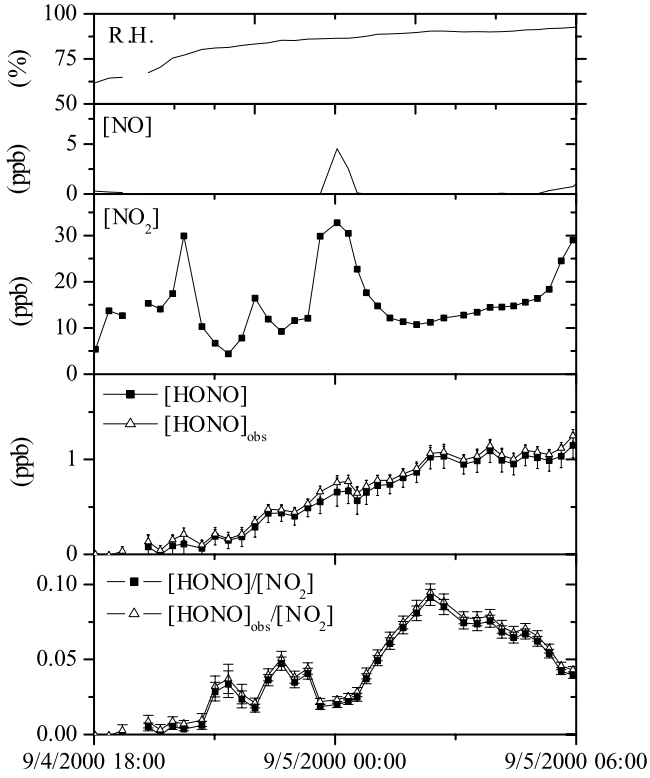

Figure 2. Behavior of [NO], [NO_2], [HONO], and RH during one night in Houston, Texas.

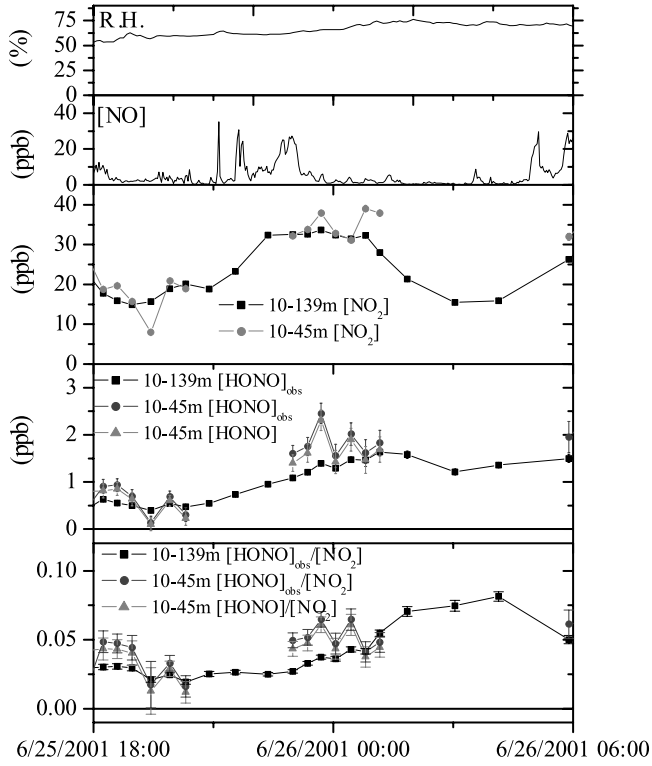

Figure 3. Behavior of [NO], [NO_2], [HONO], and RH during one night in Phoenix, Arizona. The night is characterized by relatively high nocturnal RH. See color version of this figure at back of this issue.

~20 ppb afterward (Figure 1). HONO mixing ratios started to increase right after sunset and reach a maximum level of 0.8 ppb at midnight, after which [HONO] stayed fairly constant until sunrise around 0530. During this night in Nashville, the correction of direct HONO emissions was negligible. The [HONO]/[NO_2] ratio in Nashville showed a similar temporal behavior as [HONO] due to the relatively constant NO_2 levels. The maximum [HONO]/[NO_2] ratio reached during this night was ~5%.

[33] The behavior of the RH in Houston (Figure 2) during the night of 4–5 September 2000 is similar to that in Nashville (Figure 1). NO levels in Houston were low, except for one plume event around midnight. This plume is also reflected in the increase of NO_2 mixing ratios at midnight. The normal NO_2 levels in Houston were between 10 and 20 ppb, somewhat lower than in Nashville, except for the two plumes at 2000 and 0000 hours (Figure 2). As in Nashville (Figure 1), HONO mixing ratios in Houston started to increase right after sunset and reached a maximum of 1 ppb at 0230. We included both the observed HONO, $[HONO]_{obs}$, and emission-corrected HONO, [HONO], data in Figure 2 to illustrate the effect of the correction with equation (6). The difference between [HONO] and $[HONO]_{obs}$ was ~10%. The [HONO] build-up showed a leveling off at 0230 and [HONO] remained constant from 0230 to 0600. The behavior of the [HONO]/[NO_2] ratio in Houston is not as clear, since the two plumes with elevated [NO_2] and [NO] lead to a dip in the [HONO]/[NO_2] ratio. We suspect that the plumes originated from a nearby industrial source. It is likely that a conversion of NO_2 to HONO in the

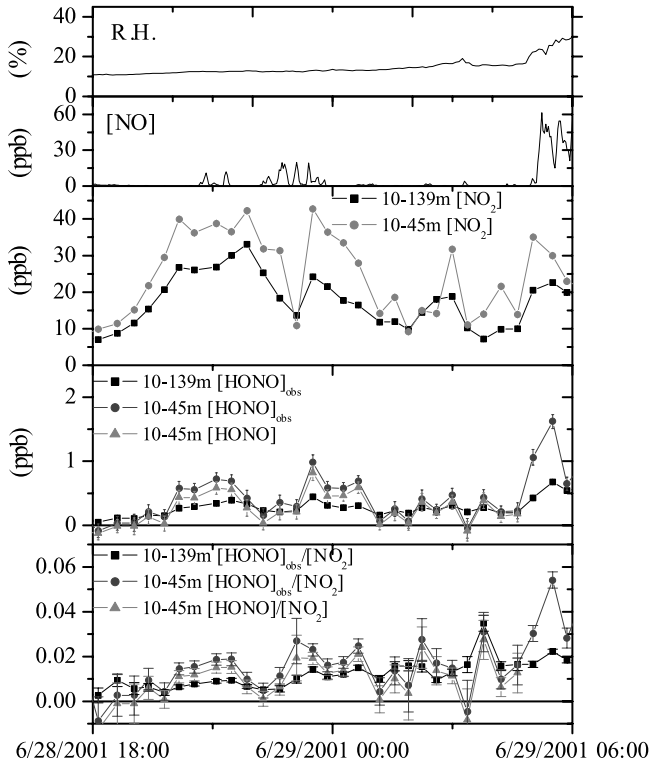

Figure 4. Behavior of [NO], [NO_2], [HONO], and RH during one night in Phoenix, Arizona. The night is characterized by very low nocturnal RH below 35%. [HONO] is not shown after 0430, when the onset of photolysis and strong emissions during rush hour make an emission correction unreliable. See color version of this figure at back of this issue.

relatively freshly polluted air masses has not yet proceeded as far as in other air masses, thus leading to [HONO]/[NO_2] ratios more like those encountered at the beginning of the night. Despite the larger variation of [HONO]/[NO_2], a clear trend of increasing ratios towards a maximum of ~8% was observed. The ratio decreases somewhat after this maximum to a value of ~6%.

[34] Both nights in Nashville and Houston have in common that HONO mixing ratios level off and remain constant in the second part of the night. We have observed this leveling off of [HONO] in other locations [*Stutz et al.*, 2002] and believe it is a common feature of the NO_2 to HONO conversion in urban areas.

[35] Two nights from our measurements in Phoenix are shown in Figures 3 and 4. The figures are organized in a similar way as those of Nashville and Houston. The large gaps in the 10–45 m [NO_2] and [HONO] data in Figure 3 are caused by the poor time resolution and problems in the calculation of the 10–45 m data. To bridge these gaps, we have also included the original long path data averaged over a height interval of 10–139 m. Because [NO_2] and [HONO] generally showed larger mixing ratios near the ground in Phoenix, the 10–139 m data can be considered as a lower estimate for the 10–45 m values.

[36] Phoenix typically has a much dryer climate during the early summer than Nashville or Houston. Nocturnal RH often does not exceed 20%. We have, however, encountered one night during our measurements in Phoenix (25–26 June 2001) when the RH increased to 70% (Figure 3). NO mixing ratios during this night were generally below 5 ppb, except for a period between 2100 and midnight and after sunrise. The high NO levels before midnight were not reflected in any of the DOAS data, and we suspect that the in situ monitor observed an air mass that was transported locally, for example from the street canyon under the sampling site. [NO_2] varied slowly between 20 and 30 ppb. Little difference was seen between the path-averaged and 10–45 m NO_2 mixing ratios, indicating that the air was vertically fairly well mixed. This night started out with relatively high [HONO] and [HONO]/[NO_2] due to a dense cloud cover during the afternoon that reduced HONO photolysis and thus increased HONO mixing ratios. Despite the higher starting levels of [HONO], we observed an increase of [HONO] and [HONO]/[NO_2] until ~0200 to about 1.5–2 ppb and 0.06, respectively, in the 10–45 m height interval. In general, the data in the 10–45 m height interval were slightly higher than the path-averaged values. Because the 10–45 m data between 2000 and 2300 and after 0200 are missing, we will use the path-averaged data as lower limits for $[HONO]_{obs}$ and $[HONO]_{obs}/[NO_2]$. The path-averaged HONO data showed a leveling off after 0200. This was also reflected in the [HONO]/[NO_2] data, which leveled off at a value of ~0.08. The emission-corrected HONO, [HONO], which is only shown for the 10–45 m data, was up to ~10% lower than the direct HONO observations, $[HONO]_{obs}$. The behavior of [HONO], in particular the leveling off of the [HONO]/[NO_2] values at 0.06–0.08 at 0200, was similar to our example nights in Nashville and Houston. We attribute this to the relatively high RH of 70% during the second half of the night in Phoenix.

[37] Most nights in Phoenix, however, were rather dry. The night of 28–29 June 2001 (Figure 4) showed a RH after sunset of ~10%, which increased only slowly throughout the night. NO mixing ratios were below 10 ppb and only increased after sunrise and the onset of traffic in the morning. NO_2 mixing ratios in the 10–45 m height interval were ~40 ppb before midnight and decreased to values between 10 and 20 ppb later during the night. A comparison with the path-integrated data shows that the levels of [NO_2] close to the ground were higher during this night, implying that vertical mixing was weak. As for [NO_2], [HONO] levels showed considerable differences between the 10–139 m path averaged and the 10–45 m data, in particular in the first half of the night. At the beginning of the night there was also a ~10% difference between observed and emission-corrected HONO values. Later in the night, both values agreed better due to the lower NO_x levels. Although the [HONO] data showed considerable temporal changes, it appeared that an increase of [HONO] and [HONO]/[NO_2] was observed during the first half of the night. After midnight [HONO]/[NO_2] did not increase further, and remained at an average below 0.015, with maximum values of 0.03. [HONO] levels were below 0.5 ppb during this time. After 0500 the contributions of traffic emissions of NO, NO_2, and HONO, as well as the onset of photolysis at sunrise, were observed.

[38] It is interesting to compare the two nights in Phoenix shown in Figures 3 and 4. Both nights showed [NO_2] levels

between 10 and 40 ppb in the 10–45 m interval. Both nights also showed high [NO_2] values before midnight and lower values after midnight. The behavior of [HONO] and [HONO]/[NO_2], however, was drastically different between the two nights. While during the night of 25–26 June 2001 [HONO] steadily increased to ~1.5–2 ppb, HONO values remained below 0.8 ppb on 28–29 June 2001. This becomes even more clear if one compares the [HONO]/[NO_2] data, which reached up to 0.08 during the first night but only 0.03 on 28–29 June 2001. The main difference between these two nights was the much higher RH during the night of 25–26 June 2001. Vertical mixing may have played a role in the first part of the night of 28–29 June 2001, but a comparison of the path-averaged and 10–45 m data showed that the air was better mixed in the second part of the night.

4. Discussion

[39] The phenomenological description of the different behavior of HONO in humid and dry nights in Figures 1 to 4 is a first step in the understanding of the influence of RH on HONO chemistry. In the following section, we continue to derive a more statistical description of RH influence on HONO chemistry.

4.1. Theoretical Consideration

[40] To understand the behavior of the NO_2-HONO system in more detail and to provide a theoretical basis for the interpretation of our observations, we will first develop a simple analytical description of the temporal behavior of [HONO]. The chemical formation of HONO will be described as a first order process in NO_2 occurring on surfaces with a surface area, S, to air volume, V, ratio of (S/V) [*Finlayson-Pitts et al.*, 2003; *Jenkin et al.*, 1988; *Kleffmann et al.*, 1998; *Pitts et al.*, 1984b; *Sakamaki et al.*, 1983; *Svensson et al.*, 1987]. We incorporate the influence of water observed in various laboratory studies [*Finlayson-Pitts et al.*, 2003; *Jenkin et al.*, 1988; *Kleffmann et al.*, 1998] by using a RH-dependent reactive conversion probability $\gamma_{NO2\rightarrow HONO}$(RH), without further specifying the functional dependence on RH. The second process influencing HONO concentrations is the heterogeneous loss of HONO. We assume a loss that is first order in HONO. Evidence for this reaction order will be given below. Whether the HONO loss depends on the surface adsorbed water is unknown. In analogy to the observed water dependence of NO_2 and HNO_3 uptake [*Finlayson-Pitts et al.*, 2003; *Saliba et al.*, 2001], we will assume that HONO also has a RH-dependent uptake probability, γ_{HONO}(RH). A RH dependence was recently observed by *Syomin and Finlayson-Pitts* [2003], between 0% and 50% RH. Equation (7) describes this simple model mathematically [*Finlayson-Pitts and Pitts*, 2000]:

$$\frac{d[HONO]}{dt} = \gamma_{NO2\rightarrow HONO}(R.H.) \times \frac{S}{V} \times \frac{v_{NO2}}{4} \times [NO_2] - \gamma_{HONO}(R.H.) \times \frac{S}{V} \times \frac{v_{HONO}}{4} \times [HONO]. \quad (7)$$

[41] Here ν_{NO2} and ν_{HONO} are the mean molecular velocities of the respective species. At the beginning of the night, when HONO levels are generally low, the first term in equation (7) dominates, and equation (7) predicts an increase in [HONO]. As the night proceeds and HONO accumulates, the HONO loss term will gain importance, counterbalancing the formation rate, thus ultimately leading to a pseudo steady state and constant [HONO] as observed in Figures 1–4.

[42] By further simplifying equation (7), we can derive an analytical expression for the temporal behavior of the [HONO]/[NO_2] ratio. We will assume that the change of [NO_2] due to the conversion to HONO and other reactions is small. We therefore assume that the NO_2 concentration is constant with time. Since the mean velocities of NO_2 and HONO only differ by ~2%, we will set both to $\bar{v}$ for the following calculation. Another simplification in our equation is that we consider the reaction probabilities and S/V to be time independent, although we know that both parameters can change throughout the night. Equation (7) therefore becomes

$$\frac{d\left(\frac{[HONO]}{[NO_2]}\right)}{dt}(t) = \frac{S}{V} \times \frac{\bar{v}}{4} \times \gamma_{HONO}(R.H.) \times \left(\frac{\gamma_{NO2\rightarrow HONO}(R.H.)}{\gamma_{HONO}(R.H.)} - \left(\frac{[HONO]}{[NO_2]}\right)(t)\right). \quad (8)$$

[43] The analytical solution for this equation, assuming that [HONO]/[NO_2] = 0 at the beginning of the night (t = 0), is

$$\left(\frac{[HONO]}{[NO_2]}\right)(t) = \frac{\gamma_{NO2\rightarrow HONO}(R.H.)}{\gamma_{HONO}(R.H.)} \times \left(1 - \exp\left(-\frac{S}{V} \times \frac{\bar{v}}{4} \times \gamma_{HONO}(R.H.) \times t\right)\right). \quad (9)$$

[44] Equation (9) describes an exponential increase of the [HONO]/[NO_2] ratio with a time constant of $\frac{S}{V} \times \frac{\bar{v}}{4} \times \gamma_{HONO}(R.H.)$. It is interesting to note that this time constant depends only on the surface to volume ratio and the heterogeneous reaction probability of HONO but is independent of the NO_2 to HONO conversion probability.

[45] The dependence of the time constant on S/V requires a more detailed discussion. In a laboratory-type setting, S/V is clearly defined by the reaction vessel geometry. This approach is often also applied to the atmosphere by assuming a well-mixed nocturnal boundary layer with the ground as reactive surface. In this case, S/V is defined by the surface area of the ground and other reactive surfaces and the volume determined by the assumed height of the nocturnal boundary layer (NBL). However, the concept of a well-mixed boundary layer is often not justified during the night. Thus a "volume" cannot be easily defined [*Stutz et al.*, 2002]. If the ground is the dominant reactive surface in the nocturnal boundary layer, the S/V cannot be interpreted directly as a surface to volume ratio since trace gases may be unevenly distributed with altitude. The degree of mixing throughout the boundary layer depends on the magnitude of vertical transport at

night. We therefore have to interpret S/V in equation (9) as a parameter that depends mainly on the strength of vertical mixing, i.e., S/V is large during strong vertical stability (because the effective volume is small) and becomes smaller as the NBL becomes less stable. It should also be noted that if S/V is interpreted in this way, a change in vertical mixing during the night could lead to a change of S/V. It is also likely that aerosol particles contribute to the reactive surface in the NBL. In this case, S/V is a combination of the aerosol surface to volume ratio and the influence of vertical mixing.

[46] Equations (7) and (9) show that the NO_2-HONO system will ultimately reach a pseudo steady state (PSS), which is determined by the ratio of the two reaction probabilities $\gamma_{NO2\rightarrow HONO}$ and γ_{HONO}

$$\left(\frac{[HONO]}{[NO_2]}\right)_{PSS} = \frac{\gamma_{NO2\rightarrow HONO}(R.H.)}{\gamma_{HONO}(R.H.)}. \quad (10)$$

[47] It is essential for our further interpretation to understand that the chemical system will always try to reach this PSS. The [HONO]/[NO_2] ratio can exceed the PSS value only if direct emissions add HONO to the system without adding a corresponding amount of NO_2. The system will then, however, move back into the PSS by an increased loss of HONO onto the surface.

[48] The fact that the HONO-NO_2 system moves into a PSS makes the interpretation of the influence of direct HONO emission difficult. As we have argued above, the true PSS lies between the emission corrected HONO mixing ratio, [HONO], and the direct observation $[HONO]_{obs}$ (equation (6)). As shown in the comparison of $[HONO]_{obs}$ and [HONO] in Figures 2–4, the difference between these two values is typically between 0 and 10% and can reach 20% in extreme cases (not shown here). Keeping this systematic uncertainty in mind, we will use the emission-corrected HONO mixing ratio for the following interpretation of our data.

[49] From the discussion above, one expects that under meteorologically favorable conditions the [HONO]/[NO_2] ratio attains a constant level when the system reaches the PSS. This leveling off of the HONO-to-NO_2 ratio was indeed found during many nights in Nashville, Houston, and Phoenix, (section 3, Figures 1–3) and at other sites [e.g., *Stutz et al.*, 2002]. Because of the strong influence of S/V and therefore vertical mixing, the time that is required to reach the PSS can, however, vary considerably. Our observations suggest that it is likely to find the NO_2-HONO system in a PSS at the end of a night. It is, however, also possible that the PSS is not reached, for example, if vertical mixing is too strong. Indeed, examples as in Figures 1–3 are not encountered in every night. In the further analysis we will therefore use the complete nocturnal data set, without considering the time of the night, to investigate the average behavior of the system.

4.2. Order of HONO Loss

[50] We first test our hypothesis that the heterogeneous HONO loss is a first-order process. Figure 5 shows all nocturnal, emission-corrected HONO measurements during the three campaigns plotted against their respective NO_2 mixing ratios. To determine the order of the HONO loss, we included three linear functions describing the dependence of [HONO] on [NO_2], as predicted for the PSS by equation (10). The three functions were calculated for reaction probability ratios $\gamma_{NO2\rightarrow HONO}/\gamma_{HONO}$, of 0.04, 0.06, and 0.08. The linear curves in Figure 5 describe the maximum values of [HONO] fairly well, considering that different reaction probability ratios may have been encountered. We also included the curve expected for a second order loss of HONO. In this case, [HONO] would depend on the square root of [NO_2] (compare with equation (7)). It is evident that this curve does not describe the maxima over the entire NO_2 range in Figure 5. Only below 6 ppb NO_2, the quadratic dependence appears to describe the [HONO] maxima as well as the linear dependence. We conclude, based on our entire data set, that the assumption of a first order HONO loss is justified.

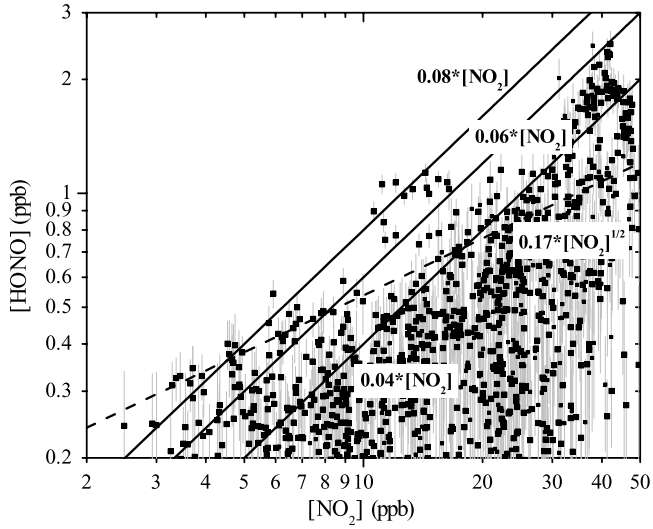

Figure 5. The maximum HONO mixing ratios from the three field experiments show a linear dependence of [NO_2]. The three continuous curves show a linear relation between [HONO] and [NO_2], as predicted for the PSS in equation (10) with a heterogeneous reactivity ratio of 0.04, 0.06, and 0.08. For comparison, the expected curve for a second order loss of HONO is also included (dashed line).

4.3. RH Dependence of HONO Chemistry

[51] Figure 6 shows all nocturnal [HONO]/[NO_2] ratios observed during the three field experiments plotted against their respective relative humidities. It should be noted that we removed data of three nights from the Phoenix data set due to the influence of dust storms that showed extremely high [HONO]/[NO_2] ratios. The results of these nights are discussed by *Wang et al.* [2003a]. To supplement our data, we have also included the nocturnal [HONO] maxima observed by *Harris et al.* [1982] in the Los Angeles Basin. Our observations in Figure 6 are color-coded according to the time periods before and after midnight.

[52] To interpret Figure 6 we will rely on the theoretical discussion of the behavior of [HONO] and the [HONO]/[NO_2] ratio in section 4.1. For each RH, [HONO]/[NO_2] ratios can be influenced by the time of the night, the surface to volume ratio (equation (9)), and other parameters, such as advection. These dependencies lead to a range of [HONO]/[NO_2] values in Figure 6. Independent from

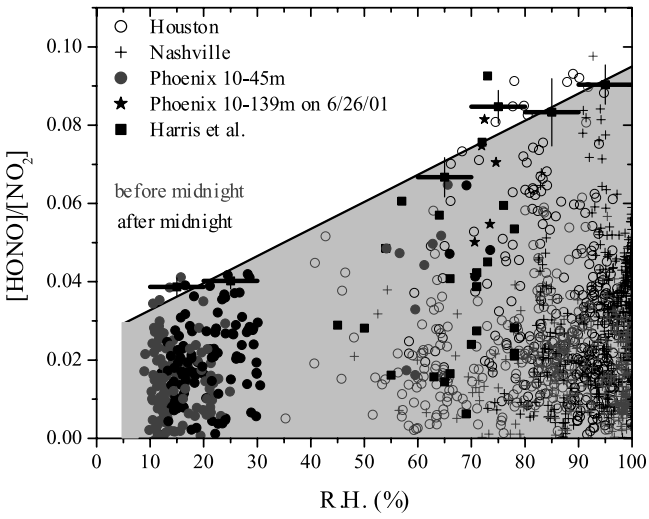

Figure 6. [HONO]/[NO_2] ratios versus RH for four different locations in the United States. Errors for [HONO]/[NO_2] are in the range 0.002–0.01 and were omitted in this plot for clarity. See color version of this figure at back of this issue.

these parameters is, however, that the NO_2-HONO system can reach a pseudo steady state, which is characterized by a maximum [HONO]/[NO_2] ratio. Concentrating solely on these maxima in Figure 6 will therefore eliminate much of the uncertainty connected with the influence of other parameters. To provide a better description of these maxima, we calculated the average of the five highest [HONO]/[NO_2] values in RH intervals of 10%. These averaged maxima are shown in Figure 6 as black horizontal bars, where the lengths of the bars indicate the RH interval. The standard deviation of the five maxima is also shown. Because data between 30 and 60% RH are sparse, the average of the maxima in these intervals is not displayed. Also shown in Figure 6 is a linear least squares fit through the averaged maxima.

[53] The maxima and their averages in Figure 6 show a clear dependence on the RH. While the maximum values in the 10–30% RH interval are in the range between 0.03 and 0.04, they reach 0.08–0.09 at RH between 70 and 95%. The few data points between 30 and 60% RH seem to have maximum ratios around 0.04–0.06. The averaged maxima lie on a line that describes the general behavior of all maxima well. It appears, however, that the [HONO]/[NO_2] ratios between 95 and 100% RH are lower than the values at 70–95% RH.

[54] The different symbols in Figure 6 show that the RH range between 10 and 35% is solely filled by data from Phoenix. Above 40% RH, all three campaigns and the data by [*Harris et al.*, 1982] contribute. It is important to note that the humid night in Phoenix (Figure 3) agrees well with the values of Nashville and Houston around 70% RH. This night therefore provides the link between the four data sets and shows that the influence of the location on the [HONO]/[NO_2] ratio is less important than the dependence on RH.

[55] We can use equation (10) and the maximum [HONO]/[NO_2] ratios in Figure 6 to analyze the RH dependence of the ratio between the heterogeneous reaction probabilities $\gamma_{NO2\rightarrow HONO}(RH)$ and $\gamma_{HONO}(RH)$. While we cannot determine which of the two parameters changes, we can conclude that the RH dependence of $\gamma_{NO2\rightarrow HONO}(RH)$ must be stronger than that of $\gamma_{HONO}(RH)$ to explain the observations:

$$\frac{d(\gamma_{NO2\rightarrow HONO}(R.H.))}{d(R.H.)} > \frac{d(\gamma_{HONO}(R.H.))}{d(R.H.)}. \qquad (11)$$

[56] It is important to note that there is currently little information of the RH dependence of $\gamma_{HONO}(RH)$. It is possible that this mechanism is only weakly dependent or even independent of RH, at least over a certain range of RH. In this case the observed change is purely due to the RH dependence of the NO_2 to HONO conversion. Since the [HONO]/[NO_2] maxima in Figure 6 are linearly dependent on RH, we can conclude in this case that the NO_2 to HONO conversion would be proportional to the RH, $\gamma_{NO2\rightarrow HONO}(RH) \propto RH$. This is in agreement with various laboratory results that find a linear dependence on RH. *Syomin and Finlayson-Pitts* [2003] recently reported that the HONO loss decreases with increasing RH between 0% and 50% RH, which would lead to a negative $d(\gamma_{HONO}(RH))/d(RH)$. If this is the case for the entire RH range, the RH dependence of $\gamma_{NO2\rightarrow HONO}(RH)$ could be less than linear, or $\gamma_{NO2\rightarrow HONO}(RH)$ could even be independent of RH.

[57] While the dry nights in Phoenix (e.g., Figure 4) seem to show that a PSS is reached, the low [HONO] levels make it difficult to prove that this is indeed the case. Since our interpretation thus far is based on the PSS assumption, we therefore need to consider the possibility that [HONO]/[NO_2] ratios are lower at lower RH because a PSS was not yet reached. A closer look at the exponential term in equation (9) reveals that a smaller $\gamma_{HONO}(RH)$ at lower RH ($d(\gamma_{HONO}(RH))/d(RH) > 0$) would increase the time to reach the PSS. Because $\gamma_{HONO}(RH)$ is also in the denominator in the first term of equation (9), a sole change in $\gamma_{HONO}(RH)$ would, however, also lead to higher PSS [HONO]/[NO_2] ratios and thus to higher ratios during dry nights, which contradicts our observations. We can therefore conclude that $\gamma_{NO2\rightarrow HONO}(RH)$ also has to change with RH. The relation between the RH dependencies is somewhat more complicated, and we can distinguish between three different cases based on our observations that at RH > 70% a PSS is reached. In the first, $d(\gamma_{HONO}(RH))/d(RH)$ is smaller than $d(\gamma_{NO2\rightarrow HONO}(RH))/d(RH)$, and the time to reach the PSS will be longer and the final [HONO]/[NO_2] ratio will be smaller at lower RH than at higher RH. This case would explain our observations and is in agreement with equation (11) and the explanation through a PSS. In the case that $d(\gamma_{HONO}(RH))/d(RH)$ is approximately equal to $d(\gamma_{NO2\rightarrow HONO}(RH))/d(RH)$ the time to reach PSS is still longer at lower RH, but the PSS [HONO]/[NO_2] ratio will not change with RH. This case can, in principle, also explain our observations at low RH. The case of $d(\gamma_{HONO}(RH))/d(RH)$ being larger than $d(\gamma_{NO2\rightarrow HONO}(RH))/d(RH)$ leads to an increase of the PSS at lower RH and, except for cases where the difference is small, will lead to higher [HONO]/[NO_2] ratios at the end of drier nights. From our consideration we can conclude that in the case a

PSS is not reached in the dry nocturnal boundary layer the following relation applies:

$$\frac{d(\gamma_{NO2\rightarrow HONO}(R.H.))}{d(R.H.)} \geq \frac{d(\gamma_{HONO}(R.H.))}{d(R.H.)}. \quad (12)$$

[58] If the $d(\gamma_{HONO}(RH))/d(RH)$ is negative, as suggested by *Syomin and Finlayson-Pitts* [2003], the steady state should be reached earlier at lower RH. In this case our observations in Phoenix would be in a PSS and equation (11) would apply.

[59] A dependence of S/V on RH could also influence the $[HONO]/[NO_2]$ increase (equation (9)), depending on the involved reactive surface. In the case of aerosol surfaces, one expects larger S/V values at higher RH. In the case of the ground as reactive surface, S/V will depend on the magnitude of vertical mixing. Since the magnitude of vertical mixing in Phoenix was generally smaller (more stable boundary layers) than in Houston and Nashville, we expect higher S/V at lower RH. The contribution of the RH dependence is therefore not clear, but one can calculate that the available S/V from ground surfaces is higher in nocturnal urban environments than from the aerosol under normal conditions. Thus a slower increase of $[HONO]/[NO_2]$ due to a change in S/V is not expected for drier conditions.

[60] In summary, we can conclude that the RH dependence of the $[HONO]/[NO_2]$ maxima observed in urban areas is due to the dependence of the reaction and uptake probabilities of NO_2 and HONO. While we can only determine the ratio of the two probabilities, our derivation indicates that the dependence of the reaction probability of NO_2 on RH is larger than that of the uptake probability of HONO.

4.4. Comparison to Literature

[61] Earlier work on HONO formation often showed a first-order dependence of the formation rate on the concentration of water vapor [*Jenkin et al.*, 1988; *Pitts et al.*, 1984b; *Sakamaki et al.*, 1983; *Svensson et al.*, 1987]. Most of these studies were performed in laboratory settings under conditions of constant temperatures. The water vapor concentration and thus the formation of HONO was therefore proportional to the RH.

[62] Other studies have suggested that the parameter that influences the NO_2 to HONO conversion is the amount of surface adsorbed water [*Finlayson-Pitts et al.*, 2003; *Kleffmann et al.*, 1998]. In a first approximation, one would expect that the amount of surface adsorbed water is proportional to the RH. *Saliba et al.* [2001], for example, determined that the number of water monolayers on glass followed a Brunauer, Emmett, and Teller (BET) isotherm. The data shows that the dependence can be approximated by a linear function between 10 and 70% and increases more strongly at higher RH. *Lammel* [1999] shows that the water coverage of various materials, expressed as number of monolayers of water, increases steadily with RH. In the case of stone and soil, the coverage around 20% RH is around 1 monolayer. The coverage increases to 3–5 monolayers at 80% RH. Above 80% RH, the coverage rapidly increases. *Goodman et al.* [2001] found a similar behavior on oxide particles. Qualitatively, the results of the different studies agree and the water coverage can therefore clearly be related to the RH. We want to caution, however, about taking too literal a view of a monolayer for atmospheric surfaces. The complex surface structure of natural surfaces will most likely lead to a mixture of areas with little surface adsorbed water and areas with many layers of water molecules. The functional dependence of the water coverage on the RH resulting from this averaging is not clear. For our case we will therefore assume that the water coverage is proportional to the RH below 80–90% RH. Above 95% RH a change in coverage may occur [*Lammel*, 1999], which could explain the lower $[HONO]/[NO_2]$ ratios observed in this range. Below 10% RH, where less than one monolayer is present on the surface [*Lammel*, 1999; *Goodman et al.*, 2001], the amount of adsorbed water decreases rapidly to zero at 0% RH. One would thus expect a fast decrease of the $[HONO]/[NO_2]$ ratios in Figure 6 below 10% RH. Because nocturnal RH is typically above 10% in the atmosphere, no information for HONO and NO_2 in this range is available.

[63] As we discussed above, under the assumption that the HONO uptake is independent or only weakly dependent on RH, our data shows a proportionality of the NO_2 to HONO conversion probability and the RH, $\gamma_{NO2\rightarrow HONO} \propto$ RH. It therefore appears that our results are in agreement with the laboratory findings that predict a first-order dependence on the RH or the amount of surface-adsorbed water. In contrast, the recent observation of a negative RH dependence of $\gamma_{HONO}(RH)$ by *Syomin and Finlayson-Pitts*, [2003] imply that the $\gamma_{NO2\rightarrow HONO}$ dependence on RH could be less than linear.

[64] *Saliba et al.* [2001] describe that in the uptake of NO onto a surface previously exposed to HNO_3, the maximum uptake occurs around a 3 monolayer coverage. They explain their results by a particular hydrogen bonding of HNO_3 in the surface layer. While the results of *Saliba et al.* [2001] apply to a different chemical reaction, surface adsorbed HNO_3 is also expected to play a role in the HONO loss on surfaces (see reaction (R5)). Our data, however, shows no clear change around a 3 monolayer coverage expected at 50–60% RH. Considering that natural surfaces will not have a uniform water coverage, as the glass surfaces in the study by *Saliba et al.* [2001], we suspect that any possible effect was averaged out to an extent that it would not be visible in our observations.

5. Conclusions

[65] Measurements of $[NO_2]$, [HONO], and RH from three different locations were analyzed with respect to the dependence of HONO chemistry on RH. Examples of the nocturnal behavior of [HONO] and the $[HONO]/[NO_2]$ ratio show a leveling off in the later part of the night. Following earlier results by *Stutz et al.* [2002], we interpret this behavior as a pseudo steady state (PSS) between the heterogeneous conversion of NO_2 to HONO and the loss of HONO on surfaces. A simplified mathematical description shows that the PSS $[HONO]/[NO_2]$ ratio solely depends on the ratio of the heterogeneous reaction probabilities of NO_2 and HONO, $\gamma_{NO2\rightarrow HONO}/\gamma_{HONO}$. The surface to volume ratio, which can be interpreted as a measure for vertical mixing if the ground is the reactive surface, and the reactive HONO uptake, γ_{HONO}, influence the time constant that is needed to reach the PSS.

[66] Based on these theoretical considerations, we associate the observed maximum [HONO]/[NO_2] ratios at various RH with the PSS of the NO_2-HONO system. A plot of all the [HONO]/[NO_2] ratios determined at night in the three field experiments clearly shows that the maximum [HONO]/[NO_2] ratio depends on the RH. From this observation we can conclude that the dependence on RH of the reaction probability of the NO_2 to HONO conversion is stronger than that of the loss of HONO. In the case that the reactive HONO uptake probability, γ_{HONO}, is independent of RH, our data would predict a linear dependence of $\gamma_{NO2\rightarrow HONO}$ on RH, in agreement with laboratory observations. For a negative RH dependence of γ_{HONO}, [*Syomin and Finlayson-Pitts*, 2003] our results imply that $\gamma_{NO2\rightarrow HONO}$ is less dependent on RH or perhaps even independent of RH.

[67] Many air pollution models currently employ a simplified NO_2 to HONO conversion mechanism that does not take RH dependence into account. *Aumont et al.* [2003], for example, parameterize HONO formation solely as a first-order conversion of NO_2. A parameterization omitting the influence of the RH, or surface-adsorbed water, will lead to a number of misrepresentations of HONO formation. It will, for example, overestimate the daytime HONO formation, since the RH is typically lower during day than during night. It also has implications for the applicability of a model to different locations such as those shown in our study.

[68] The apparent dependence of the NO_2 to HONO conversion on RH in environments with natural surfaces needs further investigation. Our study shows that water, most likely in its surface adsorbed form, can have a considerable influence on heterogeneous reactions in the atmosphere. It is very likely that a RH dependence of other heterogeneous reactions can also be found on natural surfaces.

[69] **Acknowledgments.** This study was supported by the NOAA Health of the Atmosphere Research Program, the EPA-Southern Oxidant Study program (grant 1995-1786-09), the Texas Natural Resource Conservation Commission, (grant 582-2-48650), and the Department of Energy (grant DE-FG03-01ER63094).

References

Ackermann, R. (2000), Auswirkungen von Kraftfahrzeugemissionen in der urbanen Atmosphäre, Ph.D. thesis, Univ. of Heidelberg, Heidelberg, Germany.

Alicke, B., U. Platt, and J. Stutz (2002), Impact of nitrous acid photolysis on the total hydroxyl radical budget during the Limitation of Oxidant Production/Pianura Padana Produzione di Ozono study in Milan, *J. Geophys. Res.*, *107*(D22), 8196, doi:10.1029/2000JD000075.

Alicke, B., A. Geyer, A. Hofzumahaus, F. Holland, S. Konrad, H.-W. Pätz, J. Schäfer, J. Stutz, A. Volz-Thomas, and U. Platt (2003), OH formation by HONO photolysis during the BERLIOZ experiment, *J. Geophys. Res.*, *108*(D4), 8247, doi:10.1029/2001JD000579.

Ammann, M., M. Kalberer, D. T. Jost, L. Tobler, E. Rossler, D. Piguet, H. W. Gaggeler, and U. Baltensperger (1998), Heterogeneous production of nitrous acid on soot in polluted air masses, *Nature*, *395*, 157–160.

Andres-Hernandez, M. D., J. Notholt, J. Hjorth, and O. Schrems (1996), A DOAS study on the origin of nitrous acid at urban and non-urban sites, *Atmos. Environ.*, *30*(2), 175–180.

Aumont, B., F. Chervier, and S. Laval (2003), Contribution of HONO sources to the $NO_x/HO_x/O_3$ chemistry in the polluted boundary layer, *Atmos. Environ.*, *37*(4), 487–498.

Barney, W. S., and B. J. Finlayson-Pitts (2000), Enhancement of N_2O_4 on porous glass at room temperature: A key intermediate in the heterogeneous hydrolysis of NO_2?, *J. Phys. Chem. A*, *104*(2), 171–175.

Bongartz, A., J. Kames, U. Schurath, C. George, P. Mirabel, and J. L. Ponche (1994), Experimental determination of HONO mass accommodation coefficients using 2 different techniques, *J. Atmos. Chem.*, *18*(2), 149–169.

Calvert, J. G., G. Yarwood, and A. M. Dunker (1994), An evaluation of the mechanism of nitrous acid formation in the urban atmosphere, *Res. Chem. Interm.*, *20*(3–5), 463–502.

Finlayson-Pitts, B. J., and J. N. Pitts (2000), *Chemistry of the Upper and Lower Atmosphere: Theory, Experiments and Applications*, Academic, San Diego, Calif.

Finlayson-Pitts, B. J., L. M. Wingen, A. L. Sumner, D. Syomin, and K. A. Ramazan (2003), The heterogeneous hydrolysis of NO_2 in laboratory systems and in outdoor and indoor atmospheres: An integrated mechanism, *Phys. Chem. Chem. Phys.*, *5*, 223–242.

Gerecke, A., A. Thielmann, L. Gutzwiller, and M. J. Rossi (1998), The chemical kinetics of HONO formation resulting from heterogeneous interaction of NO_2 with flame soot, *Geophys. Res. Lett.*, *25*(13), 2453–2456.

Goodman, A. L., G. M. Underwood, and V. H. Grassian (1999), Heterogeneous reaction of NO_2: Characterization of gas-phase and adsorbed products from the reaction, $2NO_2(g) + H_2O(a) \rightarrow HONO(g) + HNO_3(a)$ on hydrated silica particles, *J. Phys. Chem. A*, *103*(36), 7217–7223.

Goodman, A. L., E. T. Bernard, and V. H. Grassian (2001), Spectroscopic study of nitric acid and water adsorption on oxide particles: Enhanced nitric acid uptake kinetics in the presence of adsorbed water, *J. Phys. Chem. A*, *105*(26), 6443–6457.

Harris, G. W., W. P. L. Carter, A. M. Winer, J. N. Pitts, U. Platt, and D. Perner (1982), Observations of nitrous acid in the Los Angeles atmosphere and implications for the predictions of ozone-precursor relationships, *Environ. Sci. Technol.*, *16*(2), 414–419.

Harrison, R. M., J. D. Peak, and G. M. Collins (1996), Tropospheric cycle of nitrous acid, *J. Geophys. Res.*, *101*(D9), 14,429–14,439.

Jenkin, M. I., R. A. Cox, and D. J. Williams (1988), Laboratory studies of the kinetics of formation of nitrous acid from the thermal reaction of nitrogen dioxide and water vapour, *Atmos. Environ.*, *22*(3), 487–498.

Kaiser, E. W., and C. H. Wu (1977), A kinetic study of the gas phase formation and decomposition reactions of nitrous acid, *J. Phys. Chem.*, *81*(18), 1701–1706.

Kalberer, M., M. Ammann, F. Arens, H. W. Gaggeler, and U. Baltensperger (1999), Heterogeneous formation of nitrous acid (HONO) on soot aerosol particles, *J. Geophys. Res.*, *104*(D11), 13,825–13,832.

Kessler, C. (1984), Gasfoermige salpetrige Saeure (HNO_2) in der belasteten Atmosphaere, Ph.D. thesis, University of Cologne, Köln, Germany.

Kirchstetter, T. W., R. A. Harley, and D. Littlejohn (1996), Measurement of nitrous acid in motor vehicle exhaust, *Environ. Sci. Technol.*, *30*(9), 2843–2849.

Kitto, A. M. N., and R. M. Harrison (1992), Nitrous and nitric acid measurements at sites in South-East England, *Atmos. Environ.*, *26*(2), 235–241.

Kleffmann, J., K. H. Becker, and P. Wiesen (1998), Heterogeneous NO_2 conversion processes on acid surfaces: Possible atmospheric implications, *Atmos. Environ.*, *32*(16), 2721–2729.

Kleffmann, J., K. H. Becker, M. Lackhoff, and P. Wiesen (1999), Heterogeneous conversion of NO_2 on carbonaceous surfaces, *Phys. Chem. Chem. Phys.*, *1*(24), 5443–5450.

Kurtenbach, R., K. H. Becker, J. A. G. Gomes, J. Kleffmann, J. C. Lorzer, M. Spittler, P. Wiesen, R. Ackermann, A. Geyer, and U. Platt (2001), Investigations of emissions and heterogeneous formation of HONO in a road traffic tunnel, *Atmos. Environ.*, *35*(20), 3385–3394.

Lammel, G. (1999), Formation of nitrous acid: Parameterisation and comparison with observations, *Rep. 286*, 36 pp., Max-Planck-Inst. für Meteorol., Hamburg, Germany.

Longfellow, C. A., A. R. Ravishankara, and D. R. Hanson (2000), Reactive and nonreactive uptake on hydrocarbon soot: HNO_3, O_3, and N_2O_5, *J. Geophys. Res.*, *105*(D19), 24,345–24,350.

Mertes, S., and A. Wahner (1995), Uptake of nitrogen dioxide and nitrous acid on aqueous surfaces, *J. Phys. Chem.*, *99*(38), 14,000–14,006.

Pitts, J. N., H. W. Biermann, A. M. Winer, and E. C. Tuazon (1984a), Spectroscopic identification and measurement of gaseous nitrous acid in dilute auto exhaust, *Atmos. Environ.*, *18*(4), 847–854.

Pitts, J. N., E. Sanhueza, R. Atkinson, W. P. L. Carter, A. M. Winer, G. W. Harris, and C. N. Plum (1984b), An investigation of the dark formation of nitrous acid in environmental chambers, *Int. J. Chem. Kinet.*, *XVI*, 919–939.

Platt, U. (1986), The origin of nitrous and nitric acid in the atmosphere, in *Chemistry of Multiphase Atmospheric Systems*, edited by W. Jaeschke, pp. 299–319, Springer-Verlag, New York.

Platt, U. (1994), Differential Optical Absorption Spectroscopy (DOAS), in *Monitoring by Spectroscopic Techniques*, edited by M. W. Sigrist, John Wiley, Hoboken, N.J.

Sakamaki, F., S. Hatakeyama, and H. Akimoto (1983), Formation of nitrous acid and nitric oxide in the heterogeneous dark reaction of nitrogen dioxide and water vapor in a smog chamber, *Int. J. Chem. Kinet.*, 1013–1029.

Saliba, N. A., M. Mochida, and B. J. Finlayson-Pitts (2000), Laboratory studies of sources of HONO in polluted urban atmospheres, *Geophys. Res. Lett.*, *27*(19), 3229–3232.

Saliba, N. A., H. Yang, and B. J. Finlayson-Pitts (2001), Reaction of gaseous nitric oxide with nitric acid on silica surfaces in the presence of water at room temperature, *J. Phys. Chem. A*, *105*(45), 10,339–10,346.

Sjödin, A., and M. Ferm (1985), Measurement of nitrous acid in an urban area, *Atmos. Environ.*, *19*(6), 985–992.

Spindler, G., E. Brüggemann, and H. Herrmann (1999), Nitrous acid concentration measurements and estimation of dry deposition over grassland in Eastern Germany, in *Proceedings of EUROTRAC Symposium '98*, vol. 2, edited by P. M. Borrell and P. Borrell, pp. 218–222, Wentworth Inst. of Technol., Boston, Mass.

Stutz, J., B. Alicke, and A. Neftel (2002), Nitrous acid formation in the urban atmosphere: Gradient measurements of NO_2 and HONO over grass in Milan, Italy, *J. Geophys. Res.*, *107*(D18), 8192, doi:10.1029/2001JD000390.

Svensson, R., E. Ljungström, and O. Lindqvist (1987), Kinetics of the reaction between nitrogen dioxide and water vapour, *Atmos. Environ.*, *21*(7), 1529–1539.

Syomin, D. A., and B. J. Finlayson-Pitts (2003), HONO decomposition on borosilicate glass surfaces: Implications for environmental chamber studies and field experiments, *Phys. Chem. Chem. Phys.*, *5*(23), 5236–5242.

Syomin, D., K. A. Ramazan, and B. J. Finlayson-Pitts (2002), HONO reactions on clean and nitric acid doped glass surfaces, *Eos Trans. AGU*, *83*(47), Fall Meet. Suppl., Abstract A22B-0081.

TenBrink, H. M., and H. Spoelstra (1998), The dark decay of HONO in environmental (SMOG) chambers, *Atmos. Environ.*, *32*(2), 247–251.

Wang, S., R. Ackermann, J. D. Fast, C. W. Spicer, M. Schmeling, and J. Stutz (2003a), Atmospheric observations of enhanced NO_2-HONO conversion on mineral dust particles, *Geophys. Res. Lett.*, *30*(11), 1595, doi:10.1029/2003GL017014.

Wang, S., R. Ackermann, A. Geyer, J. C. Doran, W. J. Shaw, J. D. Fast, C. W. Spicer, and J. Stutz (2003b), Vertical variation of nocturnal NOx chemistry in the urban environment of Phoenix, paper presented at Annual Meeting, Am. Meteorol. Soc., Long Beach, Calif.

Williams, E. J., et al. (1998), Intercomparison of ground-based NO_y measurement techniques, *J. Geophys. Res.*, *103*(D17), 22,261–22,280.

R. Ackermann, B. Alicke, A. Geyer, J. Stutz, and S. Wang, Department of Atmospheric Sciences, University of California, Los Angeles, CA 90095-1565, USA. (ralf.ackermann@al-lightning.com; bjoern.alicke@web.de; andreas@atmos.ucla.edu; jochen@atmos.ucla.edu; shw@atmos.ucla.edu)

J. D. Fast, Pacific Northwest National Laboratory, Richland, WA 99352, USA. (jerome.fast.pnl.gov)

C. W. Spicer, Battelle Science and Technology International, Columbus, OH 43201-2693, USA. (spicerc@battelle.org)

E. J. Williams, Aeronomy Laboratory, National Oceanic and Atmospheric Administration, Boulder, CO 80309, USA. (eric@al.noaa.gov)

A. B. White, Environmental Technology Laboratory, National Oceanic and Atmospheric Administration, Boulder, CO 80309, USA. (allen.b.white@noaa.gov)

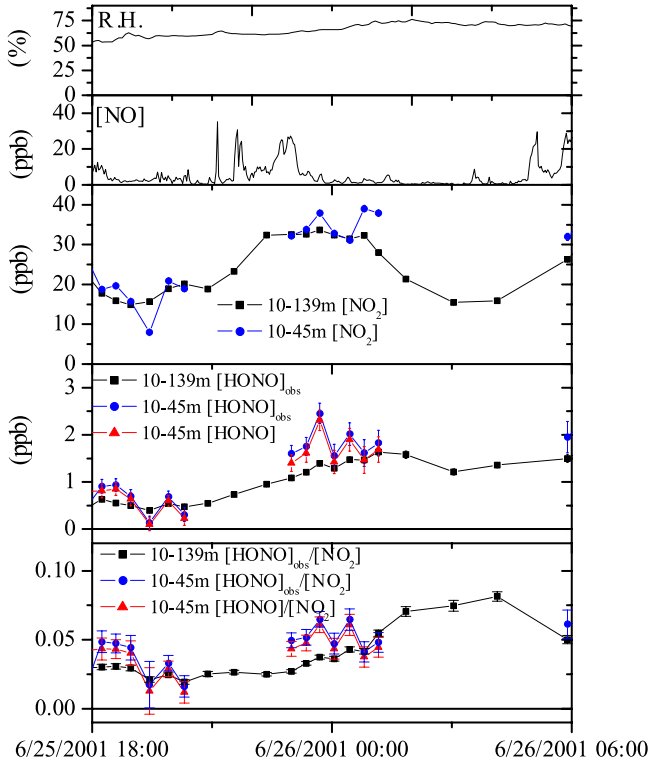

Figure 3. Behavior of [NO], [NO_2], [HONO], and RH during one night in Phoenix, Arizona. The night is characterized by relatively high nocturnal RH.

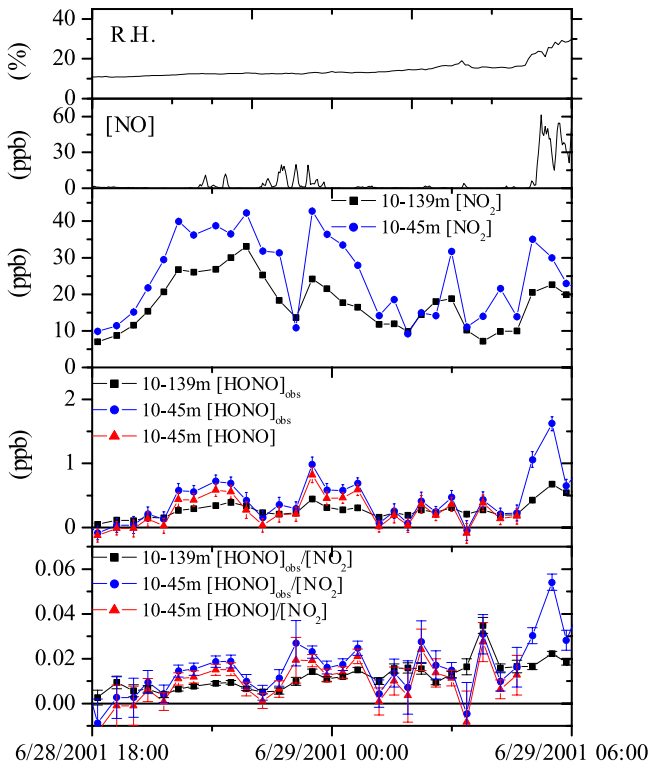

Figure 4. Behavior of [NO], [NO_2], [HONO], and RH during one night in Phoenix, Arizona. The night is characterized by very low nocturnal RH below 35%. [HONO] is not shown after 0430, when the onset of photolysis and strong emissions during rush hour make an emission correction unreliable.

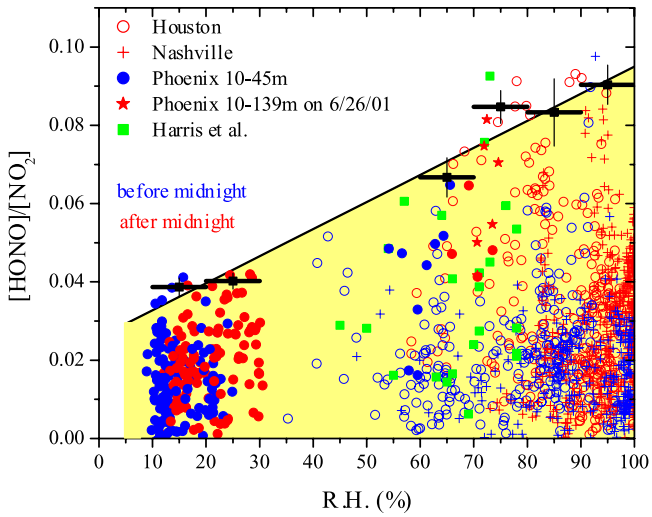

Figure 6. [HONO]/[NO_2] ratios versus RH for four different locations in the United States. Errors for [HONO]/[NO_2] are in the range 0.002–0.01 and were omitted in this plot for clarity.

Atmospheric observations of enhanced NO_2-HONO conversion on mineral dust particles

Shuhui Wang,[1] Ralf Ackermann,[1] Chester W. Spicer,[2] Jerome D. Fast,[3] Martina Schmeling,[4] and Jochen Stutz[1]

Received 29 January 2003; revised 23 March 2003; accepted 9 April 2003; published 14 June 2003.

[1] Nitrous acid is an important precursor for OH radicals in the polluted troposphere. The heterogeneous conversion of NO_2 to HONO, however, is currently not well understood. Measurements of HONO and NO_2 in Phoenix in summer 2001 using long path DOAS show ratios of chemically formed secondary [HONO] to [NO_2] that rarely exceeded 3%. During two nocturnal dust storm events, however, a significant increase of this ratio was observed. The unprecedented high ratios near 19% suggest a highly efficient NO_2 to HONO conversion process on mineral dust particles. The particle composition in Phoenix is similar to other mineral dusts, implying that the enhanced NO_2 conversion could be an important HONO, and therefore also OH, source in regions where pollution and dust storms coincide. *INDEX TERMS:* 0305 Atmospheric Composition and Structure: Aerosols and particles (0345, 4801); 0345 Atmospheric Composition and Structure: Pollution—urban and regional (0305); 0365 Atmospheric Composition and Structure: Troposphere—composition and chemistry. **Citation:** Wang, S., R. Ackermann, C. W. Spicer, J. D. Fast, M. Schmeling, and J. Stutz, Atmospheric observations of enhanced NO_2-HONO conversion on mineral dust particles, *Geophys. Res. Lett.*, *30*(11), 1595, doi:10.1029/2003GL017014, 2003.

1. Introduction

[2] The photolysis of nitrous acid (HONO) is an important OH source in the polluted atmosphere. It is well established today that HONO is formed by a conversion of NO_x on surfaces [*Finlayson-Pitts et al.*, 2003]. The mechanism and kinetics of this conversion, are, however, still poorly understood. Laboratory evidence points to a mechanism with the following stochiometry as the main source of HONO in the atmosphere (see references in [*Finlayson-Pitts et al.*, 2003; *Lammel and Cape*, 1996])

$$2NO_2 + H_2O_{surf} \rightarrow HONO + HNO_{3,surf} \quad (1)$$

[3] Most studies have reported that mechanism 1 is first order in NO_2 (for example [*Finlayson-Pitts et al.*, 2003; *Kleffmann et al.*, 1998; *Svensson et al.*, 1987]). The dependence on water is less clear, but it is suggested that the NO_2 to HONO conversion efficiency depends on the amount of surface adsorbed water [*Barney and Finlayson-Pitts*, 2000; *Finlayson-Pitts et al.*, 2003]. The role of the surface involved is also not well known. While most experiments have been performed on glass or teflon, a number of recent studies have investigated the NO_2 chemistry on mineral oxides or dust particles. [*Underwood et al.*, 1999, 2001] found that the heterogeneous reaction of NO_2 on dehydrated ($p_{H2O} < 10^{-6}$ Torr) Al_2O_3, Fe_2O_3 and TiO_2 particles, as well as on Saharan and Gobi dust samples, leads to surface adsorbed nitrite and nitrate at low NO_2 and high NO_2 pressure respectively. The gas phase product is mainly NO. HONO was not detected. [*Goodman et al.*, 1999] investigated the heterogeneous processes on SiO_2 particles at relatively high R.H. (relative humidity). The NO_2 reaction in this case followed mechanism (1).

[4] Mineral dust can provide large surface areas for chemical transformation of trace gases [*Dentener et al.*, 1996]. In particular, dust storms over Asia have recently received considerable attention due to the unique mixture of aerosol and pollutants. Typical aerosol mass loadings in dust storms are $1-1000\ \mu g\ m^{-3}$, with particle sizes ranging from 0.1 to above 40 μm. The main components of mineral dust are SiO_2, Al_2O_3, Fe_2O_3, CaO, and often also $CaCO_3$ [*Goudie*, 1978].

[5] In this study we present measurements of HONO and NO_2 during two nocturnal dust storms in Phoenix, AZ. The behavior of HONO and NO_2 is compared to times without mineral dust particles. The potential impacts of our observations on tropospheric chemistry are discussed.

2. Experimental Section

[6] In summer 2001 (6/17–6/30) we made long-path Differential Optical Absorption Spectroscopy (DOAS) [*Platt*, 1994] measurements of HONO and NO_2 in the downtown area of Phoenix, AZ. The DOAS sending and receiving telescope was set up on the 39th floor of the BankOne building, 140 m above ground level. The light paths were folded by quartz cube corner retroreflectors, which were mounted at a distance of about 3.3 km, on top of two buildings in uptown Phoenix (ADEQ and Hilton) at the heights of 110 m and 45 m, respectively [*Wang et al.*, 2003]. The average concentrations of NO_2 and HONO along these two absorption paths were monitored by periodically alternating the aiming direction of the telescope. Details of the setup and the analysis methods used can be found in [*Stutz et al.*, 2002].

[7] Meteorological measurements were made close to the retroreflectors on top of the two buildings using Campbell Scientific Inc. weather stations. Mixing ratios of NO and the scattering coefficient b_{scat} were measured by chemilumines-

[1]Department of Atmospheric Sciences, University of California, Los Angeles, California, USA.
[2]Battelle Columbus Operations, Columbus, Ohio, USA.
[3]Pacific Northwest National Laboratory, Richland, Washington, USA.
[4]Loyola University, Chicago, Illinois, USA.

0094-8276/03/2003GL017014$05.00

cence (ThermoEnvironmental 42S) and nephelometry (Meteorology Research Inc. Model 1550) respectively on the 16th floor (73 m) and 39th floor (140 m) of the BankOne building. In addition, atmospheric particles were collected on top of the BankOne building with a time resolution of 1.5 hours. The trace elemental composition of these samples was analyzed by total reflection X-ray fluorescence spectrometry (TXRF) [*Schmeling*, 2001].

[8] To separate secondary HONO, $[HONO]_{corr}$, formed by chemical processes, from direct emissions which originate primarily from cars, we used a $[HONO]/[NO_x]$ emission ratio of 0.35% for an average American car fleet, as determined in traffic tunnel measurements by [*Kirchstetter et al.*, 1996]:

$$[HONO]_{corr} = [HONO] - 0.0035 \times [NO_x] \quad (2)$$

[9] $[NO_x]$ for the two light paths were calculated as the sum of the [NO] on the 39th and 16th floor and the $[NO_2]$ for upper and lower light paths, respectively. For most nights during our study the calculated HONO emissions contributed about 20% to the total [HONO]. During dust storms, however, $[NO_x]$ was so low that the influence of direct HONO emissions was negligible.

3. Results and Discussion

[10] The results of the night of June 20–21 (Figure 1) show a sudden increase of b_{scat}, indicating a high concentration of dust particles, correlated with strong winds at the onset of the storm around 21:45. The direction of the wind

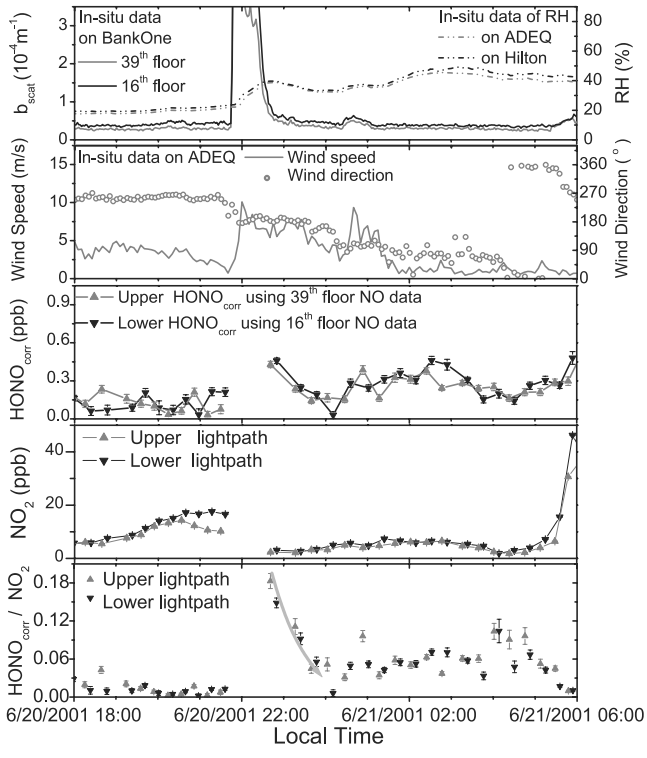

Figure 1. b_{scat}, R.H., wind speed and direction, $[NO_2]$, $[HONO]_{corr}$, and $[HONO]_{corr}/[NO_2]$ during the night of June 20–21, 2001 in Phoenix. The error bars show the 1σ standard deviation.

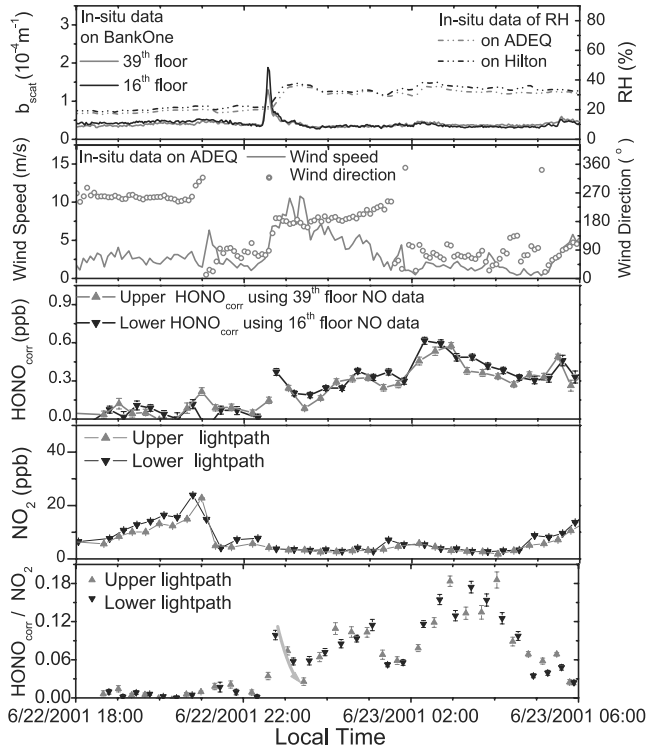

Figure 2. Observation results at the night of June 22–23, 2001 in Phoenix.

also changed abruptly from weak local winds to a larger scale south-southwest wind flow. Due to the strong light extinction during the dust storm the time resolution of DOAS measurement was reduced temporarily and DOAS data shows a gap in Figure 1. Immediately following this gap significantly higher $[HONO]_{corr}$ and lower $[NO_2]$ were observed. Enhanced vertical mixing and advection of the less polluted air mass from outside of Phoenix most likely contributed to the lower $[NO_2]$. The doubled $[HONO]_{corr}$ at the end of the dust storm and its decrease afterwards, however, suggest that a highly efficient HONO production pathway was active. $[HONO]_{corr}/[NO_2]$ ratios reached a level of (18.3 ± 1.2)% during the storm (Figure 1). Coincidentally, as b_{scat} decreased after the storm, the $[HONO]_{corr/[NO2]}$ also fell below 5%. Throughout the rest of the night $[HONO]_{corr}/[NO_2]$ steadily increased to a relatively high final value of around 10% before dawn.

[11] The data of June 22–23 (Figure 2) are similar to that of June 20–21. A narrow peak of b_{scat} around 22:30, together with the sudden change of wind speed and direction, indicates a weaker dust storm compared to June 20. $[HONO]_{corr}/[NO_2]$ reached 10% at the tail of the storm, and decayed to below 5% afterwards. The main difference during this night is that $[HONO]_{corr}/[NO_2]$ increased throughout the night and reached a much higher value of (18.6 ± 1.3)% than on June 21. It is currently unclear why such high $[HONO]_{corr}/[NO_2]$ values were observed at the end of the night on June 22–23. One reason could be the presence of dust particles that were too small to be observed by the nephelometer which has a low detection efficiency for particles smaller than 0.2 μm diameter. The difference could also be explained by the different wind patterns.

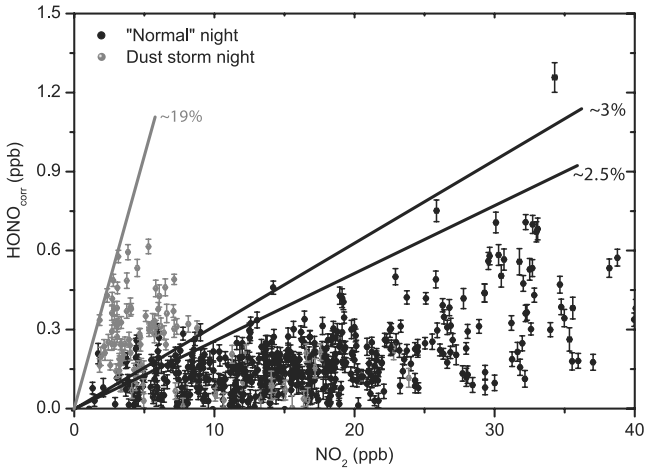

Figure 3. Comparison of $[HONO]_{corr}$ and $[NO_2]$. Dust storm night data include data of the entire nights with dust storm events. The maximum $[HONO]_{corr}/[NO_2]$ ratios can be interpreted as a lower estimate of the PSS value that can be reached.

While on the night of 20–21 the wind turned slowly to the east after the storm, thus blowing away the dust particles and the processed air, on 22–23 the wind shifted suddenly from southwest to east near 2am, implying that the dust processed air blown to the east could have been brought back to our site.

[12] We calculated 24-hour backtrajectories with the Hybrid Single-Particle Lagrangian Integrated Trajectory (HYSPLIT) Model by NOAA. The backtrajectories for both dust storms are very similar, showing that the dust particles originated from the same areas south-west of Phoenix and thus have similar mineral composition.

[13] To show the influence of the dust storms we correlated $[HONO]_{corr}$ with $[NO_2]$ during dust storm nights and "normal" nights in Figure 3. Meteorological conditions during "normal" nights differed considerably from dust storm nights. In particular the lower wind speeds make it unlikely that elevated dust levels were present, as was also confirmed by the nepheolometer data. Data from "normal" nights includes all measurements with R.H. < 50%. One night with a high R.H. of up to 70% was not included because the property of surface adsorbed water changes at R.H. above 50% [*Saliba et al.*, 2001], and accordingly the chemistry of NO_2 and HONO may be different. Figure 3 clearly shows that the $[HONO]_{corr}/[NO_2]$ ratio was rarely above 3% under "normal" conditions, but reached near 19% under the influence of dust storms.

[14] Table 1 lists the aerosol composition during June 20 in downtown Phoenix. The collection during 20:30–22:00, which covered the first 15 minutes of the dust storm, shows large amounts of Fe, Ca, and Al, which are often used as key tracers for mineral dust, with concentrations of up to 8 times those collected before the storm. Although Si was not analyzed in our study because of the usage of quartz glass material in TXRF particulate measurement, it is believed that Si is the most abundant element in the mineral dust we observed [*Goudie*, 1978].

[15] The use of the $[HONO]_{corr}/[NO_2]$ ratio as a parameter for the study of the NO_2-HONO conversion requires more consideration. The HONO formation rate by reaction (1) is first order in NO_2, depends on the surface adsorbed water, and increases with S/V, the surface area per unit volume of air. The main HONO loss will occur on surfaces [*Finlayson-Pitts et al.*, 2003; *Stutz et al.*, 2002], which is suggested to be a first order loss [*Syomin et al.*, 2002]. The temporal change of HONO can therefore be expressed with equation (3). γ_1 and γ_2 are HONO formation and destruction reaction probabilities that depend on surface properties as well as atmospheric R.H. $\bar{\nu}$ is the mean velocity of a gas species.

$$\frac{d[HONO]}{dt} = \gamma_1(R.H.) \times \frac{\overline{\nu}_{NO_2}}{4} \times \frac{S}{V} \times [NO_2] - \gamma_2(R.H.) \times \frac{\overline{\nu}_{HONO}}{4} \times \frac{S}{V} \times [HONO] \quad (3)$$

[16] The initial increase of HONO will be dominated by the first term on the right of equation (3). As more HONO is formed the second term becomes more important. In the end HONO and NO_2 will reach a pseudo steady state (PSS), which is determined by:

$$\frac{[HONO]}{[NO_2]} = \frac{\gamma_1(R.H.) \times \overline{\nu}_{NO_2}}{\gamma_2(R.H.) \times \overline{\nu}_{HONO}} \quad (4)$$

[17] It is interesting to note that this PSS is independent of S/V. On the other hand, a high S/V, as in a dust storm, will accelerate the surface reactions and the PSS will be reached in a very short time. We can now distinguish two scenarios in our dust storms. If a PSS was reached during the storm period, the PSS ratio of $[HONO]/[NO_2]$ based on our observations must be around 18%. In the case that a PSS was not yet reached for the observed air mass at the end of the storm, the PSS $[HONO]/[NO_2]$ ratio should be even higher than our observations.

[18] Under "normal" conditions, $[HONO]_{corr}/[NO_2]$ ratios in Phoenix rarely exceeded 3%. While it is currently not clear if a PSS was reached during these nights, the $[HONO]/[NO_2]$ PSS value in a dust storm is clearly higher when mineral dust is present. This is also confirmed by comparison of literature $[HONO]/[NO_2]$ ratios measured at other urban and suburban sites, which range from 1% to 12% [*Lammel and Cape*, 1996]. The ratios we observed are therefore higher than any other atmospheric observations we are aware of, with the exception of recent daytime findings in and above snow [*Zhou et al.*, 2001].

[19] Our observations show that the heterogeneous chemistry on mineral particles is different from the chemistry on other surfaces, such as the ground and buildings. We are unable to distinguish whether the change in the heterogeneous chemistry is related to an enhanced uptake and conversion of NO_2, or to a decreased loss of HONO on

Table 1. Aerosol Composition Before and During the Dust Storm on June 20, 2001 in Phoenix

	Concentration of measured element (ng/m3)					
Collection time	Al	K	Ca	Ti	Mn	Fe
16:00-17:35	430.8	255.0	1339.5	20.9	21.3	33.0
20:30-22:00	2132.5	1372.8	9282.1	79.2	227.8	254.8

the surface, but the observations show that the net HONO formation (HONO formed per NO_2) is enhanced. We can only speculate about the mechanism responsible for the enhanced net conversion. Laboratory studies on dehydrated mineral oxide particles showed a heterogeneous reaction mechanism of NO_2 without gaseous HONO product [*Underwood et al.*, 2001]. Due to the very low water vapor pressure used in these studies, this data is most likely not representative for our case in Phoenix where R. H. 30–50% were observed in the dust storms. In the investigation of NO_2 reactivity on "wet" SiO_2 particles [*Goodman et al.*, 1999] and "wet" porous glass [*Barney and Finlayson-Pitts*, 2000], gaseous HONO and surface adsorbed HNO_3 were detected as products, in agreement with reaction (1). We believe that this is the most likely reaction occurring on mineral dust particles, which contain adsorbed water under atmospheric conditions. Why this mechanism is different on dust particles compared to other surfaces is, however, unclear.

4. Conclusions

[20] During nighttime dust storms in Phoenix in summer 2001, we observed very high values of secondary [HONO] to [NO_2] ratios around 18%, while this ratio rarely exceeded 3% during non-dust-storm nights. We propose an efficient heterogeneous net NO_2 to HONO conversion process on dust particles to explain our results. The steady-state [HONO]/[NO_2] ratio that can be reached in the presence of mineral dust particles must be at least 18%.

[21] Our results suggest a significant impact of dust storms on the tropospheric nitrogen chemistry. If more NO_2 is converted into HONO over night under the influence of dust storms, more OH radicals will be produced by HONO photolysis in the morning, ultimately oxidizing NO_2 and VOCs. At the same time, the NO_2-HONO conversion process by reaction (1) results in the transformation of NO_2 to surface HNO_3, and can thus contribute to the denoxification of the troposphere. In addition, this enhanced NO_2-HONO conversion can impact the chemistry in daytime dust storms. Faster HONO formation can lead to an increase of OH radical formation rate in dust storms also during the day.

[22] It is estimated that 1000–3000 Tg of mineral aerosols are emitted annually into the atmosphere [*Jonas et al.*, 1995]. The emissions are expected to increase substantially as arid regions expand due to vegetation loss, erosion, and industrial activities [*Sheehy*, 1992]. The preexisting deserts and the large scale desertification have caused severe seasonal dust storms over many regions, including East Asia, West Africa, and South America [*Dentener et al.*, 1996]. On the other hand, the increasing population and industry in East Asia as well as the biomass burning in Africa and South America, will contribute increasing amounts of NO_x to the troposphere. Our study shows that seasonal dust storms have the potential to change the distribution of nitrogen compounds and the level of reactive species significantly in the troposphere.

[23] **Acknowledgments.** We gratefully acknowledge the support of the Department of Energy, grant DE-FG03-01ER63094. The assistance of Arizona Department of Environmental Quality is greatly appreciated. We would also like to thank C. Berkowitz, C. Doran, and R. Redman for their help in establishing the measurement site.

References

Barney, W. S., and B. J. Finlayson-Pitts, Enhancement of N_2O_4 on porous glass at room temperature: A key intermediate in the heterogeneous hydrolysis of NO_2?, *J. Phys. Chem. A*, *104*, 171–175, 2000.

Dentener, F. J., et al., Role of mineral aerosol as a reactive surface in the global troposphere, *J. Geophys. Res.*, *101*(D17), 22,869–22,890, 1996.

Finlayson-Pitts, B. J., et al., The heterogeneous hydrolysis of NO_2 in laboratory systems and in outdoor and indoor atmospheres: An integrated mechanism, *Phys. Chem. Chem. Phys.*, *5*, 223–242, 2003.

Goodman, A. L., G. M. Underwood, and V. H. Grassian, Heterogeneous reaction of NO_2: Characterization of gas-phase and adsorbed products from the reaction, $2\ NO_{2(g)} + H_2O_{(a)} \rightarrow HONO_{(g)} + NO_{3(a)}$ on hydrated silica particles, *J. Phys. Chem. A*, *103*, 7217–7223, 1999.

Goudie, A. S., Dust storms and their geomorphological implcations, *J. Arid. Environ.*, *1*, 291–310, 1978.

Kirchstetter, T. W., R. A. Harley, and D. Littlejohn, Measurement of nitrous acid in motor vehicle exhaust, *Environ. Sci. Technol.*, *30*(9), 2843–2849, 1996.

Kleffmann, J., K. H. Becker, and P. Wiesen, Heterogeneous NO_2 conversion processes on acid surfaces: Possible atmospheric implications, *Atmos. Environ.*, *32*, 2721–2729, 1998.

Lammel, G., and J. N. Cape, Nitrous acid and nitrite in the atmosphere, *Chem. Soc. Rev.*, *25*(5), 361–369, 1996.

Platt, U., Differential Optical Absorption Spectroscopy (DOAS), in *Monitoring by Spectroscopic Techniques*, edited by M. W. Sigrist, pp. 27–84, John Wiley, New York, 1994.

Saliba, N. A., H. Yang, and B. J. Finlayson-Pitts, Reaction of gaseous nitric oxide with nitric acid on silica surfaces in the presence of water at room temperature, *J. Phys. Chem.*, *105*(45), 10,339–10,346, 2001.

Schmeling, M., Total reflection X-ray fluorescence—A tool to obtain information about different air masses and air pollution, *Spectrochim. Acta B*, *56*(11), 2127–2136, 2001.

Sheehy, D., A perspective on desertification of grazingland and ecosystems in North China, *Ambio*, *21*, 303–307, 1992.

Stutz, J., B. Alicke, and A. Neftel, Nitrous acid formation in the urban atmosphere: Gradient measurements of NO_2 and HONO over grass in Milan, Italy, *J. Geophys. Res.*, *107*(D22), 8192, doi:10.1029/2001JD000390, 2002.

Svensson, R., E. Ljungström, and O. Lindqvist, Kinetics of the reaction between nitrogen dioxide and water vapour, *Atmos. Environ.*, *21*, 1529–1539, 1987.

Syomin, D., K. A. Ramazan, and B. J. Finlayson-Pitts, HONO reactions on clean and nitric acid doped glass surfaces, *Eos Trans. AGU*, *83*(47), Fall Meet. Suppl., Abstract A22B-0081, 2002.

Underwood, G. M., et al., Heterogeneous reactions of NO_2 and HNO_3 on oxides and mineral dust: a combined laboratory and modeling study, *J. Geophys. Res.*, *106*(D16), 18,055–18,066, 2001.

Wang, S., et al., Vertical variation of nocturnal NOx chemistry in the urban environment of Phoenix, in *Extended Abstracts, Fifth Conference on Atmospheric Chemistry in the 83rd AMS Annual Meeting*, pp. 1.1, Am. Meteorol. Soc., Long Beach, Calif., 2003.

Zhou, X., et al., Snowpack photochemical production of HONO: A major source of OH in the Arctic boundary layer in springtime, *Geophys. Res. Lett.*, *28*, 4087–4090, 2001.

R. Ackermann, J. Stutz, and S. Wang, Department of Atmospheric Sciences, University of California, Los Angeles, CA 90095-1565, USA. (jochen@atmos.ucla.edu)

J. D. Fast, Pacific Northwest National Laboratory, 902 Battelle Boulevard, Richland, WA 99352, USA.

M. Schmeling, Department of Chemistry, Loyola University, 6525 North Sheridan Road, Chicago, IL 60626, USA.

C. W. Spicer, Battelle Columbus Operations, 505 King Avenue, Columbus, OH 43201, USA.